2007-2010

China National Report on Physical Sciences of the Oceans

For

The 25th General Assembly of IUGG

Melbourne, Australia, 28 June - 7 July 2011

Prepared by Chinese National Committee for

The International Union of Geodesy and Geophysics

March 5, 2011

PREFACE

This quadrennial report is the third report in the new millennium, which is one of the China National Reports (2007-2011), prepared by the Chinese National Committee for IAPSO for the XXV IUGG General Assembly of the International Union of Geodesy and Geophysics to be held in Melbourne, Australia, 28 June - 7 July 2011.

This report composes of 13 pappers which reviewed the main work done and the major progress made in physical oceanography and air-sea interaction in Mainland China as well as the new trend that the physical sciences of the ocean are becoming multi-disciplinary sciences, since researches into sediment dynamics, ecosystem dynamics and biogeochemistry of the ocean are come into together in China. It should be noted that this report only provides an overview of the subjects mentioned in the 13 papers, but it does show encouraging progress in physical sciences of the oceans in Mainland China over the past four years. It is pleasant to see the fact that most of papers in this report have been written by the younger scientists, which shows that the younger generation of marine scientists in China has grown up.

I would like to take this opportunity, on behalf of the Chinese National Committee for IAPSO, to express my deep appreciation to all the authors for their contributions, to Dr. CHEN Xueen, the secretary general of Chinese Committee of IAPSO, who made a great contribution to organizing the writing group for this report, and to Mr. ZHENG Peng, who carefully corrected some mistakes in texts of some papers. Finally, the editing of this report was supported by several projects like State 863 project 2007AA09Z117 and SOA project 200905001.

ZHAO Jinping

Editor-in-Chief

Chairman, Chinese National Committee for IAPSO

CONTENTS

PROGRESS IN ARCTIC PHYSICAL OCEANOGRAPHY AND SEA ICE PHYSICS DURING 2007-2010

Yong CAO and Jinping ZHAO

(Ocean University of China, Qingdao, China, 266100)

Ⅰ Introduction

During 2007-2010, a good opportunity for Arctic scientists is the 4th International Polar Year (IPY), during which there are more field observation cruises and international collaborations. The scientific activities and research results of physical oceanography in China are introduced in this report.

In 2007, Chinese government approved the "China's Action Plan for the International Polar Year", including the activities in both Arctic and Antarctic. Two cruises to the Arctic Basin were planned in this project. The other part of the project in the Arctic is promotion of the research in the scientific base, Huanghe Station, located in the Sverbard Islands. The expeditions in the Arctic Ocean were carried out in summer in 2008 and 2010. The plan also supports scientists to participate international cooperation and collaborative studies.

In 2008 the scientific goal of the third Chinese National Arctic Research Expedition was "Rapid Change on the Arctic Climate and Environment". The expedition regions include the Bering Sea, the Chukchi Sea, the Beaufort Sea, the Canada Basin and the Chukchi plateau. The expeditions including the physical oceanography and the ocean optics in the context of ocean physics were carried out. At the same time two sets of the subsurface buoys were deployed to study the coupled variation between the sea-ice-air in the Arctic, the changes of the Arctic Ocean responding to the sea ice, the influence of the climate in China responding to the variation of the Arctic, and so on. In 2010 the goal of the fourth Chinese National Arctic Research Expedition was "Rapid Changes of the Arctic Sea Ice and the response of the marine ecosystem in the Arctic Ocean". The physical oceanography and the optics expedition regions were same as the third expedition but northward station was reached to 87°N. A series of observations at the North Pole were carried supported by a helicopter.

At the same time the Chinese scientists participate in the expeditions of the international cooperation. Eight expeditions included three cruises of the U.S. Icebreaker Healy (2007, 2008, and 2009), one cruise of the Canada LSSL Icebreaker (2009), three cruises of Canada Amundsen Icebreaker (2007, 2008ab), and one cruise supported by the aircraft on the sea ice around the north slope of Canada.

Most Arctic expeditions were in summer. For the winter in the Arctic was very dark and cold, there were few opportunities to visit in winter. During the 4th International Polar Year, the "Circum Polar Flaw Leads (CFL)" program was carried out for a whole year by Canada. The scientists from Ocean University of China attended the two legs in winter and one leg in summer. The observations of the physical oceanography and several tests of the sea ice optics were implemented during these expeditions.

For the rapid change of the sea ice in Arctic, the studies of physical oceanography of China emphasis on the physical structure of the ocean response to the variation of the sea ice, especially the studies of the structure and the energy distribution of the upper ocean. The "Rapid Arctic sea ice retreat

and the associated climate, ecological effects" as a system topic of the variation of the sea ice which was proposed for in the 4th International Polar Year.

Based on the observation data obtained from the previous Arctic Expeditions, a series of results were acquired in the Arctic Ocean, sea ice and climate of China. The studies focused on the temporal and spatial variations of the upper ocean and the sea ice, the sea ice optics and the ocean optics, the core region of the Arctic Oscillation and so on. These studies established the basis of the physical oceanography of the Arctic and strengthened the relationship between the climate and the ocean in the Arctic.

Ⅱ The upper ocean in the Arctic

There is close relationship between the rapid change of sea ice and the upper ocean temperature and salinity in the Arctic. In summer, melting of the sea ice causes the sea surface water fresher. More solar radiation penetrating through ice heats seawater and leads the decreasing of the sea ice concentration and ice thickness. At the same time, the heat absorbed by the upper ocean accelerates sea ice melting, which forms the positive heat feedback mechanism of the upper ocean to the sea ice in the Arctic. The results of Chinese scientists on the upper ocean of the Arctic are summarized as followed.

1 Near Surface Temperature Maximum

Zhao et al. (2003) found that there was a temperature maximum water layer near the sea surface in the summer marginal ice zone of Chukchi Sea by using the CTD data collected by the first Chinese National Arctic Research Expedition in 1999. The water was named as Subsurface Warm Water and the depth of the temperature maximum peak was observed as about 20m. Jakson et al. (2010) gave it a better name as Near Surface Temperature Maximum (NSTM). The formation mechanism of NSTM was the heating of the solar radiation and the cooling by the sea surface (Zhao et al., 2003). There was a halocline above the depth of the temperature peak so that the NSTM might be maintained. NSTM usually occurred in the ice-covered water, sometimes might occurred in the open water (Cao et al. 2010). The result from the CTD data collected in the Beaufort Sea, Chukchi Sea and the Canada Basin from 1993 to 2008 showed that NSTM often occurred in the open water of the shelf and the marginal ice zone before 2004 and the temperature maxima were high. From 2004, the NSTM occurs more and more extensively, covering most of the Canada Basin (fig 1). The reason is that large sea ice melted in these years. More solar radiation penetrating the sea ice is absorbed by the near surface water with the decreasing of the sea ice concentration (Cao et al. 2010). The depth of the NSTM, the temperature peaks and the its temporal variation are related with the halocline which is determined by the ice melting water and lowers the vertical turbulent diffusivity. Zhang et al. (2007) calculated the vertical distributions using the temperature, salinity and the current profile data in the Canada Basin (74^{o}N-78^{o}N, 144^{o}W-164^{o}W) obtained from the Chinese Arctic Research Expedition cruise of summer 2003. The results showed that the distributions was consistent in some respects which was large in both surface and at the depth of 60m and smaller in the middle layer especially at the depth of halocline. Therefore, the NSTM needs not only the solar radiation heating and surface cooling, but also the stratification. Chen et al. (2010) studied the NSTM by a thermodynamic column model coupled by a sea ice model and an upper ocean model. The results verified that the solar radiation is the dominant energy source and the thin ice and the leads are the main energy channels of solar radiation. Meanwhile, long-wave flux, air temperature, and atmospheric humidity played important roles in determining the relative intensity of NSTM.

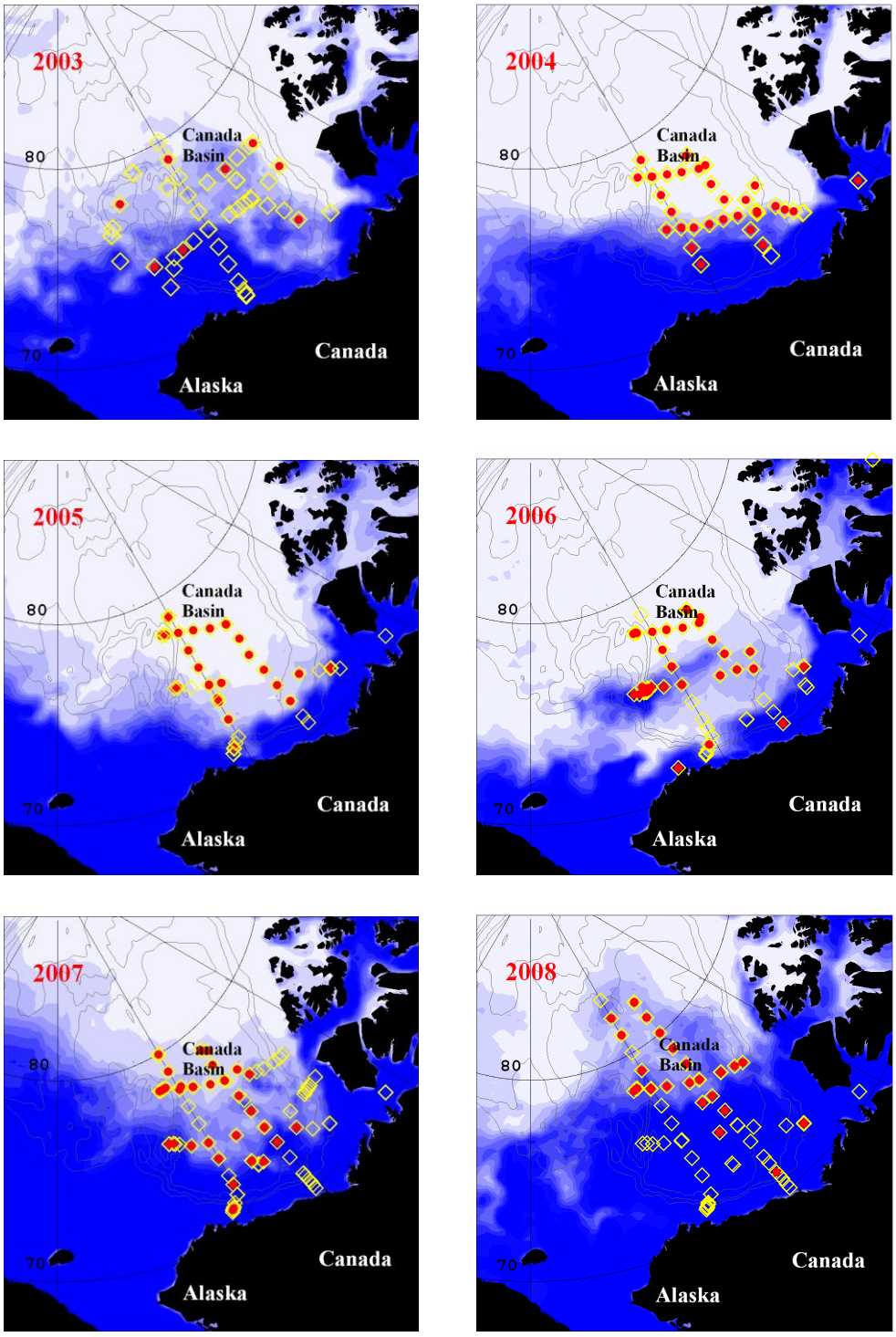

Fig 1 Spatial distribution of NSTM in 2003-2008

Locations of CTD are expressed by yellow squares and the locations with NSTM are expressed by red dots. The filled counter lines are the averaged ice concentration in August.

2 Water Mass Structure during Ice Melting Period

Chinese icebreaker, "Xue Long", entered the Chukchi Sea on July 14th, 1999 during the 1st Chinese Arctic Research Expedition. The sea ice seriously delayed the sailing of the vessel for the sea ice

concentration was up to 60%. In the next four days, the ship struggled in the ice to look for the north access around the Herald Shoal, and deployed CTD and took water samples during the voyage. Zhao et al. (2010) analyzed the ocean structure of Chukchi Sea around the Herald Shoal. Besides temperature and salinity,the nutrients and chlorophyll-a was also considered to study the water structure around the Harold Shoal. The results showed that there were two water masses existing in this region. One was the Anadyr Water (AW) that entered in winter or spring with lower temperature, higher salinity and higher silicate. The other was the Bering Shelf Water (BSW) with higher temperature, lower salinity and lower silicate. The dividing line between the two water masses was consistent with the margin of the ice edge. During the ice melting process, the AW retreated northward with the ice edge, indicating that the BSW flows north simultaneously with ice melting. The northward tongues of water with low salinity and low silicate represented the main channel of the northward currents.

3 Water Properties and Convection under Sea Ice in Winter

The convection under sea ice in winter Amundsen Gulf without solar heating is studied by Li et al. (2010). The data were from Circumpolar Flaw Leads System Study project (CFL) during the time of polar night from November 2007 to the end of January 2008. The results showed that the vertical haline convection was the main character of the sea water in winter time in this region. The thickness of the mixed layer varied from meters to tens of meters. No static instability was found, i.e. the density of the water in mixed layer was lower than that of the water below. Unlike the convection others studied, the convection was caused by continual released haline parcel. The temperature of the water in the mixed layer was almost at the freezing point, which was the result of the haline /density convection during the period of the ice formation. Below the mixed layer, there was a warm layer. But the temperature decreased with time during the observation period. The main reason for it was the energy exchange with the water in mixed layer. According to the results, the salinity and thickness of the mixed layer coincided in early winter, while the thickness decreased in late winter with the salinity increasing. The study also analyzed the temperature and salinity data from 3 stations which are coarsely at the same position and found that the salinity of the mixed layer increased and the temperature of the warm layer decreased during the observation period.

4 Polynyas in Bering Sea

A polynya is a large area of open water or an area covered by very thin ice that persists in the middle of winter sea ice in the polar regions. In winter, a lot of latent polynyas appear regularly in the shelf of Northern Bering Sea. They have made great contributions to local ecological system and the Arctic halocline. A Los Alamos Sea Ice Model (CICE) with a horizontal resolution of 6.37km had been implemented to simulate a full year of sea-ice growth and decay starting on November 1, 2002 in the Bering Sea (Fu et al., 2009). The total sea ice area from the model results and one from AMSRE /Aqua satellite observations had a good consistency. Their correlation coefficient of daily mean total sea ice area was 0.97. Model results showed that polynyas in southern domains of east-west coasts were formed by means of southward movements of sea ice, which were mainly forced by offshore northeast wind. Fu et al. (2010) studied variations of temperature and salinity in seawater under sea ice using hydrologic data collected from polynyas south of the St. Lawrence Island during March of 2008 and 2009. The results indicated that the high-salinity water found during the cruises of 2008 and 2009 was due to the formation of polynyas. The salinity observed in 2008 was higher than that in 2009 as a result of higher salt production in 2008. The spatial distributions of high-salinity cores differed between the

two cruises. In March 2008, a southeastward flow was formed under the persistent northerly wind in the observation region, which transported the high-salinity water produced by the polynyas to the southeast. The similar flow, however, did not exist in March 2009 because the northerly wind over the study area was interrupted by a southerly wind. Accordingly, the polynyas and the high-salinity water produced by them existed for a short time. As a result, the high-salinity water in 2009 did not spread very far, and stayed within the polynyas. In addition, during the 2009 cruise, two stages of observations in the polynyas showed the core of high-salinity water was shifted to the southwest of the St. Lawrence Island. This result suggested that a southwestward flow might have existed in the area at the onset of the northerly wind, which was consistent with the alongshore and/or offshore flows caused by the northerly wind.

5 Structure of a Subsurface Eddy

An Arctic Ocean eddy in subsurface layer was analyzed by Shi et al. (2007) with temperature, salinity and current profile data obtained at an ice camp in the Canada Basin during the second Chinese Arctic Expedition in summer of 2003. In the vertical temperature section, the eddy showed itself as an isolated cold water block at the depth of 60 m with a minimum temperature of 1.5^{o}C that is -0.5^{o}C colder than the ambient water. Isopycnals in the eddy formed a pattern of convex, which indicated the eddy is anticyclonic. Although maximum velocity near 0.4 ms^{-1} occurred in the current records observed synchronously, the current pattern is far away from a typical eddy. By further analysis, inertial frequency oscillations with amplitudes comparable with the eddy velocity were found in the subsurface layer currents (fig 2). After removing the inertial current and mean current, an axial symmetric current pattern of an eddy with maximum velocity radius of 5 km is obtained. The analysis of the T-S characteristics of the eddy core water and its ambient waters supported the conclusion that the eddy was formed on the Chukchi Shelf and migrated northeastward into the northern Canada Basin.

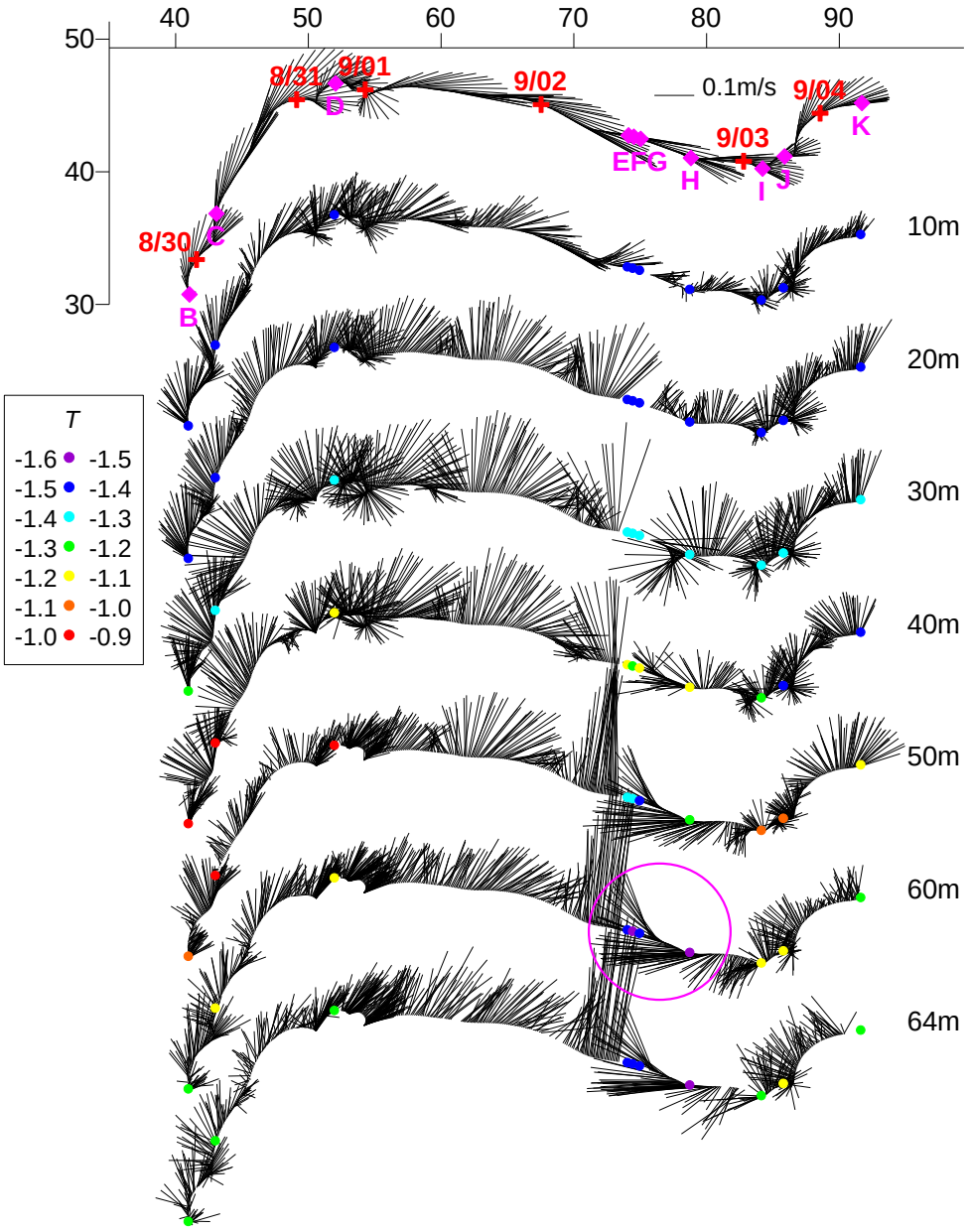

Fig 2 Vectors of ice camp drift velocity (top) and absolute current velocity at 7 depths plotted along ice camp drift track

6 Observation Technology of the Physical Oceanography

During the Second and the third Chinese National Arctic Research Expedition in 2003 and 2008, mooring systems were deployed in the Bering Strait and the Chuckchi Sea. The technical designment and deployment process related with mooring system in polar region were discussed (Jiao et al., 2007). Selection of observing stations and layers, design of mooring system and the steps of deployment were presented in their studies, which gave the references to deploy anchored system in the low temperature and ice covered ocean.

A newly-developed profiler with an automatic winch was applied for deploying CTD down to 1000 m from an ice hole on the ice covered ocean (Jiao et al., 2010). The profiler was mounted on the ice

camp and observed more than 100 profilers in 2008.. It is a useful tool together with a ADCP for capturing subsurface eddies on a drifting pack ice.

Ⅲ Ocean optics in Arctic

Beside CTD and LADCP profiling, the ocean optics and the sea ice optics were one of the main observations in the third Chinese National Arctic Research Expedition in 2008. It was the first time that the ocean optics was taken into action and 80 optical ptofiles were acquired. In addition, there were a series of other cruise for the sea ice optics observation in the Bering Sea, Beaufort Sea, and Canadian Basin by the cooperation with Canadian and American scientists in 2007, 2008, and 2009. These efforts not only greatly expand the physical oceanographic observations and research areas, and gained valuable knowledge and innovative

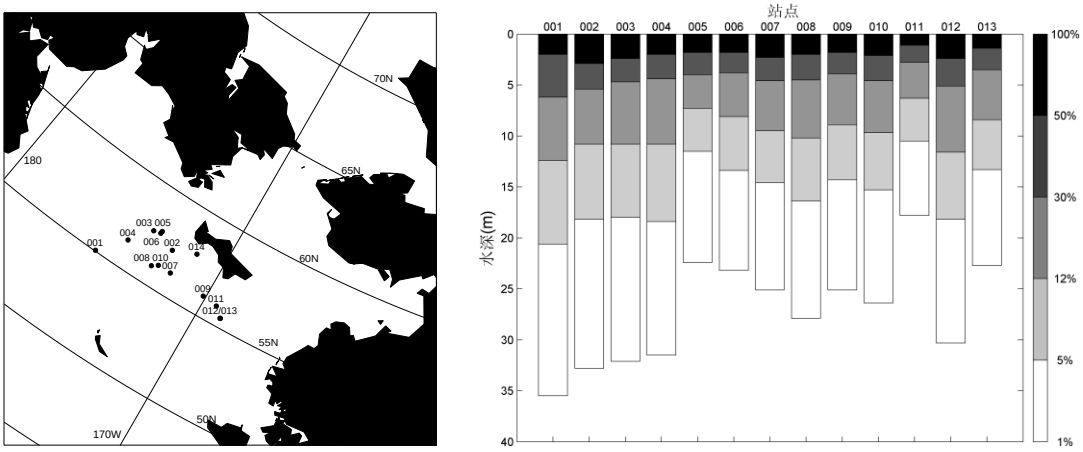

Fig 3 PAR attenuation depth.
Left one is the 13 stations in Bering Sea in 2008; the right one shows the depth of the PAR attenuation to 50%, 30%, 12%, 5%, 1%.

The downwelling irradiance at the sea surface and some factors are simultaneously measured during the marine optical observation with much higher sampling rate of 0.2s, which is benefit to study the high frequency variation in the irradiance record (Zhao et al., 2010b). The data obtained in Bering Sea of 2007 spring was used to analyze main factors causing the high frequency variation of the irradiance. The influences of cloud, fog, and sea wave on the irradiance were distinguishable. The variations of irradiance by the cloud are usually with lower frequency and higher amplitude, whereas those caused by fog express complex variation with higher amplitude and varying periods from several to a hundred seconds. The complexity was useful to distinguish fog influence from that of cloud. Under the clear sky condition, the steady incident solar radiation was reflected at the sea surface, modulated by the wave oscillation and then scattered from the particles in the air to the collector of the instrument. So the sea wave signal appeared in the irradiance record with short period and low amplitude, clearly different from the influence of cloud and fog. In their study, the influence of cloud, fog, and wave on irradiance was analyzed and calculated, which was valuable for understanding the irradiance and the corresponding variation in the under water record.

Photosynthetically Available Radiation (PAR) is an important bio-optical parameter related to marine primary production. PAR is usually measured by a broadband sensor and can also be calculated

by multispectral data. When the PAR is calculated by multispectral data in polar region, four factors are possible error sources. PAR could be overestimated as the wavelengths of multispectral instrument are usually chosen to evade main absorption zones of atmosphere. However, both PARs calculated by hyperspectral and multispectral data are consistent with the error less than 1%. By the fitting function proposed, Zhao et al. (2010c) calculated the PAR by multispectral data has the same accuracy with that by hyperspectral data. To calculate the attenuation rate of the PAR under the surface needs PAR0. Here, an approach is proposed to calculate PAR0 by the best fit of the irradiance profile of 1-5 m with a content attenuation coefficient under surface. It is demonstrated by theory and data observed in different time at same location that the attenuation coefficient of PAR is independent of the intensity of radiation. But under sea ice, the attenuation coefficient of PAR is little bit different, as the spectrum of the light has been changed by selective absorption through the sea ice. Therefore, the difference of inclusions inside sea ice will result in different PAR, and impact the attenuation of PAR. By the results of this study, PAR can be calculated reliably by multispectral data.

Ⅳ Sea Ice Optics

Sea ice is an important component of the climate system. But also because of its sensitivity to climate change, the sea ice is known as an indictor of climate change. In the past decade, Arctic sea ice extent and thickness have shown rapid decreasing trend. In summer 2007, the coverage of the Arctic sea ice has reached its lowest level since satellite data record. There are more complex research proposition in the air-sea-ice coupled process with the rapid reduction of the Arctic sea ice. Sea ice needs to absorb enough energy to be melted. The short-wave solar radiation is the main source of the energy. So the sea ice optics is the core to study the sea ice and the solar radiation. From 2006, a number of observations and studies for the sea ice optics were carried out by the scientists of Ocean University of China. A lot of data of the sea ice optics in the Arctic Ocean have been obtained from more than 10 cruises optical inspection.

1 Light Lateral Scattering in the sea ice

A winter optical experiment by an artificial lamp was conducted in the Amundsen Bay of Arctic ocean from November of 2007 to January of 2008. The radiation field emitted from an artificial lamp was measured and was introduced, and the optimized experiment project was discussed by Zhao et al. (2008). It was demonstrated that the minimum size allowed of the lamp is determined by both the field of view (FOV) of optical instrument and the measuring distance from the lamp. Some problems that might influence on the experiment results often occurred for a simple lamp, such as instability, spatial non-uniformity, light divergence, effect of lamp temperature, etc. The experiment indicated that the reliable results can be obtained only when the optical measurement is coordinated with the radiation field of artificial lamp. The measured radiation property of the lamp was used to advise the field experiment to minimize mearuring error.

As the experiment by artificial lamp was the first attempt in the Arctic Ocean, the experience given by this study is a valuable reference to the correlative studies. A measurement method was proposed and applied whereby a recording instrument was buried in the sea ice and an artificial lamp was moved across the instrument (Zhao et al., 2010d). With the exception of blue and red lights, the attenuation coefficient changed little with wavelength, but changed considerably with depth. The vertical decrease of the attenuation coefficient was found to be correlated with salinity: the greater the salinity, the greater the attenuation coefficient. A clear linear relation of salinity and the lateral attenuation

coefficient with $R^2 = 0.939$ exists to address the close correlation of the attenuation of LPL with the scattering from the brine.

2 Solar Radiation Absorbed by the Sea Ice

Based on the optical data for transmission radiation through sea ice in the winter Arctic of 2007, the transmission of solar radiation under the condition with very low solar altitude was studied (Zhao et al., 2010e). The basic feature of the solar radiation was that the light with shorter wavelength was significantly reduced to form a two peek spectral structure. The reflection was lower than that in summertime because of the thin thicknesses of ice and snow, allowing more ratio of heat to enter the sea ice. The reflection of the ice with longer wavelength decreased and more light with longer wavelength entered sea ice. However, the light with wavelength of 490 nm was again dominant, which meant the light with longer wavelength was mostly absorbed by sea ice. Although the light penetrating sea ice was quite weak, the sea ice obtained more heat by the absorption of sea ice for longer wavelength light, which would postpone the freezing of the sea ice.

The solar energy absorbed by the packed ice in the central Arctic was studied by Zhao et al. (2009) based on the optical observations of the Third Chinese Arctic Expedition on an ice camp during the period of August 21-27, 2008 (fig 4). The transmission, albedo, and the absorption rates of the sea ice and their variation with ice thickness were calculated from the observed data. On average, the absorption rate of sea ice for shortwave solar radiation was about 16%, meanwhile, about 77% of the incident energy was reflected back to the space. A three-day optical observation was conducted to determine the amount of the arriving solar radiation. Although the solar radiation arriving on the upper atmosphere was still strong in August, but about 57% of them was reduced by the atmosphere, as the coverage of cloud and fog caused obvious absorption to the shortwave radiation. Therefore, the heat flux absorbed by sea ice was only 10.2 W m^{-2}, corresponding to the heat in melting 2.6 mm ice per day or 1m ice within 380 days. It means that the weak heat flux did not provide sufficient heat to melt the sea ice there. Therefore, the packed ice still covered the central Arctic Ocean even though the ice coverage becomes nearly the minimum in the whole Arctic. However, the result also indicated that some other factors, if appeared, could cause the increased melting of the packed ice, such as the decrease of cloud and fog, the total melting of snow layer, the reduction of ice thickness, and the increase of the ponds which could especially endanger the permanent packed ice. In the future, it is possible for the sea ice in central Arctic to collapse if more heat is absorbed under the condition different to that of the summer of 2008.

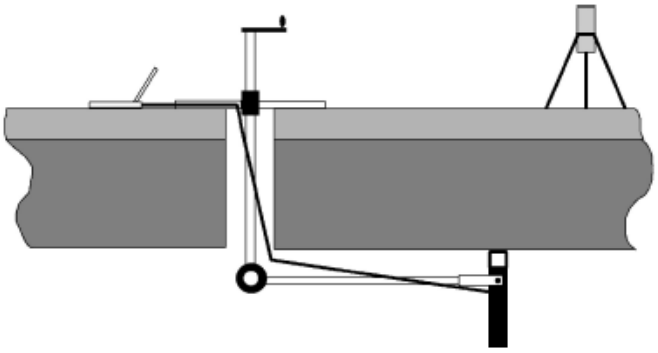

Fig 4 Sketch for sea ice observation system

3 Optical Properties of Snow on the Sea Ice

From November 2007 to February 2008, a series of optical measurements of light transmission in the snow on the ice were carried out in the Amundsen Gulf of the North Polar Region. By the

experiments, Li et al. (2010) have studied the optical extinction properties of artificial light between 313-875 nm in the snow of the polar night. The results validated that the radiant intensity was attenuated by exponential form with snow thickness increasing, and the snow attenuation was greater than that of ice. On the basis of the observation results with different snow thickness, the optical extinction coefficients in the snow can be calculated. The results showed that the spectral extinction coefficients with in 465-625 nm were minima, and were almost constant with the meaning value $20m^{-1}$. When the light wavelength is out of this range, the extinction coefficients increase abruptly, and even exceed 30 m^{-1}. According to the observation results, we have an analysis that the effect of snow density on the optical extinction properties in the snow is different with the variation of light wavelength. With the longer wavelength, the effect of snow density is greater.

Ⅴ Kinematics of the Sea Ice

The sea ice is an important factor of the climate in the northern hemisphere. In recent years, the sea ice extent and the sea ice thickness keep decreasing continuously. These changes are from gentle to intense. The variation of Arctic sea ice depends not only on the internal process of the Arctic, but also on the ocean process of the sub-polar regions, such as the warm water from the Pacific and the Atlantic Ocean. The runoff is also an important factor influencing the Arctic sea ice. Now, the studies on the Arctic sea ice are mainly the morphological of the sea ice by the numerical model and the temporal variation of the sea ice in different regions.

1 Vertical Melting Process of the Sea Ice

By the description of the thermodynamic and kinetic parameters of the sea ice, the mathematical representation of sea ice behavior can be provided by the climate forecasting models. At the same time the physical basis and the parameters of the program to simulate the Arctic sea ice also base on these parameters. Kinetic parameters of the sea ice can be divided into the sea ice concentration, the sea ice thickness, the ice surface roughness and the ice motion (Li et al., 2007). Based on the investigated data of sea ice physical processes during the Second Chinese National Arctic Research Expedition in the summer of 2003, the sea ice dynamical characteristics were analyzed and the parameters expressing these characteristics were given. While the floe moved toward Northeast, the rotation angle increases step by step with the maximum of 37.8^{o}, and while the floe moved toward Southeast, its rotation angle decreased step by step. The oscillation period of the floe was 12.45h consistent with that of the inertia current at the same latitude, which showed the contribution of the inertia current to the ice floe movement. The feedback mechanism of the snow/ice-albedo is the intensity contrast of the solar radiation reflection, absorption and transmission by the open water and the snow/ice which is an important reason to enlarge the polar warming. The Arctic sea ice plays an important role in the feedback mechanism. Currently, a diversity of sea ice albedo parameterizations are used in climate system models and standalone sea ice models, ranging from simple to complex. Yang et al. (2010) reviewed previous studies on the evaluations of the snow/ice albedo parameterizations, and discussed some problems of the satellite-derived surface albedo for the ice covered ocean. They put forward some on going issues related to further developments of the albedo parameterizations as climate warms, including melt ponds and leads. The thermodynamics mechanism of the system involving a floe and a small lead in the Arctic Ocean has been observed during the ice-camp period in the third Chinese Arctic Research Expedition from 20 to 28 August, 2008 (Lei et al., 2010). The field measurements include surface air temperature above the floe, albedo of the lead, seawater temperature in the lead and under

the floe, the lateral and bottom mass balance of the floe. The results showed that the surface of the lead was frozen-up by 23 August. From then onward, the albedo of the thin ice-covered lead in band of 320-950 nm was 0.46, the vertical seawater-temperature gradient in the lead, as well as the seawater temperatures both in the lead and under the floe decreased gradually, while the oceanic heat under the ice was being at a low level.

2 Variation of the Sea Ice Cover

The sea ice has obvious seasonal variation (Wei et al., 2007; Li et al., 2007) and lag response properties (Zhang et al., 2009). The seasonal variation of the sea ice in Arctic can be simply distributed as melting in spring and freezing in autumn, which also can be divided into dense ice phase, the slope of cracking phase, the westward melting phase, the full melting phase and the freezing phase by the sea ice concentration and the extent. The dates of these phases beginning are different in different regions and different years, the minima and the corresponding dates of the sea ice extent are also different. Though the Arctic sea ice decreasing continuously for recent years, there are annual variations of the sea ice in different regions. Zhu et al. (2007) indicated that the sea ice extent in Chukchi Sea had a variation progress from light (1997) - heavy (2000-2001) - light (2002-2005). The duration of ice melting correlated well with the ice condition. In the light ice year, the melting begins earlier and freezes-up later. The minimum sea ice cover appear in the late September to early October each year, whose areas are quite different, 4 % in the light ice years and more than 50 % in the heavy ice years. But the satellite remote sensing data that there were heavy conditions of sea ice in the East Siberian Sea in 1997-2001 while there were light conditions of sea ice in this region in 2002-2005 (Li et al., 2009). With the methods of moving-t abrupt test and wavelet analysis, abrupt changes of the ice extent (1953—2004) in Bering Sea and Chukchi Sea were found separately in the late of 1970s. The results showed that there were an abrupt change of the mean value in Bering Sea and a frequency shift in Chukchi Sea (Hu et al., 2007). There are many factors influence the variation of the Arctic sea ice, such as the air temperature, the air pressure, wind and other changes. The anomalies of the large-scale circulation, the heat carried by the Pacific inflow and the increasing of the long-wave radiation by the greenhouse gases may cause the variation of the sea ice too (Hu et al., 2007; Zhu et al., 2007; Zhou et al., 2007; Li Et al., 2009; Zhang et al., 2009). The variation of the global climate is deeply respond to the Arctic sea ice (Fan, 2007; Wu et al., 2009)

3 Distribution and Variation of the Sea ice in the Northwest Passage

"Northwest Passage" refers to the passage from the Atlantic to the Pacific which begins from the Canada's Baffin Island, north of the northeastern sea area as a starting point, from east to west, through a series of deep Strait in the Canadian Arctic Archipelago (CAA, Canadian Arctic Archipelago) to the Beaufort Sea north of Alaska, finally into the Pacific Ocean by the Bering Strait. In recent years, rapid warming of Arctic has made the Northwest Passage navigation possible. Su et al. (2010) studied the characters of variation of sea ice concentration around the Northwest Passage using AMSR-E sea ice concentration product with the resolution of 6.25 kilometers from 2002 to 2008. By analyzing melting period, ice-free period, slight-ice period, ice-free days, slight-ice days, as well as some details of the variation and distribution of sea ice in main ice choke points along the passages, the results gave a deeper understanding of the main features of sea ice seasonal and inter-annual variation and distribution, especially the information related to the navigation possibility of Northwest Passage. Their research showed that the south route was easier to navigate than the north route. Sea ice often began to

melt near the place where polynya and Circumpolar Flaw Lead occurred. For each route, the period of ice choke pointed existing represented a decreasing trend, while ice-free and slight-ice days showed an increasing trend. The spatial distribution of sea ice in the research region and its mechanism were discussed and an index which named ice-free or slight-ice days along the whole route was set to estimate navigation extent.

Ⅵ Arctic impact on global climate change

Arctic Oscillation (AO) is defined by the first mode of Empirical Orthogonal Function (EOF) of the sea level pressure (SLP) north of 20 ºN, and the time coefficient of EOF-1 is defined as the Arctic Oscillation Index (AOI). It has been used as a representative atmospheric circulation index to express climate change in North Hemisphere (NH). Compared with the pattern of the annular circulation mode of the lower stratosphere in the Southern Hemisphere, which has been extensively documented, AO is in essence the annular mode of the lower stratosphere in NH. The Arctic region is experiencing obvious climatological warming at a rate which is nearly twice of the global average during the past decades. Most climatological indicators show a linear trend. The notable ones include the decline of the perennial ice coverage at a rate of 9% per decade, and the thinning of the ice draft for more than a meter from two to four decades ago to the 1990s. However, AO behaves differently from such regularities. In AO, instead, a seesaw-like oscillation is dominant.

1 Core Region of the Arctic Oscillation

As we know that Arctic Oscillation (AO) is a seesaw pattern in which sea level pressure (SLP) at the polar and middle latitudes in North Hemisphere fluctuates between positive and negative phases. It has been used as a representative atmospheric circulation index to express climate change. Arctic region is experiencing significant climate warming, with many climate change factors are reflected

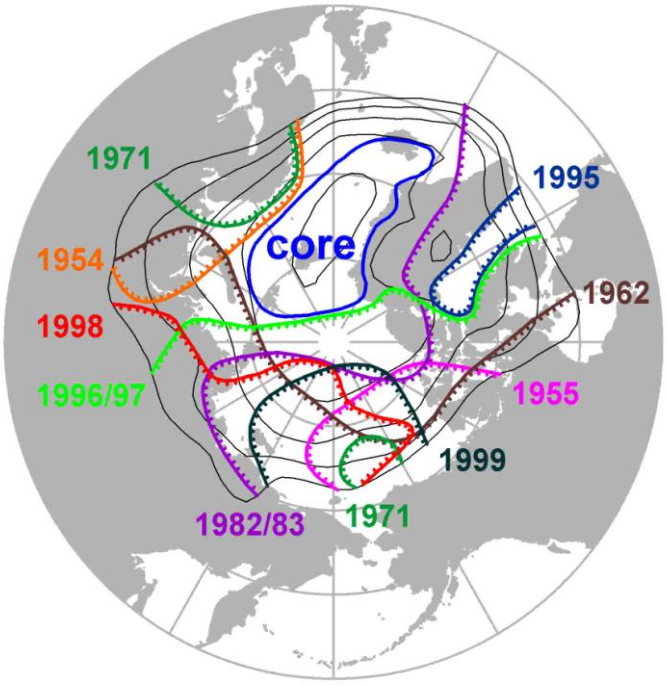

Fig 5 Impacted of events on Arctic in 1950–2002.
Marked with 'Core' is called as Arctic Oscillation Core Region. Several strong processes influenced the area outside of AOCR.

linear trends, most notably the reduction of sea ice extent and sea ice thickness decreases. But only the change of AO is different, it remains to seesaw as the main type of change. By calculating the correlation coefficients of AO Index with all the gridded SLPs, Zhao et al. (2006) revealed a special region named as Arctic Oscillation Core Region (AOCR), where the running correlation coefficients (RCC) between averaged SLP in AOCR and AO index are all negative. The averaged SLP of this region correlates significantly with the AO index, with the correlation coefficient -0.97. The correlations between SLPs and AO index outside of AOCR are weaker than those inside. RCC analysis reveals several strong discrepant events different from AO (fig 5). These events occurred in the years of 1954, 1955, 1962, 1971, 1982/83, 1995, 1996/97, 1998, and 1999. A comparison of these events and the ENSO or PDO indices suggests that the events in 1982/83 and 1998 are probably associated with the ENSO processes. Events centered in other years are likely connected with PDO, which reached their minima in the years of 1950, 1955, 1962 and 1971. The result in this study provides an alternative insight to look at the mechanism of the variation of Arctic Oscillation.

2 Spatial Variation of the Arctic Oscillation

The Arctic Oscillation (AO) is spatially varied, but lack of study. Zhao et al. (2010f) defined the spatial variation of AO as the temporal variation of the ensemble of grids with SLP varying consistent with the AO index in certain time span. The region of the ensemble is called as 'AO-dominant region',

identified by the running correlation coefficient (RCC) of gridded SLP with the AO index. The positive and negative AO-dominant regions show that the SLP oscillated sometimes between the polar and mid-latitude regions and sometimes between land and ocean. Along the Atlantic-Pacific Section, the North Atlantic Oscillation exists as a stationary seesaw-like dipole, while on the Pacific side the oscillation is intermittent with lower intensity and swinging boundary. The long-term spatial variation of the AO with three stages is clearly identified by the relative area of the SLP anomaly regions. Positive SLP anomaly area dominated before 1970, showing the state before the global warming. Negative SLP anomaly area dominated during 1971-1995, indicating the effect of global warming before the Arctic warming being apparent. Since 1996 both positive and negative SLP anomaly areas are all small, being possibly caused by the sea-ice retreat during the Arctic warming.

Ⅶ Conclusion

In the last four years, the studies of the Arctic physical oceanography of China were closely linked with the 4th International Polar Year, and focused on the rapid changes of the Arctic sea ice and the variation of the ocean and the climate corresponding to the sea ice change. Faced to the scientific issues, we participated a mount of filed expeditions to study the variation processes of sea ice, ocean and atmosphere. The studies of the physical oceanography were focused on the variation of the upper ocean, the ocean optics, the sea ice optics, the variation of the structure of the sea ice and the coupled variation of air-sea-ice, which discovered the variation of the climate in response to the variation of the Arctic. At the same time, the observation technology, the automatic continuous profiler technology, the satellite remote sensing technology, and the numerical model are developing in China. The abilities of the data acquirement and the numerical forecast are enhanced by these technologies.

Chinese scientists have made considerable progress in Arctic physical oceanography. By the international cooperation the studies on the Arctic are put into the international Arctic science community and play an important role in promoting the global Arctic research. After the International Polar Year, China will set up polar research project which will enhance the research on the Arctic and promote the development of Arctic science.

Reference

Cao Yong , Jie Su , Jinping Zhao , Shujiang Li , Dong Xu, 2010，The Study on Near Surface Temperature Maximum in the Canada Basin for 2003-2008 in Response to Sea Ice Variations，Proceedings of the Twentieth (2010) International Offshore and Polar Engineering Conference，Beijing, China, 1238-1242

Chen Zhihua, Zhao Jinping, 2010, The thermodynamics of Subsurface Warm Water in the Arctic Ocean, Oceanologia et Limnologia Sinica, 41(2), 167-174.

Fan Ke, 2007, The Sea Ice in the North Pacific Ocean, a Northwest Pacific Typhoon Frequency Predictor? Science in China Series D, 37(6), 851-856.

Fu Hongli, Zhao Jinping, 2009, A Modeling of Bering Sea Polynyas and Analysis of Key Factors Impacting Simulation Accuracy, Advances in Earth Science, 24(5), 538-547.

Fu Hongli, Jinping Zhao, Jiuxin Shi, Yutian Jiao, 2010, Formation and transportation of high-salinity water produced by polynyas south of the St. Lawrence Island. J. Ocean University of China, DOI 10.1007/s11802-010-1734-9, 9(4): 317-326.

Hu Xianmin, Su Jie, Zhao Jinping, 2007, Variation Characteristics of the Sea Ice Extent in Bering-Chukchi Seas, Journal of Glaciology and Geocryology, 29(1), 53-60.

Jiao Yutian, Zhao Jinping, Shi Jiuxin, Wu Wei, Zhang Hongxin, 2007, The Design and Deployment of Mooring System in Polar Region, Chinese Journal of Polar Research, 19(4), 305-313.

Jiao Yutian, Shi Jiuxin, Zhao Jinping, Zhang Xueming, Hou Jiaqiang, 2010, Auto CTD Profiling Observation System and Application in the Ice-Covered Ocean, Ocean Technology, 29(4), 31-33.

Lei Ruibo, Li Zhijun, Cheng Bin, Ynag Qinghua, Li Na, 2010, Observation on the Thermodynamics Mechanism of the Floe-lead System in the Arctic Ocean During Summer, Chinese Journal of Polar Research, 22(3), 286-295.

Li Shujiang, Zhao Jinping, Li Xiang, Li Tao, 2010, The Optical Properties of Snow on the Ice in the North Polar Region, Periodical of Ocean University of China, 40(7),9-14.

Li Tao, Zhao Jinping, Zhu Dayong, 2007, Seasonal Variations of Sea Ice Cover in the East Siberian Sea and its Main Driving Factors, Chinese Journal of Polar Research,19(2), 87-98.

Li Tao, Zhao Jinping, Zhu Dayong, 2009, Variations of Sea Ice Cover in East Siberian Sea of Arctic Ocean in 1997-2005, Journal of Glaciology and Geocryology, 31(5), 822-828.

Li Xiang, Zhao Jinping, Li Tao, Li Shujiang, 2010, A Study of Water Properties and Convection under Sea Ice in Winter Amundsen Gulf, Chinese Journal of Polar Research,22(4), 404-414.

Li Zhijun, Zhang Zhanhai, Lu Peng, Dong Xilu, Cheng Bin, Chen She, 2007, Some Parameters on Arctic Sea Ice Dynamics from the Expedition in Summer of 2003, Advances in Water Science, 18(2), 193-197.

Shi Jiuxin，Zhao Jinping, Jiao Yutian and Cao Yong，2007, An Arctic Ocean eddy in inertial currents in sub-surface layer，Chinese Journal of Polar Science， 18(2)： 135-146.

Su Jie, Yang Bo, Ji Shunying, and Du Ling, 2010a. Thin ice thickness measured by upward-looking sonar in a marginal sea. In Proceedings of the Twentieth (2010) International Offshore and Polar Engineering Conference, Beijing, China, 1141-1147.

Su Jie, Zha Jinping, Xu Dong, Li Xiang, 2010b, Features of Northwest Passage Sea Ice's Distribution and Variation under Arctic Rapid Warming Condition, Chinese Journal of Polar Research, 22(2),104-124.

Wei Lixin, Zhang Zhanhai, 2007, Analysis of Arctic Sea Ice Variation, Marine Forecasts, 24(4), 42-48.

Wu Bingyi, Zhang Renhe, 2009, Study on the Variation of Precipitation of China and the Arctic Sea Ice in Summer, China Meteorological Society 26th Annual Meeting of Cryosphere and Polar Meteorology Session Proceedings.

Yang Qinghua, Zhang Zhanhai, Liu Jiping, Wu Huiding, Zhang Lin, 2010, Review of Sea Ice Albedo Parameterizations, Advances in Earth Science, 25(1), 14-21

Zhao J., Y. Cao, and J. Shi, 2006, Core region of Arctic Oscillation and the main atmospheric events impact on the Arctic, Geophys. Res. Lett., 33, L22708, doi: 10.1029/2006GL027590.

Zhao Jinping, Shi Jiuxin, Gao Guoping, Jiao Yutian, Zhang Hongxin, 2006. Water mass of the northward throughflow in the Bering Strait in the summer of 2003, Acta Oceanologica Sinica, 25(2), P25-32.

Zhao Jinping, David Barber, Tao Li, Shujiang Li, and Xiang Li, 2008. Radiation of lamp and optimized experiment using artificial light in the Arctic Ocean, Chinese Journal of Polar Science， 19(2): 249-260.

Zhao Jinping, Li Tao, Zhang Shugang, Jiao Yutian, 2009, The Shortwave Solar Radiation Energy Absorbed by Packed Sea Ice in the Central Arctic, Advances in Earth Science, 24(1), 35-41.

Zhao Jinping, Shi Jiuxin, Jin Mingming, Li Chaolun, Jiao Yutian, Lu Yong, 2010a, Water Mass Structure of the Chukchi Sea During Ice Melting Period in the Summer of 1999, Advances in Earth Science, 25(2), 154-162

Zhao Jinping, Wang Weibo, Jiao Yutian, 2010b, Analysis for the High-Frequency Variation of the Downwelling Irradiance Caused by Different Atmosphere and Sea Surface Condition, Periodical of Ocean University of China, 40(4), 1-8.

Zhao Jinping, Wang Weibo, Cooper, Lee, 2010c, Calculation of photosynthetically available radiation using multispectral data in the Arctic. Chinese Journal of Polar Science, 21(2):113-126.

Zhao Jinping, Tao Li, David Barber, Jingping Ren, Monika Pucko, Shujiang Li, and Xiang Li，2010d. Attenuation of artificial lateral propagating light in winter Arctic sea ice, Cold Regions Science and Technology, 61: 6–12

Zhao Jinping , Li Tao, 2010e, Solar radiation penetrating through sea ice under very low solar altitude, Journal of Ocean

University of China (Oceanic and Coastal Sea Research), DOI 10.1007/s11802-010-0116-7, 116-122.

Zhao Jinping, Cao Yong and Shi, Jiuxin, 2010f, Spatial Variation of the Arctic Oscillation and its Long-Term Change, TELLUS, July DOI: 1 0.1111/j.1600- 0870.2010.00472, 62A, 661-672.

Zhang Lu, Zhang Zhanhai, Li Qun, Wu Huiding, 2009, Status of the Recent Declining of Arctic Sea Ice Studies, Chinese Journal of Polar Research, 21(4), 344-352.

Zhang Ying, Zhao Jinping, Shi Jiuxin, 2007, The Estimation of Vertical Turbulent Diffusivity in the Surface Layer in the Canada Basin, Periodical of Ocean University of China, 37(5), 695-703.

Zhou Botao, Wang Huijun, 2007, The Relationship between the Variation of Hadley Circulation and the Sea Ice in the Bering Sea, Chinese Science Bulletin, 52(18), 2194-2198.

Zhu Dayong, Zhao Jinping, Shi Jiuxin, 2007, Study on the Multi-year Variations of the Sea Ice Cover of Chukchi Sea in Arctic Ocean, Acta Oceanologica Sinica, 29(2), 1-9.

PROGRESS OF CHEMISTRY RESEARCH IN THE COASTAL WATERS, CHINA (2007-2010)

Yong ZHANG and Dongyan LIU

(Yantai Institute of Coastal Zone Research, Chinese Academy of Science, 264003, P.R. China)

Abstract The research progress of chemistry research in coastal waters that achieved by Chinese scientists from the middle of 2006 to 2010 is reviewed. This overview focused mainly on the biogeochemical process of marine carbon cycling, dynamical process of nutrients, persistent organic pollutants (POPs) and heavy metals in coastal waters. Related research area covered two major estuaries (Yangtze River and the Pear River), some small rivers and almost the whole China coastal waters including the South China Sea (SCS), the East China Sea (ECS) and the Yellow Sea (YS).

Keywords Chemical oceanography, marine carbon cycling, nutrient dynamics, persistent organic pollutants, heavy metals

Ⅰ Biogeochemical process in marine carbon cycling

1. Sea-air exchange of CO_2 and its controls

Sea-air exchange of CO_2 is an important component of the global carbon cycle and accurate estimation of the sea-air CO_2 fluxes is essential for the study of climate change. Over the last five years, most of studies were carried out in the largest estuaries of China (e.g., Yangtz River and Pearl River) and margin seas.

The inner Yangtze River Estuary, as indicated by (Zhai et al., 2007), is generally a significant source for atmospheric CO_2. Surface partial pressure of carbon dioxide (pCO_2), based on shipboard underway measurement, which ranged from 650-1440 □ atm in the upper reach of the estuary and 200-1000 □ atm in the estuarine mixing zone. The inner estuarine CO_2 degassing fluxes ranged mostly from 0-100 □ $molm^{-2}day^{-1}$, which were lower than some European inner estuaries (100-760 □ $molm^{-2}day^{-1}$ (Frankignoulle et al., 1998). The total CO_2 degassing flux in the inner estuary of the Yangtze River ranged 2.5-5.5×10^{10} mol yr^{-1}. The outer Yangtze Estuary served as a moderate or significant sink of atmospheric CO_2 in winter, spring and summer, while it turned to a net source in autumn. Surface pCO_2 ranged 320-380 □ atm in winter, 180-450 □ atm in spring, 150-620 □ atm in summer and 120-540 □ atm in autumn. The intergraded sea-air flux in the outer Yangtze Estuary was estimated as -1.9±1.3 mol m^{-2} yr^{-1}, which is double the sea-air flux estimation for the northern ECS (Zhai and Dai, 2009; Shim et al., 2007). In contrast, pCO_2 level in the Pearl River estuary is higher in warm and wet seasons than in cold and dry seasons. As a consequence, CO_2 emission from the Pearl River Estuary system in summer was ~ 6 times of that in winter. The annual CO_2 emission was estimated to be ~3×10^{10} molC, which is equivalent to ~6% of the total DIC export flux to the SCS from the Pearl river system (Guo et al., 2009).

Based on four field investigation (March 2005, April 2006, May 2005 and July 2001) in the southern Yellow Sea, (Zhang et al., 2010) indicated that the near shore area generally was a source of atmospheric CO_2, whereas the offshore area shifted from a source in winter to a sink in spring. The author also indicated that in the shallow nearshore area, the vertical mixing all year round caused the oversaturation of pCO_2, which was also affected by the terrestrial inputs and the upwelling of bottom water along the shelf in July. In the offshore area, the major process influencing pCO_2 varied seasonally. In winter, surface waters mixed well with the CO_2-enriched bottom waters so that surface CO_2 was oversaturated. During spring, phytoplankton bloom occurred leading to a sink of atmospheric CO_2. During summer, the CO_2 sink was located in the Yangtze dilute water plume, beyond which pCO_2 was oversaturated owing to the limitation of nutrient for phytoplankton.

The SCS is one of the world's largest marginal seas. Field observations suggest that the SCS is a source of atmospheric CO_2 (Zhai et al., 2005). Significant diurnal change of surface pCO_2 as 1.0-1.6 Pa in the offshore and oligotrophic sites of SCS was discovered (Dai et al., 2009). Zhu et al. (2009) presented an empirical approach for the estimation of the pCO_2 and sea-air CO_2 fluxes in the northern SCS using satellite-derived sea surface temperatures, chlorophyll-a concentrations, and wind fields. The estimated spatial mean flux was 7.65 □ mol CO_2 $m^{-2}day^{-1}$ from sea to air in July 2000, quite similar to the field–measured flux (7.50 □ mol CO_2 $m^{-2}day^{-1}$; Zhai et al., 2005). The well-matched results suggest a potential usage of remote-sensing technique in the estimation of sea-air CO_2 fluxes. Compared to field measurement, remote-sensing technique can realize broad spatial and temporal coverage.

The mechanism that modulates pCO_2 variability and sea-air CO_2 fluxes was also studied. Temperature was found to be a primary controlling factor in the oligotrophic SCS (Zhai et al., 2005; Dai et al., 2009). Biological metabolism may exceed the temperature effect in the south YS and coastal zone of northern SCS, and also in the coral reef system. Additionally, physical processes (such as vertical mixing and tidal effects) are important in nearshore (Dai et al., 2008; Dai et al., 2009; Zhang et al., 2010).

The underway measurement of pCO_2 has already been carried out in the SCS, the ECS, and the YS in different seasons. Preliminary results showed that the southern SCS is a weak source of atmospheric CO_2 year round. The northern SCS is a weak source in summer and autumn, however a sink in winter and spring. The northern ECS is a source in autumn while sink in other seasons (Prof. Minhan Dai's unpublished data).

2．Biogeochemical behavior of DOC and POC

Terrestrial organic carbon transported by river runoff represents an important carbon source to the coastal waters. In the upper reach of the Pearl River Estuary, DOC comes mainly from sewage inputs and is rapidly removed by microbial degradation, resulting in a non-conservative behavior with salinity. In the mixing zone, microbial degradation removes ～31% of total DOC. In the lower estuary, the heterotrophic removal almost balanced by the autotrophic production, leading to a linear distribution of DOC with salinity. Organic composition changes rapidly along the estuary, showing a selected removal of carbohydrates and amino acids within the DOC pool in the upper reach and mixing zone, and an autotrophic source of polysaccharides in the lower estuary (He et al., 2010).

Continental margins play a significant role in global carbon cycling. They contribute ~28% of global ocean primary production despite their relative limited surface area. This leads to a fundamental basis for continental margins to be potential carbon sinks, although the pattern and magnitude still need to be better constrained (Cai et al., 2006). In the NSCS, DOC ranges from 70-85 □ M in the mixed layer of

offshore area, while POC ranges from 1.6 to 4.0 □ M. Distributions of DOC and POC are uniform in deep and bottom layers of the deep basin areas, (43±3 □ M) and POC (1.1±0.2 □ M) respectively. Both DOC and POC are generally higher in shelf zones than in deep basins and also higher in summer than in other seasons particularly for coastal zones. Terrestrial inputs and mixing processes may primarily control the horizontal and vertical distributions of DOC and POC in the NSCS, as both correlate significantly with water density and temperature but less significant with salinity. Biological effect on DOC and POC distributions also may be significant in the central basin, as both are correlated well with chlorophyll a. The degradation rate of DOC in the mixed layer is generally higher in the Zhujiang plume than in the deep basin. The labile and semi-labile fractions of DOC account for roughly 42-50% of total DOC in the mixed layer. The increase of C/N or C/P ratio with depth in deep-basin waters implies a preferential decay of phosphorus (nitrogen) over carbon (Hung et al., 2007). (Dai et al., 2009) reported an excess TOC (3.2±1.1 □ mol kg^{-1}) in the intermediate layer of the SCS at 1000-1500m compared to the North Western Pacific. This excess TOC in the outflowing intermediate water may carry 3.1±2.1 Tg C yr^{-1} of organic carbon out from the SCS. Taking into account of the short residence time of the SCS deep water, the author pointed out that the exported TOC was likely from the recently fixed organic carbon within the SCS. ^{234}Th-derived POC downward export fluxes out of the euphotic zone in the northern SCS ranges from 5.3 to 26.6 □ mol C m^{-2} d^{-1} (Chen et al., 2008), while 9.40-14.78 □ mol C m^{-2} d^{-1} with an average value of 11.91 □ mol C m^{-2} d^{-1} in the central SCS (Ma et al. 2008), and -10.7±1.5 □ mol C m^{-2} d^{-1} to 12.6±1.1 □ mol C m^{-2} d^{-1} with an average of 3.8±4.0 □ mol C m^{-2} d^{-1} in the southern SCS (Cai et al., 2008). The negative flux is interpreted by the author as the result of lateral input of particulate matter from nearby waters.

3. Perspective to the future research

Underway measurement of air-sea CO_2 flux has been widely conducted on many cruises. This approach is suitable in a large and homogeneous region under the condition that the cruise covers at least one diurnal cycle for the specific region. However, in some coastal areas, where tidal cycles and surface seawater pCO_2 diurnal variability are significant, underway measurement may show potential bias in its temporal representation of a particular study area. Given the fact that diurnal variability may be subject to latitudinal differences (e.g., higher biological effects at higher latitudes), underway measurement alone are not sufficient to resolve the diurnal, seasonal, and inter-annual pCO_2 variations in surface seawater. Time-series observations at varying time scales and process and mechanism analysis are essential to further improve the estimate of global air-sea CO_2 fluxes (Dai et al., 2009).

In addition, Cai et al. (2006, 2008) recommended a small volume ^{234}Th method for the determination of total ^{234}Th in seawater, which can now be used aboard for initial ^{234}Th counting.

Ⅱ The biogeochemical cycle of nutrients and eutrophication in coastal waters

In the Bohai Sea, the average concentrations of dissolved inorganic nitrogen (DIN), PO_4-P, and SiO_3-Si are 12.09±14.44, 0.23±0.12, and 8.12±3.43□ mol L^{-1}, respectively (Wang et al. 2009). Compared with historic data, the PO_4-P concentration decreased since the 1990s, while DIN concentration especially NO_3-N increased. Observed DIN/P ratio indicates PO_4-P as the primary limiting factor for phytoplankton growing in the Bohai Sea. DIN concentration is high in Liaodong Bay and the central area of Bohai Sea. Eutrophication is genenally mesotrophic in the Bohai Sea, but relatively worse in the Bohai Bay, Liaodong Bay and near the Yellow River estuary.

In the ECS and SCS connection, northward flow of seawater in the summer carries little nutrient. On

the other hand, the waters flowing southward along the coast of China in winter carry orders of magnitude higher nutrient concentrations. The outflow of subsurface waters from the SCS is the major source of new nutrients to the ECS continental shelves because these subsurface waters flow out of the Luzon Strait, join the northwardly flowing Kuroshio and enter the Okinawa trough. Around 10% of the nutrients exported from the SCS through the Luzon Strait upwell onto the ESC shelf. These inputs are larger than the aggregate of all the rivers that empty into the ECS, contributing 49% of the externally source nitrogen, 71% of the phosphorous, and 54% of the silica for the ECS(Chen 2008).

Atmospheric deposition is an important pathway by which nutrients are delivered to the surface oceans. Zhang et al. (2007) analyzed the nutrients concentrations in atmospheric deposition at Qianliyan Island in the YS and Shengsi Archipelago in the ECS. Results show clear seasonal signatures for nutrient species in both wet and dry deposition events. Most of the samples collected at Qianliyan Island have higher nutrient concentrations than those from Shensi because of relatively low rainfall and a greater influence of continental dust storms at Qianliyan Island. At both sites, wet deposition plays a comparable role to that of riverine inputs in supplying DIN to the surface ocean and to a lesser extent PO_4 and SiO_3.

Total nutrient fluxes from major Chinese estuaries to the coastal region in the summer are estimated to be 516×10^6 mol day^{-1} for NO_3^-, 24.8×10^6mol day^{-1} for NH_4^+, 4.86×10^6 mol day^{-1} for PO_4^{3-}, 777×10^6 mol day^{-1} for SiO_3, which are 3-4 times greater than those in the winter except for NH_4^+ (Liu et al., 2009).

Nutrients composition is changing in the Chinese Seas. In the Bohai Sea, NO_3^- increased, but phosphate and silicate levels decreased with DIN/P ratios increasing four times (from 3.3 to 14) and Si/DIN ratios decreasing about 10 times (from 10-1.0) in the last forty years (Liu et al., 2008b). In the East China Sea, the DIN/P ratios decreased from 30-134 in the inner shelf to 5-18 in the outer shelf region, while the Si/DIN ratios varied from 0.8-1.1 in the inner shelf to 0.5-2.0 in the outer shelf (Zhang et al., 2007b). Off the Pearl River estuary, molar ratios of DIN/P were 33-89 and Si/DIN ratios were 0.7-3.4 (Liu et al,. unpublished data; Peng et al., 2006). The changed nutrients composition may trigger the change of phytoplankton composition, and furthermore, the fishery resources in the Chinese seas.

In spite of P species in the coastal marine environment, much effort has also been focused on P species in the bottom sediments and suspended particulate matter. In the Yangtze estuary, exchangeable P, organic P, Fe-bounded P, antigenic P and refractory P were concentrated in small particle size classed, while more detrital P was found in the coarse silt and very coarse silt fractions. Particulate organic P, Fe-bound P and refractory P decreased with increasing salinity from the inside to the gate of the river mouth. The bio-available particulate P transported from the Yangtze River to the estuary was ~13.58×10^8 mol/s, which was higher than the flux of dissolved phosphorus (0.82×10^8 mol/s)(He et al., 2009).

Eutrophication, caused by rapidly expanding mariculture and increasing human population, has been a growing problem in many coastal and estuarine ecosystems. In Daya Bay, SCS, increasing DIN and decreasing DIP loading cause the change in the nature of the marine ecosystem as shifts in phytoplankton community from diatoms to flagellates, also lead to high occurrence of dinoflagellate species and numbers (Wang et al., 2006). The state of eutrophication in the Bohai Sea is mesotrophic in general; however the situation is serious in coastal waters (Wang et al., 2009). In the Yellow Sea, eutrophication may partly contribute to the massive macroalgal bloom (Liu et al., 2009). In the Yangtze Estuary, the concentration gradients of nutrients across the shelf indicate that high levels from

land-sources are constrained to the coastal and inner-shelf region by the complex circulation regime (Zhang et al., 2007). Pollution index based on DIN indicates that 41% of the rivers emptying into the Chinese Seas are at the levels between the average global conditions (52 □ M) to polluted waters (110 □ M), and the other 59% are at the levels between polluted to extremely polluted waters (347 □ M). Phosphate concentrations in thirteen rivers are at the pristine level (0.5 □ M) and in five rivers are at average level (3 □ M) compared to the global river data. Dissolved silicate levels in the rivers and areal yields in their watersheds in general are higher in the warm and wet south than in the cold and dry north of the Yangtze (Liu et al., 2009). Anthropogenic activities have increased DIN and PO_4^{3-} loading above natural fluxes by more than a factor of 3-4.

Ⅲ**Environment chemical process of the persistent organic pollutants (POPs)**

Organochlorines (OCS), such as polychlorinated biphenyls (PCBs) and Organochlorine pesticide (OCPs), represent an important group of POPs that have caused worldwide concern as toxic environmental contaminants. In the Haihe River and Haihe Estuary area, The concentration of ∑PCBs and ∑OCPs in the sediments ranged from n.d. (not detected) to 253 ng g^{-1} (average value 66.8 ng g^{-1}) and from 0.997 to 2447 ng g^{-1} (average value: 738ng g^{-1}), respectively. Among the OCPs, the range of concentrations of hexachlorocyclohexane and its isomers (HCHs), dichlorodiphenyltrichloroethane and its metabolites (DDTs) and hexachlorobenzene (HCB) were 0.997–1620 ng g^{-1} (547 ng g^{-1}), n.d. – 155 ng g^{-1} (18.5 ng g^{-1}) and n.d. – 835 ng g^{-1} (173 ng g^{-1}), respectively (Zhao et al. 2010). In the Yangtze estuary, total HCHs' and total DDTs' levels in surface sediments ranged from 0.5 to 17.5 ng g^{-1} with an average of 6.0 ng g^{-1}, and from 0.9 to 33.1 ng g^{-1} with an average 8.2 ng g^{-1}, respectively. Total HCHs's and total DDTs's levels in suspended particulate matters (SPM) varied from 6.2 to 14.8 ng g^{-1} with a mean value of 12.3ng g^{-1} and were from 3.4 to 25.7 ng g^{-1} with an average of 16.4 ng g^{-1}, respectively (Liu et al., 2008). In the atmosphere over the Peal River Estuary and adjacent SCS, the OCPS mainly consisted of HCHS, DDTS and chlordane. Their concentrations were higher in spring (10-106, 429-1003, 1724-9638 pg m^{-3}, respectively) than in winter (13-99, 73-390, 63-224 Pg m^{-3}, respectively), higher at sites close to continent and lower in outer sea, indicating land-based source plays a key role in the delivery of atmospheric OCPs (Liu et al., 2008). The levels of total HCHs in water of PRE varied from 213 to 3116 pg L^{-1} and in sediments they ranged from 181-1388 pg g^{-1} dry weight. The levels of DDTs were in the range of 228- 3284 pg L^{-1} in water and 57- 2244 pg g^{-1} dry weight in sediments, respectively. Total organic carbon, salinity and total suspended particulate matter may control the transport and fate of these two pollutants in the marine environment (Yu et al., 2007).

Polybrominated diphenyl ethers (PBDEs) and perfluorooctane sulfonate (PFOS) and perfluorooctanoic acid (PFOA) are newly listed as POPS under the Stockholm Convention (2009). PBDEs are a class of additive flame retardants that are widely used in plastics, textiles, and electronic appliances. Concerns about the impact of PBDEs on wild animals and human health are mounting because of their ubiquitous presence in the environment and their bioaccumulative ability. Temporal trend of PBDEs' contamination in the Pearl River Delta have revealed apparent increase of such contamination during the past 20 years since 1980s (Chen et al., 2007). In the Peal River Estuary, the concentrations of 10 PBDE congeners (BDEs-28, 47, 66, 85, 99, 100, 138, 154, 153 and 183) ranged from 34.1 to 444.5 ng g^{-1} lipid and from 9.88 to 39.0 ng g^{-1} organic carbon in biota and sediment, respectively (Xiang et al., 2007). The current $\sum_{10}$PBDEs (sum of the BDE congeners, BDE- 28, 47, 66, 85, 99, 100, 138, 154, 153 and 183) and BDE 209 fluxes to the Pearl River Estuary were 2.1 and 29.7

ng cm^{-2} yr^{-1}, respectively, and the total burden of PBDEs were estimated at 8.6 metric tons (Chen et al., 2007). The annual outflows of $\sum_{10}$PBDEs and BDE-209 were estimated at 126 and 940 kg yr^{-1}, respectively from the Pearl River Estuary to coastal ocean (Guan et al., 2009). Both the levels of ∑PBDEs and BDE 209 in Beijiang River were lower than those of the Zhujiang River and Dongjiang River, which together are three major branches of PRE (Chen et al., 2009). In the Bohai Sea, BDE 209 was the predominant congener with a mean value of 7000 pg g^{-1} dry weight, two orders of magnitude higher than other BDE congeners (Pan et al., 2010). In the Laizhou Bay, $\sum_{11}$PBDEs concentrations in sediment ranged from 1.3 to 1800 ng g^{-1} dry weight, with BDE 209 as the predominant congener, which consistent with the fact that deca-BDE technical mixtures are the dominant PBDEs product in this region (Jin et al., 2008).

Greater concentrations of PFOS and PFOA were observed in southern and eastern China than in other areas of China. PFOS and PFOA were reported to be 20.5 ng L^{-1} and 1590 ng L^{-1} respectively in the Huangpu River (Chen et al., 2009). The median concentration was found to be 4.2ng L^{-1} for PFOS and 5.4ng L^{-1} for PFOA in the Yangtze River (Jin et al., 2009). In the Daliao River system in northeast China, Eight Perfluorinated compounds (PFCs) including perfluorobutane sulfonate (PFBs), perluorohexane sulfonate (PFHxS), perfluorooctane sulfonate (PFOS), perfluorooctanoic acid (PFOA), perfluoronoanoic acid (PFNA), perfluorodecanoic acid (PFDA), perfluorododecanoic acid (PFDoA) and perfluorotetradecanoic acid (PFTA) were determined based on the upper 10cm surface sediment samples. Total concentrations of PFCs ranged 0.29-1.03 ng g^{-1} dry weight. PFOS and PFOA are two dominant species, with a range of <LOQ to 0.37 ng g^{-1} and < LOQ -0.17 ng g^{-1} dry weight, respectively, while those of the other six target analytes are blow their limit of quantification (LOQ) at most of the sampling sites (Bao et al., 2009).

Polycyclic aromatic hydrocarbons (PAHs) are among the most carcinogenic, mutagenic and toxic contaminates found in aquatic system. Investigations of PAHs in estuarine systems are intensive. In the Daliao river system, total PAH concentration ranged from 570.2 to 2318.6 ng L^{-1} in surface water, from 151.0 to 28483.8 ng L^{-1} in SPM, from 102.9 to 3419.2 ng L^{-1} in sediment and from 6.3 to 46.4 □ gL^{-1} in pore water (Guo et al., 2009). The total PAH contents varied from 10.8 to 252 ng g^{-1} in Yellow River Estuary sediment, and from 84.6 to 620 ng g^{-1} in Yangtze River Estuary sediment. The mean total PAH content was approximately two times higher in the latter than that in former (Hui et al., 2009). High concentration of PAHs in river water usually attributes to the influence of storm runoff demonstrated by the research conducted in the Peal River Estuary (Luo et al., 2007) and in Xijiang River (Deng et al., 2006).

Ⅳ Major and minor elements in marine environment (four familiar heavy metals (e.g., Cu, Zn, Pb, Cd and rare elements))

Since the Industrial Revolution, large amounts of toxic metal-containing wastewater and solid wastes has been directly disposed into coastal environment. Sediments of bays and estuaries have represented huge sinks of heavy metals (Wang et al., 2010). Distribution of pollution levels of heavy metals in rivers, estuaries, and seawaters have been extensively investigated in China in the past few years.

In the sediments of the Jinzhou Bay, the highest concentration of Cd, Cu and Pb were up to 64, 400 and 460 mg Kg^{-1}, which was 100, 13 and 7 times higher than the national guideline (GB 18668-2002). 39%-61% of Cd was exchangeable fractions indicating that Cd in the sediments posed a high risk to

local environments. Cu and Pb were at medium risk level for local ecosystem. Nonferrous smelting activities are the major source of the heavy metals contamination (Wang et al., 2010).

In the water body of Bohai Bay, high levels of Cu, Zn, Pb and Hg were detected, with maximum concentrations in the year 1996-2005 of 16.30, 422.0, 40.40, 0.23 □ gL^{-1} respectively. The concentration of Cu, Zn and Pb descended from the coastline to the central area of the bay, while high concentrations of Hg and Cd occurred not only in inshore but also in offshore area (Dai et al., 2009). In the sediment of the Bohai Bay, high levels of Cu, Zn, Cd, Pb and Hg were observed not only along the shoreline but also in the inner part of the bay, suggesting the contamination sources of heavy metals from both terrestrial inputs and the atmospheric deposition (Zhan et al., 2010).

Contamination caused by heavy metals was found in the Yangtze River estuary. In the water column of the Yangtze River estuary, dissolved Cu, Zn, Pb and Cd ranged from 22.26±2.31, 30.15±3.18, 15.74±1.36, and 0.76±0.12 □ g dm^{-3} respectively (Quan et al., 2010). In the sediments of the Yangtze river estuary, As, Hg, Cd, Cu, Cr, Zn and Pb were found to be 6.49-17.6, 0.0164-0.0987, 0.059-0.319, 11.7-46.6, 10.5-11.3, 44.5-125, 14.8-32.7 □ g kg^{-1}, respectively (An et al., 2009).

In the sediment of the Daya Bay, the average values of As, Pb, and Zn were found to be 18.6, 38.1, and 74.9 mg kg^{-1} respectively, which were clearly higher than those of natural abundance, showing that there was pollutant of As, Pb and Zn (Du et al., 2008).

The surface sediment of Xiamen Bay and its adjacent areas were contaminated by Cd, Pb, Zn and As, with the highest value of Zn (68-268 mg kg^{-1}) followed by Pb (27-71 mg kg^{-1}). Data from sequential extractions showed that Cd posed a medium ecological risk, whereas, Cr posed low risk and the mobility of heavy metals decreased in the order of Cd>Pb>Cu>Zn>Hg>As>Cr (Yan et al., 2010).

The sediments of the Pearl River estuary was significantly contaminated by Cd, Zn and Ni with concentration ranges of 2.79-4.65, 239.4-345.7 and 24.8-122.1 mg kg^{-1}, respectively. 34.6-46.8% of Pb, Cd, and Zn was strongly associated with exchangeable fractions, while Cu, Ni and Cr were predominantly associated with organic fractions, residual, and Fe-Mn oxide (Li et al., 2007). The concentration of Hg ranged from 1.5 to 201 ng g^{-1} (average 54.4 ng g^{-1}), decreased with distance from the estuary to the open SCS. The variations in Hg fluxes in sediment cores correlated obviously with the economic development and urbanization that has occurred in this region (Shi et al., 2010). Ip et al. (2007) demonstrated that heavy metals in the Pear River estuary came mainly from anthropogenic inputs. Heavy metal associated with coarse particles mainly deposited on the upstream area of PRE, while dissolved heavy metals and heavy metals associated with fine particulates could be transported downstream or even to its surrounding coastal area by physical transportation.

Acknowledgement

This work was supported by Natural Science Foundation of China (No. 40976097) and by the External Cooperation Program of the Chinese Academy of Sciences (No. GJHZ200811).

References

An, Q., Y. Q. Wu, J. H. Wang and Z. E. Li (2009). Heavy metals and polychlorinated biphenyls in sediments of the Yangtze River estuary, China. Environmental Earth Sciences 59(2): 363-370.

Bao, J., Y. H. Jin, W. Liu, X. R. Ran and Z. X. Zhang (2009). Perfluorinated compounds in sediments from the Daliao River system of northeast China. Chemosphere 77(5): 652-657.

Cai, P. H., W. F. Chen, M. H. Dai, Z. W. Wan, D. X. Wang, Q. Li, T. T. Tang and D. W. Lv (2008). A high-resolution study of particle export in the southern South China Sea based on Th-234: U-238 disequilibrium. Journal of Geophysical Research-Oceans 113(C4).

Cai, P. H., M. H. Dai, D. W. Lv and W. F. Chen (2006). How accurate are Th-234 measurements in seawater based on the

MnO2-impregnated cartridge technique? Geochemistry Geophysics Geosystems 7.

Cai, P. H., M. H. Dai, D. W. Lv and W. F. Chen (2008). Reply to comment by Chin-Chang Hung et al. on "How accurate are Th-234 measurements in seawater based on the MnO2-impregnated cartridge technique?". Geochemistry Geophysics Geosystems 9.

Cai, W. J., M. H. Dai and Y. C. Wang (2006). Air-sea exchange of carbon dioxide in ocean margins: A province-based synthesis. Geophysical Research Letters 33(12): 4.

Chen, C. L., Y. L. Lu, X. Zhang, J. Geng, T. Y. Wang, Y. J. Shi, W. Y. Hu and J. Li (2009). A review of spatial and temporal assessment of PFOS and PFOA contamination in China. Chemistry and Ecology 25(3): 163-177.

Chen, C. T. A. (2008). Distributions of nutrients in the East China Sea and the South China Sea connection. Journal of Oceanography 64(5): 737-751.

Chen, L. G., Y. M. Huang, X. C. Peng, Z. C. Xu, S. K. Zhang, M. Z. Ren, Z. X. Ye and X. H. Wang (2009). PBDEs in sediments of the Beijiang River, China: Levels, distribution, and influence of total organic carbon. Chemosphere 76(2): 226-231.

Chen, S. J., X. J. Luo, Z. Lin, Y. Luo, K. C. Li, X. Z. Peng, B. X. Mai, Y. Ran and E. Y. Zeng (2007). Time trends of polybrominated diphenyl ethers in sediment cores from the pearl river estuary, south china. Environmental Science & Technology 41(16): 5595-5600.

Chen, W. F., P. H. Cai, M. H. Dai and J. F. Wei (2008). Th-234/U-238 disequilibrium and particulate organic carbon export in the northern South China Sea. Journal of Oceanography 64(3): 417-428.

Dai, M. H., Z. M. Lu, W. D. Zhai, B. S. Chen, Z. M. Cao, K. B. Zhou, W. J. Cai and C. T. A. Chen (2009). Diurnal variations of surface seawater pCO(2) in contrasting coastal environments. Limnology and Oceanography 54(3): 735-745.

Dai, M. H., F. F. Meng, T. T. Tang, S. J. Kao, J. R. Lin, J. H. Chen, J. C. Huang, J. W. Tian, J. P. Gan and S. Yang (2009). Excess total organic carbon in the intermediate water of the South China Sea and its export to the North Pacific. Geochemistry Geophysics Geosystems 10.

Dai, M. H., W. D. Zhai, W. J. Cai, J. Callahan, B. Q. Huang, S. L. Shang, T. Huang, X. L. Li, Z. M. Lu, W. F. Chen and Z. Z. Chen (2008). Effects of an estuarine plume-associated bloom on the carbonate system in the lower reaches of the Pearl River estuary and the coastal zone of the northern South China Sea. Continental Shelf Research 28(12): 1416-1423.

Dai, M. X., S. T. Peng, J. Xu, C. G. Liu, X. L. Jin and S. F. Zhan (2009). Decennary Variations of Dissolved Heavy Metals in Seawater of Bohai Bay, North China. Bulletin of Environmental Contamination and Toxicology 83(6): 907-912.

Deng, H. M., Peng, P. A., Huang, W. L., & Song, J. Z. (2006). Distribution and loadings of polycyclic aromatic hydro-carbons in the Xijiang River in Guangdong, South China. Chemosphere, 64, 1401–1411.

Du, J. Z., H. D. Mu, H. Q. Song, S. P. Yan, Y. J. Gu and J. Zhang (2008). 100 years of sediment history of heavy metals in daya bay, china. Water Air and Soil Pollution 190(1-4): 343-351.

Frankignoulle, M., G. Abril, A. Borges, I. Bourge, C. Canon, B. Delille, E. Libert and J.-M. Théate (1998). Carbon Dioxide Emission from European Estuaries. Science 282: 434 - 436.

Guan Y.F., O.S. SamuelSojinu, S. M. Li and Eddy Y. Zeng，2009. Fate of polybrominated diphenyl ethers in the environment of the Pearl River Estuary, South China. Environmental Pollution 157：2166-2172.

Guo, W., M. C. He, Z. F. Yang, C. Y. Lin, X. C. Quan and B. Men (2009). Distribution, partitioning and sources of polycyclic aromatic hydrocarbons in Daliao River water system in dry season, China. Journal of Hazardous Materials 164(2-3): 1379-1385.

Guo, X., M. Dai, W. Zhai, W.-J. Cai, and B. Chen (2009), CO_2 flux and seasonal variability in a large subtropical estuarine system, the Pearl River Estuary, China, J. Geophys. Res., 114, G03013, doi:10.1029/2008JG000905.

He, B. Y., M. H. Dai, W. D. Zhai, L. F. Wang, K. J. Wang, J. H. Chen, J. R. Lin, A. G. Han and Y. P. Xu (2010). Distribution, degradation and dynamics of dissolved organic carbon and its major compound classes in the Pearl River estuary, China. Marine Chemistry 119(1-4): 52-64.

He, H. J., H. T. Chen, Q. Z. Yao, Y. W. Qin, T. Z. Mi and Z. G. Yu (2009). Behavior of different phosphorus species in suspended particulate matter in the Yangtze estuary. Chinese Journal of Oceanology and Limnology 27(4): 859-868.

Hui, YM; Zheng, MH; Liu, ZT, Gao LR. 2009. Distribution of polycyclic aromatic hydrocarbons in sediments from Yellow River Estuary and Yangtze River Estuary, China

Hung, J. J., S. M. Wang and Y. L. Chen (2007). Biogeochemical controls on distributions and fluxes of dissolved and particulate organic carbon in the Northern South China Sea. Deep-Sea Research Part Ii-Topical Studies in Oceanography 54(14-15): 1486-1503.

Jin, J., W. Z. Liu, Y. Wang and X. Y. Tang (2008). Levels and distribution of polybrominated diphenyl ethers in plant, shellfish and sediment samples from Laizhou Bay in China. Chemosphere 71(6): 1043-1050.

Jin, Y. H., W. Liu, I. Sato, S. F. Nakayama, K. Sasaki, N. Saito and S. Tsuda (2009). PFOS and PFOA in environmental and tap water in China. Chemosphere 77(5): 605-611.

Li, Q. S., Z. F. Wu, B. Chu, N. Zhang, S. S. Cai and J. H. Fang (2007). Heavy metals in coastal wetland sediments of the Pearl River Estuary, China. Environmental Pollution 149(2): 158-164.

Liu, D. Y., J. K. Keesing, Q. U. Xing and P. Shi (2009). World's largest macroalgal bloom caused by expansion of seaweed aquaculture in China. Marine Pollution Bulletin 58(6): 888-895.

Liu, G.Q., G. Zhang, et al. (2008). Source and Distribution Characteristic of Atmospheric Organochlorine Pesticides in the Pearl River Estuary and Adjacent South China Sea. Huanjing Kexue 29(12): 3320-3325.

Liu, M., S. B. Cheng, D. N. Ou, Y. Yang, H. L. Liu, L. J. Hou, L. Gao and S. Y. Xu (2008). Organochlorine pesticides in surface sediments and suspended particulate matters from the Yangtze estuary, China. Environmental Pollution 156(1): 168-173.

Liu, S. M., G. H. Hong, J. Zhang, X. W. Ye and X. L. Jiang (2009). Nutrient budgets for large Chinese estuaries. Biogeosciences 6(10): 2245-2263.

Liu, S. M., J. Zhang, H. W. Gao and Z. Liu (2008b). Historic changes in flux of materials and nutrient budgets in the Bohai. Acta Oceanol. Sin. 27: 1-17.

Luo, X.J., B.X. Mai, Q.S.Yang, S.J. Chen and Eddy Y. Zeng. Distribution and partition of polycyclic aromatic hydrocarbon in surface water of the Pearl River Estuary, South China. Environmental Monitoring and Assessment, Volume 145, Numbers 1-3, 427-436, DOI: 10.1007/s10661-007-0051-2

Ma, H., Z. Zeng, J. H. He, L. Q. Chen, M. D. Yin, S. Zeng and W. Y. Zeng (2008). Vertical flux of particulate organic carbon in the central South China Sea estimated from Th-234-U-238 disequilibria. Chinese Journal of Oceanology and Limnology 26(4): 480-485.

Mei Yu, Xiaojun Luo, Shejun Chen, Bixian Mai, Eddy Y. Zeng. 2007. Organochlorine pesticides in the surface water and sediments of the Pearl River Estuary, South China.

Pan, X. H., J. H. Tang, J. Li, Z. G. Guo and G. Zhang (2010). Levels and distributions of PBDEs and PCBs in sediments of the Bohai Sea, North China. Journal of Environmental Monitoring 12(6): 1234-1241.

Peng, X., X. R. Ning, J. Sun and F. F. Le (2006). Responses of phytoplankton growth on nutrient enrichments in the northern South China Sea. Acta Ecologica Sinica 26: 3959-3968 (in Chinese with English Abstract).

Quan, W. M., L. Y. Shi, J. D. Han, X. Y. Ping, A. Shen and Y. Q. Chen (2010). Spatial and temporal distributions of nitrogen, phosphorus and heavy metals in the intertidal sediment of the Chang jiang River Estuary in China. Acta Oceanologica Sinica 29(1): 108-115.

Shim, J., D. Kim, Y. C. Kang, J. H. Lee, S. T. Jang and C. H. Kim (2007). Seasonal variations in pCO(2) and its controlling factors in surface seawater of the northern East China Sea. Continental Shelf Research 27(20): 2623-2636.

Wang, S. F., Y. F. Jia, S. Y. Wang, X. Wang, H. Wang, Z. X. Zhao and B. Z. Liu (2010). Fractionation of heavy metals in shallow marine sediments from Jinzhou Bay, China. Journal of Environmental Sciences-China 22(1): 23-31.

Wang, X. L., Z. G. Cui, Q. Guo, X. R. Han and J. T. Wang (2009). Distribution of nutrients and eutrophication assessment in the Bohai Sea of China. Chinese Journal of Oceanology and Limnology 27(1): 177-183.

Wang, Z. H., Y. Z. Qi, J. F. Chen, N. Xu and Y. F. Yang (2006). Phytoplankton abundance, community structure and nutrients in cultural areas of Daya Bay, South China Sea. Journal of Marine Systems 62(1-2): 85-94.

Xiang, C. H., X. J. Luo, S. J. Chen, M. Yu, B. X. Mai and E. Y. Zeng (2007). Polybrominated diphenyl ethers in biota and sediments of the Pearl River Estuary, South China. Environmental Toxicology and Chemistry 26(4): 616-623.

Yan, C. Z., Q. Z. Li, X. Zhang and G. X. Li (2010). Mobility and ecological risk assessment of heavy metals in surface sediments of Xiamen Bay and its adjacent areas, China. Environmental Earth Sciences 60(7): 1469-1479.

Zhai, W. D., M. H. Dai, W. J. Cai, Y. C. Wang and H. S. Hong (2005). The partial pressure of carbon dioxide and air-sea fluxes in the northern South China Sea in spring, summer and autumn, Marine Chemistry, 103(1-2): 209-209.

Zhai, W. D., M. H. Dai and X. G. Guo (2007). Carbonate system and CO2 degassing fluxes in the inner estuary of Yangtze (Yangtze) River, China. Marine Chemistry 107(3): 342-356.

Zhan, S. F., S. T. Peng, C. G. Liu, Q. Chang and J. Xu (2010). Spatial and Temporal Variations of Heavy Metals in Surface Sediments in Bohai Bay, North China. Bulletin of Environmental Contamination and Toxicology 84(4): 482-487.

Zhang, G. S., J. Zhang and S. M. Liu (2007a). Characterization of nutrients in the atmospheric wet and dry deposition observed at the two monitoring sites over Yellow Sea and East China Sea. Journal of Atmospheric Chemistry 57(1): 41-57.

Zhang, J., S. M. Liu, J. L. Ren, Y. Wu and G. L. Zhang (2007b). Nutrient gradients from the eutorphic Yangtze (Yangze River) Estuary to the oligotrophic Kuroshio waters and re-evaluation of budgets for the East China Sea Shelf. Prog. Oceanog. 74: 449-478.

Zhang, L. J., L. Xue, M. Q. Song and C. B. Jiang (2010). Distribution of the surface partial pressure of CO2 in the southern Yellow Sea and its controls. Continental Shelf Research 30(3-4): 293-304.

Zhao, L., H. Hou, Y. Y. Zhou, N. D. Xue, H. Y. Li and F. S. Li (2010). Distribution and ecological risk of polychlorinated biphenyls and organochlorine pesticides in surficial sediments from Haihe River and Haihe Estuary Area, China. Chemosphere 78(10): 1285-1293.

Zhu, Y., S. L. Shang, W. D. Zhai and M. H. Dai (2009). Satellite-derived surface water pCO(2) and air-sea CO2 fluxes in the northern South China Sea in summer. Progress in Natural Science 19(6): 775-779.

PROGRESS OF OCEANIC REMOTE SENSING BY SATELLITE ALTIMETRY IN CHINA (2006-2010)

QIU Zhongfeng and HE Yijun

（Key Laboratory of Ocean Circulation and Waves, Institute of Oceanology, CAS, Qingdao, P.R. China）

Abstract

This paper introduces the progress of oceanic remote sensing by satellite altimetry in China since 2006. Satellite altimeter data were widely used to retrieve tides, currents, mesoscale variability, sea surface wind speed and sea surface wave by Chinese researchers. The distributions and variations of oceanic parameters in the China seas and other areas have been analyzed with altimeter data being directly used or assimilated into numerical models. Furthermore, China plans to launch the HY-2A satellite in 2011. This paper also introduces the pre-launch experiments for altimetry mounted on the HY-2A satellite.

Ⅰ Introduction

The development of satellite altimeter began in 1970s with the altimeter mounted on the satellite GEOS-3 for the first time in 1975. Altimetry permanently transmits signals to the earth and receives the echo waves from sea surface. Sea surface height (SSH hereafter) is derived from the round trip time of microwave transmitting between satellite altimeter and sea surface. With the improvements of satellite orbit determination, corrections of atmospheric refraction and tides mixing elimination, SSH has been detected from satellite altimetry more and more precisely. The satellite altimetry TOPEX/Poseidon (T/P hereafter) launched in 1992 has the ability of detecting SSH in a high precision about 4.1cm. As follow-on satellite systems of T/P, Jason-1 and Jason-2, which have been launched in 2001 and 2008, respectively, also contain the high precision of detecting SSH with lower than 3cm.

T/P, Jason-1 and Jason-2 have provided a precise data set of global SSH, sea surface wind speed (SSWS hereafter) and sea surface wave height (SSWH hereafter) and so on. Observations from satellite altimetry will facilitate applications to geodesy, geophysics, glaciology, hydrology, and atmospheric physics. Chinese researchers have made great contributions on applying altimeter data in the research fields such as oceanic currents, tides and mesoscale hydrodynamic phenomena and attained a lot of achievements. Qiu et al. (2007) have introduced the progress of oceanic remote sensing using satellite altimetry made by Chinese researchers during the period 2002-2006. Following their work this paper will present the progress since 2006.

Nowadays people realize that a long term series of data is a key to understanding the mechanism of ocean and global atmosphere. For example, Leuliette et al. (2004) declared that the global mean sea level raised with $3.2 mm a^{-1}$ based on analyzing the 12-year T/P SSH data. The satellites T/P, Jason-1 and Jason-2 have jointly provided about 18-year observations now and the records still extend. In order to increase the spatial-temporal sampling and the time series of satellite observations, China plans to launch the satellite HY-2A in 2011. A radar altimeter will be mounted on HY-2A. This paper will also

present some experiments designed for HY-2A.

Ⅱ. Applications of Altimeter Data

1 Tides Retrieval

With the optimized orbit phasing the satellite altimetry, such as T/P, is able to attain periodical observations in a same area. Various tide components are available to be discriminated each other or from non-periodical sea level variations because of their own fixed periods. The long time series of satellite altimeter data have widely used in tides retrieval (Qiu et al., 2007). These results have improved our knowledge of tides and helped correct the altimetric data for tide effects.

Models of unprecedented accuracy (2-3cm RMS) have been produced for the main diurnal and semi-diurnal components based on satellite altimeter data. Wang et al. (2010) assessed the accuracy of 7 global ocean tidal models derived from satellite altimeter data using observations at 152 tidal gauge stations. The RMS values of tidal height differences are in the range from 1.0cm to 1.3cm for M_2, and from 2.0cm to 2.3cm for 7 other principal constituents (S_2, K_1, O_1, N_2, K_2, $P_1$and Q_1).

Due to shallow and large gradients of water depths, small spatial scales and complex distributions of tides in the China seas, it is hard to retrieve tides using those global ocean tidal models, even though they process successfully in the open ocean (Hu, 2007). Researchers then developed various models for tides in the shallow waters based on the tidal gauge observations and satellite altimeter data. One representative of them is the adjoint assimilation tide model. Based on variational principle and optimization, the best open boundaries and bottom friction coefficients of the model are determined by the constraint of oceanic hydrodynamics. Tidal gauge observations and satellite altimeter data are assimilated into the model to achieve tidal simulations in high precision.

Sun and Lv (2007), Zhang (2008) extracted the harmonic constants of tidal constituents from over 10 years altimeter data. After estimating the optimized bottom friction coefficients using the adjoint assimilation model, they simulated tides in the Bohai Sea, the Yellow sea and the East China Sea in high precision. They made some numerical experiments to compare different methods to optimize the bottom friction coefficients. The results showed that the method of selecting the independent bottom friction coefficients according to the spatial characteristics of ocean topography was helpful to increase the simulation precision even if a small number of independent parameters considered.

Internal tides are mainly derived from the interactions between barotropic tides and ocean topography, which have the same frequencies as the induced tides. Satellite altimeter data are applied to estimate the distributions of internal tides and the energy flux. Jiang and Lv (2007) investigated the distributions of the internal tides, which are deduced by the surface tides (M_2, S_2, K_1 and O_1) in the Bohai Sea, the Yellow Sea and the East China Sea using a three dimensional model. They compared the simulated surface tides with the T/P data. The results showed that internal tides were effectively generated over prominent topographic features such as the northeast of Taiwan and the continental shelf slope in the China seas. Yao (2009) used a three dimensional ocean model HAMSOM to simulate the internal tide in Hawaiian area, which was induced by M_2 tide under the condition of rough topography. Satellite altimeter data were used to extract the signals of M_2 internal tides and compute the energy flux in the magnitude from $100Wm^{-1}$ to $1kWm^{-1}$.

2. Research of Currents and Mesoscale Variability

Mesoscale variability has typical spatial scales of 30-300 km and time scales of 1-3 months. It is mainly associated with strong current instabilities, eddy formation, and propagation, which are very energetic and have a key role in heat transport from low to high latitudes. In the coastal domain there is a complex, mesoscale or short-scale activity involving many processes such as the accumulation of organic matter and fresh water transported by rivers, dense water formation, and coastal tides, plus the influence of the open ocean through interactions between coastal currents and open ocean circulation. Understanding such complex processes requires the development of very specific models and the use of various data sources, including altimetry.

The altimeter data are usually applied to the research of mesoscale variability in two ways (He, 2007). One is to retrieve the characteristics of mesoscale eddies directly from altimeter data. The other one is to combine with ocean models using assimilation methods. Various data sources, including altimetry data, satellite derived sea surface temperature and other profiling data from buoys such as Argos, are analyzed to know the distributions and the three dimensional structures of eddies.

Yang (2008) used Jason-1 data and in situ observations of temperature, salinity, density and currents in the east areas of the Vietnam Sea in summer to determine the locations, scales and life-spans of the mesoscale eddies. He (2007) investigated the characteristics of eddies in the region of subtropical countercurrent in the northwest Pacific using the 10-year satellite SSH data from 1996 to 2005. The results showed that the number of cyclonic eddies were more than that of anticyclonic eddies. About 50-70 mesoscale eddies appeared each year with different seasonal distributions. Eddies were more frequently observed in this area in spring and summer than those in other seasons. Also the intensities were stronger and the life-spans were longer too. Cheng and Qi (2008) obtained the distribution and propagation activity of mesoscale eddies in the global oceans by using the merged altimeter data of more than 12 years. The results showed that the distribution of the mesoscale eddies was a remarkable zonal in the subtropics. Numbers of cyclonic eddies were almost equal to those of anticyclonic eddies.

The Kuroshio is a strong western boundary current in the northwestern Pacific with high temperature and high salinity. It begins off the east coast of Philipphine and flows northeastward from the east coast of Taiwan past the continental shelf of the East China Sea to Japan, where it merges with the easterly drift of the North Pacific Current. When it passes the Luzon Strait, the Kuroshio will deform and penetrate into the South China Sea (SCS hereafter) because of lacking western boundary. Due to the penetrations the Kuroshio exchanges the mass, momentum and energy with the water in the SCS through the Luzon Strait and therefore influence the circulation in the SCS (Hu, 2008). As the important data sources, satellite altimeter data and buoy observations are widely used to the research of the Kuroshio and the interactions between the Kuroshio and mesoscale eddies.

Ma (2006) derived the sea surface current fields in the Kuroshio and adjacent regions from the Argos drifter buoy observations and satellite altimeter data. The seasonal variability of the Kuroshio was investigated by analyzing the time series current fields. They also used a method of subsidiary lines to extract the axis and the primary variability periods at different sections of the Kuroshio. The results showed the primary variability period changed at different sections of the Kuroshio and that was caused mainly by ocean waves, regional winds and topography.

Zhou et al. (2007) investigated the vertical structure of eddies off the east coast of Taiwan by using the Argo profiling observations and altimeter data. The results indicated that those eddies were very

energetic with a vertical extent of 2000m and a horizontal scale of 200km. The tangential velocity at the surface was about 60cms^{-1}, which was almost equal to that of the Kuroshio.

By analyzing the in situ observations at the Luzon Strait and altimeter data, Zhao (2007) indicated that eddies on both sides of the Kuroshio can affect the current path. The main axis of the Kuroshio tended to be attracted when encountering cyclonic eddies and that tended to deviate westward when anticyclonic eddies occurring. The results also showed the eddy-shedding events, which occurred about 49 times during 1992-2005.

Hu (2008) analyzed the characters of the upper circulations in the northeast SCS by using the altimeter data and numerical model outputs. The nonlinear characteristics of the Kuroshio's intrusions to the SCS and the interactions between the Kuroshio and mesoscale eddies were analyzed by using a 1.5-layer gravity reduced shallow water model. The results showed that mesoscale eddies usually dissipated or drifted northward with the Kuroshio when they transported westward and encountered the Kuroshio at the Luzon Strait. However eddies are capable of transferring energy from the Pacific to the SCS when the Kuroshio is weak.

On a scale of several days and tens kilometers, currents can be approximately treated as geostrophic balance except for in the equatorial areas. Current velocities and directions can be derived from the pressure gradient of equipotential surface by using altimeter data. Guo et al. (2006) analyzed the distributions of the sea surface circulations in the SCS based on 11-year altimeter data by using the empirical orthogonal function method. T/P data during 1992-2001 have been used to analyze the seasonal and interannual variations of surface geostrophic current in the southeast Pacific by Lin and Hu (2006). Qiu and Li (2007) analyzed the characters and rules of seasonal evolution of the upper circulation in the Bay of Bengal by reproducing climatological monthly surface dynamic topography using T/P data from 1993 to 2003 and historical hydrographic data. Zhang et al. (2008) determined the bifurcation latitude and investigated its seasonal and interannual variations by using 12-year altimeter data.

Mean sea level is a pertinent indicator of global warming. Various data sources including altimetry and numerical models are used to estimate the sea level trend. Gao et al. (2007) analyzed the variations of mean sea level in the extent areas of the Kuroshio and the distributions of eddies by using the 12-year SSH data merged from T/P, Jason-1 and ERS/ENVISAT. The results showed that the mean sea level in the extent areas of the Kuroshio increased with the speed 8.89 mma^{-1}. Zhai et al. (2007) analyzed the high frequency fluctuation with the period shorter than 165 days and the spatial distributions of energy by using the altimeter SSH data from 1992 to 2006. Qiao and Chen (2008) analyzed the temporal and spatial variations of the sea level in the China seas by using 11-year T/P and Jason-1 data. The results showed that the raising speed of the sea level in the China seas was about 0.593 cma^{-1}. Shi et al. (2008) found the sea level in the areas of the Pearl River estuary raised with the speed 0.30 ± 0.05 cma^{-1} by analyzing the altimeter data during 1993-2006. Rong et al. (2008) investigated the variations of sea level in the global ocean and the SCS during 1993-2004 by using the altimeter data. The results showed that the raising speeds of the sea level in the global ocean and the SCS are 2.5 ± 0.2 mma^{-1} and 4.8 ± 1.2 mma^{-1} respectively. They also found that the variations of sea level in low frequency related to El Nino.

3.Sea Surface Wind Speed Retrieval

SSWS is one of the main motivations for the surface dynamic processes such as waves and circulations. It plays a vital role on the transfer of energy and heat flux between ocean and atmosphere. There is an inversed relationship existing between the backscatter cross section and SSWS, which has been named the Geophysical Model Function. The sea surface toughness will increase as SSWS becomes larger, which will enlarge the energy of side scatter of radar and therefore reduce the backscatter cross section. With the Geophysical Model Function the backscatter cross section detected by altimetry can be transformed to SSWS.

Yang (2007) analyzed the temporal and spatial distributions of SSWS in the northwest Pacific by using Jason-1 SSWS data. The buoy observations have been used to validate the altimeter SSWS data. Chen et al. (2007) investigated the effects of the wave state on the altimeter wind speed retrieval based on the observations in the Gulf of Mexico. The results showed that the wave state affected significantly on the altimeter SSWS retrieval. When considering the effects of the wave state they presented a new wind wave spectrum model, which could retrieve SSWS from altimeter data more accurately than the normal retrieval method with the root mean square difference and the averaged bias between retrieved SSWS and buoy observations reduced 30% and 83%, respectively. Gu (2009) developed a method to detect SSWS in the range of 10-40ms^{-1} based on the observations in weather stations and high speed wind data from satellite. They used the method to retrieve the high speed wind from Jason-1 data. The results showed that the proposed method would increase the precision of SSWS retrieval from altimeter data when wind speeds were larger than 20ms^{-1}. Furthermore, a neural net algorithm for retrieving SSWS from altimeter data has been established based on T/P data and the NDBC buoy observations (Ren et al., 2007).

Sea surface toughness is also observed by altimetry. In addition to the range, an altimeter provides estimates of SSWS and SSWH, which are of both scientific and operational values to marine meteorology. Guo et al. (2007) estimated the sea surface roughness in the Pacific by using wind speed data derived from T/P. The results showed that the mean sea surface roughness was greatest in winter and smallest in spring. Cui and Chen (2006) proposed a modified method on the relationship between altimeter sea surface roughness and gas transfer by further considering the influence of the chemical enhancement effect. They used the method to estimate the CO_2 gas transfer velocities at the air/sea interface in the tropical areas. The results showed that the influence induced by the chemical enhancement can be up to 31.98% in summer.

4. Wave Parameters Retrieval

Satellite altimeter SSWH data are mainly applied into wave parameters retrieval in two aspects. One is that SSWH data are assimilated into ocean wave numerical models to provide appropriate initial conditions, to improve model settings and to validate model results. The other one is that SSWH are used to analyze the wave characteristics in the global ocean or the regional areas.

Zhou and Yang (2008) simulated the wave distributions in the SCS affected by cold air using the ocean model WWATCH and validated the results by using Jason-1 data. Yan et al. (2009) simulated the wave during hurricane Dean in August 2007 using SWAN nested in WAVEWATCH with altimeter SSWH as validation data. Zheng et al. (2010) simulated the process of wave caused by cold wave and strong wind in the Bohai Sea based on the wave model SWAN by using self nested method to provide the spectral type boundary. T/P data and near shore buoy observations were used to compare with the simulations and the results showed that the spatial-temporal distributions of the wave were well

simulated in the period of cold wave in the Bohai Sea. Wang and Yu (2009) assimilated Jason-a data into the wave model to perform a numerical experiment of forecasting three days' wave in the northwest Pacific. The results showed that a considerable improvement was observed for wave forecast with assimilating altimeter data.

Chen et al. (2009) analyzed the temporal and spatial distribution of the wave height during the typhoon RANANIM in August 5-13, 2004 by using wave height data from GFO, T/P, Jason-1 and Envisat. Xie et al. (2009) investigated the characteristics of the waves with significant wave height greater than 4m in the surrounding waters of the Taiwan Island by using TOPEX data. The results showed that seasonal variations were observed in the distributions of the waves. Chen et al. (2006) analyzed the seasonal characteristics and temporal variations of waves in the China seas using TOPEX data from 1992 to 2005. The results showed that the average wave height was greatest in winter and the high wave areas were mainly located in the Taiwan Strait, the northern SCS, the areas southeast to the Indo-China Peninsula and the regions outside of the Luzon Strait. The average wave height was the smallest in summer.

Besides significant wave height satellite altimeter data are used to retrieve other wave elements such as period. Wang (2006) proposed a new wave period retrieval model based on the relationships between wave age and non-dimensional wave height. They retrieved the wave period in the Gulf of Mexico and the Hawaii sea area by using this model and altimeter data and the NDBC observations. Li (2007) retrieved significant wave period from satellite altimeter data using a new algorithm and compared the computations with buoy data. The results showed that the algorithm was suitable for wave period retrieval, especially in the wind wave areas.

Ⅲ. Data Corrections and Retrieval Methods

Satellite altimeter data are usually assimilated into numerical models as initial conditions or forcing fields. Various assimilation methods are used by different researches due to the differences of research objects or mathematic algorithms used. Zhu et al. (2007) established an ocean variational analysis system (OVALS) based on the three dimensional variational method and applied the model to assimilate oceanic observations in the tropic areas of the Pacific. Lu et al. (2010) developed the parallel algorithm for the OVALS. Gao et al. (2007) simulated mesoscale eddies by combining the OVALS with the ocean model POM. The results showed that assimilation improved the precision of mesoscale eddies simulations by using circulation models. Xiao et al. (2007) used a three dimensional variational method to assimilate altimeter data into the ocean model POM. They considered the error correlations of each orbit and optimized data using a recursive filtering method. Furthermore, ensemble data assimilation (Wan, 2006), adjoint assimilation (Wu et al., 2008) and a four dimensional variational assimilation system (Liu et al., 2008) were used to assimilated altimeter data into ocean models, in order to optimize model settings and improve the precision of model results.

Yu (2006) compared parameters derived from Jason-1 and T/P, including sea surface wind speed, significant wave height, sea surface height and backscatter coefficient, during the verification phrase in the China seas and the northwest Pacific. The results showed that ocean circumstance parameters derived from Jason-1 were consistent with those from T/P. As a follow-on mission Jason-1 provides a continuous, high-accuracy altimetric survey. Chen et al. (200) compared T/P data with synchronous buoy observations to verify significant wave height and wind speed derived from T/P. The results showed that differences between T/P data and buoy observations were reduced by using narrow space

window and long sequence.

Significant wave height and wind speed are derived from the shape and intensity of the returned radar waveform, respectively. The error of altitude caused by the mispointing angle will influence severely the returned radar waveform received by altimetry. Liu (2006), Xu and Liu (2008) estimated and corrected the errors of the mispointing angle to improve the accuracy of altimeter data.

SSH data in the areas with lower than 50km close to coast lines are not able to be derived precisely by satellite altimetry. Jiang and Song (2010) indicated that reasons were from several aspects. The effect range of microwave sidelobe due to lands is about 5km. The adjustment distances are about 15km for stable positing when satellites fly across the land/sea interface. Another source of data loss is from microwave radiometer, which is used to correct atmospheric refraction. Because water vapor amount in the air can only be estimated accurately in the areas 50km away from coast lines.

Nowadays, the most limitation of altimeteric technology is that only SSH at nadir points can be derived from altimeter. The spatial and temporal samplings are not adequate, which limits the ability of altimeter data to access to shorter scale oceanic processes. To solve this problem, it is a good method to merge different satellite data sets. Chen et al. (2009) used several data fusion methods, such as inverse distance to a power, Kriging and successive correction, to merge significant wave height data from GFO, Jason-1 and Envisat. After numerical tests they found the suitable models and parameters. They analyzed the distributions of significant wave height in the China seas by using the models.

Besides merging different satellite data sets, new generation satellite altimeter with observing in wide swath can also be used to improve the spatial sampling. Yang (2007) designed a radar altimeter system based on the synthetic aperture technique. He applied the synthetic aperture technique and the echo signal processing technique into the traditional altimeter system. The Center for Space Science and Applied Research of the Chinese Academy of Sciences has designed a new radar altimeter, the China Imaging Altimeter, by integrating three techniques together, the off-nadir looking and height tracking measurement technique, the synthetic aperture technique and the interferometric technique (Zhang et al., 2009). This radar altimeter can increase the effective measurement point and reduce the time interval of sampling, which meets the requirement of modern marine research and the applications for spatial and temporal intervals of the parameters. Therefore, it has good application prospects in the observation of three-dimensional ocean surface, marine geoid surface, ocean currents, mesoscale eddies, ocean surface winds, waves, and tides and so on.

Ⅳ. Research of Chinese Satellite Altimetry

Based on the successful experiences of T/P and other satellite altimetry, China plans to launch the Chinese ocean dynamic environment satellite HY-2A in 2011. Altimeter is an important remote sensor mounted on the HY-2A satellite. This mission is helpful to improve the spatial-temporal sampling frequency for global ocean altimeter observations. A great amount of pre-launch experiments have been performed for the HY-2A satellite, including analysis of returned wave form, calibration, internal calibration, data process and retrieval algorithm.

The space borne altimeter flown on Chinese spacecraft Shenzhou-4 (SZ-4) has provided waveform data for the first time in China. Ji et al. (2007) analyzed the characteristics of the waveform data and performed the pro-process for the data. After eliminating abnormal waveforms and removing thermal noise they obtained normalized waveforms. And then they computed the range retracking correction

and the altimeter antenna pointing angle. The results showed that the antenna pointing angle was relatively stable while the range retracking correction varied considerably so that it should be considered as an error source when extracting the sea surface height.

Zhang and Lin (2007) introduced the methods of absolute backscatter calibration by transponder and microwave radiometer. Based on satellite altimeter's characteristics they presented some suggestions on choosing the calibration site and introduced some successful calibration sites and the calibration results. The work is objective to present the information on the Chinese satellite altimeter in the near future.

Xu et al. (2007) chose an internal calibration scheme for engineering design after comparing the methods used in different satellite altimetry. They estimated the attenuation and delay parameters and analyzed the error sources occurring in calibration channels.

Supported by the construction of HY-2 ground application system, Xu (2009) researched the data process and retrieval method of the HY-2 satellite altimeter. Refer to the data classification and the procedure of data processing used in Jason-1, the data classification method suitable for the HY-2 satellite altimeter has been established and the data were divided into level 0, level 1 and level 2. The data process of level 1B and level 2 were introduced in detail. The SZ-4 altimeter data were used as simulations for significant wave height retrieval. The methods to retrieve significant wave height have been performed in 6 steps, which included waveform's 1s average, thermal noise elimination, normalization, half power point calculation, waveform integration and significant wave height calculation. The method to estimate antenna mispointing angle has also been investigated. Furthermore, Xu et al. (2009) introduced some factors relate to altimeter orbit and sampling patterns, which included orbit height, eccentricity, orbit inclination and repeat cycle and so on. By analyzing the T/P altimeter orbit parameters, they presented the scheme of the HY-2 satellite altimeter orbit design and the sampling pattern.

Ⅴ. Conclusions

This paper introduces the progress of oceanic remote sensing by satellite altimetry in China since 2006. Satellite altimeter data were used to retrieve tides, currents, mesoscale variability, sea surface wind speed and sea surface wave by Chinese researchers. The data corrections and retrieval methods were also been investigated. The distributions and variations of oceanic parameters in the China seas and other areas have been analyzed with altimeter data used directly or assimilated into numerical models. Furthermore, China plans to launch the HY-2A satellite in 2011. This paper introduces the pre-launch experiments for altimetry mounted on the HY-2A satellite.

With the development of altimeter remote sensing technique, the precision of detecting will improve. And the time series of data sets will prolong on the basis of about 18 years. Furthermore, improvements of existing satellite altimeter remote sensing technique will enhance the spatial-temporal covering of data sets. Such as the next generation altimeter SWOT, which was introduced by Jiang and Song(2010). The SWOT is a kind of wide swath interfere altimeter using synthetic aperture radar technique, which works at the Ka waveband (about 35GHz). The scanning swath reaches 110km. The data cell of observations is 1km×1km with the data precision 1cm。There is no doubt that satellite altimeter data will be more widely used to detect oceanic parameters and operational applications, with the time series getting longer and the improvements of spatial-temporal sampling and precision of the data.

Reference

1. Chen H.,Hua F.,Yuan Y.,2006. Seasonal characteristics and temporal variations of ocean wave in the chinese offshore waters and adjacent sea areas, Advances In Marine Science, 24(4):407-415 (In Chinese).

2. Chen X.,Yang J.,Huang W.,Wang J.,Wang H.,Zhang R.,2009a. Research on the fusion methods of significant wave height data from multisatellite altimeters, Acta Oceanologica Sinica, 31(4):51-57 (In Chinese).

3. Chen X.,Yang J.,Huang W.,Zhang R.,Wang J.,2009b. Analysis on the temporal and spatial distribution of the wave height during Typhoon RANANIM with altimeter data, Journal of Marine Sciences, 27(4):10-16 (In Chinese).

4. Cheng, X., QI Y., 2008. Distribution and propagation of mesoscale eddies in the global oceans learnt from altimetric data, Advances IN MARINE SCIENCE, 26(4): 447-453 (In Chinese).

5. Cheng Y.,Liu Y.,Xu Q.,Zeng H.,Wen F.,2007. Effects of the wave state on TOPEX/Poseidon altimeter for retrieving winds, Marine Science Bulletin, 26(5): 11-16 (In Chinese).

6. Cheng Y.,Xu Q.,Liu Y.,Li C.,Gu Y.,2008. Verification and comparison of wind speed and significant wave height from TOPEX /Poseidon and Jason-1, Journal of Geodesy and Geodynamics, 28(6):117-122 (In Chinese).

7. Cui L.,Chen R.,2006. Study on gas transfer velocity of carbon dioxide across air-sea interface from dual-frequency altimeter measurements, Periodical of Ocean University of China, 36(Sup.Ⅱ):145-150 (In Chinese).

8. Gao L., Liu Y., Rong Z., 2007. Sea level anomaly and mesoscale eddies in the Kuroshio extension region, Transactions of Oceanology and Limnology, 1：14－23 (In Chinese).

9. Gao S.,Wang F.,Li M.,Chen Y.,Yan C.,Zhu J.,2007. Simulations of mesoscale eddies by assimilating altimeter data, Science in China, 37(12):1669-1678 (In Chinese).

10. Gu Y., 2009.Study on Wind Retrieval Algorithm for Altimeter at High Wind Speeds,Ocean University Of China, Master thesis (In Chinese).

11. Guo J., Fang W., Fang G., Chen H., 2006. The spatial and temporal variations of surface circulations in the South China Sea by analyzing 11-year altimeter data, Science Bulletin, 51(Sup.Ⅱ）:1－8 (In Chinese).

12. Guo J.,Guo P.,Zhou L.,2007. Calculation of sea surface roughness and extraction of wavelength in the Pacific Ocean, Transactions of Oceanology and Limnology, 1:24-29 (In Chinese).

13. He, Z., 2007. Study of mesoscal eddies in the subtropical ocean of the northwest Pacific and adjacent area, Ocean University of China, Doctor Thesis (In Chinese).

14. Hu, J., 2007. Studies about tidal harmonic analysis and climate changes from altimetric data, Ocean University of China, Master Thesis (In Chinese).

15. Hu, P., 2008. Interactions of ocean mesoscale eddies and the beginning of the Kuroshio, Institute of Oceanology, Chinese Academy of Sciences, Doctor Thesis (In Chinese).

16. Ji Y.,Zhang J.,Zhang Y.,Meng J.,2007. The pretreatment and information retrieval of waveform data of chinese spacecraft SHENZHOU-4 borne altimeter, Oceanologia Et Limnologia Sinica, 27(3):99-102 (In Chinese).

17. Jiang, B., Lv X., 2007. Three-dimensional numerical simulation of internal tides in the Bohai sea, the Yellow sea and the east China sea, Transactions of Oceanology and Limnology, 1: 30-37 (In Chinese).

18. Jiang X.,Song Q.,2010. Satellite microwave measurements of the global oceans and future missions, Science and Technology Review, 28(3):105-111 (In Chinese).

19. Leuliette, E.W., Nerem R.S. and Mitchum G.T., 2004. Calibration of TOPEX/Poseidon and Jason altimeter data to construct a continuous record of mean sea level change, Marine Geodesy, 27(1): 79-94.

20. Li R., 2007. Research on various periods of sea waves, Ocean University of China, Master Thesis (In Chinese).

21. Lin L., Hu J., 2006. Seasonal and interannual variations of sea surface geostrophic current in the Southeast Pacific, Marine Sciences, 30(6): 51－58 (In Chinese).

22. Liu B., 2006. The estimation and correction of mispointing on radar altimeter, The Center for Space Science and Applied Research of the Chinese Academy of Sciences, Master Thesis (In Chinese).

23. Liu J.,Wang B.,Yu Y.,Liu H.,2008. Assimilation of TOPEX/Poseidon data into a global ocean model and its analysis, Climatic and Environmental Research, 13(6):697-707 (In Chinese).

24. Lu F.,Song J.,Zhu X.,2010. A study of the parallel computation of the OVALS ocean data assimilation system, Computer Engineering and Science, 32(1):113-116 (In Chinese).

25. Ma, C., 2006.The variability of the Kuroshio and its effects on the current in the Taiwan strait, Ocean University of China, Master Thesis (In Chinese).

26. Qiao X. and Chen G., 2008. A preliminary analysis on the China sea level using 11 years'TOPEX/Poseidon altimeter data, Marine Sciences, 32(1): 60－64 (In Chinese).

27. Qiu Y. and Li L., 2007. Annual variation of geostrophic circulation in the Bay of Bengal observed with TOPEX/Poseidon altimeter data, Acta Oceanologica Sinica, 29(3): 39－46 (In Chinese).

28. Qiu, Z., He, Y., Li H. and Wang L., 2007. Progress of Oceanic Remote Sensing by Satellite Altimetry in China (2002-2006), 2003-2006 China National Report on Physical Sciences of the Oceans, Chinese National Committee for IAPSO.

29. Ren J.,Yan W.,Wang Y.,2007. Neural network method for retrieving sea surface wind speed from satellite altimeter, Ocean Technology, 26(2):47-50 (In Chinese).

30. Rong Z., Liu Y., Chen M., Zong H., Xiu P., Wen F., 2008. Mean sea level change in the global ocean and the south China sea and its response to ENSO, Marine Science Bulletin, 27(1): 1－8 (In Chinese).

31. Shi, X., Chen T., Yu K., 2008. Sea-level changes in Zhujiang estuary over last 40 years, Marine Geology and Quaternary Geology, 28(1): 127－134

32. Sun, L., Lv X., 2007. Study on bottom friction coefficient in the Bohai, Huanghai and east China seas, Transactions of Oceanology and Limnology, 2: 7-12 (In Chinese).

33. Wan L., 2006. Ensemble methods and applications to altimetry data assimilation in the Pacific, Institute of Atmospheric Physics, Chinese Academy of Sciences, Doctor Thesis (In Chinese).

34. Wang X., 2006. Researeh on retrieving wave period from satellite a1t1meters, Ocean University of China, Master Thesis (In Chinese).

35. Wang, Y., Fang G., Wei Z., Wang Y., Wang X., 2010. Accuracy assessment of global ocean tide models base on satellite altimetry, Advances in Earth Science, 25(4): 353-359 (In Chinese).

36. Wang Y.,Yu Z.,2009. Validation of impact of assimilation of altimeter satellite significant wave height on wave forecast in the northwest Pacific, Acta Oceanologica Sinica, 31(6):1-8 (In Chinese).

37. Wu Z., 2008. The Applications of Adjoint Method in Simulating Tides, Mathematics In Practice And Theory, 38(11):61-66 (In Chinese).

38. Xiao J.,Wang D.,Yan C.,Zhu J.,2007. Three-dimension variational assimilation model and its validation in the South China Sea, Progress In Natural Science, 17(3):353-361 (In Chinese).

39. Xie X.,Li Y.,Xu W.,Zheng L.,Lin M.,2009. The analysis of the characterstics of wind and wave fields over the surrounding waters of Taiwan Island using TOPEX satellite altimeter data, Acta Oceanologica Sinica, 31(5):1-9 (In Chinese).

40. Xu X.,Liu H.,2008. Accuracy of altimeter attitude angel estimation by waveform tracking, Journal of the Graduate School of the Chinese Academy of Sciences, 25(1):54-60 (In Chinese).

41. Xu X.,Liu H.,Xu K.,2007. Engineering design and error analysis of HY-2 radar altimeter in-orbit calibration, Remote Sensing Technology and Application, 22(2): 141-146 (In Chinese).

42. Xu Y.,2009, The study on retrieval method of significant wave height of HY-2 satellite altimeter, Ocean University of China, Master Thesis (In Chinese).

43. Yan T.,Zhang Y.,Hu B.,2009. Simulating wind-generated waves in hurricane DEAN with SWAN nested in WAVEWATCH, Transactions of Oceanology and Limnology, 4: 1-7 (In Chinese).

44. Yang L.，2007，Temporal and spatial characteristics analysis of sea surface wind on the northwest Pacific based on remote sensing data，The first Institute of Oceanography, SOA, Master Thesis (In Chinese).

45. Yang, S., 2008.Observations and research on Vietnam cold eddies and eddy-induced upwelling current, Ocean University of China, Master Thesis (In Chinese).

46. Yang, S., 2007. Technology research of radar altimeter based on synthetic aperture techniques, The Center for Space Science and Applied Research of the Chinese Academy of Sciences, Doctor Thesis (In Chinese).

47. Yao, X., 2009.Research of M_2 internal tide energy flux in Hawaii ocean based on HAMSOM model simulation, Ocean University of China, Master Thesis (In Chinese).

48. Yu Z., 2006. The cross-calibration,validation and merging of Jason-1 and TOPEX/Poseidon data in the China seas and northwest Pacific Ocean, Ocean University of China, Master Thesis (In Chinese).

49. Zhai P., Lin X., Wu D., 2007. The characteristics of high frequency oscillations in the world ocean, Periodical of Ocean University of China, 37(Sup.Ⅱ): 39－43

50. Zhang, J., 2008.Development and application of a three-dimensional numerical barotropic adjoint assimilation tidal model, Ocean University of China, Doctor Thesis (In Chinese).

51. Zhang R.,Yang J.,Huang W.,Zhang H.,Chen X.,Wang J.,2009. Imaging mechanism and possible oceanographic applications of China Imaging Altimeter, Journal Of Marine Sciences, 27(3):99-102 (In Chinese).

52. Zhang X., Xiu Y., Liu J., Su G., Wang Q., 2008. The determination about the bifurcation latitude of the NEC and its variations, Marine Forecasts, 25(2): 33－41 (In Chinese).

53. Zhang Y.,Lin M.,2007. Hemolytic Activity Inspection of a New Red Tide Organism Karlodinium micrum, Marine Science Bulletin, 26(3): 87-116 (In Chinese).

54. Zhao, W., 2007.Seasonal variation of the water exchange in Luzon Strait, Institute of Oceanology, Chinese Academy of Sciences, Doctor Thesis (In Chinese).

55. Zheng G.,Zhao H.,Xu F.,2010. Numerical simulation of wind waves in Bohai Sea induced by“98·04”cold wave, Port and Waterway Engineering, 2: 36-39 (In Chinese).

56. Zhou, H., Guo P., Xu J., Liu Q., 2007. The characteristics of the eddies east of Taiwan island and the Kuroshio in east China sea, Periodical of Ocean University of China, 37(2): 181-190 (In Chinese).

57. Zhou Z.,Yang X.,2008. Numerical simulation of wave filed in South China Sea using WWATCHⅢ, Journal Of Tropical Oceanography, 27(2):1-6 (In Chinese).

58. Zhu J.,Zhou G.,Yan C.,Fu W.,You X.,2007. Design and primary applications of a three dimensional ocean variational assimilation system, Science in China, 37(2): 261-271 (In Chinese).

MODEL STUDIES ON THE EFFECTS OF PHYSICAL PROCESSES TO THE COASTAL ECOSYSTEMS

Hao WEI [1],Liang ZHAO[2],Yuheng WANG[2],Jie SHI[2],Luning WANG[2] and Chengyi YUAN[2]

(1 Tianjin University of Science and Technology, College of Maine Science and Engineering, Tianjin, 300457 .

2 Key Lab of Physical Oceanography, Ocean University of China, 238. Rd., Songling, Qingdao, Shandong, 266100, PR China. E-mail: weihao@ouc.edu.cn)

Physical and biological coupled NPZ-like ecosystem models are developed in the Bohai Sea, Yellow Sea and East China Sea. The annual cycle of phytoplankton biomass, nutrients concentration and new production are simulated reasonably. Their distribution and seasonal variations are reproduced by three dimensional studies. Numerical experiments show that vertical mixing can both affect the vertical transportation of nutrients and the horizontal distribution of primary production. The weaker the mixing, the higher the primary production when the nutrients and temperature adequate. Water column steadiness (PEA) almost the trigger of the spring blooms. Weak turbulence under weak monsoon could maintain the alge in the euphotic zoon longer and allow the quick increasing of phytoplankton biomass. Horizontal advection affects the relative magnitude of the phytoplankton bloom and convergence along tidal fronts could induce high biomass and new production. The migration of anchovy in the Yellow Sea is also modeled using an Individual-Based Model (IBM). Hydrodynamic model(HYCOM) and planktonic ecosystem model（NEMURO）were used to provide physical environments and food for different ages of anchovy. Swimming speed was determined by food and temperature conditions fit for their living. Interannual variation from 1982-2004 were simulated. Two production peaks in a year were found. The overwinter ground was consistent with the extent of the Yellow Sea Warm Current. An IBM for *Calanus sinica* (zooplankton) is in construction now. Twelve life stages are considered and the influence of Yellow Sea Cold Water Mass on zooplankton growth was tested with one dimensional model. The cold water as the refuge of C. Sinica induced its diapause in summer which could affect on the zooplankton distribution and secondary production. A 3D biophysical model was developed in a typical mariculture area, Sangou Bay, to estimate the biomass of kelp grow there on the raft. The drags induced by the rafts at the surface and by the kelp in the water column were added to the hydrodynamic model. It was found that the establishments and kelp could damp the tidal current in the bay by 45% and increase the water exchange time by 75%. Thus the nutrients input from the outside and release from the bottom is limited which limited the maximum biomass of the kelp. Decrease the mariculture density to 90% of nowadays could get the most fitted current. A microloop model was also developed by adding bacteria as variable in NEMURO in the Yellow Sea. Food from microloop was estimated to be 14-30% of the total consumption of zooplankton in different seasons.

References:

1. WEI Hao, SUN Jun, Andreas Moll and ZHAO Liang，Phytoplankton dynamics in the Bohai Sea--observations and modelling，Journal of Marine System, 2004,vol.44：233-251

2. Liu Zhe，WEI Hao, Liu Guangshan and Zhang Jing. Simulation of water exchange time in Jiaozhou Bay with Half-life time concept. Estuary, Coast and Shelf Sea Science, 2004,61:25-35

3. Tian Tian, Wei Hao, Su Jian, Chung CS. Simulations of annual cycle of phytoplankton production and the utilization

of nitrogen in the Yellow Sea. Journal of Oceanography, 2005, vol.61（2）：343-357.

4. Zhao Liang and Wei Hao. The influence of physical factors on the ecosystem dynamic of the Bohai Sea. Journal of Oceanography ,2005，vol.61(2), pp.335-342.

5. Zhao Liang, Wei Hao et al. An adjoint data assimilation approach to estimate key parameters for a three-dimensional coupled physical and biological model. Ecological Modeling, 2005，186, 234-249.

6. Liu Z. Y., H. Wei. Estimation to Turbulent Kinetic Energy Dissipation Rate and Bottom Shear Stress in the Tidal Bottom Boundary Layer of the Yellow Sea. Progress in Nature Sciences, 2007,vol.17(3):289-297

7. Liu, Z., H. Wei, J. Zhang, J. Bai, D.Y. Liu, S. Liu. Nutrients seasonal variation and budget in Jiaozhou Bay, China: A 3-dimensional physical-biological coupled model study, Water, Air & Soil Pollution Focus, 2007, 7:607-623

8. Shi Jie, Wei Hao, Zhao Liang, Fang Jianguang, Zhang Jihong. Multi-species aquaculture ecosystem model study in a typical raft culture bay of China. GLOBEC News Letter，Sept. 2009

9. Wei Hao, Shi Jie, Lu Youyu, Peng Yuan. Hydrographic changes in the Yellow Sea as a response to climate events. Deep-Sea Research II，2010，57：1025–1034

10. Fan Xing, Wei Hao, Zhao Liang and Yuan Ye. The Effects of Aquaculture Establishments on Hydrodynamic Structures in Coastal Mariculture Area. Accepted by CSR，

11. Shi Jie, WEI Hao, Zhao Liang, Fang Jianguang, Zhang Jihong. Milti-trophic level aquaculture ecosystem model in Sangou Bay I—model establishment and sensitive analysis. Advances in Fishery Science. 2010, 31(4): 26-35(in Chinese with English abstract)

12. Shi Jie, WEI Hao, Zhao Liang, Fang Jianguang, Zhang Jihong. Milti-trophic level aquaculture ecosystem model in Sangou Bay II—simulation to annula cycle of alge biomass and nutrients. Advances in Fishery Science. 2010, 31(4): 36-42(in Chinese with English abstract)

13. Shi Jie, WEI Hao, Zhao Liang, Fang Jianguang, Zhang Jihong. Milti-trophic level aquaculture ecosystem model in Sangou Bay III—numerical study on the kelp culture capacity. Advances in Fishery Science. 2010, 31(4): 43-52(in Chinese with English abstract)

14. Jun HAN, Hao WEI, Jie SHI, Liang ZHAO. Observations of the phytoplankton spring bloom in the central Southern Yellow Sea: effects of horizontal advection，Acta Oceanologia Sinca，accepted

15. Zhao Liang, Wei Hao, Simulation on phytoplankton system variation of Jiaozhou Bay for recent 40 years. 3rd China-Japan-Korea GLOBEC, Hokodate, Dec, 11-16, 2007

16. Wei Hao and Zhao Liang. Ecosystem model study in the coastal water of China. PICES 17th annual meeting, Dalian, Oct. 2008

17. Shi Jie, Wei Hao and Zhao Liang. Aquaculture carrying capacity model in a typical raft culture bay of China. 18th PICES annual meeting, Oct. 2009, Cheju, Korea

18. Wang Yuheng, J. Kishi, Wei Hao. IBM of anchovy in the Yellow Sea. LMEYS, Xiamen, Feb，2010, China

19. Wang Yuheng, Wei Hao, Zhao Liang & Kishi. Simulation to the interannual variation of the Anchovey population in the Central Yellow Sea. 4th CJK GLOBEC, May. 2010, Cheju Island, Korea.

THE KUROSHIO AND THE INTERACTION WITH CURRENTS IN ITS NEIGHBORING CHINESE SEAS AND THE RYUKYU CURRENT

YUAN Yaochu, YANG Chenghao and LIAO Guanghong

(State Key Laboratory of Satellite Ocean Environment Dynamics, Second Institute of Oceanography, State Oceanic Administration, Hangzhou 310012, P.R. China)

On the study of the Kuroshio and the interaction with Currents in its neighboring Chinese Seas, a lot of the works were made and reviewed by the Chinese scientists during July of 2006- July of 2010. In this paper these works will be reviewed and can be divided into four aspects, namely the Kuroshio near the Luzon Strait and east of Taiwan, Kuroshio in the East China Sea (ECS), Numerical computed results for the Kuroshio and the currents east of the Ryukyu Islands.

Ⅰ Kuroshio near the Luzon Strait and east of Taiwan

1. Numerical computed results with the observed currents and hydrographic data

The Luzon strait is the deepest passage from the Pacific Ocean to the South China Sea (SCS). There have been studies on the westward intrusion of the Kuroshio into SCS via the Luzon Strait for several decades. We shall discuss and review these works by the Chinese scientists during July of 2006- July of 2010 as follows.

On the basis of the wind data from NCEP and hydrographic data obtained from April 22-May 24, 1998, Yuan et al. (2007) computed the circulation in the South China Sea（SCS）using three dimensional diagnostic models. The main numerical results with SSHA derived from T/P altimeter were as follows: most of intruded Kuroshio bypasses. However, a part of Kuroshio intrudes westward above 300 m levels. This intruded westward flow is narrowly confined to the continental slope south of China. Their most important dynamical mechanism is due to the joint effect of the baroclinity and relief. The second dynamical mechanism is due to the interaction between the wind stress and relief. The topography effect is more important than the ß effect (Yuan et al., 2007). In the spring season in the other years there were the following works:

On the basis of current measurements at the mooring station and hydrographic and wind data obtained in the Luzon Strait during spring 2002, the numerical calculation and comparison of circulation were implemented by the aid of a diagnostic model with a modified inverse method (Yuan et al., 2008b). Their numerical results showed that at depths above 400 m, most of the Kuroshio bypasses the South China Sea (SCS) near the Luzon Strait. However, both the observed and modeled results show part of the Kuroshio flows westward to intrude into the area around the continental slope south of China, and the net westward volume transport across the longitudinal section of 120°33′ E is about 0.82 ×106 m3s-1 in the upper layers from the sea surface to 400 m level. At depths below 400 m, the directions of flow east of 120°57′ E are mostly eastward, and the net eastward volume transport across the longitudinal sections of 121°09′ E and 121°15′ E both are about 2.4 × 106 m3s-1 in the middle layers between 500 m and 1200 m. This indicates the SCS water with a higher oxygen concentration flows eastward into the eastern side of the Luzon Strait in the middle layer. Comparison between the observed and modeled results shows they agree basically with each other (Yuan et al., 2008b).

Yuan et al. (2009b) pointed out that 1）the vertical structure of the currents in the Luzon Strait suggests strongly the sandwiched structure of the LST, even though the bottom part of the profile is not resolved by the observational grid. 2) The spectral analyses show the following periods of significant spectral peaks: (a) the tidal currents variability in the vertical direction; (b) the period about 4－6 d for the two cases of frequency f＞0 and f＜0 at the 200 and 500 m levels, but at the 800 m level only for the case of f＞0; (3) The fluctuation in the period range is about 2－3 days for the two cases of f＞0 and f＜0 at the 200, 500 and 800 m levels, namely the Luzon Strait currents exhibit significant synoptical variability throughout the water column up to 800 m deep. Both direct current measurements and in situ hydrographic and satellite survey suggest no Kuroshio loop current in the Luzon Strait during the spring of 2002(Yuan et al., 2009b).

Wind data from NCEP and Hydrographic data obtained during March 8 to 27, 1992 had been used to compute circulation in the Luzon Strait and the northern South China Sea using three-dimensional diagnostic models with a modified inverse method (Yuan et al., 2009a). Their numerical results are as follows: the main Kuroshio is located above 800 m levels. It has two intrusive branches of the Kuroshio in the areas above 400 m. One part intrudes anti-cyclonically northwestward, then flows through the area above 200 m southwest of Taiwan and into the Taiwan Strait. The other part intrudes westward and flows cyclonically in the areas north of the cyclonic eddies, then flows southward through the southern boundary of the region. The net westward volume transport (VT) through Section at 120°15′E between Luzon Island and Taiwan Island is about 3.0 Sv, net northward VT through northern boundaries into the Taiwan Strait is about 1.4 Sv and net southward VT through southern boundaries is about 1.6 Sv, which finally flows into the Karimata and Mindoro Straits. In the areas above 400 m east of 117°15′E, the circulation is mainly dominated by the basin-scale cyclonic gyre, which consists of two cyclonic eddies. However, in the areas below 400 m east of 119°00′E, the circulation is mainly dominated by basin-scale anti-cyclonic gyre. The joint effect of baroclinity and relief and interaction between wind stress and relief are important in different area respectively for the pattern of the depth-averaged flow across contours of fH^{-1} (Yuan et al., 2009a).

For winter season Liao et al (2008) computed the three-dimensional structure of circulation in the South China Sea (SCS) using a three-dimensional diagnostic model on the basis of hydrographic data obtained from 28 November to 27 December, 1998. Their results showed that the net westward volume transport through section CD at 119.125°E from 18.975° to 21.725°N is about 10.3×10^6 m^3s^{-1} in the layer above 400 m level. The most important dynamic mechanism generating the circulation in the SCS is a joint effect of the baroclinicity and relief (JEBAR), and the second dynamical mechanism is an interaction between the wind stress and relief (IBWSR).

Yuan et al (2008a) computed the circulation in the northern South China Sea and near Luzon Strait using three-dimensional diagnostic models with a modified inverse method on the basis of wind data from NCEP and hydrographic data obtained from August 28 to September 10, 1994. The numerical results showed that the main Kuroshio is located above 400 m levels near Taiwan's eastern coast and above 800 m levels away from it. Near Luzon Strait above 400 m levels a branch of the Kuroshio joins with a part of the northward current, which comes from an area west of Luzon's western coast and intrudes northwestward, then it branchs into western and eastern parts near 20°30′N. The eastern part flows northward into an area east of Taiwan, while its western part continues to intrude northwestward, flowing through an area southwest of Taiwan. Net westward intruded volume transport through longitude Section AB at 121°00′E from 19°00′N to 21°43′N is about 3.5×10^6 m^3s^{-1} in a layer above

400 m levels. The joint effect of baroclinity and relief and interaction between wind stress and relief both are important for real forcing of flow across contours of fH^{-1} in effecting the circulation pattern (Yuan et al, 2008a).

CTD measurements along 120 ℃E (18.5 ° N—21.5 ° N) during July and August, 2007 are used to examine water exchange in the Luzon Strait (Bao et al., 2009). The distribution characteristics of temperature，salinity and density are analyzed．Bao et al. (2009) calculated the velocity and the volume transport through the strait by using dynamic calculation．Their major results show that the water flows from the South China Sea (SCS) to the Pacific between 19º 30'N and 20 º 30'N, but from the Pacific to the SCS to the south of 19º 30'N and from 20 º 30'N to21 º 30'N．Water exchange is mainly from the SCS to the North Pacific with the total volume transport of about 3.15 Sv．Moreover，the maximum velocity at the surface flowing out and into the SCS can reach 1.3 m／s and 60 cm／s respectively, while the latter appears to the south of 19º 30'N．

Based on the long series of current velocity data from the new version of SODA reanalysis, and data of temperature and salinity on 137 ℃E section, Cai et al. (2009) calculated the transport on 4 main sections of the source and adjacent areas of Kuroshio and analyzed the annual cycle and long-term variations. Their results indicated that 1) the transport of the main Kuroshio sections have strong seasonal and striking inter-annual and inter-decadal variations. 2) The correlation analysis showed that there were strong independences among the variations of the transport in main sections of Kuroshio. Among them the short climate changes are likely related to the tropical Pacific inter-annuM variation, while the inter-decadal variation could be possibly associated with the North Pacific inter-decadal variations and subtropical meso-scale eddy.

2.Numerical simulation and the dynamics of Kuroshio in the Luzon Strait

Zhao et al. (2007) used the Princeton Ocean Model (POM) to simulate the seasonal variation of water exchange in the Luzon Strait．The model domain covers the North Pacific(20 ℃S—60 ℃N, 100 ℃E—70 ℃W) with closed boundaries．A variable horizontal grid was set up with the finest grid of 0.25 °in the South China Sea(SCS)．Their results showed that 1) the Luzon Strait Transport (LST) had seasonal variations．Except for the eastward LST in May(1.0Sv) and June(0.9Sv)，westward LST dominates from July to the next April．The LST increases rapidly from July (1.6 Sv) to November(14.0 Sv)，and decreases from December (13 8 Sv)to the next April (3.1 Sv). In the depth above 500m, a clear branch of the Kuroshio intrudes the SCS from winter to spring, and this branch disappears from summer to fall．Below 500m, the Kuroshio affects the LST less significantly because the bifurcation latitude of the North Equatorial Current moves northward．Furthermore, they divided the velocity field of Luzon Strait into upper and lower layers at the depth at which the flow direction remains the same to the surface one．They called it the sign-changing depth．2) The annual mean net transport is -7.6Sv in the upper layer and 1.8 Sv in the lower layer ("-"" indicates the net LST is to the westward). The sign-changing depth varies seasonally to an extent of several hundred meters with the maximum depth near l800 m in the middle of the section．

Chen et al (2009) studied the seasonal variation of Kuroshio in Luzon Strait, and the regional ocean modeling system (ROMS) was applied to simulate the current pattern in Luzon Strait. ROMS was used to simulate the monthly averaged zonal velocity and zonal volume transports at the 120. 75 ℃E cross-section and compared with the measured data and other results. Their results indicated that the Kuroshio exists in the form of front in spring and summer, there are flows originated from the SCS afflux into the Kuroshio in summer. But in fall and winter, the Kuroshio flows invade the SCS in the form of a current loop, with a part of it turns back into the main current along the south of Taiwan.

Especially in winter, a branch of it invades the SCS.

The dynamics of eddy-induced Kuroshio variability in the Luzon Strait are studied using a 1.5 layer reduced gravity quasi-geostrophic model (Yuan and Li, 2008). Their model experiments suggest that 1) when the Kuroshio is close to the critical states of hysteresis, both cyclonic and anti-cyclonic meso-scale eddies can induce transition of the Kuroshio path from an anti-cyclonic intrusion to a gap-leaping state in the Luzon Strait, whereas only cyclonic eddies can force the Kuroshio from the leaping path to an penetrating path. 2) The dynamics of the path transition is related to the hysteresis of the Kuroshio in the Luzon Strait, whereby multiple steady states exist in the nonlinear system so that the path of the Kuroshio cannot return to its initial state after the external force is removed. 3) When the Kuroshio is far away from the critical states of hysteresis, its path is not sensitive to eddy perturbation. In this case, the gap-leaping Kuroshio blocks the westward propagation of meso-scale eddies in the Luzon Strait and pushes the eddies to migrate northward along the eastern side of the Luzon Strait.

3.Studies of the Kuroshio and the eddies using data from the ARGO profiling data and Altimeter data

Zhou et al. (2007) studied the vertical structure of the eddies east of Taiwan Island by using the ARGO profiling data and Altimeter data. Their analysis indicated 1) that these eddies are very energetic with a vertical extent of 2 000 m and a horizontal scale of 200 km. The tangential velocity at the surface is about 60 cm/s, which is almost equal to that of the Kuroshio while the tangential velocity at 1 000 m is about 8cm/s. 2) According to the altimeter data, these eddies are caused by the westward propagating Rossby wave which generated from the STCC. The Rossby deformation radius is about 43 km with a phase speed of 4.2 cm/s. 3) The drifting speed of the ARGO Profiling Float suggests that the Kuroshio in the East China Sea can be divided into three parts at 1 000 m.

Ⅱ Kuroshio and its interaction with the currents and the mesoscale eddies in the East China Sea

As Chen et al. (2009) stated, off the east coast of the Taiwan Island, the Kuroshio strides over the Ilan Ridge and flows into the East China Sea, where it encounters the continental break. The Kuroshio then turns right and flows along the Okinawa Trough; its main axis does not show significant swaying there due to topographic restrictions. This stream continuously flows eastward southwest of Kyushu and feeds into the sea south of Japan. This section of the Kuroshio is named as "the East China Sea Kuroshio". We review on the study of the Kuroshio and its interaction with currents and the mesoscale eddies in the East China Sea by the Chinese scientists during July of 2006- July of 2010 as follows.

1.Overview of studies on the Kuroshio and some cyclonic and anti–cyclonic eddies in the East China Sea

Overview of studies on the Kuroshio and some cyclonic and anti–cyclonic eddies were made in the East China Sea (Yuan and Guan, 2007). In the continental shelf above 200 m level in the East China Sea (ECS), they discussed mainly an anti-cyclonic eddy in southwestern part of the ECS, a cyclonic mesoscale eddy southwest of Cheju Island and a cyclonic eddy northeast of Changjiang. In the region near continental slope and both sides of the Kuroshio in the ECS, there are some mesoscale eddies with the different scales, and one of their dynamical causes may be due to the Kuroshio meander in the ECS. The second dynamical causes are related to the topographic relief and existence of Ryukyu Islands. There are two types of the meanders of the Kuroshio in the ECS: the Kuroshio front meander and the Kuroshio path meander. For the Kuroshio front meander, their time and space scales and the structure of the Kuroshio frontal eddy were reviewed (see Yuan and Guan, 2007). For the Kuroshio path meander, Yuan and Guan (2007) discussed the mesoscale cyclonic and anti-cyclonic eddies on both sides of the

Kuroshio and the variability of their character. Especially, they discussed with emphasis the interaction between the Kuroshio path meander and the mesoscale eddy, and pointed out that the following fact. When the growing cyclonic eddy in the northern Okinawa Trough dominates variability at periods of 1-3 months and its scale grows to about 200 km corresponding to the zonal scale grows to about Okinawa Trough, the Kuroshio path translates from the southern path to southern one. Yuan and Guan (2007) also reviewed the interaction between the volume transport of the Kuroshio in the ECS and the mesoscale eddy.

2. Variability of structure of the Kuroshio and volume transport (VT) of the Kuroshio in the East China Sea

On the basis of the data obtained in cruises of April and May 2002 onboard the R/V Chofu Maru of Japan Meteorological Agency and the satellite wind data of QuikSCAT during April and May 2002, the velocity and volume transport (VT) of the currents in the East China Sea were computed by using the modified inverse method (Yang et al., 2007). In the meantime, analyzing the ARGOS satellite-tracked drifters data in 2002 and the simultaneous sea surface height anomalies merged data of CLS AVISO, Yang et al. (2007) pointed out that 1) The Kuroshio only has one core at the section PN. the net northeastward VT through Section PN is about $34.7\times10^6 m^3/s$, including Taiwan Warm Current, Kuroshio in the East China Sea and the anticyclonic eddy east of the Kuroshio, 2) The Kuroshio has two cores in the Tokara strait, and its VT is about $25.6\times10^6 m^3/s$, and then flows towards Section ASUKA. 3) The VT of Kuroshio through Section ASUKA in the first layer mostly comes from the Kuroshio in the Tokara strait. In the second and third layers, it comes from the northward current east of the Amami-Oshima Island and the Kuroshio in the Tokara Strait, and their VTs equal approximately. From analyzing the drifts' data, a part of current east of the Amami-Oshima Island comes from the area east of Section AM, and then it flows through Section ASUKA.

Chen et al. (2009) collected long-term hydrographic temperature and salinity transect data in the East China Sea from June 1955 to November 2001, 175 data sets are analyzed in order to examine the geostrophic velocity and the structure of the Kuroshio current. Chen et al. (2009) pointed out that 1) the structure of the Kuroshio Current is divided into three basic forms, a single-core structure, a double-core structure and a multi-core structure; the appearance percentage of the three forms are 53.1%, 31.4%, and 15.4%, respectively. 2) The analysis suggests that multi-core structures have significant seasonal and interannual variabilities that are not fully understood but may relate to variations in transport and associated flow instabilities. 3) The Kuroshio's spatial character is also analyzed in detail by applying a simplified model of motion instability into this multi-core structure of the East China Sea Kuroshio. The theoretical analysis indicates that the space between cores is consistent with the observations, while the growth time scale and the moving speed calculated from the simplified model suggest that the sub-circulations have enough time to be developed in the main Kuroshio current.

3 Studies of the Kuroshio using data from the satellite remote sensing and tracing technology, Argos satellite-tracked surface drifters

Recently, with the development of the satellite remote sensing and tracing technology, Argos satellite-tracked surface drifters have been widely used in ocean circulation studies, such as the Tropical Ocean Global Atmosphere program (TOGA) and the World Ocean Circulation Experiment-Surface Velocity Program (WOCESVP). Since the 1990s, China has used Argos drifters in some oceanographic research projects and released a great number of drifters in the KC and adjacent regions. Ma et al. (2010) combined Argos drifter buoys and TOPEX/POSEIDON altimeter data and

established the time serried of sea-surface velocity fields in the Kuroshio Current (KC) and adjacent regions. Their results showed that the variability of the KC from the Luzon Strait to the Tokara Strait is studied based on the velocity fields. The results show that the dominant variability period varies in different segments of the KC: The primary period near the Luzon Strait and to the east of Taiwan Island is the intra-seasonal time scale; the KC on the continental shelf of the ECS is the steadiest segment without obvious periodicity, while the Tokara Strait shows the period of seasonal variability. The diverse periods are caused by the Rossby waves propagating from the interior ocean, with adjustments in topography of island chain and local wind stress.

Hu et al. (2008) studied the multi-year averaged surface current field and seasonal variability in the Kuroshio and adjacent regions. The data used in this study are trajectories and (1 / 4 °) latitude by (1 / 4 °). Longitude mean currents derived from 323 Argos drifters deployed by Chinese institutions and World Ocean Circulation Experiment from 1979 to 2003. Their results showed that the Kuroshio surface path adapts well to the western boundary topography and exhibits six great turnings. The branching occurs frequently near anticyclonic turnings rather than near cyclonic ones. At the Luzon Strait, the surface water intrusion into the South China Sea occurs only in fall and winter. The Kuroshio surface path east of Taiwan appears nearly as straight lines in summer, fall, and winter, when anticyclonic eddies coexist on its right side; while the path may cyclonically turning in spring when no eddy exists. The Kuroshio intrusion northeast of Taiwan often occurs in fall and winter, but not in summer. The running direction, width and velocity of the middle segment of the Kuroshio surface currents in the East China Sea vary seasonally. The northward intrusion of the Kuroshio surface water southwest of Kyushu Occurs in spring and fall, but not in summer. The northmost position of the Kuroshio surface path southwest of Kyushu occurs in fall, but never goes beyond 31 °N. The northward surface current east of the Ryukyu Islands exists only along Okinawa—Amami Islands from spring to fall. In particular, it appears as an arm of an anticyclonic eddy in fall.

Feng et al. (2010) also use the data of the Argos drifters at the selected area (21 °~33 °N, 120 °~132 °E) from 1979 to 2008 to analyze the characteristics of Kuroshio in the East China Sea (ECSK) and the seasonal variability. Especially at the middle segment of ECSK, the current speed is stronger, the current width is wider, and the volume transport is greater. All those features at the middle segment of ECSK become the most significant and the most stable.

4 Interaction between the Kuroshio and the currents in the East China and Yellow Seas

Swath data from the Tropical Rainfall Measuring Mission microwave imager of sea-surface temperatures (SST) from 1998 to 2005 have been used to analyze the climatology and seasonal variability of the SST fronts in the Yellow and East China Seas (YES) by Huang et al. (2010). Huang et al. (2010) pointed out that seven fronts have been identified and placed into three categories, namely, (1) the shelf-break front (Kuroshio Front), (2) the coastal fronts (Zhe-Min, Jiangsu, Shangdong Peninsula, Western Korean, and Western Chejudo Fronts), and (3) the shelf front (Western Yellow Sea Shelf Front). They revealed that the Kuroshio Front exists from December through May, with the maximum SST gradient and highest frontal probability in April. The five coastal fronts exist year-round, all with their maximum SST gradient and highest frontal probability in February. The shelf front in the western Yellow Sea exists only from January to March. Frontogenesis in winter is due to effects of both air–sea heat exchange and advection by currents. The coastal fronts in the stratifiedmonths are expressed as tidal fronts. The coastal frontal zones coincide with the major spawning grounds of fish in the YES. The overwintering fishery ground in the Yellow Sea overlaps with the narrow band of favorable water temperature in the frontal zone. The overwintering grounds in

the East China Sea are broad and bounded by fronts.

Qu et al. (2010) studied the dynamic response of the East China Sea shelf-water to the strong shear of the Kuroshio. They considered the potential vontex equation for homogeneous sea water, the horizontal friction, the bottom friction, and the topographic uplifting effect, and Fourier transform is employed to obtain the analytic solution of the equation. Their results showed that the current loop induced from the shear and the water upwelling were limited into the sea area closely adjacent to the shear, consistent with the satellite images in which a cold eddy is located in the sea are northeast of Taiwan Island.

Zhou et al. (2009) studied variations of the Changjiang Diluted Water between August of 1999 and 2006. They found that 1) a large area of low dissolved oxygen bottom water has been a distinctive oceanic phenomenon in the Changjiang River Estuary and its adjacent areas in recent years. The hypoxic zone shows distinct year-to-year variations. These great changes are related to the tremendous reduction of the freshwater discharge and variations of wind fields between these two years. 2) the monthly mean intrusion of Kuroshio and its branches has increased in the north of East China Sea (ECS), but decreased in the south of ECS in August 2006 comparing with 1999 on the base of general circulation models. 3) The Regional Ocean Modelling Systems is applied to the ECS to evaluate the contributions and relative importance of impacts from the river discharge, wind forcing and open boundary data. The simulations reproduce the phenomena that more fresh water extends northeastward in 2006 and forms a negative SSS anomaly to the northeast of the river mouth comparing with 1999, which is consistent with observations. The five group numerical tests suggest that the wind forcing dominates the CDW variations followed by the Kuroshio and its branches (Zhou et al, 2009).

Zheng et al. (2009) studied the relationship between the Taiwan Warm Current (TWC) and Tsushima Warm Current (TSWC) using the ocean baroclinic model. Their results showed that the TWC has little effect on the TSWC, while the TSWC has a significant effect on the TWC. A source-sink driven mechanism along isobaths may be used to explain this phenomenon. The perennial northward flow through the Tsushima Strait pumps the response over the northern shelf in the ECS that gives rise to the TWC. Although the TSWC is located at the “downstream” region, it could induce about 0.5 Sv to TWC in annual mean values.

Ⅲ Numerical computed results for the Kuroshio

YANG et al (2010) used the two dimensional global free surface diagnostic model, combined with dynamic calculation to investigate the world ocean circulation; the model has a horizontal resolution of 1/4 °×1/4 °. Their simulated results agreed well with the results of other models and observations. The distribution of Stream Function suggested that the main circulation systems in the world ocean had been represented, including oceanic currents strengthened in the oceanic western. Be close to the observed results, the net mass transport of the Kuroshio axes is estimated about 54Sv; The distribution of the horizontal circulation in each layer shows that the main circulation systems in the world ocean are well simulated, for example, the Kuroshio and the Antarctic Circumpolar Current can go down to the bottom layer, but the Gulf Stream cannot, and its direction reverses at the depths of 1 000 to 2 000 m.

Zhao et al (2009) used a Hybrid Coordinate Ocean Model (HYCOM) to simulate the current field of the Northwestern Pacific. Their result using the Northwest Pacific regional model showed 10 the typical characteristic of Kuroshio Current. 2) The interplay of Kuroshio with Luzon strait reveals the multiple equilibrium, which is influenced by topography and beta effect. 3) There are several types of Kuroshio’s meander South of Japan whose time scales are apparently different from seasonal to

interannual). 4) In addition to the stability of Kuroshio at PN section(East China Sea), its velocity structure agrees with corresponding observations. 4) The volume transport of Kuroshio at East Taiwan. East China Sea and Turara Strait accord with the observation although they are distinctive.

Bai at el. (2010) used a triply nested HYbrid Coordinate Ocean Model (HYCOM) to simulate the climatological Kuroshio in the East China Sea. Their numerical results showed that (1) The higher-resolution model can improve the simulation results of Kuroshio, which is mostly caused by better representation of topography and baroclinicity; (2) The higher-resolution model results reproduce the water vertical structure of PN section, and generally reflect seasonal following conclusions can be deduced from the variation rule of current velocity and volume transport at PN section. In summer, current velocity is the strongest and volume transport is the largest, while in autumn, current velocity is the weakest and volume transport is the least, and the values in winter and spring are between those of summer and autumn; (3) The model successfully simulates the countercurrent east of Kuroshio, which is steady and comparatively larger in summer; (4) The model simulates the double core structure of Kuroshio at PN section.

Ⅳ Currents east of the Ryukyu Islands

Yuan and Guan (2007) summarize the studies of some oceanographic surveys, pointed out that in the regions east and south of the Ryukyu Islands there are some mesoscale cyclonic and anticyclonic eddies with different scales, and the variability of their character were reviewed (see Yuan and Guan, 2007).

On the basis of twelve repeated hydrographic section data collected from 2004 to 2006, Zhu and Huang (2008) used an inverse calculation to study the velocity structures and volume transports, the results proved that the Ryukyu current (RC) is dominated by subsurface velocity core with maximum velocities vary from 15.1 to 80.0 cm s^{-1}, the positions of subsurface core distribute between 100m and 600m and 27.2°~28.2°N along the AE line, east of Amami-Ohshima. The mean volume transports (VTs)of the AE line in winter, spring, summer, autumn and all twelve observations are 10.9, 10.1, 5.9, 23.9 and 12.7×10^6 m^3 s^{-1}, respectively. The seasonal mean velocity sections exhibit that the RC is the strongest in autumn and the weakest in summer.

Yang et al. (2007) use the measuring data of R/V *Chof Maru* of JMA, Argos satellite-tracked drifters data, etc, to study the currents on the both sides of the Ryukyu Islands in April and May 2002, the results show that the VT of RC is about 8.8×10^6 m^3 s^{-1} in the southeast area to the Okinawa Island, then flows towards the AE line. The VT of Kuroshio through Section ASUKA in the surface layer mostly origins from the Kuroshio in the Tokara Strait. But, in the mid-layer, the contributions of Kuroshio in the Tokara Strait and the RC along the AE line are equal approximately.

Zhu et al. (2008) traced a cyclonic and an anticyclonic eddy southeast of Okinawa Island, time series of sea surface height anomaly (SSHA) map confirmed that these two eddies originated from the North Pacific Subtropical Countercurrent region near 20°~30°N and 150°~160°E, propagated westwards with a mean speed about 6 cm/s. Bottom pressure sensors measured no variation related to these eddy activities, which indicated that the two eddies were dominated by baroclinicity.

Because of the scarcity of measuring data, Zheng et al. (2008) took use of the reanalysis data to study the Ryukyu current (RC), it is found that there is a maximum core velocity of 20 cm s^{-1} at 600~1200m over the shelf slop. Because the water exchange through the ocean trough in the southwest of the Okinawa Island can affect the VT of Kuroshio in the East China Sea (KECS), the mean VT of KECS steadily increases from south to north, which is 28×10^6~35×10^6 m^3 s^{-1}; the transport of the western boundary current in the east of Ryukyu Islands is less an order of magnitude than that of KECS,

whose mean value is less than the standard deviation; because of the current through the ocean trough in the southwest of Okinawa, the transport in the east of Okinawa is less than that in the east of Amami-ohshima. The Rossby wave propagating westward in the east of Ryukyu Islands could influence the western boundary current in the east of Ryukyu Islands distinctly, so the distinct period of the transport of the western boundary current in east of Ryukyu Islands is approximately 100 d. The KECS in the south of the ocean trough is mainly controlled by the Kuroshio in the east of Taiwan, so the period of its transport is also approximately 100 d. But the KESC in the north of the ocean trough does not have this feature.

Hu et al. (2007) overviewed the researches of KESC and RC, and listed some scientific items to be solved. Zhu (2008) reviewed studies on the RC, it is pointed out that the RC is strongly influenced by the mesoscale eddy, its velocity and volume transport exhibits subsurface maximum structure. The RC remarkably develops between the Okinawa and Amami-Ohshima Islands. The following three points need to better address: (1) the origin of the RC, the formation mechanism and its temporal and spatial variations; (2) dynamic processes of formation and maintaining of the subsurface maximum structure, the development of RC from the northern of the Okinawa Island, and (3) the contributions of volume and heat transport to the Kuroshio.

References

Bai, Z. P., S. Gao, H. T. Wang (2010): A HYbrid Coordinate Ocean Model (HYCOM) for simulating the climatological Kuroshio in the East China Sea. Marine Science Bulletin, 29(2): 121-129. (in Chinese) .

Bao, X. W., X. Ju, D. X. Wu (2009): Characteristics of Water Exchange Across 120°E Section in the Luzon Strait. Periodical of Ocean University of China, 39(1) : 1-6. (in Chinese) .

Cai, R. S., Q. L. Zhang, Q. H. Qi (2009): Characters of transport variations at the source and adjacent area of Kuroshio. Journal of Oceanography in Taiwan Strait. 28 (3): 299-307. (in Chinese).

Chen, H. X., F. L. Qiao, T. Ezer, et al. (2009): Multi-core structure of the Kuroshio in the East China Sea from long-term transect observations. Ocean Dynamics, 59: 477-488 DOI 10.1007/s10236-009-0182-9.

Chen, Z. Y., Z. C. Zhang, Y. W. Jiang (2009): Seasonal Variation of Kuroshio at Luzon Strait Studied with Argos and Numerical Model. Journal of Xiamen University, 48(5): 719-724. (in Chinese) .

Feng, Y., H. X. Chen, Y. L. Yuan (2010): Analysis of Argos Drifter Data for Kuroshio Characteristics in East China Sea. Advances in Marine Science, 28 (3): 275-284. (in Chinese)

Huang, D. J., T. Zhang, F. Zhou (2010): Sea-surface temperature fronts in the Yellow and East China Sea from TRMM microwave imager data. Deep-Sea Research Ⅱ, 57: 1017-1024.

Hu, P., Y. J. Hou, K. T. Le, et al. (2007): Study advances on the Kuroshio in the East China Sea and currents in the region east of Ryukyu Islands. Studia Marina Sinica, 48:28-34. (in Chinese) .

Hu, X. M., X. J. Xiong, F. L. Qiao, et al. (2008): Surface current field and seasonal variability in the Kuroshio and adjacent regions derived from satellite-tracked drifter data. Acta Oceanologica Sinica, 27(3): 11-29.

Hu, Y. M., X. J. Xiong, F. L. Qiao, et al. (2008): Surface current field and seasonal variability in the Kuroshio and adjacent regions derived from satellite-tracked drifter data. Acta Oceanologica Sinica, 30(6): 1-16. . (in Chinese).

Liao, G. H., Y. C. Yuan and X. H. Xu (2008): Three Dimensional Diagnostic Study of the Circulation in the South China Sea during winter 1998. *Journal of Oceanography*, 64 (5): 803-814.

Ma, C., D. X. Wu, X. P. Lin (2009): Variability of surface velocity in the Kuroshio Current and adjacent waters derived from Argos drifter buoys and satellite altimeter data. Chinese Journal of Oceanology and Limnology, Vol. 27 No. 2, P. 208-217, 2009 DOI: 10.1007/s00343-009-9260-6.

Ma, C., D. X. Wu, X. Ju (2010): The analysis of the Kuroshio intrusion to the South China Sea using Argos drifting buoys

data. Transaction of Oceanology and Limnology, 2010 (2): 1-5. (in Chinese) .

Qu, Y. Y., Q. H. Zhang, Y. Ma (2010): Danamic Response of Shelf Water in the East China Sea to Strong Shear in Kuroshio. Advances in Marine Science, 28 (3): 292-298. (in Chinese) .

Wang, Y. P. and X. P. Sun (1990): A study on t he features of Ryukyu Current. Proceedings of investigation of Kuroshio , No. 2. Beijing : China Ocean Press , 1990 : 237 —245.

Yang, C. H., Y. C. Yuan, H. Q. Wang (2007): The currents on the both sides of the Ryukyu Islands in April and May 2002. Acta Oceanologica Sinica, 29(3): 1-13. (in Chinese) .

Yang, Y., W. D. Zhou, D. P. Dong (2010): Diagnostic Calculation of the Oceanic Circulation. Marine Science Bulletin, 12(1): 30-38.

Yuan, D. L. and R. X. Li, (2008): Dynamics of eddy-induced Kuroshio variability in Luzon Strait. Journal of Tropical Oceanography, 27(4): 1-9. (in Chinese) .

Yuan, Y. C. and B. X. Guan (2007): Overview of studies in the China seas and their adjacent seas Ⅱ.The East China Sea and the region east of the Ryukyu Islands. Acta Oceanologica Sinica, 29(2): 1-17. (in Chinese) .

Yuan Y. C., G. H. Liao and X. H. Xu (2007) Three dimensional diagnostic modeling study of the South China Sea circulation before onset of summer monsoon in 1998. Journal of Oceanography, 63 (1): 77-100.

Yuan Y. C., G. H. Liao and C. H. Yang (2008a): The Kuroshio near the Luzon Strait and circulation in the northern South China Sea during August and September 1994. *Journal of Oceanography*, 64 (5): 777-788.

Yuan Y. C., G. H. Liao, W. B. Guan, H.Q. Wang, R. Y. Lou and H. Chen (2008b): The circulation in the upper and middle layers of the Luzon Strait during spring 2002. *J Geophys.Res*, 113, C06004, doi:10.1029/2007JC004546.

Yuan Yaochu, Liao Guanghong, Yang Chenghao (2009a) : A diagnostic calculation of the circulation in the upper and middle layers of the Luzon Strait and the northern South China Sea during March 1992. Dynamics of Atmospheres and Oceans, 47: 86-113.

Yuan YaoChu, Liao GuangHong, Wang HuiQun, Lou RuYun, Chen Hong (2009b): Variability of the currents in the Luzon Strait during spring of 2002 obtained from observations and satellite geostrophic currents and spectral analyses. *Science in China (Series D*) , 52 . 4 : 519-531 .

Zhao, J., D. X. Wu, X. E. Chen (2009): Simulation of Kuroshio with eddy resolution model. Marine Science Bulletin, 28(5): 13-20.

Zhao, W., Y. J. Hou, K. T. Le, et al. (2007): Numerical study on seasonal water exchange in the Luzon Strait. Oceanologia Et Limnologia Sinica, 38(6): 495-503. (in Chinese)

Zheng, P. N., D. X. Wu, X. P. Lin (2009): The relationship between the Taiwan Warm Current and Tsushima Warm Current. Journal of Hydrodynamics, 2009, 21(2):212-218 DOI: 10.1016/S1001-6058(08)60138-9.

.Zheng, X. T., Q. Y. Liu, H. B. Hu, et al. (2008): The Study of the temporal and.spatial characteristics of western boundary current East of Ryukyu submarine ridge and the transport of Kuroshio in East China Sea. Acta Oceanologica Sinica, 30(1): 1-9. (in Chinese) .

Zhou, F., J. L. Xuan, X. B. Ni, et al. (2009): A preliminary study of variations of the Changjiang Diluted Water between August of 1999 and 2006. Acta Oceanologica Sinica, 28(6): 1-11.

Zhou, H., P. F. Guo, J. P. Xu, et al. (2007): The Characteristics of the Eddies East of Taiwan Island and the Kuroshio in East Chian Sea. Periodical of Ocean University of China, 37(2) : 180-190. (in Chinese) .

Zhu, X. H. and D. J. Huang (2008): The Ryukyu Current east of Amami-Ohshima during 2004 to 2006. Chinese Journal of Geophysics, 51(5): 1354-1363. (in Chinese) .

Zhu, X. H., J. H. Park, D. J. Huang (2008): Observation of baroclinic eddies sout heast of Okiniawa Island [J / OL] . Science in China Series-D, doi :10. 1007/ s 1430 - 008 - 0146 - 9.

Zhu, X. H. (2008): Overview of studies on the Ryukyu Current. Acta Oceanologica Sinica, 30(5): 1-8. (in Chinese) .

ADVANCES IN OCEAN COLOR REMOTE SENSING IN CHINA 2007-2010)

Zhao D.Z.[1)], Wang L.[1)], LIU Y.H.[2)] and Wang X.[1)]

(1. National Marine Environmental Monitoring Center, Dalian, 116023, P.R. China 2. Ocean University of China, Qingdao, 266100, P.R. China)

Ⅰ Introduction

Ocean occupies 70% of the earth's surface. Accompanied with the acceleration of human development, utilization and protection on the ocean, the condition of marine environment and resources is undergoing significant changes. Also, governments of countries all around the world are paying more and more attention to ocean's sustainable development. A variety of high-tech observing and monitoring methods have been put into use. Among them, ocean color remote sensing, which can remotely obtain information of water body such as concentrations of phytoplankton pigments (PP), suspended solids (SS), and dissolved organic matter (DOM) by processing some correction and inversion algorisms to the visible and near-infrared sea-surface upstream spectral radiation received by sensors borne on aero- and aircrafts, is significantly important to investigation and research on ocean primary productivity, marine ecological environment, marine flux, fishery resources and many other aspects.

Chinese scientists' research on ocean color remote sensing dates back to 1980's. In 2002 and 2007, Chinese government has launched its own ocean color satellites "HY-1A" and "HY-1B", respectively. Together with earth resource satellite "CBERS-02B", meteorological satellite "FY-3A", and small satellites for environmental and disaster monitoring and forecasting "HJ-1A / B" which are launched in Sep 2007, May and Sep 2008, respectively, they greatly enrich Chinese data source of ocean color remote sensing.

In recent years, Chinese researchers have achieved breakthrough in many technological aspects of ocean color remote sensing, including measurement and analysis of marine bio-optical properties, quantitative retrieval of ocean color information, atmospheric correction algorithms and so on, which greatly contributed to the operational applications and development of ocean color remote sensing and the gradually developed remote monitoring application systems in China.

Ⅱ Recent development of ocean color remote sensing satellite in China

1.Haiyang-1 series satellites (HY-1)

HY-1A, launched in May 2002, is China's first operational satellite for experimental remote sensing of ocean color. It carries 10-band Chinese Ocean Color and Temperature Scanner (COCTS) and 4-band Coastal Zone Imager (CZI). General technical features show in Table 1. The real-time observation area of HY-1A covers the Bohai Sea, Yellow Sea, East China Sea, South China Sea and coastal zone of China. The main objective observations include water optical properties, chlorophyll concentration, sea surface temperature, suspended sediment concentration, dissolved organic matter, and ocean pollutants, also taking into account Sea Ice, shallow sea topography, currents, and atmospheric aerosols. The monitoring data obtained during operation has played important roles in various fields such as monitoring of red tides, forecasting of sea ice and temperature, fisheries, monitoring and managing of coastal zone. The successor of HY-1A, HY-1B, has been launched in April 200. It also carries 10-band COCTS and a 4-band CZI (detailed in Table 1). The new satellite was developed base on HY-1A, so its technical features and performances are better than former one.

Tab.1 The parameters for HY-1series

		HY-1A	HY-1B
Orbit		Near-sun-synchronous	sun-synchronous
Local Pass		8:30~9:30am	10:30am
COCTS	Bands(nm)	412,443,490,520,565,670：±10nm 765,865：±20nm 10.4~11.4,11.5~12.5	412,443,490,520,565,670,750：±10nm 865：±20nm 10.4~11.4,11.5~12.5
	Pixels	1024	1664
	Swath（km）	1500	2000
	Resolution（km）	1	1
	FOV（°）	±45	±55
CZI	Bands(nm)	420~500,520~600,610~690,760~890,	443,555,665,685：±10nm
	Pixels	2048	2048
	Swath（km）	500	500
	Resolution（m）	250	250

2.Fengyun series satellites (FY-1/2/3A)

The FY series are China's meteorological satellites, which carries sensors with visible and near infrared bands using for ocean color remote sensing. FY-1 is China's first generation of meteorological satellite. There are four FY-1 series satellites launched from 1988 to 2002, among which FY-1A/1B are test satellites and FY-1C/1D are operational ones. FY-1C had retired on 2004 after 6 years operation, while FY-1D is currently running in good condition. FY-2 is the first generation of operational geostationary meteorological satellite developed by China. The process of development and launch can be divided into two batches.The first batch includes two satellites, FY-2A and FY-2B, which were launched in 1997 and 2000, respectively and retired in late 2009. The latter batch, FY-2C and FY-2D, were launched in 2004 and 2006, respectively and are working well now.

FY-3 series, developed on the basis of FY-1, is China's second generation of polar-orbiting meteorological satellite. FY-3A was successfully launched in 2008, whose detection performances are much better than FY-1. In addition to Visible and InfraRed Radiometer (VIRR), many other instruments are borne, such as MicroWave Temperature Sounder (MWTS), MicroWave Humidity Sounder (MWHS), MicroWave Radiation Imager (MWRI), InfraRed Atmospheric Sounder (IRAS), MEdium Resolution Spectral Imager (MERSI), Solar Backscatter Ultraviolet Sounder (SBUS), Total Ozone Unit (TOU), Solar Irradiation Monitor (SIM), Earth Radiation Measurement (ERM), and Space Environment Monitor (SEM). Relying on these instruments, FY-3 has the capability of acquiring multi-spectral, three-dimensional, quantitative environmental parameters of global earth's surface, ocean and space in all-weather. Instruments can be used for ocean color remote sensing are detailed in Table 2 and 3.

Tab.2 The channel parameters for VIRR

Band	Wave Length（μm）	Noise Equivalent Reflectance(%)/Temperature Difference（K）	Dynamic Range
1	0.58~0.68	0.1%	0~100%
2	0.84~0.89	0.1%	0~100%
3	3.55~3.93	0.3K	180~350K
4	10.3~11.3	0.2K	180~330K
5	11.5~12.5	0.2K	180~330K
6	1.55~1.64	0.15%	0~90%
7	0.43~0.48	0.05%	0~50%
8	0.48~0.53	0.05%	0~50%
9	0.53~0.58	0.05%	0~50%
10	1.325~1.395	0.19%	0~90%

Tab.3 The channel parameters for MERSI

Band NO.	Center Wavelength（μm）	Band Width（μm）	Spatial Resolution（m）	Noise Equivalent Reflectance(%)/ Temperature Difference（K）	Dynamic Range
1	0.470	0.05	250	0.45	100%
2	0.550	0.05	250	0.4	100%
3	0.650	0.05	250	0.3	100%
4	0.865	0.05	250	0.3	100%
5	11.25	2.5	250	0.4K	330K
6	0.412	0.02	1000	0.1	80%
7	0.443	0.02	1000	0.1	80%
8	0.490	0.02	1000	0.05	80%
9	0.520	0.02	1000	0.05	80%
10	0.565	0.02	1000	0.05	80%
11	0.650	0.02	1000	0.05	80%
12	0.685	0.02	1000	0.05	80%
13	0.765	0.02	1000	0.05	80%
14	0.865	0.02	1000	0.05	80%
15	0.905	0.02	1000	0.10	90%
16	0.940	0.02	1000	0.10	90%
17	0.980	0.02	1000	0.10	90%
18	1.030	0.02	1000	0.10	90%
19	1.640	0.05	1000	0.05	90%
20	2.130	0.05	1000	0.05	90%

CBERS-02B Satellite

This satellite was successfully launched from Taiyuan Satellite Launch Center on September 19th, 2007. The first earth observation image was acquired on September 22nd, 2007. CBERS-02B has earth observation capability of all the high, medium and low spatial resolution. The employment of High Resolution (HR) camera with 2.36 meter resolution broke the long-term monopoly of foreign high-resolution satellite data in China. This satellite plays an important role in various fields such as

land resources, urban planning, environmental monitoring, disaster prevention, agriculture, forestry, water conservation projects and others Main parameters of borne instruments are shown in Table 4.

Tab.4 The channel parameters for CBERS-02B

Platform	Instrument	Band No.	Spectral range (μm)	Spatial resolution (m)	Swath width (km)	Swing capability	Recurrent period (day)	Data rate (Mbps)
CBERS-02B	CCD camera	B01	0.45～0.52	20	113	±32°	26	106
		B02	0.52～0.59	20				
		B03	0.63～0.69	20				
		B04	0.77～0.89	20				
		B05	0.51～0.73	20				
	High Resolution camera (HR)	B06	0.5～0.8	2.36	27	/	104	60
	Wide Field Imager (WFI)	B07	0.63～0.69	258	890	/	5	1.1
		B08	0.77～0.89	258				

HJ-1-A, B satellite

A and B stars of small satellite constellations for environment and disaster monitoring and forecasting (HJ-1A / 1B) were launched at 11:25 on September 6th, 2008. HJ-1A is equipped with CCD camera and Hyper Spectral Imager (HSI), while HJ-1B is equipped with CCD camera and InfraRed Scanner (IRS).The CCD cameras borne on both satellites are of exactly the same design, placed symmetrically to the nadir. They process a joint pushbroom imaging on ground field with 700 km swath width, 30 meters ground pixel resolution at 4 spectral bands by parallel scanning on equally split fields.The HSI loaded on HJ-1A has ability to process pushbroom imaging on 50-km-wide, 100-meter-ground-pixel-resolution field at as many as 110 ~ 128 spectral bands, with ± 30 ° swing capability and onboard calibration function. The IRS loaded on HJ-1B has ability to process imaging on 720-km-wide, 150/300-meter-ground-pixel-resolution field at 4 spectral bands. Main parameters of borne instruments are shown in Table 5.

Tab.5 HJ-1-A, B satellite main load parameters

Platform	Instrument	Band	Spectral range (μm)	Spatial resolution	Swath width	Swing capability	Recurre	Data rate

		No.		(m)	(km)		nt period (day)	(Mbps)
HJ-1A	CCD camera	1	0.43-0.52	30	360 (single), 700 (two sets)	-	4	120
		2	0.52-0.60	30				
		3	0.63-0.69	30				
		4	0.76-0.90	30				
	Hyper spectral imager (HIS)	-	5 (110-128 spectral bands)	100	50	±30 °	4	
HJ-1B	CCD camera	1	0.43-0.52	30	360 (single), 700 (two sets)	-	4	60
		2	0.52-0.60	30				
		3	0.63-0.69	30				
		4	0.76-0.90	30				
	Infrared Scanner (IRS)	5	0.75-1.10		720	-	4	
		6	1.55-1.75	150 (NIR)				
		7	3.50-3.90					
		8	10.5-12.5	300 (10.5-12.5 μm)				

Ⅲ Measurement and analysis of water bio-optical characteristics

1 Implementation and development of Specifications for marine optical parameters monitoring

Acquisition and analysis of water bio-optical data is the basis of development and optimization of the ocean color remote sensing retrieval model.

The series National Specifications “Specifications for oceanographic survey”, which was composed by China’s State Oceanic Administration and published via “Announcement of Newly Approved National Standards of P.R.China, 2007 No.8 (Total No.108)” by Standardization Administration of the People’s Republic of China, was put into execution on February 1st, 2008. The Part 5 of this series: Survey of acoustical and optical parameters in the sea (GB / T 12763.5-2007) was prepared by The First and Third Institute of Oceanography, SOA and National Satellite Ocean Application Service. This standard specifies the technical requirements, measurement methods, data recording and finishing of

acoustical and optical parameters survey, which provides a scientific foundation for the apparent optical measurements with spectrometer and underwater profiler and inherent optical measurements with absorption and attenuation meters.

In 2008, the Part 7 of “Technical specification for marine monitoring”, “Satellite remote sensing methods” was drafted by National Marine Environmental Monitoring Center, SOA. Currently this set of industry standards is under final review and trusted to be an indispensable part of China’s ocean color remote sensing specification system. The set includes a part about “determination of absorption coefficient of ocean color factors (spectrophotometric method), which provides a scientific foundation for laboratory determination of inherent optical of water color factors such as absorption coefficients.

In addition, National Marine Environmental Monitoring Center, SOA submitted a "measurement of water backscattering coefficients" specification project application in June 2010, which will eventually make up the lack of *in-situ* measurement specification for backscattering coefficient.

The publications of these national and industrial oceanographic survey specifications in recent years, in coordination to China's current laws and regulations and related technical specifications, which not only reflect the development level of science and technology, but also adapt to actual situation of survey techniques in China, are scientific, advanced and practical. They will play an important role in the guidance of the Chinese marine survey, observation activities, ensuring the quality of survey data, promoting the development of marine science and better serving domestic economic and national defense construction.

2 Research on measurement of marine bio-optical data

On the research on bio-optical measurement methods, Zhu Jianhua *et al.* acquired the path-length amplification factor in particulate absorption coefficient measurement with integrating sphere. The results showed good comparability with traditional path-length amplification factor. They not only proved the TR method is suitable for measurements of absorption coefficient on various types of particulate and various zone, but also verified the superiority of TR method in the application in high turbid water zone. Zhou Hongli *et al.* compared the influence of different path-length amplification factors on particulate absorption spectra in typical Chinese coastal water based on different particulate absorption coefficients and shape of absorption spectra Dong Qiang *et al.* focused on the TR method and the method that places the colorimetric plate inside integrating sphere and achieved more precise correction to path-length amplification effect. Song Qingjun *et al.* presented two backscatter coefficient correction methods based on actual measurement situations, one of which used scattering coefficient calculated according to the relationship model between backscattering and scattering coefficient, while the other one used observed data measured data for substitution. Results showed these two methods have obvious advantages compared to traditional correction method, and meet the water inherent optical properties better.

3 Research on water scattering properties

On the research on water scattering properties, Song Qingjun *et al.* established relationship model between water backscattering coefficient and concentration of total suspended matter (TSM) in the Yellow and East China Sea. Liu Wei *et al.* established backscattering probability (b_{bs}) model and relationship model of unit scattering coefficient (b^*_s) between different spectral bands of TSM, based on research on b_{bs} and b^*_s of TSM in the Yellow and East China Sea. Zhou Wen *et al.* analyzed the influence of algal cell physical properties on its optical properties based both on their simulation of absorption and scattering properties of mineral particles with different particle size distributions and complex refractive indexes according to Mie theory and Aden-Kerker scattering theory. They also

processed comparative analysis to the optical properties of uniform sphere algal cell, and established phytoplankton scattering forward model under assumption of uniform spherical structure algal cell. The scattering spectra of model estimates and experiments achieved good agreement. Zhou Wen *et al.* also analyzed the spectral variation of water backscattering rate and influencing factors in Daya Bay, South China Sea based on bio-optical data collected in buoy fixed voyages.

4 Research on water absorption properties

On the research on water absorption properties, Wang Lin *et al.* analyzed pheophytin's influence on phytoplankton absorption properties based on *in-situ* measurements in Dalian Bay, North Yellow Sea. They also found evident seasonal variation of phytoplankton absorption coefficient in Changhai County coastal area according to *in-situ* measurements. Liang Shaojun *et al.* studied the variation of phytoplankton size structure and established a mixed spectrum model based on phytoplankton size parameters (S<f>) extracted from phytoplankton absorption spectra according to *in-situ* bio-optical data acquired in Northern South China Sea, Daya Bay and the Pearl River Estuary. Wang Guifen *et al.* established an absorption spectra ($a_p(\lambda)$) decomposition model of total particulate matter based on correlation between absorption spectra, and achieved separation between the absorption spectra of phytoplankton ($a_{ph}(\lambda)$) and non-algal particles ($a_{NAP}(\lambda)$) using a constrained nonlinear optimization algorithm. They also found that both pigment packaging effects and variation in pigment composition have great contribution to the variation of phytoplankton absorption coefficient, and phytoplankton spectral slope S calculated from 443 and 510nm bands has relative high sensitivity to the variation of size structure. Zhou Wen *et al.* retrieved pigment concentrations of chlorophyll a, chlorophyll b, chlorophyll c, photoprotective carotenoids and non-photoprotective carotenoids from phytoplankton absorption spectrum with multi-layer perceptron model. Han Bing *et al.* analyzed absorption spectral properties of the Chlorella, flat algae and Gymnodinium and studied the spectrum decomposition method under multi-species natural mixed state.

Wang Guifen *et al.* found the average non-algal particulate absorption spectral slope (S_{NAP}) of $0.0103nm^{-1}$ in Guangdong coastal area and the northern South China Sea according to *in-situ* observations. Zhou Wen *et al.* based on survey results of CDOM absorption properties in southern Taiwan Strait, found an average $a_g(355)$ as $0.13m^{-1}$ and an average spectral slope S_g as $0.022nm^{-1}$. They also confirmed that the main source of CDOM in study area is field production. Xing Xiaogang *et al.* studied the absorption coefficients of non-pigment particles and CDOM in the Bohai Sea and obtained the average spectral slopes as 0.012 and $0.014nm^{-1}$, respectively, which is consistent with the results from foreign researchers. Lei Hui *et al.* established models of CDOM spectral and absorption coefficient distribution in typical bands for various water body types in East China Sea such as high turbid water in Hangzhou Bay, the Yangtze River plume water, and the open sea water based on CDOM spectral absorption data acquired in four seasons during 2006-2007. Wang Guifen *et al.* found that non-algal materials, especially colored dissolved organic matter, have strong absorption contribution before and after algal blooms. Zhou Hongli *et al.* obtained the characteristics of non-pigmented particle absorption spectrum based on the analysis of non-pigmented particle absorption spectrum data collected in southern Yellow Sea and the Pearl River estuary during different seasons.

Li Meng *et al.* studied the absorption properties of CDOM in Jiulong River Estuary, Western area, Tongan Bay and East Watercourse of Xiamen Bay. They also analyzed the "estuary behavior" of CDOM and discussed the relationship between CDOM absorption properties and fluorescence properties Liu Xianping *et al.* established the quantitative analysis method of CDOM in water with complex composition based on the linear relationship between emission spectra peak area and

concentration of CDOM in low concentration condition for the first time, which extends the application of fluorescence analysis in CDOM research. Wang Lin *et al.* discussed the uncertainty in the relationship between $a_g(440)$ and S_g in coastal and open ocean water types, respectively. The results showed that in both coastal and open ocean waters, there is great (small) probability to show a negative (positive) correlation.

Ⅳ Development of ocean color remote sensing algorithm model in China

1 Research on remote sensing algorithm of chlorophyll concentration

Zhao Dongzhi *et al.* assessed the performances of MODIS ocean color algorithm CZCS_pigm, chlor_MODIS, chlor_a_2 and chlor_a_3 in Liaodong Bay of Bohai Sea based on *in-situ* measurements of chlorophyll-a concentration and remote sensing reflectance. The results showed a necessity to establish local chlorophyll-a retrieval algorithm for this area. Cong Pifu *et al.* setup 2 local chlorophyll-a retrieval models in Liaodong Bay based on their comparative studies on the single-band and band ratio methods. Zhang Hongliang established a chlorophyll FLH algorithm based on MERIS data, which is suitable for deep area of the Bohai Sea with low suspended solids concentration. Zhang Yanzhe *et al.* processed regression analyses between chlorophyll concentration (ρ) and NDPI (Normalized Difference Pigment Index) calculated from MODIS remote sensed band reflect ratio with 250m spatial resolution, then established a retrieval model of chlorophyll concentration from MODIS level-1B data for the Bohai Sea. Xiu Peng *et al.* made a comprehensive analysis of water optical properties in the Bohai Sea, especially the inshore area. They also developed the retrieval algorithm of vertical maximum chlorophyll concentration, which provided a new approach for the further expansion of ocean color remote sensing application from the sea surface into interior. Qiu Zhongfeng *et al.* obtained empirical coefficient from red tide observation data during 2002-2004 voyage in the East China Sea, and then developed a semi-analytical algorithm of chlorophyll concentrations for the high red tide incidence area in the East China Sea.

Ma Jinfeng *et al.* processed a fitness test on the applicability in the Pearl River Estuary of Gitelson model, which is a conceptual model based on remote-sensing reflectance (Rrs) in red and two NIR bands. On this basis, they built up an estimation model of chlorophyll-a concentration from remote sensing data for the Pearl River Estuary. Yang Jinkun *et al.* established chlorophyll fluorescence algorithms for the Pearl River Estuary area based on measured Rrs with 1nm bandwidth and simulated MERIS data. Hao Yingzhen built up an evolving neural network model based on genetic algorithm for retrieval of chlorophyll concentration in the Pearl River through comparison with traditional neural network and optimization. Xi Hongyan *et al.* developed an empirical correlation model between chlorophyll-a concentration and pigment absorption coefficient aph(675) for Hong Kong adjacent waters, and then established a semi-analysis algorithm of chlorophyll-a concentration for the usage in low chlorophyll-a concentration area. Xu Dazhi *et al.* setup two local empirical algorithm for accurate calculation of chlorophyll-a concentration in northern South China Sea based on the relationship between ratios of Rrs in different bands (Rrs (433) / Rrs (555)) and chlorophyll-a concentrations.

Mao Zhihua *et al.* established data processing model for China's Moderate Resolution Imaging Spectrometer (CMODIS) using chlorophyll-a concentration retrieved from SeaWiFS data as reference. They also setup three sets of chlorophyll-a concentration retrieval algorithm based on blue-green band ratio method. Wen JianGuang *et al.* processed chlorophyll-a concentration retrieval via mixed-spectra model based on first order differential of measured data and then built up a quantitative model for remote monitoring of chlorophyll-a concentration. Wei Zhiqiang *et al.* retrieved sea surface

chlorophyll-a concentration through the use of Raman calibration normalization method and employment of China's first airborne laser-induced marine fluorescence radar systems developed by Ocean University of China. They also retrieved the attenuation coefficient of sea water from measured data and the laser radar equation. Gao Yan developed a high-spectral feature retrieval algorithm of algae species via focusing on *Chlorella vulgaris* and *Microcystisaeruginosa*, and then applied it to chlorophyll-a retrieval mode. Ma Yong *et al.* retrieved the density of algae suspended particulates and other information through the use of infrared laser, and ultimately built up a detection model for phytoplankton, CDOM and suspended particles by 1.064μm laser in seawater. Fu Dongyang *et al.* studied the influence of typhoon on chlorophyll-a concentration based on MODIS and SeaWiFS level-3A data.

2 Research on remote Sensing Algorithm of suspended sediment concentration

Cui Tingwei *et al.* established a retrieval algorithm for suspended matter based on band R_{rs} at 555 and 670 nm bands according to and spectral collected in the Bohai Bay and Laizhou Bay. Based on their model, they analyzed the spatial and temporal distribution features of suspended matter in the Bohai Sea from ENVISAT MERIS data. Zhao Wenjing established empirical retrieval model of suspended matter concentrations for different remote sensors in adjacent area of the Yellow River estuary according to measured datasets of suspended matter concentration and spectral. Fan Hui *et al.* established model of suspended matter concentration at different temporal phase for the same area. Pang Chongguang *et al.* established suspended matter concentration vertical distribution model for different seasons and regions in the East China Sea based on their research on vertical distribution features of suspended matter concentration in this area. Test results showed that the model is a high degree of confidence, and can better forecast the suspended matter concentrations in upper layer. Kong Dexing *et al.* retrieved surface suspended sediment concentration via linear extrapolation method from *in-situ* measurements in the Yangtze River estuary and identified the relationship between suspended sediment concentration and backscatter intensity calculated from sonar equation. They also retrieved suspended sediment concentration in different seasons with BP artificial neural network algorithm. Zhang Minwei *et al.* established a retrieval algorithm of total suspended matter concentration in the Yellow and East China Seas from MODIS imagery. Lin Qiang *et al.* processed correlation and regression analyses between remote sensing images and quasi-simultaneous measurements of the Xiamen Bay. Their results indicated that model that includes quadratic regression between surface sediment concentration and remote sensing parameter with combination form of two different band-ratios will produce higher accuracy. Liu Fenfen *et al.* established a piecewise retrieval algorithm for suspended sediment concentration in the Pearl River estuary based on MERIS data. Liu Dazhao *et al.* calculated suspended sediment concentration distribution in the Pearl River estuary with mixed spectral decomposition model.

Xu Xiaojun built up a based on standard reflectance according to suspended sediment concentration, particle size and spectral data. He also established suspended sediment concentration retrieval model which had remove the effect of particle size according to the influence of particle size on reflectance. Xu Jingping *et al.* established a NIR band bio-optical model based on the simplification of water inherent optical properties in NIR, which can effectively extract the suspended matter concentration in Case-II turbid water. Wang Fan *et al.* established the empirical and semi-analytical model of suspended matter concentration and inherent optical properties, respectively, based on datasets of water apparent optical properties, inherent optical properties and component concentrations. They also analyzed the short-period variability of suspended matter inherent optical properties taking account of tidal

dynamics, then analyzed the influence factors for its spatial and temporal variation from the perspective of the concentration and composition. Wu Chuanqing *et al.* tried to find the spectral range and characteristics position that can avoid interference of chlorophyll-a on suspended sediment retrieval through research on spectral curves with different concentrations of suspended sediment and a certain concentration of chlorophyll-a. They setup several models through correlation analyses and selected the best one for further research.

3 Research on retrieval of inherent optical properties and other optical parameters

Cui Tingwei *et al.* established an empirical retrieval model of the backscattering coefficient $b_b(\lambda)$ from R_{rs} spectra based on measured datasets collected in inshore area of the Bohai Sea. The model proved to be suitable for the coastal turbid water in the Bohai Sea, and could be used for analyses of spatial and temporal distribution of water optical parameters and retrieval of optical components based on inherent optical properties. Yang Wei *et al.* put forward an algorithm to calculate absorption and backscattering coefficient of each component in water according to reflectance spectra of water samples with known concentration, and verified the rationality of the algorithm using bio-optical spectral data generated by bio-optical model. Shen Hong *et al.* tried to retrieve CDOM concentration from MODIS data at 443 and 488 nm bands, which were found to have the highest correlations with *in-situ* measured CDOM data. Then they established a CDOM retrieval model based on MODIS data for the Liaodong Bay and Dalian Bay. Wang Xiaoyong *et al.* built up a local seasonal empirical model between apparent and inherent optical properties based on bio-optical data collected during the Yellow and East China Sea experiment in 2003 and during "908" Special Program marine optical investigation in 2007. Wang Xiaomei *et al.* setup a statistical retrieval model of water absorption coefficient at several bands for the use in coastal Case-II water of the Yellow and East China Sea. Zhan Haigang *et al.* improved the quasi-analysis algorithm (QAA) based on Bayesian inversion theory. They extracted the total absorption and scattering coefficients at reference bands and then extended the estimation results to other bands according to the empirical formula of backscatter coefficient spectral shape.

Yang Jinkun *et al.* established optimized retrieval model of the three elements of ocean color for the Case-II water in Pearl River Estuary. The mean relative error between retrieved and measured values are 14.9%, 12.1%, 13.6% for chlorophyll, suspended sediment, and CDOM, respectively. Zhang Tinglu *et al.* built up an artificial neural network algorithm for ocean color elements in Case-II water based on COASTLOOC and PMNS datasets. Sun Liran applied modified Powell algorithm, simulated annealing algorithm and genetic algorithms to the retrieval of ocean color parameters to solve the sophisticated multi-dimensional and nonlinear andidate parameters problems in bio-optical model.

Hu Lianbo proposed a retrieval algorithm for diffuse attenuation coefficient at 490nm band Kd(490) in the East China Sea based on *in-situ* optical observations collected in April and December, 2006 and February 2007. Cui Tingwei *et al.* built up an empirical Kd(490)retrieval model from Rrs (λ) based on bio-optical dataset collected in the Bohai Sea coastal area during 2005. Zhang Tinglu *et al.* established a Kd(490)retrieval algorithm with artificial neural network based on NOMAD dataset. Xing Xiaogang *et al.* proposed a theoretical algorithm, which is called φ algorithm, to estimate fluorescence quantum yield based on MODIS data. Zhao Wenjing *et al.* focused on radiation transfer simulation of sea surface spectral response and analyzed the variation of sea surface spectra with thickness and suspension depth of *Enteromorpha*, water turbidity, and other environmental conditions. LI Xiaobin *et al.* setup an inorganic nitrogen concentration estimation model for the Pearl River Estuary area employing partial least squares regression based on *in-situ* measurements of Rrs and total inorganic nitrogen (TIN) at 36 stations during 2 cruises.

Ⅴ Atmospheric correction

China's operational observations of marine aerosol

Marine aerosols is one of the important parameters of climate change, which not only has direct and indirect influences on climate by altering the radiation balance of climate system, but also plays an important role in many geophysical and geochemical processes. The main tasks and purposes of operational monitoring of marine aerosol by field observing and remote sensing are: building marine aerosol observation network covering China's whole sea area; obtaining long-term, continuous, entire-area-covering observations of aerosol through on-board observations and island- or coast-based fixed-point observations; establishing operational satellite remote sensing aerosol monitoring system based on *in-situ* observations; achieving spatial and temporal dynamic monitoring of marine atmospheric environmental parameters; analyzing the impact of aerosols on climatic dynamics and air quality; and providing scientific basis for establishment and improvement of atmospheric correction algorithm in ocean color remote sensing.

China's government has built three island- or coast-based aerosol optical depth (AOD) monitoring stations equipped with CE318 sun photometers since 2009 at Small Mai Island in southern Yellow Sea, Sansha in the East China Sea, and Yuan Island in northern Yellow Sea, respectively. The Station located in the South China Sea is currently under construction. In addition, hand-held sun photometers are employed for on-board operational observations by National Marine Environmental Monitoring Center and branch monitoring centers of SOA. All of these provide adequate data to support the establishment of atmospheric correction algorithm of ocean color remote sensing.

2 Research on atmospheric correction algorithm

Ding Jing *et al.* first proposed classification that divides coastal turbid water into 2 classes according to different turbidities and gave a preliminary criterion for the classification. They processed atmospheric correction to higher turbidity water with spectral optimization method and got satisfactory results. Li Hua *et al.* improved MUMM (The Management Unit Mathematical Models) atmospheric correction algorithm for the use in Case-II water of the Pearl River Estuary area by re-calculating the ratio of aerosol scattering at 765 and 865nm bands according to local water pixel spectral information and then re-calculating a new atmospheric correction factor e and water leaving radiance at every band based on atmospheric correction factor calculation in Gordon quasi-single-scattering approximation algorithm for clean water.

Yu Kun *et al.* proposed an atmospheric correction algorithm to solve the problem that SEADAS cannot calculate water leaving radiance and simply set it to zero in inshore Case-II water, which is suitable for the Case-II water in Chinese coastal area. Liu Liangming *et al.* revised Gordon atmospheric correction algorithm according to radiative transfer theory and proposed to use analytical method to separate the water leaving radiance and contribution of aerosol at 748 and 869 nm bands and then achieve atmospheric correction in coastal Case-II water, which should be more suitable for China's coastal area with high concentration of suspended sediment aerosol. Wang Feng *et al.* proposed an atmospheric correction algorithm for Case-II water that assumed water leaving radiance at short-wave infrared (SWIR) band to be zero. They applied the algorithm to coastal waters and lakes in eastern China and compared the results with observations and those of regular algorithm. Results showed the new algorithm can effectively remove atmospheric effects. Xu Meng *et al.* processed atmospheric correction to EOS / MODIS visible and NIR channel data with 6S model and then optimized the calculation of atmospheric model parameters and atmospheric profile in 6S model. Chen Jin *et al.* proposed a new retrieval method of aerosol optical properties above turbid water for MODIS data,

which provided technical basis for Research on atmospheric correction to data collected by HY and FY series satellites.

Xing Qianguo *et al.* established a single window algorithm for retrieval of coastal sea surface temperature taking into account the atmospheric effects based on Landsat TM, ETM+ thermal infrared data. Their algorithm only needs surface air temperature relative humidity as input and doesn't need definition of atmospheric model. Chen Yunzhi *et al.* established an atmospheric correction algorithm of MERIS data for the Taiwan Strait according to the characteristics of MERIS Level-1B products. Their algorithm can maintain a good consistency between the corrected spectra curves with *in-situ* data. Zhang Minwei *et al.* established their atmospheric correction algorithm based on POLDER multi-angle observations, from which AOT and water reflectivity can be retrieved.

Liu DaZhao *et al.* obtained AOT of northern South China Sea from multi-band sun photometer measurements. He Xianjiang *et al.* calculated the radiation polarization component for pure Rayleigh atmosphere (no aerosol) and atmosphere with AOT of 0.2 with the use of ocean-atmosphere coupled vector radiative transfer model PCOART. Deng Xueliang *et al.* directly calculated the optical depth of artificial and dust aerosol above China's sea area based on the relationship between 550nm AOT and ratio of small particles in MODIS aerosol products. Deng Xueliang *et al.* validated MODIS-C005 aerosol products in China's sea area by comparing MODIS AOT product with sun photometer measurements obtained at several AERONET stations in this area. Chen Qing *et al.* studied the spatial distribution of multi-annual mean AOT in Taiwan Strait and adjacent area and found a banded distribution lying along the coast and decreasing exponentially with offshore distance.

Ⅵ Conclusion

Detecting and providing marine environmental elements from satellite is an important part of the three-dimensional marine environment monitoring system. China's government has carried out the corresponding operational applications on monitoring suspended solids concentration, chlorophyll-a concentration, water temperature, sea ice and others. FY-1C and FY-1D of Fengyun series, HY-1A and HY-1B of Haiyang series are mainly used on marine monitoring; while HJ-1 and CBERS (China and Brazil earth resources satellite) are mainly used for small water body such as inland waters and coastal bays. Based on current situation of marine remote sensing technology and the development plan of marine satellite remote sensing for the next 10 years, the development of marine remote sensing technology will have the following features: more oriented by environmental monitoring application; more industry participation and commercialization trends; higher analysis accuracy and quantitative analysis trends; higher frequency, longer sequence monitoring and operational trends; multi-platform monitoring data assimilation trends and synthesis of core technology trends. Considering current international conditions and trends of development, the main development strategy of China's marine remote sensing technology is: to carry out the operational monitoring of marine environmental remote sensing, to strengthen the development degree of application to the high quality marine remote sensing products in market, and to form a team with Chinese characteristics which is working on operational monitoring and product application development of marine remote sensing.

References

CHEN Jin, MA Jin-ji, WANG Jia-cheng. Atmospheric Correction of MODIS Image for Turbid Coastal Waters. Journal of Atmospheric and Environmental Optics, 2007, 2(4): 306-311.

CHEN Yun-zhi, WANG Xiao-qin, GAO Zhong-ling. Atmospheric correction of MERIS data over the Taiwan Straits. Marine Sciences, 2008, 32(3): 62-67.

CONG Pi-fu, QU Li-mei, LIU Chang-an, et al. Remotely sensed retrieval model of chlorophyll a in Liaodong Gulf based on MODIS band simulation. Ecology and Environmental Sciences, 2009, 18(6): 2057-2060.

CUI Ting-wei, ZHANG Jie, MA Yi, et al. Diffuse attenuation coefficient Kd(490) retrieval model for nearshore area of Bohai sea. Journal of Remote Sensing, 2009, 13(3): 411-422.

CUI Ting-wei, ZHANG Jie, MA Yi, et al. Backscattering Coefficient Retrieval Model for Nearshore Area of Bohai Sea. Acta Optica Sinica, 2008, 8(11): 2041-2045.

CUI Ting-wei, ZHANG Jie, MA Yi, et al. The study on the distribution of suspended particulate matter in the Bohai Sea by remote sensing. Acta Oceanologica Sinica, 2009, 31(5): 10-18.

DENG Xue-liang, PAN De-lu, HE Dong-yan, et al.Anthropogenic and dust aerosol components estimated by satellite data over the China's seas. Acta Oceanologica Sinica, 2009, 31(4): 58-68.

DENG Xue-liang, PAN De-lu, HE Dong-yan, et al. Validation of MODIS Aerosol Optical Depth Retrievals over the China Sea. Journal of Nanjing Institute of Meteorology, 2008, 28(12): 558-564.

DING Jing, TANG Jun-wu, SONG Qing-jun, et al.Atmospheric Correction for Chinese Coastal Turbid Waters Using Iteration and Optimization Method. Journal of Remote Sensing, 2006, 10(5): 732-741.

DONG Qiang, HONG Hua-sheng, SHANG Shao-ling. A New Approach to Correct for Pathlength Amplification in Measurements of Particulate Spectral Absorption by the Quantitative Filter Technique. Journal of Xiamen University (Natural Science), 2008, 47(4): 556-561.

FAN Hui, HUANG Hai-jun, TANG Jun-wu. Spectral Signature of Waters in Huanghe Estuary and Estimation of Suspended Sediment Concentration from Remote Sensing Data. Geomatics and Information Science of Wuhan University, 2007, 32(7): 601-604.

FU Dong-yang, DING You-zhuan, LIU Da-zhao, et al. Delayed effect of typhoon on marine chlorophyll-a concentration. Journal of Tropical Oceanography, 2009, 28(2): 15-21.

FU Dong-yang, PAN De-lu, DING You-zhuan, et al. Quantitative study of effects of the sea chlorophyll-a concentration by typhoon based on remote-sensing. Acta Oceanologica Sinica, 2009, 31(3): 46-56.

GAO Yan. HyperSpectral feature extraction of algae and application on the Chl-a inversion[D]. Dissertation of master's Degree of Peking University, 2007.

HAN Bing, ZHOU Hong-li, ZHU Jian-hua, et al. Study on Spectral Unmixing of Mixed Algae in Laboratory. Ocean Technology, 2009, 28(4): 58-62.

HAO Ying-zhen. The Study of Chlorophyll remote sensing in Case II Waters Based on the neural network and genetic algorithms—Take the Pearl River estuary for instance[D]. Dissertation of master's Degree of SUN YAT-SEN University, 2006.

HE Xian-qiang, PAN De-lu, BAI Yan, et al.Effect of Aerosol Scattering on Polarization Correction of Ocean Color Remote Sensing. Journal of Atmospheric and Environmental Optics, 2009, 4(2): 88-96.

HU Lian-bo.Research on the diffuse attenuation coefficients in the East China Seas[D]. Dissertation of master's Degree of Ocean University of China, 2007.

LEI Hui，PAN De-lu，TAO Bang-yi, et al. The spectral absorption and distri bution characteristics of CDOM in the typical waters of the East China Sea. Acta Oceanologica Sinica, 2009, 31(2): 57-62.

LI Hua. The Study on Atmospheric Correction Algorithm of Case-2 Turbid Water and The Infection in The Extraction of Ocean Color Information[D]. Dissertation of master's Degree of Zhongshan University, 2006.

LI Meng, GUO Wei-dong, XIA En-qin, et al. A study on optical absorption properties of

chromophoric dissolved organic matter in Xiamen Bay. Journal of Tropical Oceanography, 2006, 25(1): 9-14.

LI Xiaobin, CHEN Chuqun, et al.SHI Ping, Retrieval of total inorganic nitrogen concentration in pearl river estuary by remote sensing. Acta Scientiae Circumstantiae, 2007, 27(2): 313-318.

LIANG Shao-jun, CAO Wen-xi, WANG Gui-fen, et al. Retrieval of phytoplankton size parameter from phytoplankton absorption spectra. Journal of Tropical Oceanography,

2010, 29(2): 59-64.

LIN Qiang, CHEN Yi-mei, HUANG Yong-ge . An Analysis of Distribution of Suspended Sediment in Estuary by Using Remote Sensing Technology. Port & Waterway Engineering. 2008, 412: 19-22.

LIU Da-zhao, TIAN Li-qiao, YANG Jin-kun, et al.Study of aerosol optical thickness over northern south china sea. Journal of Tropical Meteorology, 2008, 24(2): 205-208.

LIU Da-zhao, CHEN Chu-qun, LIU Fen-fen, et al. Estimation of suspended sediment concentration at Zhujiang River Mouth based on decomposition of mixing spectrum. Journal of Tropical Oceanography, 2009, 28(5): 43-48.

LIU Fen-fen, CHEN Chu-qun, TANG Shi-lin, et al. A piecewise algorithm for retrieval of suspended sediment concentration based on in situ spectral data by MERIS in Zhujiang River estuary. Journal of Tropical Oceanography, 2009, 28(1): 9-14.

LIU Liangming, ZHANG Hongmei, ZHANG Feng .Atmospheric Correction of MODIS Imagery for Turbid Coastal Waters. Geomatics and Information Science of Wunan University, 2007, 32(2): 104-107.

LIU Wei，LI Tong-ji，ZHU Jian-hua, et al. Study of Scattering Properties of Total Suspended Matter in the Yellow Sea and East China Sea. Ocean Technology, 2007, 26(2): 42-46.

LIU Xian-ping, LI Lei, DAI Jin-feng, et al. Determination of Chromphoric Dissolved organic Matter in Water from Different Sources. Spectroscopy and Spectral Analysis, 2007, 27(10): 2083-2087.

KONG Fan-xing. The Simulation of Suspended Sediment Concentration and its Transportion Trend in Changjiang Esturay[D]. Dissertation of master's Degree of Shanghai Ocean University, 2009.

MA Jin-feng, ZHAN Hai-gang, CHEN Chu-qun, et al. Remote sensing retrieval of chlorophyll-a in turbid, productive estuaries: A case study of Zhujiang River estuary. Journal of Tropical Oceanography, 2009, 28(1): 15-20.

MA Yong, LIN Hong, AI Qing, et al. Transmitting characteristics of 1.064μm laser in seawater. Laser Technology, 2008, 32(5): 502-507.

MAO Zhi-hua ZHU Qian-kun GONG Fang , et al. The development of inversion models of chlorophyll-a concentration from CMODIS data. Acta Oceanologica Sinica, 2006, 28(3): 57-63.

PANG Chong-guang, HAN Dan-xiu, ZHAO En-bao. Characteristics and regression equations for vertical distribution of suspended sediment concentration in the Yellow Sea and East China Sea. Journal of Sediment Research, 2009, 5: 69-75.

QIU Zhong-feng, XI Hong-yan, HE Yi-jun, et al. Semi-Analysis Algorithm to Retrieve Pigment Concentrations in the Red Tide Area Of the East China Sea. Environmental Science, 2006, 27(8): 1516-1521.

SHEN Hong. The Research of the Optical Characteristic of CDOM and MODIS Algorithm to Estimate CDOM in the Typical Bays of China[D]. Dissertation of master's Degree of Dalian Maritime Universtiy. 2006.

SONG Qing-jun, TANG Jun-wu, MA Rong-hua. Correction of Backscattering Coefficients in Different Water Bodies. Ocean Technology, 2008, 27(1): 48-52.

SUN Li-ran. Study on Algorithm for Retrieval of Water Constituents from Ocean Color Remote Sensed Data in Case Ⅱ Waters [D]. Dissertation of Doctor's Degree of Beijing Normal Universtiy, 2009.

WANG Fan. Estuary Water Suspended Matter Inherent Optical Property and Concentration Remote Sensing Inversion Model[D]. Dissertation of Doctor's Degree of Zhejiang University, 2008.

WANG Feng, ZHOU Yi, YAN FuLi, et al. Atmospheric correction algorithm for modis imagery over case Ⅱ waters based on SWIR. Journal of Infrared And Millimeter Waves, 2009, 28(5): 346-349.

WANG Gui-fen, CAO Wen-xi, XU Da-zhi, et al. Variations in the Light Absorption Coefficients of Non-algal Particels in the North of the South China Sea. Ocean Technology, 2007, 26(1): 45-49.

WANG Gui-fen, CAO Wen-xi, XU Da-zhi, et al. Effects of size structure and pigment composition of algal population on phytoplankton absorption coefficients in the South China Sea. Acta Oceanologica Sinica, 2007, 29(1): 38-48.

WANG Gui-fen, CAO Wen-xi, YANG Ding-tian, et al. Decomposing Total Suspended Particle Absorption Based on the Spectral Correlation Relationship. Spectroscopy and Spectral Analysis. 2009, 29(1): 201-206.

WANG Gui-fen, CAO Wen-xi, YANG Yue-zhong, et al. Variations of absorption coefficient of seawater in the Pearl River Estuary and a hyperspectral retrieval model for an algal bloom. Journal of Tropical Oceanography. 2010, 29(2): 52-58.

WANG Gui-fen, CAO Wen-xi, ZHOU Wen, et al. Retrieval of phytoplankton size structure based on the spectral slope of phytoplankton absorption in the northern South China Sea. Journal of Tropical Oceanography, 2010, 29(2): 25-32.

WANG Lin, ZHAO Dong-zhi, FU Yun-na, et al.Discussion on the correlation between absorption coefficient ag(440) and the slope Sg of CDOM. Journal of Dalian Maritime University, 2007, 33(S2): 179-182.

WANG Lin, ZHAO Dong-zhi, XING Xiao-gang, et al. The effects of pheophytin on absorption characteristics of phytoplankton. Oceanologia et Limnologia Sinica, 2009, 40(5) : 596-602.

WANG Lin, ZHAO Dong-zhi, YANG Jian-hong, et al. Study on seasonal variation of phytoplankton absorption coefficient in north Yellow Sea. Marine Environmental Science, 2010, 29(1): 60-65.

WANG Xiao-Mei, TANG Jun-Wu, SONG Qing-Jun, et al.The statistic inversion algorithms and spectral relations of total absorption coefficients for the Huanghai sea and the East China Sea. Oceanologia Et Limnologia Sinica, 2006, 37(3): 256-263.

WANG Xiao-yong LI Tong-ji LIU Wei, et al.Empirical Models Between Apparent and Inherent Optical Properties in the East China Sea and Yellow Sea. Ocean Technology, 2008, 27(1): 58-64.

WEI Zhi-Qiang ZHANG Kai-Lin WU Dong. Algorithmic Research for Measuring Chlorophyll-a Concentration in the Sea Surface Layer by Using Airborne Ocean Fluorescence Lidar. Periodical of Ocean University of China. 2007, 37(1):157-162.

WEN Jian-guang, XIAO Qing, YANG Yi-peng, et al. Spectral mixing model and its stability of chlorophyll-a concentration extraction based on hyperspectral data. Advances In Water Science, 2007,18(2): 270-276.

WU Chuang-qing, WANG Qiao, WANG Chang-zuo. Sea Concentration Reverse Model with Choraphyll-a Influence Removing. Environmental Monitoring in China, 2009, 25(2): 26-30.

XI Hong-yan, ZHANG Yuan-zhi, QIU Zhong-feng, et al. A semi-analytical algorithm to retrieve chlorophyll-a concentrations in the coastal region of Hong Kong and its vicinity. J. Lake Sci, 2009, 21(2): 199-206.

XING Qian-guo, CHEN Chu-qun, SHI Ping. Atmospheric correction of using Landsat data to retrieve sea surface temperature in coastal waters. Acta Oceanologica Sinica, 2007, 29(3): 23-30.

XING Xiao-gang, Zhao Dong-zhi, Liu Yu-guang, et al. A new MODIS algorithm for estimation of chlorophyll fluorescence quantum yield in natural waters. Chinese High Technology Letters, 2008, 18(1): 77-83.

XING Xiao-gang, ZHAO Dong-zhi , LIU Yu-guang, et al. Absorption characteristics of de-pigmented particle and yellow substance in Bohai Sea. Marine Environmental Science, 2008, 27(6): 595-598.

XIU Peng. Studies on Ocean color Remote Sensing in the Bohai Sea of China. [D]. Dissertation of Doctor's Degree of Ocean University of China, 2008.

XU Da-zhi, CAO Wan-xi, WANG Gui-fen. A bio--optical model for retrieval of chlorophyll-a concentration in northern South China Sea. Journal of Tropical Oceanography. 2007, 26(2): 15-21.

XU Jing-ping, ZHANG Bai, SONG Kai-shan, et al. Bio-Optical Model of Total Suspended Matter Based on Reflectance in the Near Infrared Wave Band for Case-Ⅱ Waters. Spectroscopy and Spectral Analysis, 2008, 28(10): 2273-2277.

Xu Meng, Yu Fan, Li Ya-Chun, et al.The Method of Atmospheric Correction on the EOS/MODIS Data with 6S Model. Journal of Nanjing University(Natural Sciences), 2006, 42(6): 582-589.

XU Xiao-jun. Analysis and remote sensing of suspended particle in Southern Yellow Sea coastal water[D]. Dissertation of master's Degree of Nanjing Normal University, 2007.

YANG Jin kun, CHEN Chu-qun, TANG Shi-lin, et al. Research on chlorophyll fluorescence properties of water in Zhujiang River estuary. Journal of Tropical Oceanography, 2007, 26(4): 15-20.

YANG Jin-kun, CHEN Chu-qun.An optimal algorithm for retrieval of chlorophyll, suspended sediments and gelbstoff of case Ⅱ waters in Zhujiang River estuary. Marine Science Bulletin, 2009,11(1): 15-20.

YANG Wei, Matsushita Bunkei1, CHEN Jin. Deriving inherent optical properties through training samples with known concentration of water constituents and reflectance spectra. Journal of Lake Sciences. 2009, 21(2): 207-214.

YU Kun, LU Dian-mei. Atmospheric correction of modis data for case-ii water and research of monitoring and retrieving chlorophyll concentration in the Bohai Sea.Marine Science Bulletin, 2009, 28(5): 21-27.

ZHANG Hong-liang. Evaluation research on chlorophyll concentration retrieval by FLH algorithm in Bohai sea[D]. Dissertation of master's Degree of Inner Mongolia University, 2007.

ZHANG Min-wei, TANG Jun-wu, CHEN Liang-fu, et al. Study on the POLDER ocean color atmospheric correction algorithm. Marine Science Bulletin, 2009, 28(5): 95-100.

ZHANG Min-wei, TANG Jun-wu, Dong Qing, et al. Retrieval of total suspended matter concentration in the Yellow and East China Seas from MODIS imagery. Remote Sensing of Environment, 2010, 114: 392–403.

ZHANG Ting-Lu, LI Xiao-Xia.A Remote Sensing Method for the Determination of Seawater Diffuse Attenuation Coefficient Based on Artificial Neural Networks. Periodical of Ocean University of China.2007,37(4):676-680

ZHANG Ting-lu, QIU Guo-qiang. Algorithms based on artificial neural network for retrieval of oceanic constituents in Case Ⅱ waters. Journal of Lake Sciences, 2009, 21(2): 173-181.

ZHANG Yan-zhe, ZHENG Xiao-shen, ZHANG Bo. Study on Retrieval of Chlorophyll Concentration by Remote Sensing in Bohai Sea. Journal of Tianjin University of Science＆Technology, 2010, 25(1): 51-53.

ZHAN Hai-gang, SHI Ping, CHEN Chu-qun. Quasi-analytical algorithm of inherent optical properties of seawater based on Bayesian theory. Chinese Science Bulletin, 2006, 51(2): 204-210.

ZHAO Dong-zhi, YANG Jian-hong, ZHAO ling, et al. MODIS Bio-optical algorithms in Liaodong Bay(Ⅰ) Algorithms assessment. Marine Environmental Science. 2007, 26(5): 401-407.

ZHAO Wen-jing. Researching on the inversion model of suspended particle matter concentration and applications of different sensors for the Yellow river estuary[D]. Dissertation of master's Degree of The First Institute of Oceanography, SOA, 2007.

ZHAO Wen-jing, ZHANG Jie, CUI Ting-wei, et al. Enteromorpha Prolifera Underwater Spectral Research Based on Simulation of Radiation Transmission. Spectroscopy and Spectral Analysis, 2009, 29(6): 1656-1660

ZHOU Hong-li, HAN Bing, LI Tong-ji, et al. Variations in the Light Absorption Coefficients of De-pigment Particles in South Yellow Sea and Zhu Jiang Kou of China. Ocean Technology, 2007, 26(3): 114-117.

ZHOU Hong-li, ZHU Jian-hua, HAN Bing, et al. The Effect of Different Pathlength Amplification Correction Factor to the Typical Absorption Spectrum of Seawater in China. Ocean Technology, 2010, 29(1): 46-50.

ZHOU Wen, CAO Wen-xi, LI Cai. Modeling absorption and scattering properties of mineral particles suspended in seawater based on Mie theory. Journal of Tropical Oceanography, 2008, 27(1): 22-26.

ZHOU Wen, CAO Wen-xi, LI Cai, et al. Spectral Scattering Property of Phytoplankton Calculated by Absorption Coefficient and Size Distribution. ACTA OPTICA SINICA. 2008, 28(8): 1429-1433.

ZHOU Wen, CAO Wen-xi, YANG Yue-zhong, et al. Spectral variability of particulate backscattering ratio in the Daya Bay. Journal of Tropical Oceanography. 2010, 29(2): 39-45.

ZHOU Wen, CAO Wen-xi, LI Cai, et al. Effects of algal cell structure on the optical properties of phytoplankton. Journal of Tropical Oceanography. 2010, 29(2): 33-38.

ZHOU Wen, CAO Wen-xi, WANG Gui-fen, et al. Retrieval of pigment concentrations from the absorption spectra of phytoplankton by multilayered perceptrons. Journal of Tropical Oceanography, 2010, 29(2): 46-51.

ZHOU Wen, WU Jing-yu, SHANG Shao-ling, et al. Characteristics of Chromophoric Dissolved Organic Matter Absorption in the Southern Taiwan Strait During Summer 2005. Journal of Xiamen University (Natural Science), 2007, 46(4): 538-542.

ZHU Jian-hua, ZHOU Hong-li, LI Tong-ji.Research on Optical Path Enlargement Emendation Factor of optical transmission-Light Reflex Methods. Ocean Technology, 2008, 27(1):53-57.

ZHU Jian-hua, ZHOU Hong-li, LI Tong-ji, et al. Study on Applicability of Pathlength Amplification Correction Factor with T-R Method Based on Chlorella Vulgaris. Ocean Technology, 2010, 29(1): 40-45.

RECENT PROGRESS OF MARINE INFORMATION TECHNOLOGY IN CHINA: 2006-2010

Ge CHEN, Wenqing LI, Qianqian KONG, Shouxin LIU,

Chongjing LV and Fenglin TIAN

(Engineering Research Center of Marine Information Technology, Chinese Ministry of Education,College of Information Science and Engineering, Ocean University of China,238 Songling Road, Qingdao 266003, China .Email: gechen@ouc.edu.cn)

Abstract

In this article, the progress of marine information technology in China during 2006-2010 is reviewed with emphasis on marine geographical information system (GIS), virtual marine environment and digital ocean system. The marine GIS can be divided into two categories: Thematic system and generic system, recent achievements of which by Chinese researchers are summarized respectively. Several suggestions for future development of marine GIS in China are proposed. Meanwhile, an overview of the applications of virtual reality and visualization technology to ocean simulation in the context of marine environment, digital ocean and marine engineering operation is presented, and their trend of development is addressed.

Key words: marine geographical information system, virtual reality, digital ocean, dynamic visualization, ocean simulation.

With the rapid development of science and technology accompanied by serious challenges of population growth, environmental degradation, resource depletion, climate anomalies and other issues, people are paying more attention to the ocean which comprises 71% of the earth's surface. As a powerful tool for dealing with ocean issues, marine information technology has been attached increasing importance by not only sea experts but also decision makers, among which geographical information system (GIS) and virtual reality (VR) are of particular interest. The marine GIS with its prototype came into being in 1980s can be currently divided into two categories: The thematic system and the generic system. The former is considered as a transformation from land-oriented commercial software to oceanographic applications in the form of "secondary development". In the latter category, an original kernel-related software platform is developed with GIS functionalities specialized in dynamic marine data management, spatiotemporal analysis and multi-dimensional ocean visualization. Meanwhile, virtual marine environment and digital ocean become new areas of active research in marine information technology. The powerful capacity and potential applications of 3-demensional (3D) virtual reality characterized by "immersion, interaction and imagination" (the so-called '3I') are widely recognized. In this article, the research and development progress of marine information technology in China during 2006-2010 is reviewed with emphasis on oceanographic applications of GIS and VR technologies, the future trends of which are also discussed.

Ⅰ Marine Geographic Information System

The huge amount of multi-source data brings challenges to its storage, management, maintenance,

fast access, intelligent analysis, visualization, and automatic mapping. As a common technology of spatial information processing and a powerful tool for dealing with complex spatiotemporal problems, more and more attention are paid to GIS by the sea experts.

In recent years, the development of marine GIS can mainly be classified into two categories: The thematic system and the generic system. The former refers to oceanographic applications closely related to human activities, such as ocean environment monitoring, ocean functional zoning, ocean resources exploitation, and so on. It is usually treated as an extension from land to ocean. However, the latter focuses more on the characteristics of the ocean itself. The multi-dimensional and dynamic nature of marine environment determines that marine GIS has tremendous differences from traditional land-oriented GIS in many aspects, such as data management, spatiotemporal analysis and visualization, etc.

1 Thematic Marine GIS

In this section, three kinds of thematic system are introduced: Ocean environment monitoring, ocean functional zoning and ocean resources exploitation.

(1) Marine GIS for Ocean Environment Monitoring

Marine disasters not only bring great damages to the safety of people's lives and properties, but also cause huge losses to many industrial facilities. Ocean environment monitoring is essential in marine disaster mitigation.

Ocean monitoring is usually applied to environmental protection. Yu et al. [1] introduce GIS technology into the protection of marine environment and develop an environmental protection GIS of Hebei province, which has been provided an effective method for ocean management and ocean environmental protection.

Nowadays, Internet has become an important way of ocean monitoring information dissemination, it can decrease the losses caused by early warning of marine disasters. Based on distributed database and web geographic information system (WebGIS), Chen et al. [2] design a marine dynamic environment monitoring system for marine monitoring and information sharing in Fujian Province.

Ma [3] designs a marine extensive makeup language (XML) schema for data exchange between heterogeneous platforms and different monitoring systems. He develops a client-based marine geographic information system (MGIS) based on Map-objects and marine XML. Some key technologies such as data rendering, vector query and attribute query are depicted in detail.

Based on components technology, Kong et al. [4] develop a marine meteorology information system using MapX5.0, Visual Basic 6.0 and SQL Server 2000, which realizes GIS-based applications in the marine meteorological disaster prevention and mitigation.

Focusing on the monitoring and the information publication, Li [5] conducts a deep study to enhance and guarantee's real-time capability of system.

In order to meet different users' demands for ocean monitoring in real time, Jiang et al. [6] combine WebGIS with other information technologies, and establish a marine information network system based on ArcIMS platform. This system delivers its information in the form of diagram, data file, product-report, etc.

(2) Marine GIS for Ocean Function Zoning

Ocean function zoning is to divide the sea into different functional areas, according to different

natural resources, environment conditions and ocean exploitation. Reasonable ocean function zoning can effectively control and guide the ocean exploitation activities, protect marine ecological environment, and keep the development of marine economy sustainable.

Liu [7] develops an ActiveX component to integrate multi-source spatial-data. With the component, a maritime management system is established to realize a number of functions such as ocean function zoning, multi-source spatial-data integration, dynamic display of Jiaozhou Bay pollutant dispersion, and so on.

Combining ArcEngine with Google Earth API, Xie et al. [8] develop a Shanghai ocean function zoning system. It integrates 2D and 3D display services. The system is a very good reference for the development of 3D GIS.

After deep analysis of the function zoning and function utilizing of sea areas, Qi et al. [9] develop a marine information management system. The system realizes highly efficient edit, query, update and other functions, and provides a strong support for sustainable use of the South China Sea.

(3) Marine GIS for Ocean Resources Exploitation

The purpose of marine research is to develop and utilize the ocean more effectively, among which ocean resources exploitation is of high priority, but is also a difficult task. Marine GIS can provide people with ocean information intuitively and in real-time, and guide marine production activities effectively.

Li et al. [10] develop a marine hydrological information system by using the functions provided in MapObjects. This system realizes the functions of data management, map browsing, information query, automatic drawing of hydrological thematic map, etc. It solves the problem of query, visualization and analysis in traditional management system.

Using C# and MapX component technology, Wang [11] develops a multi-functional information analysis system, which provides not only basic functions of GIS but also some models for seabed sediment data management and analysis. This greatly enriches the seabed sediment database.

According to the background of PANDA (The Prydz Bay, Amery Ice Shelf and Dome A Observatories-A Chinese Key International Program for IPY) section marine information database development project, Zhou et al. [12] realize the data query function of the visualizing network data sharing system based on WebGIS. The means of displaying and querying is diversified, through which the share and application of the marine information data are promoted.

Feng et al. [13] design and implement a database management system (DBMS) for marine geological survey. The methods of implementing key functions such as distance and area measures, contours generation, spatial distribution analysis are discussed. It has certain reference value to the design and practice of similar GIS.

Niu and Zhao [14] review the applications of RS and GIS technologies in marine fisheries in two aspects: Sea surface temperature (SST) and chlorophyll concentration. They make a discussion to problems in the applications. In order to meet the needs of construction of offshore oil industry, Zhang et al. [15] propose a GIS model which is developed by establishing a GIS spatial-object database and introducing a Service Oriented Architecture (SOA). This model can integrate application services of several professional databases such as offshore oil exploration, development, engineering and so on. Through its development in various projects, the comprehensive application of all professional information in cross system has been realized.

2. Generic Marine GIS

Current commercial GIS softwares mainly focus on land environment, and they are not suitable for multi-dimensional dynamic marine data expression, management, processing and analysis. As a result, the research and development of a generic marine GIS become an urgent task.

(1) Marine Data Integration and Sharing

Marine data integration and sharing plays an important role in marine GIS. To construct an effective frame for marine environment information system, Li [16] carries on research about data warehouse based marine environment data integration, component based marine environment data processing methods integration, Web Services, and ontology respectively based marine knowledge integration. Based on these research achievements, he develops new generation of MAGIS (Marine and Atmospheric Geographical Information System).

Aiming at the characteristics of marine information sharing, Zhang et al. [17] study the directory service of metadata based marine information. They design a marine information resource directory service system, which provides the efficient search, security access and management control functions to users.

Based on the study of complexity of spatial-temporal analysis, Shao et al. [18] discuss the characteristics of the order service mode in MAGIS. With multi-thread, Web Service and batch technology, they develop a new integration solution with order and spatial-temporal analysis as its key.

Taking the South China Sea as study area, Xiao et al. [19] choose three kinds of representative marine environmental example to build a prototype system of multi-source marine environmental information grid platform. It has been proved to be feasible.

To make full use of massive marine data, Zhang et al. [20] design an ocean information sharing system based on the ASP.NET three-layer framework. The system can obtain ocean data with the information acquisition subsystem and provide sharing service of ocean information with sharing and service subsystem.

According to the demand of moving the management of marine observation data from manual to computer intelligent of currently domestic marine environmental monitoring job, Li et al. [21] design a practical data management system for marine environmental monitoring. This system integrates the data of existing observation equipment, and implements intelligent management. It reduces the management cost of marine observing system effectively, and provides more information for the dynamic marine information website.

By researching in the geographic information system, grid technology, Web service technology as well as remote visualization technology. Taking the South China Sea as the experimental zone, He et al. [22] realize a prototype system of marine environment information grid service platform. This prototype system can greatly improve efficiency, reduce duplicated investment and solve the problems of heterogeneity, distribution and efficiency triggered in networking.

(2) Marine Data Visualization

With the exponential increase of marine and atmospheric remote sensing data, more and more attention is paid to the development of specialized visualization software to present these data. Considering the characteristics of marine environment data, Huang [23] proposes a marine environment-oriented spatial and temporal data organization model and a GIS-based visualization technology integration framework. Analyzing the deficiency of existing GIS data model in marine environment, he designs the object-oriented data model which integrated field and feature. With the dynamic organization of resources, he designs a multi-grid system architecture for marine environment

data visualization.

Xu et al. [24] develop a multi-dimensional animated visualization system for marine and atmosphere. The system is developed on Java platform, while using special graphics packages of Java and the API of VisAD, the interactive visualization system is realized, the rendering of multi-dimensional data of marine and atmosphere environment is implemented, and a human system interface is also provided.

To satisfy the need of marine data remote visualization, Tang et al. [25] construct the remote visualization environment using grid technology. It can deal with a static and dynamic massive marine data service dynamically, highly, precisely and in real-time.

Taking the data type and collection manner of ocean temperature into account, Tu [26] analyzes the feature of 3D ocean temperature field and uses the multi-quadratic interpolation method to create an uninterrupted 3D ocean temperature field. With volumetric visualization technique, 3D ocean temperature fields are classified, an effective method to realize 3D visualization of ocean temperature field is also developed.

Based on the analysis of the recent network visualization technologies for massive data and characteristics of spatial-temporal process of marine scalar field, Liu et al. [27] discuss the network visual expression for point process and polygon process of marine scalar field. A new method to realize the remote realization for the marine spatial-temporal process has been proposed. A prototype system has been set up to visualize the SST of Taiwan Strait through the Web. In this system, some functions are accomplished, such as the value query in the whole process, the process curve drawing of any random point in the SST field and the visual analysis for the polygon process in the SST field.

For the visualization of vector data, Yang et al. [28] analyze the need for real-time dynamic internet visualization of marine vector fields and its technologic difficulties, and then introduce web service and network GIS technologies which are the theoretical base of the system. They discuss the method and structure of vector fields visualization of Ocean environment system in detail. Finally, taking ocean current data as an example, they realize network real-time visualization platform of ocean current data with the support of network service from ArcGIS and visualization service from ArcEngine.

Analyzing the type of ocean hydrological data for visualization methods, Liu [29] proposes a number of marine hydrological data visualization methods, and achieves the visualization of current data and sediment data based on GIS technology.

Ma [30] uses the multi-level topology approach to simplify the topology image based on traditional topology visualization results. She introduces the steps of multi-level topology visualization: (1) The critical point using the traditional topology visualization methods is obtained. The critical point that can be ignored based on the principle of statistics is filtered, and the integral curve is drawn. (2) The method is applied to ocean flow field. According to the experimental results, the multi-level topology visualization can show the main features of flow field without excessive cluttering while maintaining the global structure of flow field.

Ⅱ Virtual Marine Environment and Digital Ocean

3D virtual reality is quite popular in the area of computer simulation by providing participants with a true feeling of realism. Therefore, rendering marine scenes and expressing marine data in intuitive ways have become the most effective means to display information to users. The research and development activities can be divided into three categories: Virtual marine environment, digital ocean proto system and simulation of ocean phenomena or operation.

1 Virtual Marine Environment

In this section, we describe some aspects of virtual reality technology that are used in the context of ocean environment. It mainly includes ocean wave simulation and seabed terrain rendering. Some methods of ocean water information presentation are also contained.

(1) Virtual Sea Surface

Ocean wave is a complex natural phenomenon at the sea surface, which is irregular in both time and space. Simulation of ocean wave is one of the most difficult tasks in computer graphics, but is very important in not only ocean surveying and mililary environment simulation, but also in waterpower study, fluid and wave mechanics and entertainment.

Zhao et al. [31] simulate the variation process of ocean wave in changing winds, which is neglected in previous work of ocean wave simulation. They present a wave model using frequency spectrum and directional spectrum for a deep and fully developed sea based on the results of oceanographic observation and research. They further present a wind model designed as a segmented function, which describes the wind speed and directional changing process. Finally, they combine the wave and wind model, and simulate ocean wave transformation under changing wind. Pan and Liu [32] analyze the implementation principle of sea surface in real-time 3D scene. They study how to use direct3D and high level shader language to realize specific algorithms of the sea surface effects. They propose a method which could optimize the performance of traditional code. Shi and Jiang [33] present a method for simulating 3D shallow waves based on Longuet-Higsis model and wave spectrum, and they use the true wave spectrum to control ocean waves. In order to obtain perfect real waves effect, they propose a image processing method for improving the detail, color and illumination of waves. Moreover, they simulate 3D shallow waves. Based on Cg and OpenGL, Ma et al. [34] use some technologies including p-buffers, bump mapping, projective texture mapping and dynamic texture mapping synthetically to simulate a real-time water surface. In this simulation, some effects such as reflection, refraction, wave and caustics are realized. The water surface is constructed only by two triangles.

Wang [35] proposes a novel approach for simulating realistic ocean surface, using a statistical model and Fast Fourier Transform to provide a high performance native wave model. He also studies the marine special effects. The method he proposes can well achieve the performance required for interactive real-time 3D simulation and training.

Luo and Zhong [36] create the model based on spectrum of ocean waves and level-of-detail (LOD) technique. They render the ocean surface by lighting and texture mapping. Gao et al. [37] study two models for ocean waves, with high light on the ocean wave theory with Vega. Sun et al. [38] use stochastic number to simulate ocean waves. The location, size and undulation of ocean waves are stochastic, and new ocean waves are created randomly as ocean waves move toward the coast. They use Phong illumination model to simulate reflected light of the water surface and calculate critical points to model the images of the sun in the water. The animated large scale 3D ocean waves generated by this model will not repeat during movement. It is suitable for digital reappearance of the ocean and modeling of ocean elements.

Li et al. [39] present a practical algorithm for real-time rendering of realistic and unbounded ocean. Relying on the latest features of graphics programmable units (GPU), they adopt parallel computing technique for generating ocean surface in GPU and use efficient shading trips for rendering optical effects of ocean surface. The main features of the work concentrate on three fields: Ocean surface generation in compute unified device architecture, adaptive ocean surface tessellation based on LOD;

and sophisticated optical effects. Liu et al. [40] establish a marine environment with a realistic ocean surface using Vega Prime for interactive real-time 3D-simulation. The simulations of various waves have been developed according to numerical models or wave data sampled in experiments. By transferring CAD models to open flight models, the ship movements could be displayed in the virtual marine environments. Considering sphere shape's influence and free viewpoint, Li et al. [41] propose a new method for modeling and present rendering of ocean wave. Its kernel is the modeling of ocean waves on sphere and screen-subdivision algorithm. Yang et al. [42] present the algorithm of real-time realistic water surface rendering based on GPU. They also introduce the technique of graphics and mathematical used in water surface rendering. This algorithm accomplishes many effects such as water waves modeling through fixed vertex streams, bump mapping and texture blending, reflection and refraction by water, and so on.

Chen et al. [43] use the latest GPU shader to reduce the complexity of the water model. The water simulation is divided into four stages: Wave generation, surface tessellation, optical simulation, and water surface rendering. The result from implementing the respective stages' shader is satisfying.

(2) Virtual Seabed

Digital seabed terrain rendering in complex natural environment at high frame rates is a challenging problem in virtual ocean technology.

Wei et al. [44] systematically study the constitution of 3D ocean environment and environment modeling technology. The ocean geographic environment information is obtained from 2D electronic chart directly. The 3D landform data is translated into the DED file (a file format supported by MultiGen) which could serve as the data of landform 3D modeling.

The main idea of the Geometrical Clipmap, which is a graphic hardware-based terrain visualization algorithm, is used by Kang et al. [45] They focus on simplification of the details and discuss the methods of texture mapping. It promotes the rendering effects by a new high performance frustum culling method and crack filling technique. Their experiment results show that this approach can reach fine performance for real-time rendering of massive terrain dataset combining with the tile-pyramid model and multiple threads. Ma et al. [46] discuss several critical methods for implementing under water digital terrain models, including the dual transformation in digitizing, the DEM generating method based on depth contours, and the 3D terrain rendering on spherical surfaces. Taking the development of the Digital South China Sea system as an example, the techniques proposed are well validated.

(3) Virtual Sea Water

On the basis of the requirement of water information presentation of a digital ocean system, Liu et al. [47] propose a method for cubic water data modeling and building. Based on the 3DGIS software package, such as Terrasuite and EV-Globe, they study sea surface modeling, water information presentation, and virtual ocean scenery building, especially, they present water features with "cubic grid".

2 Prototype System of Digital Ocean

In this section, we focus on the architecture of digital ocean prototype system and modeling of various ocean elements.

Han et al. [48] define a concept of virtual marine environment and propose an integral conceptual architecture of virtual marine environment, which is composed of a computing network layer, a marine data layer, a multidimensional representation layer, a personal perception/cognition layer and a

multi-user collaboration layer. In addition, they propose a technological framework of constructing virtual marine environment according to the process of transmitting and processing information, followed by a detailed discussion about technologies and methods which are used to acquire, process, model and represent marine information. They also discuss perception/cognition of virtual environment and geo-collaboration. At last, they point out the significant and difficult issues related to construction of virtual marine environment. Based on the characteristic of marine, Su et al. [49] construct a prototype of digital sea of china (PDSC) with datum of coast line of China. With the foundation of PDSC, they emphasize on the problems with their resolutions, which differ from other space digital fields, especially on the data organization and manipulation with the datum of coastal line, the structure of "Digital Sea" and the integration method, the logic computation and the visualization method.

Chen et al. [50] propose a real-time method for simulating integrated ocean environment, including sky sphere, atmospheric system and ocean wave model. With this method, the effect of cloud floating in sky sphere is obtained through texture perturbation, while the air scattering and absorbing effect is realized in the atmospheric system. The ocean wave model constructs ocean surface mesh by sine wave and realizes the bumping effect of ocean surface through normal disturbance of bump map. For the lightening computation of ocean wave, the incident ray can be obtained by sampling the sky sphere and the reflecting light ray can be calculated through the principle of mirror reflection.

Sun et al. [51] conduct a research to the basic principle and technical frame of "Digital Ocean" and provide a solution to ocean information management. Liu et al. [52] give one kind of understanding of "Digital Ocean" in China and put forward the architecture of the china digital ocean prototype system (CDOPS). In addition, they present the design and preliminary realization of 9 sub-system functions. They also discuss some key problems in constructing CDOPS. Wang et al. [53] present an ocean model of multidimensional representation layer and architecture of whole system. They propose a kind of texture animation in Vega Prime as a substitute for particle system, which is used to implement accurate simulation of floater, foam and shoal, and take less processing resources. The simulator also provides the mathematics model of wind-generated waves and its LOD. In summary, the virtual marine environment within a certain range in a computer system is shown realistically. Chen et al. [54] develop an original digital platform (VR-Ocean) for real-time simulation and fast editing of ocean environment and marine life. They design the overall structure, work flow and interactive functions of the VR-Ocean platform. Key technologies applied include separate rendering of underwater from sea surface elements, direction oriented path planning, caustics rendering through dynamic textures, etc. Main focuses of the platform are shape and behavior simulation of ocean beings. The display of dynamic ocean effects are implemented VC++, OpenGL and GPU.

3 Simulation of Ocean Phenomena and Ocean Operation

Zhao et al. [55] use Creator and Vega to build virtual ocean geographic environment and submarine model. The six freedom motion of submarine in the application is controlled. Dai et al. [56] settle the contradiction between reality of modeling and real-time characteristics of simulation with a complete simulation model. The vision effect is generated based on Vega software environment, and the scene simulation program is written with Visual C++. Several detailed problems such as simulation driving, observer design, record and replay of the simulation are solved.

Tang et al. [57] build a virtual prototype for the heave compensation system used on a marine drilling platform. The parametric design, operation process and the performance of a fuzzy logic control on this virtual system have been simulated and investigated. Zhang et al. [58] propose new attempts to evaluate

the hazards of tsunami and large-scale numerical visualization work for tsunami simulations is done. The developing scheme of visual system based on Vega combined with the submarine's visual system in voyage training simulator is researched and presented by Xiao and Hu [59]. The situation models and virtual battlefields are established. Collision avoiding and special effects are applied in the visual system. In order to simulate the process of obstacle avoidance for autonomous underwater vehicle (AUV) on horizontal plane in virtual environment, Ma et al. [60] develop a visual simulation system of obstacle avoidance for AUV on HP workstation based on MultiGen Creator and Vega. They propose a simulation method of forward looking sonar (FLS). Utilizing the collision vector function provided by Vega and a self-defined volume collision method, the function of FLS is simulated. A fuzzy inference system is designed to derive the obstacle avoidance angle based on the position relationship of AUV and obstacle. The obstacle avoidance for AUV on the horizontal plane in virtual environment is implemented. Based on software platform Vega and MultiGen Creator, Gui et al. [61] develop a simulation system of AUV for bottom tracking. They introduce the selection of software, the model construction, the generation of virtual ocean environment and terrain, the implementation of fuzzy rules, and the application of virtual reality techniques in detail.

Yang et al. [62] adjust the real-time linear accumulation ocean wave spectrum algorithm by disturbing weighted phasic and amplitude factors which meliorate the defective smooth figure of billows and stormy waves. Based on the psychoacoustics and musical acoustics, an advanced storm wave parameter adjusting method is proposed, and a real-time sound implementation node using audio equalizer is realized. An advanced real-time combining environmental influence algorithm is presented based on the synthetic natural environment (SNE) information such as stormy level, wind level, equalized wave amplitude and average cycle. Runtime shading method for flowing texture is proposed, background texture is appended after mirror-image generation and Gauss blur distortion. They modify texture graphical quality and also reduce image noise after this underline processing. They realize a harmonic visual and audio virtual system combing SNE information which testifies the feasibility of the advanced storm wave spectrum. The storing volume of 3D models is an important problem in distributed virtual environment (DVE). Complex models are always the “bottleneck” of large scale DVE performance. Aiming at this, You et al. [63] propose a method of building DVE based on fractal technologies, and combined with OpenGL, construct a “Sea Battlefield Distributed Virtual Environment”. They analyze all kinds of 3D models fractal algorithm, including wave, seabed terrain, texture and plants. They also discuss the storing formats of 3D models and the architecture of DVE database. Li et al. [64] propose a system structure of situation display of ocean battlefield. They discuss the key technology of 3D display such as ocean modeling, and rendering of formation pattern and its transformation in the battle field. The software Creator and Vega are used by Chang et al. [65] to build a virtual marine geographic environment and the deep submergence rescue vehicle (DSRV), the virtual simulation system is created, with which the virtual simulation of docking process of DSRV and disable marine is done.

Ⅲ Summary and Perspective

Comparing to the development of land related information technology, marine information technology is relatively immature. In the near future, there is going to be a rapid development in marine related virtual reality, 4D visualization, data integration and expression methods, on the basis of which researchers are expected to do more geospatial analysis and demonstration to facilitate their research

work. With the process of marine data service, people can fully use existing data resources, and greatly reduce expenses and repeated labor in data collection greatly. Marine information technology will have a wide range of applications such as 3D navigation of marine transportation, real-time display of marine operations and simulation or forecasting of marine phenomena.

The future trends in marine information technology can be briefly summarized as the following:

1. Interactive visualization of integrated multi-data-source, multi-data-format and massive marine information: With the persistent development in the means of information acquisition, source of marine data is expanding dramatically, followed by a large variety of data formats, and an explosive growth of information content. In future, the decentralized information should be stored in local database. And a higher level data structure will be extracted as a unified expression for heterogeneous data formats. The Out-of-Core, cluster based massive data storage and other data management methods should be considered to support the visualization of massive information. The latest graphics and visualization technology will also be utilized to explore the computing power of computer hardware and deliver intuitive visual information to the user.

2. A variety of visualization methods integrated for visualizing the marine information: Obtaining the diversity of marine information, we need to use a variety of visualization methods for better communication between the data and the user, such as dynamic volume rendering, 3D vector field visualization and so on. All these information expressions are based on a global marine information platform.

3. Oceanographic information analysis with data mining: With the rapid development in information acquisition technology, more and more ocean-related data are accumulating. Traditional data processing methods have been unable to make full use of the hidden information in these data, and data mining technology is therefore needed. Data mining extracts implicit knowledge from a large number of incomplete, noisy, ambiguous and random data. People do not know the knowledge in advance, which might be potentially useful. With data mining techniques analyzing marine information, the user can get effective, accurate and relevant information interactively.

4. Real-time visualization and feedback of live data: With the development of communication technology, real-time accessing to marine live data has become possible. Users could make decisions in a timely manner with these live information. While using advanced communication technology, the sensor could be feedback and make appropriate adjustments.

5. Sample data based marine simulation technology: After analyzing the sampled marine data, certain rules can be deduced. Based on the rule, giving some necessary parameters in given circumstances, the simulation of marine information could be done, such as simulation of ocean currents, sea water surface temperature changes and so on.

6. Internet service based multi-user accessing and specific data services: The management of massive marine data could be integrated with the Internet service to simplify the distribution and access to marine data. This means that the user can either obtain the required services through the network of marine information or submit valid data through the network.

7. User-friendly and efficient data management API for secondary development: In the future, marine information management platform will be open and flexible. Based on open platform API, users will be able to choose different functions for customized applications to meet different needs.

Acknowledgements:

This work was jointly supported by the Natural Science Foundation of China under Projects 40730530 and 41076115, the National Basic Research Program of China under Project 2009CB723903, and the National High-Tech Research and Development Program of China under Project 2008AA121701.

References:

[1] Yu, Z. J., W. L. Cui, J. Q. Yang, Z. G. Bu, Z. Q. Li, Y. L. Wang, L. Qu, and D. H. Jiang, Geographic information system and application to marine environmental protection of Hebei province, *Marine Environmental Sciences*, 25, 83-86, 2006.

[2] Chen, C. B., C. C. Chen, M. H. Fan, and D. W. Zhong, Design and implement of a marine dynamical environment integrated observing and information-sharing system, *Marine Sciences*, 30, 53-58, 2006.

[3] Ma, T. X., Web-based data mining of marine environmental monitoring and dynamic information release system, Master thesis, *Shandong University*, Jinan, 2006.

[4] Kong, Z. L., H. Q. Tang, J. S. Pan, and J. Yang, Development and application of marine system based on GIS, *Journal of Southeast University*, 38, 217-220, 2008.

[5] Li, X. Q., Research on real-time performance on distributed marine environment monitoring and information publication system, Master thesis, *Shandong University*, Jinan, 2008.

[6] Jiang, D. Y., W. L. Cui, J. Q. Yang, Z. G. Piao, and X. H. Gao, Marine ecological monitoring information online analysis system design and implementation, *China Environmental Science Society Annual Conference 2009 Technology*, 430-434, 2009.

[7] Liu, C. D., Marine multi-source spatial-data collection and maritime management information system based on multi-source spatial-data, PhD thesis, *Ocean University of China*, Qingdao, 2008.

[8] Xie, W. H., Y. H. Li, and C. Su, C# implementation of marine functional zoning shanghai dimensional, three-dimensional geographic information system, *The Eleventh Symposium of Surveying and Mapping Institute in Six Provinces and One City of East China*, 54-58, 2009.

[9] Qi, F., S. Y. Jiang, and Y. B. Wen, Design and development of special marine information management system based on SuperMap, *Agriculture Network Information*, 1, 19-22, 2010.

[10] Li, Z., B. Ai, and H. X. Tao, Design and implementation of GIS-based marine hydrological information system, *Marine Geology Letters*, 8, 35-38, 2007.

[11] Wang, M., Research and design on the seabed-character information analysis system, Master thesis, *PLA Information Engineering University*, Zhengzhou, 2008.

[12] Zhou, L., H. X. Liu, Z. L. Song, and Z. Jia, Design and realization of visualizing query in PANDA section marine information database system based on WebGIS, *Marine Science*, 33, 86-91, 2009.

[13] Feng, B., J. J. Tan, S. R. Li, and C. G. Shao, Design and implementation of DBMS for marine geological survey, *Computer Engineering*, 35, 29-31, 2009.

[14] Niu, M. X., and X. Y. Zhao, Application of satellite remote sensing and GIS technology to the research of marine fishery resources, *South China Fisheries Science*, 4, 70-74, 2008.

[15] Zhang, Y. F., Q. Zhang, J. Q. Yang, Y. Ou, and F. Kan, A public GIS model based on spatial objects and its application in information system construction for offshore oil industry, *China Offshore Oil and Gas*, 21, 211-214, 2009.

[16] Li, H. T., The research on the methods of marine environment information integration and the development of new generation of MAGIS, PhD thesis, *Ocean University of China*, Qingdao, 2007.

[17] Zhang, F., S. H. Li, and H. Y. Wei, Design of marine information resource directory service system, *Geospatial Information*, 6, 81-83, 2008.

[18] Shao, C. L., B. M. Shao, Q. W. Zhao, and G. Chen. Design and implementation of MAGIS integration solution,

Geospatial Information, 7, 99-101, 2009.

[19] Xiao, R. L., Y. Y. Du, F. Z. Su, and F. Yang, Multi-source marine environmental information grid platform and its implement, *Geomatics and Information Science of Wuhan University*, 8, 932-935, 2009.

[20] Zhang, Y., Z. H. Zhou, L. F. Liu, J. Li, and Y. Guan, Design and implement of ocean technology information sharing system, *Ocean Technology*, 29, 95-100, 2010.

[21] Li, L. G., C. Y. Zhao, M. H. Qin, Y. S. Dai, and H. T. Sun, A design and implementation of the data management system for marine environment monitoring, *Marine Forcasts*, 27, 53-57, 2010.

[22] He, Y. W. , F. Z. Su, Y. Y. Du, and R. L. Xiao, The design and implement of marine environmental information grid platform, *Journal of Geo-information Science*, 12, 680-686, 2010.

[23] Huang, J., Research on modeling and visualization of marine environment spatio-temperal data, PhD thesis, *Zhejiang University*, Hangzhou, 2008.

[24] Xu, M., C. Y. Fang, Q. Zhu, and H. Lin, Design and implementation of multi-dimension and animated visualization system for ocean and atmosphere, *Geometrics and Information Science of Wuhan University*, 34, 57-63, 2009.

[25] Tang, K., B. Qin, and F. Hong, Ocean data visualization grid, *Periodical of Ocean University of China*, 39, 441-444, 2009.

[26] Tu, C., 3D visualization of ocean temperature field, *Engineering Journal of Wuhan University*, 40, 126-128, 2007.

[27] Liu, W. L., F. Z. Su, and Y. Y. Du, A study on remote dynamic visual service for spatio-temporal process of marine scalar field, *Journal of Geo-information Science*, 11, 513-519, 2009.

[28] Yang, F., Y. Y. Du, F. Z. Su, and R. L. Xiao, A study on remote visualization of "Ocean Vector Field Data" based on web service, *Journal of Geo-Information Science*, 10, 749-756, 2008.

[29] Liu, X. F., Discuss on visualization of hydrological data based on GIS, *Science & Technology*, 13, 49-50, 2010.

[30] Ma, Y. J., Multi-level topology visualization based on ocean flow field, *Journal of Shanxi University of Technology*, 26, 54-57, 2010.

[31] Zhao, X., F. X. Li, S. Y. Zhan, and Z. S. Li, Ocean wave simulation under wind change effect, *Proceedings of the First International Conference on Innovative Computing, Information and Control*, 26-29, 2006.

[32] Pan, M. Y., and D. R. Liu, Realization of achieving a surface effect in real-time 3D scenes, *Electronic Component &Device Applications*, 8, 47-49, 2006.

[33] Shi, J. D., and M. M. Jiang, Simulation of 3D shallow waves based on OpenGL, *Microelectronics and Computer*, 23, 137-140, 2006.

[34] Ma, J., H. J. Zhu, and J. H. Gong, Simulation of real-time water surface based on Cg and OpenGL, *Journal of System Simulation*, 18, 395-400, 2006.

[35] Wang, S. Z., A novel approach to dynamic ocean surfaces simulation for real-time 3D, *Computer Application*, 27, 1147-1149, 2007.

[36] Luo, Y., and L. Zhong, 3D wave simulation based on spectrum of ocean waves, *Journal of Wuhan University of Technology*: *Transportation Science & Engineering*, 32, 323-325, 2008.

[37] Gao, W., Y. Wu, and J. B. Xiao, Scenario simulation in virtual ocean based on Vega, *Chinese Journal of Ship Research*, 3, 54-56, 2008.

[38] Sun, S., Z. H. Fang, and Z. S. Ma, Simulation of ocean waves scene with light based on random number, *Computer and Modernization*, 4, 70-73, 2008.

[39] Li, B., C. Wang, Z. Y. Li, and Y. J. Chen, A practical method for real-time ocean simulation, *Proceedings of 2009 4th International Conference on Computer Science and Education*, 742-747, 2009.

[40] Liu, P., R. Yang, and J. Xu, Virtual display of ship movements in marine environments, *Royal Institution of Naval Architects-International Conference on Computer Applications in Shipbuilding 2009*, 719-723, 2009.

[41] Li, S. J., J. Jiang, B. Yang, and L. D. Wu, Research on sphere based modeling and rendering of ocean waves, *Journal of Image and Graphics*, 14, 744-752, 2009.

[42] Yang, Y., J. Z. Zhang, and X. X. He, Realistic water surface rendering based on GPU, *Computer Knowledge and Technology*, 5, 3483-3485, 2009.

[43] Chen, J., Y. Yuan, and J. W. Yang, Shader-based visual simulation of ocean wave, *2010 The 2nd International Conference on Computer and Automation Engineering*, 635-638, 2010.

[44] Wei, S. G., Y. L. Hao, Z. Z. Lu, Z. Y. Yang, and Y. Zhu, Research of true ocean environment visual simulation technology, *Journal of System Simulation*, 18, 394-397, 2006.

[45] Kang, N., Q. Xu, Y. Zhou, and C. Z. Lan, Graphic hardware-based algorithm for real-time visualization of massive terrain dataset, *Journal of System Simulation*, 19, 3988-3992, 2007.

[46] Ma, J. S., S. C. Xu, P. H. Jia, and G. Q. Gu, Key techniques for implementation of virtual under water digital terrain in digital ocean systems, *Hydrographic Surveying and Charting*, 27, 48-51, 2007.

[47] Liu, J., X. Y. Jiang, and S. H. Li, Research on the model building of water and 3d-dimensional visualization in digital ocean, *Marine Science Bulletin*, 28, 141-146, 2009.

[48] Han, L. T., Q. Zhu, and C. Y. Hou, Issues related to the construction of the virtual marine environments, *Marine Science Bulletin*, 25, 85-91,96, 2006.

[49] Su, F. Z., Y. Y. Di, X. B. Pei, X. M. Yang, and C. H. Zhou, Constructing digital sea of China with the datum of coastal line, *Geo-Information Science*, 8, 12-15, 2006.

[50] Chen, H. G., Q. C. Li, G. P. Wang, F. Zhou, X. H. Tang, and K. Yang, An efficient method for real-time ocean simulation, *Lecture Notes in Computer Science*, 4469, 3-11, 2007.

[51] Sun, C. Y., X. H. Zhou, F. H. Ma, and N. X. Mou, A study on the construction of information system in "digital ocean", *2008 International Conference on Wireless Communications, Networking and Mobile Computing*, 1-3, 2008.

[52] Liu, X. S., X. Zhang, T. H. Chi, H. Qu, and Y. W. Jiang, Study on China digital ocean prototype system, *Proceedings of the 2009 WRI World Congress on Software Engineering*, 466-469, 2009.

[53] Wang, J. H., W. S. Yan, and X. L. Liu, Virtual ocean environment modeling and rendering research, *Journal of System Simulation*, 21, 3985-3988, 2009.

[54] Chen. G., W. Q. Li, and X. N. Li, Design and implementation of an interactive VR-Ocean platform for ocean environment and marine life simulation, *Periodical of Ocean University of China*, 39, 1037-1041, 2009.

[55] Zhao, X. H., Y. Sun, and Z. Z. Lu, Virtual simulation of submarine motion in virtual ocean environment, *Journal of System Simulation*, 18, 226-229, 2006.

[56] Dai, J., H. Gu, Y. C. Zhai, and G. Y. Liu, Research and realization of visual system in virtual ocean battlefield, *Computer simulation*, 23, 4-8, 2006.

[57] Tang, X. Y., S. J. Liu, and Z. Yun, Design of an active heave compensation system for deep-ocean mining based on the virtual prototype technology, *Journal of Beijing University of Technology*, 34, 454-458, 2008.

[58] Zhang, H., Y. L. Shi, D. A. Yuen, Z. Z. Yan, X. R. Yuan, and C. F. Zhang, Modeling and visualization of tsunamis, *Pure and Applied Geophysics*, 165, 475-496, 2008.

[59] Xiao, J. B., and D. B. Hu, Simulation of the submarine's visual system based on Vega, *Journal of System Simulation*, 20, 120-123, 2008.

[60] Ma, W. J., W. S. Yan, and Z. H. Gui, Obstacle avoidance for AUV in virtual environment, *Torpedo Technology*, 16, 21-24, 2008.

[61] Gui, Z. H., W. S. Yan, J. Gao, and W. J. Ma, Application of virtual reality to bottom tracking of autonomous

underwater vehicle, *Torpedo Technology*, 16, 24-26, 2008.

[62] Yang, X. Y., G. H. Gong, B. Zhang, and Z. P. Huang, Virtual modeling and rendering technologies of high-seas environment, *Journal of Beijing University of Aeronautics and Astronautics*, 35, 493-496, 2009.

[63] You, Y. J., F. J. Kang, and K. Tang, Research of sea battlefield distributed virtual environment based on fractal, *Journal of System Simulation*, 21, 7190-7194, 2009.

[64] Li, S. J., L. D. Wu, S. C. Hu, and H. C. Song, Research of displaying system of digital sea battlefield situation, *Journal of System Simulation*, 21, 6144-6147, 2009.

[65] Chang, Y. Y., Q. X. Meng, and H. C. Wang, Research on simulation system of the interfacing apparatus of underwater vehicle based on VR, *Key Engineering Materials*, 419-420, 697-700, 2010.

PROGRESS OF OCEAN-ATMOSPHERE INTERACTION STUDIES IN CHINA

Qinyu LIU and Xiao-Tong ZHENG

During 2007-2010, Chinese scientist put attached in the role of ocean dynamics on climate variation, and their research area extended from the Pacific to globe ocean. They got some series of research activities, which have markedness on the world. According to the different time and space scale, the major research results are introduced as follows:

Ⅰ. Inteannual climate variation

1 The important role of the Ocean-Atmosphere Interaction over the Tropical Indian Ocean and effects on Monsoon in interannual variation.

Chinese scientists make great progress in understanding the tropical Indian Ocean (TIO) ocean-atmosphere interactions and related influences on the East Asian climate during recent years.

Many studies by Chinese scientists show that the TIO is very important for Asian Climate, especially for summer rainfall over East Asia. Yang et al. (2007) discover that the Indian Ocean basin mode (IOBM) following El Niño–Southern Oscillation (ENSO) can induce robust climatic anomalies over the Indo-West Pacific region in the summer, prolonging the El Niño's influence after equatorial Pacific SST anomalies has decayed. They refer the TIO as "capacitor effect": As a response to the positive IOBM, the increased precipitation over the TIO forces a Matsuno-Gill pattern in the troposphere, strengthening South Asian high and Indian summer monsoon (Yang et al. 2007). It is found that while El Niño decays rapidly in spring and vanishes by summer, the IOBM warming persists through summer and releases its influence, like a "discharging" process, that sustains electric currents after the battery is switched off.

Recent studies investigate the detail of IOBM and its "capacitor effect". Du et al. (2009) show that during boreal spring, the Southwest Indian Ocean warming causes the cross-equator SST gradients that induce an antisymmetric wind pattern. When the summer Indian monsoon onsets in May, the northeasterly anomalies act to reduce the southwest monsoon and warm the ocean, persisting the IOBM through June-August (JJA) following El Niño.

All the features are reproduced in a coupled model simulation initialized with a warming in the TIO, indicating that the IOBM is not only a passive response to ENSO but also important for summer Indo-West Pacific climate (Yang et al. 2007). Furthermore, Li et al. (2008) investigate the influence of IOBM on the East Asian climate by using experiments of multi-AGCM, confirming the IOBM's "capacitor effect".

Chinese Scientists participate in international cooperation with Prof. Shang-Ping Xie (from IPRC University of Hawaii, USA) and found the TIO warming causes tropospheric temperature to increase by a moist-adiabatic adjustment in deep convection, emanating a baroclinic Kelvin wave into the Pacific. In the northwest Pacific, this equatorial Kelvin wave induces northeasterly surface wind anomalies, and the resultant divergence in the subtropics triggers suppressed convection and the anomalous anticyclone (Xie et al., 2009).

Wu et al. (2010) investigate the relative role of local SST anomalies or IOBM in anchoring anomalous anticyclone over the Northwest Pacific using a suite of experiments in an AGCM. It is

found that both of them maintain the anticyclonic anomalies over the NWP. The IOBM play an essential role in late summer, while the local SST is important in early summer. In addition to East Asian climate, the IOBM can also influence the mid-latitude atmosphere in the boreal summer (Yang et al. 2009).

The Indian Ocean Dipole (IOD) mode that is referred as the second EOF mode of TIO SST anomalies is also investigated by Chinese scientists. Yang et al. (2010) first estimated the effect of IOB and IOD together and give a relative important of those two modes in a consistent way by using the Maximum Covariance Analyses (MCA). The IOBM is highly related with the Asian summer monsoon and atmospheric circulation. The increased evaporative moisture associated with IOBM leads more rainfall over the TIO in the summer and the IOD is highly related with the Asian winter monsoon rather than Asian summer monsoon. A positive IOD weakens Indian winter monsoon and induces more (less) rainfall over the southwest (eastern equatorial) TIO (Yang et al. 2010).

Analyses of up-to-date data from satellite-tracked surface drifters indicate that the Wyrtki Jets (WJ) of the equatorial Indian Ocean (EIO) are developed firstly in the central EIO and then propagate westward along the equator at speeds of about 0.7 m s^{-1}. Climatologically, the fall jet is both stronger and wider than its spring counterpart. This westward propagation phenomenon is supported by altimetry observation. It is suggested that the westward propagation of the jets in the western EIO is primarily forced directly by the westward propagating zonal winds. Whereas in the eastern EIO, propagation of the jet signals is ambiguous although the zonal wind pattern is observed moving east. It is also evident that the WJs are subject to strong interannual variability, which may associate with ENSO and IOD (Qiu et al. 2009).

Above results have important implications for the predictability of Indo–western Pacific summer climate. Since 2009, the IOB index has been as new index for climate prediction by the Japan Meterological Agency and used in climate Prediction seminar of National Climate Center of China. The paper about the IOBM “capacitor effect” (Yang et al. 2007) has been cited 50 times by SCI paper until first Dec. 2010.

Furthermore, Chinese scientists make great contributions to Indian Ocean observations. As an international cooperation, Dr. Yu Weidong from the first Institute of Oceanography (FIO), State Oceanic Administration of China participates the international Indian Ocean observation project. FIO plays an active role in the international coordinated efforts in implementing the Indian Ocean Observing System (IndOOS), with special contribution of deploying one surface buoy in the southeastern tropical Indian Ocean and one subsurface mooring off the coast of Java Island (McPhaden et al. 2009, 2010, Masumoto et al. 2010).

2. The effect of SST and Freshwater Flux anomaly on climate variability in Pacific

Based on observation analysis, the coupled model research explicitly demonstrates that the North Pacific oceanic warming can force a significant change of the atmospheric circulation with a strong seasonal dependence, which is characterized by a quasi-baratropic warm ridge in early winter, a transition to a quasi-baratropic warm trough in late winter, and then to a baroclinic response in summer with a trough and ridge, respectively. The North Pacific warming also forces a significant remote response over the tropical Pacific by upper-ocean meridional overturning cell and equatorial ocean dynamics (Wu and Li, 2007).

The coupled ocean-atmosphere response to the observed freshwater flux trend over the Kuroshio-Oyashio Extension (KOE) region is studied in a series of coupled model experiments (Zhang et al., 2010a). The positive E-P forcing in the KOE region can set up a cyclonic gyre straddling the

subtropical and the subpolar gyre, which induces anomalous southward cold advection in the west and northward warm advection in the interior. This leads to a formation of temperature dipole in the mid-latitudes with a cooling in the west and a warming in the east (Zhang et al., 2010a). This study is original and significant research about the climate response to freshwater loss in KOE region.

3. The major mode of SST variability and its predictability in the Atlantic

The predictability of the tropical Atlantic variability (TAV) is analyzed within the framework of a linear stochastic climate model by Wang and Chang (2008a). They suggest that under the stochastic forcing, the useful predictive skill for sea surface temperature measured by normalized error variance is limited to 2 months on average (Wang and Chang 2008a). Therefore, predicting TAV poses more challenge than predicting El Niño in the tropical Pacific. Whereas, based on the first-mode baroclinic Rossby wave model the wintertime SST anomalies can be skillfully predicted up to 3 months ahead in the tropical Atlantic, 18 months in the eastern subtropical Atlantic, and 3 years east of Newfoundland on the basis of the first-mode baroclinic Rossby wave adjustment (Zhang and Wu, 2010).

Wang and Chang (2008b) point out that the tropical Atlantic has two types of coupled modes: a meridional mode at the decadal time scale and a zonal mode at the interannual time scale. The meridional mode, which manifests itself as an interhemispheric SST fluctuation, is controlled by the thermodynamical feedback between winds, latent heat flux, and SST, further modified by ocean heat transport. The zonal mode, which manifests itself as an SST fluctuation in the eastern equatorial basin, is dominated by the dynamical feedback between winds, thermocline, upwelling, and SST (Wang and Chang 2008b).

4 Interaction between different Oceans by "Atmosphere Bridge" and "Ocean Bridge"

The atmospheric teleconnections of the tropical Atlantic SST variability have been investigated in a series of coupled ocean–atmosphere modeling experiments. It is found that the tropical Atlantic climate not only displays an apparent interhemispheric link, but also significantly influences the North Atlantic Oscillation (NAO) and the ENSO. Over the North Atlantic, the tropical Atlantic SST can force a significant coupled NAO–dipole SST response in spring that changes to a coupled wave train–horseshoe SST response in the following summer and fall, and a recurrence of the NAO in the next winter (Wu et al., 2007).

A comprehensive assessment of the observed atmospheric response to globe major ocean variability modes have been pointed out in a unified approach using the Generalized Equilibrium Feedback Analysis (Wen et al., 2010). They found that the classical response to ENSO mode is consisted of two parts, one responding to the tropical Pacific ENSO mode and the other to the tropical Indian Ocean SST anomaly Monopole mode (Wen et al., 2010). The North Pacific SST anomaly mode appears to generate an equivalent barotropic warm SST-high response locally over the Aleutian Low and to influence the North Atlantic Oscillation (NAO) downstream, while the North Atlantic SST anomaly tripole mode tends to force a local response on NAO (Wen et al., 2010).

The climate model can give us the information about global teleconnections in response to a shutdown of the Atlantic meridional overturning circulation. As response in the tropical Atlantic, a sea surface temperature (SST) dipole forms, with cooling north and warming on and south of the equator. In the tropical Pacific, a SST dipole forms in boreal spring in response to the intensified northeast trades across Central America and triggering the development of an El Niño–like warming that peaks on the equator in boreal fall. In the extratropical North Pacific, a basinwide cooling of 1℃ takes place, with a general westward increase in intensity (Wu et al., 2007a).

The inter-basin teleconnection between the North Atlantic and the North Pacific ocean–atmosphere

interaction is studied using a coupled ocean–atmosphere general circulation model (Li et al., 2009). The experiments explicitly demonstrate that the leading mode of the extratropical atmospheric internal variability plays a dominant role in shaping the hemispheric-scale response forced by oceanic variability over the North Atlantic and Pacific (Li et al., 2009).

Yang et al. (2009) found that TIO can affect the Northern Hemisphere climate variation based on the observational analyses and model experiments. IOBM persists from spring to summer, can generate significant Circumglobal Teleconnecton (CGT) in the Northern Hemisphere summer mid-latitude atmosphere. A warm IOBM enhances the Indian Summer Monsoon (ISM) through the increased precipitation in the northeastern Arabian Sea-western India, which then forms an atmosphere heat source there and in turn the atmospheric waves, exciting the CGT (Yang et al., 2009).

Ⅱ Unite mode of Globe tropical Oceans

Globe tropical atmosphere is related with the all tropical Oceans. Therefore, Chinese scientists suggested that there are the globe tropical unite mode as follows.

Liu and Fan (2009) first indentified the united mode about globe tropical Ocean and atmosphere coupled system based on the NCEP reanalyzed monthly SST and atmosphere data from Jan 1948 to Dec 2005. The variation of the leading mode is consistent with the El Niño-Southern Oscillation (ENSO) mode in the Pacific, and a anticyclone situates in the low level of the northwest Pacific and South China Sea, while there is IOBM in tropical Indian Ocean. However, the SST anomaly in Atlantic is inconspicuous. The influences to the following summer atmosphere circulation in the Leading mode mainly include the impact of Tropical Indian Ocean basin mode on the East Asia monsoon (Liu and Fan, 2009).

Wang (2010a) provides a consistent and unified solution for the two types of thermodynamical coupled modes in the atmosphere–ocean climate system: the tropical meridional mode and the subtropical dipole mode. The solution is derived analytically from a linear model that couples a simple atmosphere to a slab ocean via the wind–evaporation–SST (WES) feedback. For realistic parameter values, these thermodynamical coupled modes have periods and damping time scales in years; hence, they may play important roles in the tropical interannual-to-decadal climate variability.

A global wavenumber-3 dipole SST mode is showed to exist in the Southern Hemisphere subtropical climate variability in austral summer. A positive (negative) phase of the mode is characterized by cool (warm) SST anomalies in the east and warm (cool) SST anomalies in the southwest of the south Indian, Pacific, and Atlantic Oceans, respectively. This coherent dipole structure is largely a response of ocean mixed layer to the atmospheric forcing characterized by migration and modulation of the subtropical high-pressures, in which the latent heat flux play a leading role through wind-induced evaporation, although ocean dynamics may also be crucial in forming SST anomalies attached to the continents (Wang 2010b).

Ⅲ The ocean dynamic role in decadal climate variation

During 2007-2010, Chinese Scientists concentrate on the role of ocean dynamic in Pacific decadal climate variability. Wu et al., (2007b) demonstrate that extratropical decadal SST anomalies may propagate to the tropics through a coupled wind-evaporative-SST (WES) feedback. The study further suggests that the extratropical–tropical teleconnection provides a positive feedback to sustain the decadal changes in both the tropical and extratropical North Pacific (Wu et al., 2007b).

The Low Potential Vorticity (PV) water transport is an important cause of the decadal variation of stratification in the east of Taiwan and could contribute to Pacific Decadal Variability. Based on the data of Simple Ocean Data Assimilation, it is found that the central North Pacific (28^oN-35^oN，

150°E-170°W) is one of the main formation area of the low PV water between the isopycnal surfaces of 25.4 σ_θ to 25.8 σ_θ, and there is a channel to transport the low PV water from the central North Pacific to the east of Taiwan by the currents on the pycnocline and through this channel by 12 years (Liu and Hu, 2007, need the reference).

The entire China coastal sea climate variations have been investigated recently. It is found that there are two distinct low-frequency modes: a basin mode and north-south dipole mode. The basin mode is attributed mainly by oceanic advection, with the surface heat flux playing a damping effect due to the intensification of latent heat loss. The dipole mode varies coherently with the Pacific Decadal Oscillation, which is broadly associated with the surface heat flux due to the wind speed variations, with the oceanic advection playing a damping role over the shelf seas (Zhang et al., 2010b).

The coupled ocean-atmosphere experiment demonstrates that freshwater forcing in the western tropical Pacific can lead to a basin-wide response with the pattern resembling the Pacific Decadal Oscillation (PDO). The tropical responses are further substantiated by the positive Bjerknes feedback, and subsequently force significant changes in the extratropical North Pacific through atmospheric teleconnection (Wu et al., 2010).

To sum up, it is demonstrated that the ocean dynamic and ocean-atmosphere interaction play an important role in PDO.

Ⅳ The ocean response to globe warming

1 The response of Pacific

Based on observation data, after removing both the long term trend and decadal variation of the background climate, the ENSO has been enhanced by as much as 60% during the past 50 years. This is inconsistent with the changes in the equatorial atmosphere which shows a slowdown of the zonal Walker circulation and tends to stabilize the tropical coupling system. Yang and Zhang (2008) point out that enhanced ENSO variability is attributed by strengthened equatorial thermocline that plays as a destabilizing factor of the tropical coupling system under the global warming. The magnitude of local term and its change are controlled equally by its two components, the mean vertical temperature gradient and the "virtual vertical heat flux". The former determines the turnaround of ENSO variability in the whole global warming period. The above result has been proved by Zhang et al. (2008).

Based on a set of Intergovernmental Panel on Climate Change (IPCC) Fourth Assessment Report (AR4) models, Zhu and Liu (2009) pointed that the trend of sea surface temperature (SST) in the twentieth century is a clear signal of the enhanced equatorial response (EER) warming or exhibits a clear trend of the El Niño–like warming in the last century. Similarly, IPCC model simulations of the twentieth century are consistent with observations and the aerosol cooling effect, opposite to the greenhouse gases warming effect, plays an important role in the twentieth century. This result has been proved by Xie et al. (2010). But there is still different result, which is a La Niña–like response in the tropical Pacific to warm climate, with the equatorial upwelling have been pointed (Fang et al., 2008). This difference could be explained by Yang et al.(2009), who point out the dominant mechanism for temperature change differs in different stages of global warming.

Yang and Wang (2009) proposed that in studying the long term changes in mean climate and tropical coupled climate variabilities to use the 20°C isotherm depth as the thermocline depth is improper, because the surface layer warms more and faster than the lower layers, the depth of maximum vertical temperature gradient shoals, consistent with the enhanced thermocline.

Based on a set of IPCC AR4 models result, Luo et al. (2009) pointed out that under the warmer climate scenario, the subtropical mode waters in North Pacific are produced in lighter isopycnal surfaces and are significantly weakened in terms of their formation and evolution. These changes are due to a more stratified upper ocean and thus a shoaling of the winter mixing depth, resulting mainly from a reduction of the ocean-to-atmosphere heat loss over the subtropical region. The basin-wide wind stress may adjust the mode waters indirectly through its impact on the surface heat flux and the subduction process.

2 The response of tropical Indian Ocean and Southern Ocean

The response of the TIO SST to globe warming has been investigated by Chinese Scientist. For example, Zheng et al. (2010) examined the response of IOD to increasing greenhouse gases. It is found that during global warming, the oceanic feedback of IOD intensifies due to the thermocline shoaling in the eastern equatorial Indian Ocean (EEIO), while the atmospheric feedback of IOD weakens due to increased static stability of troposphere. The combined effect results in little change in IOD variance under global warming.

The role of westerly winds at southern high latitudes in global climate is investigated in a fully coupled ocean-atmosphere general circulation model (Ma et al. 2010). The coupled model explicitly demonstrates that a shutdown of southern high latitude wind stress induces a general cooling over the Antarctic Circumpolar Current (ACC) region, with surface Ekman flow and vertical mixing playing competitive roles. This cooling leads to an equatorward expansion of sea ice and triggers an equivalent barotropic response in the atmosphere to accelerate westerly anomalies. The shutdown of southern high latitude wind stress also significantly reduces global meridional overturning circulation (MOC). In addition, it is found that the weakening of Atlantic MOC by as much as 50% is capable of cooling the time mean subpolar Atlantic temperature by only about 1 ℃ (Ma et al. 2010).

Reference

Du, Y., S.-P. Xie, G. Huang, and K. Hu, 2009: Role of air-sea interaction in the long persistence of El Niño-induced North Indian Ocean warming. *J. Climate*, 22, 2023-2038.

Fang, C., and L. Wu, 2008: The role of ocean dynamics in tropical Pacific SST response to warm climate in a fully coupled GCM. *Geophys. Res. Lett*., 35, L08703, doi:10.1029/2007GL033097.

Ma, H., L. Wu, and C. Li, 2010: The Role of Southern High Latitude Wind Stress in Global Climate. *Advance in Atmospheric Science*, 27, 371-381.

Masumoto, Y., Yu, W., Meyers, G. & D'Adamo, N., 2010: Observing Systems in the Indian Ocean. In Proc. "OceanObs'09: Sustained Ocean Observations and Information for Society" Conference (Vol. 2), Venice, Italy, 21–25 September 2009, Hall, J., Harrison, D.E. and Stammer, D., Eds., ESA Publication WPP-306. in press.

McPhaden, M.J., G. Meyers, K. Ando, Y. Masumoto, V.S.N. Murty, M. Ravichandran, F. Syamsudin, J. Vialard, L. Yu, and W. Yu, 2009: RAMA: The Research Moored Array for African–Asian–Australian Monsoon Analysis and Prediction. *Bull. Amer. Meteor. Soc.*, 90, 459–480. doi:10.1175/2008BAMS2608.1.

McPhaden, M. J., K. Ando, B. Bourlès, H. P. Freitag , R. Lumpkin, Y. Masumoto, V. S. N. Murty, P. Nobre, M. Ravichandran, J. Vialard, D. Vousden, W. Yu, 2010: The global tropical moored buoy array, In Proc. "OceanObs'09: Sustained Ocean Observations and Information for Society" Conference (Vol. 2), Venice, Italy, 21–25 September 2009, Hall, J., Harrison, D.E. and Stammer, D., Eds., ESA Publication WPP-306. in press.

Li, C., L. Wu, Q. Wang, L. Qu, and L. Zhang, 2009: An intimate coupling of ocean–atmospheric interaction over the extratropical North Atlantic and Pacific. *Clim. Dyn.* DOI:10.1007/s00382-009-0529-4.

Li, S., J. Lu, G. Huang and K. Hu, 2008: Tropical Indian Ocean basin warming and East Asian summer monsoon: A

multiple AGCM study. *J. Climate*, 21, 6080-6088.

Liu Q. and H. Hu, 2007, A subsurface pathway for low potential vorticity transport from the central North Pacific toward Taiwan Island, *Geophys. Res. Lett*. 34, L12710, doi: 10.1029/2007GL029510.

____, and L. Fan, 2009: The Leading Mode of the Tropical Ocean-atmosphere Coupling. *Journal of Ocean University of China* (in Chinese) 39(5)，815-821.

Luo Y., Q. Liu, and L. M. Rothstein, 2009: Simulated response of North Pacific Mode Waters to global warming, *Geophys. Res. Lett.* 36, L23609, doi:10.1029/2009GL040906.

Qiu, Y., L. Li, and W. Yu, 2009: Behavior of the Wyrtki Jet observed with surface drifting buoys and satellite altimeter, *Geophys. Res. Lett.*, 36, L18607, doi:10.1029/2009GL039120.

Wang, F., P. Chang, 2008a: Coupled Variability and Predictability in a Stochastic Climate Model of the Tropical Atlantic. *J. Climate*, 21, 6247-6259.

____, ____, 2008b: A Linear Stability Analysis of Coupled Tropical Atlantic Variability. *J. Climate*, 21, 2421-2436.

____, 2010a: Thermodynamic Coupled Modes in the Tropical Atmosphere–Ocean: An Analytical Solution. *J. Atmos. Sci.*, 67, 1667-1677.

____, 2010b: Subtropical dipole mode in the Southern Hemisphere: A global view， *Geophys. Res. Lett.*, 37, L10702, doi:10.1029/2010GL042750.

Wu, B., T. Li, and T. J. Zhou, 2010: Relative role of Indian Ocean and western North Pacific SST forcing in the East Asian summer monsoon anomalies. *J. Climate*, 23, 2974-2986.

Wu, L., F. He, Z. Liu, and C. Li, 2007a: Atmospheric Teleconnections of Tropical Atlantic Variability: Interhemispheric, Tropical–Extratropical, and Cross-Basin Interactions. *J. Climate*, 20, 856-870.

____, Z. Liu, C. Li, Y. Sun, 2007b: Extratropical control of recent tropical pacific decadal climate variability: a relay teleconnection. *Climate Dyn*., 28, 99-112.

____, and C. Li, 2007: Warming of the north Pacific ocean: Local air-sea coupling and remote climatic impacts. *J. Climate*, 20, 2581-2601.

____, Y. Sun, J. Zhang, L. Z, and S. Minobe, 2010: Coupled ocean-atmosphere response to idealized freshwater forcing over the western tropical Pacific. *J. Climate*, 23, 1945-1954.

Xie, S.-P., K. Hu, J. Hafner, H. Tokinaga, Y. Du, G. Huang, and T. Sampe, 2009: Indian Ocean capacitor effect on Indo-western Pacific climate during the summer following El Niño. *J. Climate*, 22, 730–747.

____, C. Deser, G.A. Vecchi, J. Ma, H. Teng, and A.T. Wittenberg, 2010: Global warming pattern formation: Sea surface temperature and rainfall. *J. Climate*, 23, 966-986.

Yang, H., and Q. Zhang, 2008: Anatomizing the Ocean Role in ENSO Changes under Global Warming. *J. Climate*, 21, 6539-6555.

____, and L. Wang, 2008: Estimating the nonlinear response of tropical ocean to extratropical forcing in a coupled climate model. *Geophys. Res. Lett.*, 35, L15705, doi:10.1029/2008GL034256.

____, and F. Wang, 2009: A Revisit on the Thermocline Depth in the Equatorial Pacific. *J. Climate*, 22, 3856-3863.

____, F. Wang, and A. Sun, 2009: Understanding the Ocean Temperature Change in Global warming: the Tropical Pacific. *Tellus*, 61A(3), 371-380.

Yang, J., Q. Liu, S.-P. Xie, Z. Liu, and L. Wu, 2007: Impact of the Indian Ocean SST basin mode on the Asian summer monsoon. *Geophys. Res. Lett.*, 34, L02708, doi: 10.1029/2006GL028571.

____, ____, Z. Liu, L. Wu, and F. Huang, 2009: The basin mode of Indian Ocean sea surface temperature and northern hemisphere Circumglobal Teleconnection. *Geophys. Res. Lett.*, 36, L19705, doi: 10.1029/2009GL039559.

____, ____, and Z. Liu, 2010: Linking Asian monsoon to Indian Ocean SST in the observation: Possible roles of Indian Ocean basin mode and dipole mode. *J. Climate*, in press.

Zhang, H., and L. Wu, 2010: Predicting North Atlantic sea surface temperature variability on the basis of the first-mode

baroclinic Rossby wave model, *J. Geophys. Res*., 115, C09030, doi:10.1029/2009JC006017.

Zhang, L., L. Wu, and J. Zhang, 2010a: Coupled Ocean-Atmosphere Responses to Recent Freshwater Flux Changes over the Kuroshio-Oyashio Extension Region. *Journal of Climate*. doi:10.1175/2010JCLI3835.1. in press.

____, ____, X. Lin, and D. Wu, 2010b: Modes and mechanisms of sea surface temperature low‐frequency variations over the coastal China seas, *J. Geophys. Res*., 115, C08031, doi:10.1029/2009JC006025.

Zhang, Q., Y. Guan, and H. Yang, 2008: ENSO Amplitude Change in Observation and Coupled Models. *Adv. Atmos. Sci*., 25(3), 361-366.

Zheng, X-T., S.-P. Xie, G. A. Vecchi, Q. Liu and J. Hanfer, 2010: Indian Ocean dipole response to global warming: Analysis of ocean-atmospheric feedbacks in a coupled model. *J. Climate*, 23, 1240-1253.

Zhu X. J. and Z. Liu, 2009: Tropical SST response to global warming in the 20th century. *J. Climate*., 22, 1305-1312.

OBSERVATIONS AND MECHANISMS OF SEA FOGS REVIEW OF SEA FOG RESEARCH IN CHINA

ZHANG Suping

(Physical Oceanography Laboratory, and Ocean-Atmosphere Interaction and Climate Laboratory, Ocean University of China, Qingdao 266100, China)

Abstract

With the developments of atmospheric observational techniques, new facts are found about sea fogs and the mechanisms involved are better understood with the help of advanced atmospheric models. This review includes the main achievements focusing on fog climatology, atmospheric boundary layer, numerical simulation and forecast of fogs to help provide knowledge about sea fog research in China.

Key word: sea fog review, sea fog climatology, atmospheric boundary layer, observation, forecast

Ⅰ Introduction

Sea fogs often cause losses of shipping communities and disrupt aviation and other socioeconomic activities over oceans and in coastal regions due to the low visibility in fogs[*]. Figure 1 shows the number of fog days as a function of calendar month based on 30 yr of station observations. Stations on the northwest (NW) Yellow Sea coast typically record more than 50 foggy days a year near Qingdao (QD) while the maximum of over 80 days is found at Chengshantou (CST) station in the northern Yellow Sea. During the fog season (April to July), 65%-87% of the fog observations report visibility of less than 200 m at Qianliyan (QL) and Xiaomaidao (XM), with the average duration of sea fog events lasting about 2 days (Diao 1992). More attentions have been paid to the Yellow Sea fog due to its high frequency and severe influences on activities over the sea.

Most of sea fogs along the Chinese coast are known as advection cooling fogs (Wang 1983), which forms as the air that has been lying over a warm water surface is transported over a colder water surface, resulting in cooling of the lower layer of air below its dew point (Glossary of Meteorology, American Meteorological Society, http://amsglossary.allenpress.com/glossary/). Sea fog study was primarily based on observations on land for a long time in the past, which limited our understanding. In recent years, new observations from buoys, ships and towers provide us with data over seas, and data from digital soundings[1] near coast expose vertical structures in the atmospheric boundary layer (ABL). Besides, advanced atmospheric models develop quickly. Based on these new data and models, progresses have been made about sea fogs, especially in the respects of fog climatology, fog vertical structure, fog microphysical features and numerical simulation and forecast of fog. This work reviews the achievements in the past three or four years; some earlier literatures are mentioned briefly for better understanding these progresses.

Ⅱ Fog climatology

[*] Fog is reported when visibility<1000 m.

[1] Digital soundings along with L-band radar can provide temperature, humidity, pressure and wind at a vertical interval of 30 m.

Fog climatology was primarily focused on the statistics of fog frequency, favorable meteorological conditions, like the average wind speed and wind direction, the humidity and the difference between the sea surface temperature (SST) and surface air temperature (SAT) and etc. (e.g. Wang, 1983; Wang and Qu, 1997; Dao, 1992). Monthly averaged circulation patterns favorable or unfavorable for sea fogs were analyzed by Zhang et al., (2005), Zhou et al., (2004) and Wang et al., (2006), about which Zhang and Bao (2008) had a review discussion. Nowadays, fog climatology means more than those.

1 The mechanisms of seasonal variations of fog

The Yellow Sea fog season is characterized by an abrupt onset in April in the southern coast of Shandong Peninsula and an abrupt, basin-wide termination in August (Fig. 1). This step-like evolution is inexplicable from the gradual change in solar radiation. In April, land warms up much faster than the ocean. An anticyclone exists in the Yellow and East China Sea (YESA) due to the land-sea contrast (Fig. 2a). The southerlies on the west flank of this anticyclone advect warm and humid air from the south, causing the abrupt fog onset on the Chinese coast. The lack of such warm/moist advection on the east flank of the anticyclone leads to a gradual increase in fog occurrence on the Korean coast. The retreat of Yellow Sea fog is associated with a shift in the prevailing winds from southerly to easterly from July to August. The August wind shift over the Yellow Sea is part of a large-scale change in the East Asian-western Pacific monsoons, characterized with enhanced convection over the subtropical Northwest Pacific and the resultant teleconnection into the mid-latitudes, the latter known as the western Pacific-Japan pattern (Zhang et al., 2009).

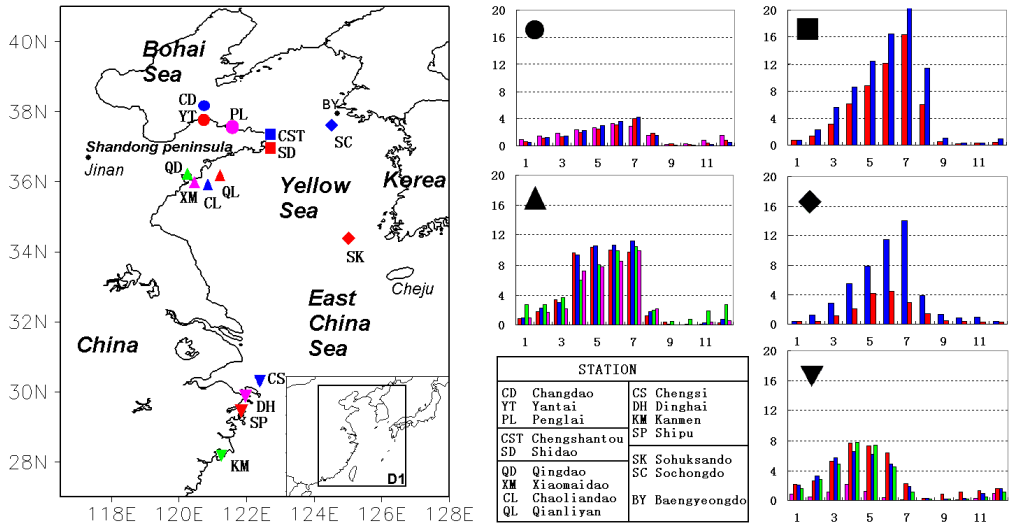

FIG. 1. Climatological seasonal cycle of the frequency (day) of fog occurrence at stations adjacent to Chinese seas. Different symbols stand for different regions: Bohai Sea (circle), northern Yellow Sea (square), northwest Yellow Sea (upward-pointing triangle), East China Sea (downward-pointing triangle), eastern Yellow Sea (diamond). Colors distinguish stations in each group. D1 is the model domain (from Zhang et al., 2009).

2 Seasonal variations in vertical structures in the ABL and fog thickness

The Yellow and East China Sea anticyclone (YESA) mentioned above is a shallow one and disappears at about 925 hPa where westerly winds blow from warm continent to cold sea in April – May (Fig. 2b). The westerly flows, both warm and dry, overlay the cold/wet sea surface to form robust

temperature inversion and dry layer. The percentage of the temperature inversion days is in excess of 50% and the stratification is extremely stable with $\frac{\partial \theta}{\partial z} > 10$ K/km from 100-400 m in April (Figs. 3a-b). Capped by so strong a stable layer, fog, once formed, can hardly develop further higher. In July, the southerly winds derived from the East Asian summer monsoon prevail and bring huge amount of moisture to the Yellow Sea to produce deep wet layer and weaker stability, favorable for fog developing upward provided that the moisture supply can meet the needs of fog maintaining. Indeed, the wet layer is much deep in July with specific humidity>12 g/kg below 600 m (Fig. 3b). The turbulence (Richardson Number Ri<1) is confined within the lowest 150 m in April and reaches to 200 m in July (Zhang et al., 2008). With the differences in the stability, in the turbulence and in the thickness of the wet layer the summer fogs are generally deeper in height than the spring fogs (Fig. 3c). Examples are demonstrated in Figures 4a-b. The relative humidity drops sharply at fog top in spring case whereas air keeps wet from surface to 1200 m in summer fog (Figs. 4a-b).

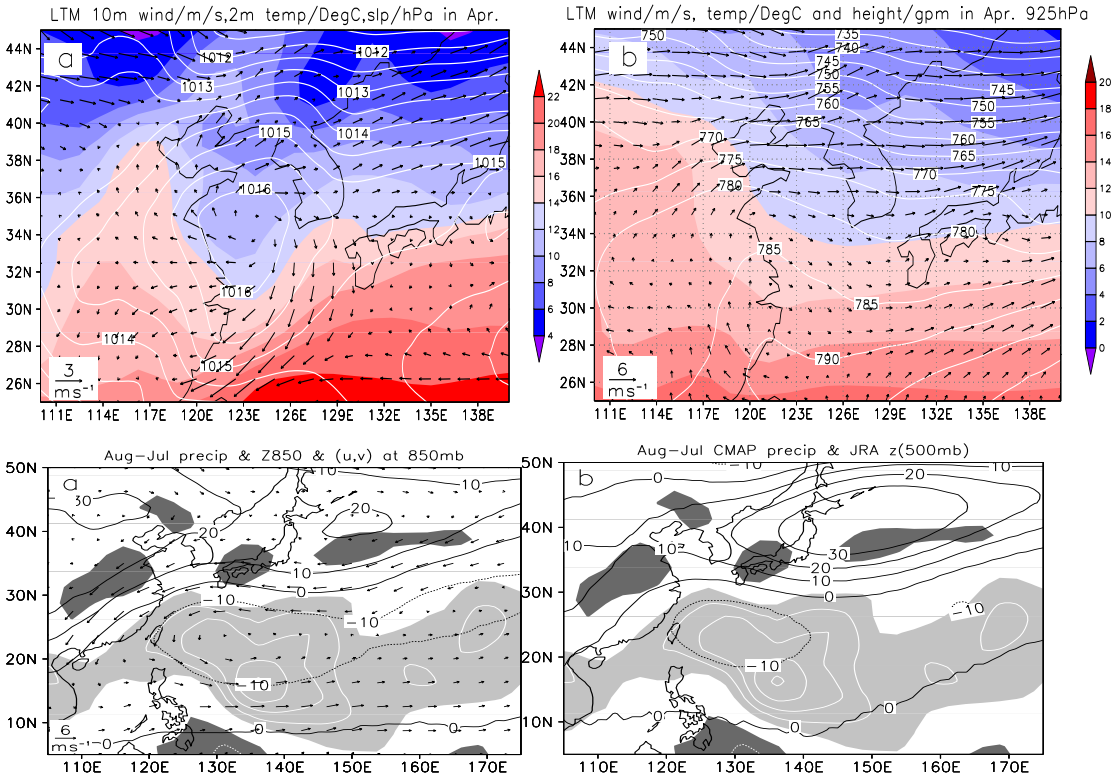

Fig. 2 (a) Surface wind velocity (m s^{-1}), temperature (℃) and sea level pressure (hPa). (b) Wind velocity (m s^{-1}), temperature (℃) and geopotential height (m) at 925hPa.
August minus July differences: precipitation (shaded in mm day^{-1}) and geopotential hight (black contours in gpm) at (c) 850 hPa and (d) 200 hPa. In (c) wind velocity (m s^{-1}) at 850hPa is superimposed. Light shaded represents positive and dark shaded negative precipitation difference, and the interval of contours is 2 mm day^{-1}. Dada based on JRA-25 and CMAP climatology.

Along with numerical simulations, the conceptual models for the mechanisms of the temperature inversion in the Northwestern Yellow Sea are figured out. In spring (April to May), air masses near the sea surface move northward driven by local southeasterlies and cool gradually by the modification of the cold sea, while those at about several hundred meters high become warmer and warmer since they

have a long land-based history, thus forming pronounced temperature inversion over the Northwestern Yellow Sea (see Figs. 2a-b). In summer, controlled by the East Asian summer monsoon, air masses in the atmospheric boundary layer (ABL) are primarily derived from the southern oceans and possess similar thermal features, thus producing weaker temperature inversion that is also related to the adiabatic sinking from the western Pacific subtropical high (Ren and Zhang, 2011). Statistics from coastal and island observations indicate more/less temperature inversion days in April/July (Huang et al., 2009a). In addition, cold air from northeast intrudes onto the Yellow Sea surface or air cools by turbulence from wind shear can also produce temperature inversion (Zhang, 2010; Gao et al., 2007).

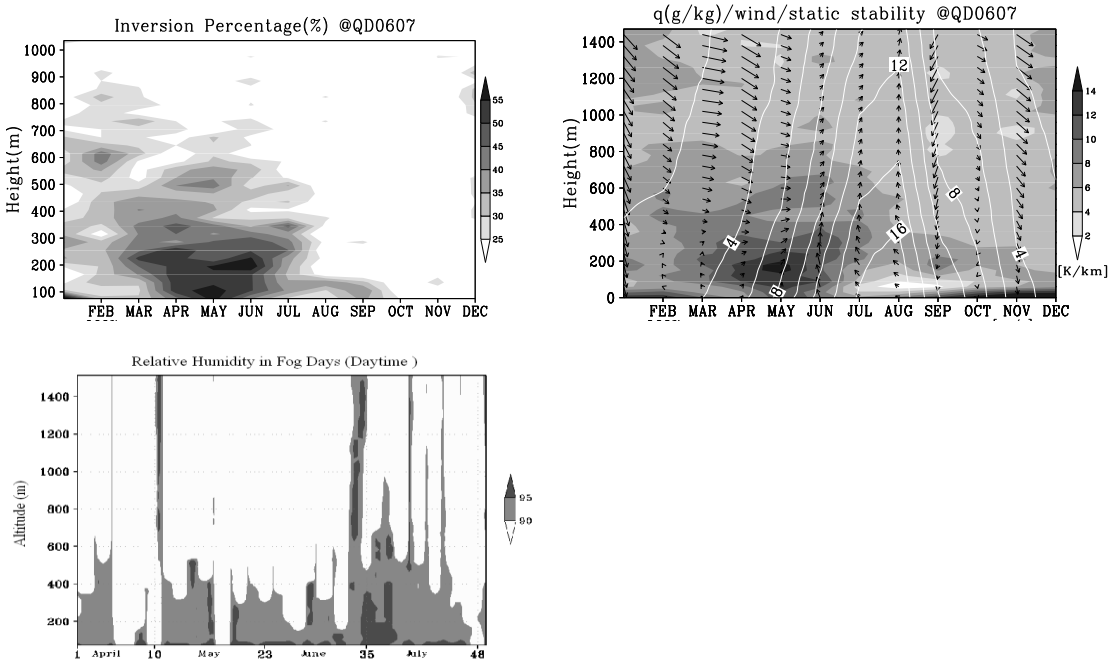

Fig. 3 (a) Days with inversion occurrence (%). (b) Monthly-mean specific humidity (white contours in g/kg), winds and static stability ($\frac{\partial \theta}{\partial z}$ in shadings). (c) Seasonal variations in fog thickness (m). Data from soundings in QD including 49 fog days from 2006-2007.

3 Sea fog with cold air

Sea fog is generally related to southerly warm/moist advection, but about 15% of the sea fogs in winter and spring are related to cold air activity in the Yellow and East China Sea (Wang and Li, 2009). Most of cold air processes during which sea fog forms are weak with daily air temperature drop less than 4 ℃ and wind speed less than 8 m/s. Northerly winds instead of southerlies lower the sea surface temperature to its dew point. The favorable temperature difference between the SAT and SST is –2 ℃ to 2 ℃. The inversion and near-isothermal state of the air near the surface almost always appear over the East China Sea when sea fog occurs in the cold air, but this condition is rarely seen in the northern Yellow Sea. These results are of great help for sea fog forecast, yet the mechanism of the formation of this kind of sea fog is not clear so far.

4 The key area for fog formation in summer

Previous studies suggested that the moisture contributed to the Yellow Sea fogs was not from local but from the tropical oceans (Zhang et al., 2005; Zhou et al., 2004; Wang et al., 2006). For the purpose

of operation, Bai et al. (2010) figured out a “key area” for fog formation in summer (June - July) where the moisture advection, wind speed and SST are different obviously (with t-test significance of 99%) between more fog and less fog years. This key area is the Northern East China Sea. More fogs are likely to occur if positive anomalies in the moisture advection, southerly wind speed and SST appear in the key areas and negative SST anomalies are in the Yellow Sea at the same time.

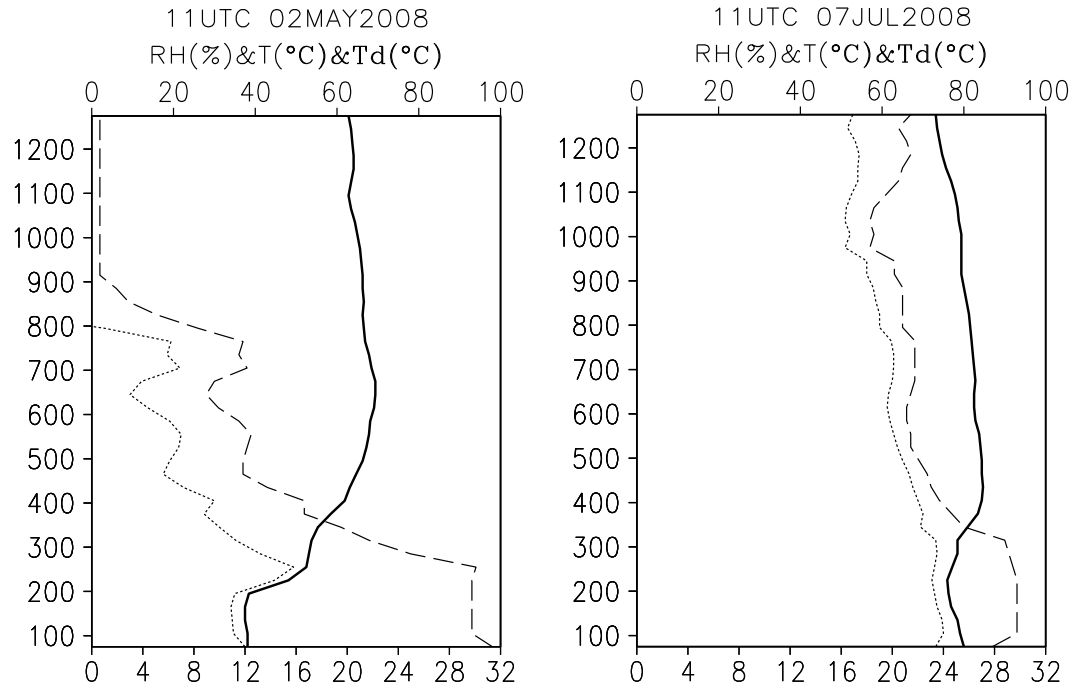

Fig. 4 Soundings at QD observatory. Temperature (solid), dew point temperature (dotted), and relative humidity (dashed). (a) 11 UTC 2 May 2008; (b) 11 UTC 7 July 2008 .

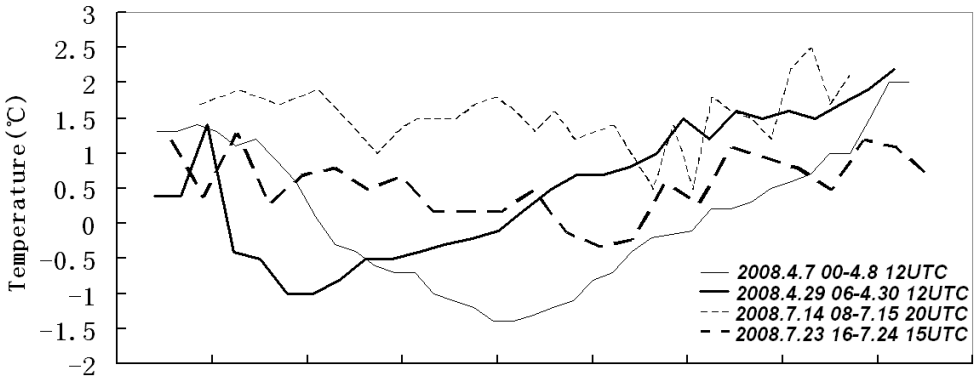

Fig. 5 The difference between the SAT and SST (SAT-SST) of four sea fog cases in 2008.

Ⅲ Air-sea interface in sea fogs

The advanced buoys were put into operational use three years ago when the 2008 Olympic sailing competition was held near Qingdao coast, with which we can learn the variations of SAT (air temperature 2 m above sea surface) and SST (water temperature 1 m below sea surface) that is hardly to be known before. From buoy observations, cold phases (SAT<SST) oftern occur in spring fogs and

warm phases (SAT>SST) are common in summer fog, though SATs are higher than SSTs before fog formations, overall. Figure 5 shows some examples.

The SAT is largely influenced by the radiative cooling effect based on the numerical simulations. In spring, the cooling effect intensified by the dry layer above fogs can transport downward to cool the SAT so heavily that it turns into cooler than the SST in shallow fogs, thus forming cold phase. In summer the radiative cooling is weaker and fogs are deep influenced by the East Asian summer monsoon. The radiative cooling effect can hardly affect the surface air temperature efficiently thus resulting in SAT>SST easily. Under the conditions of SAT<SST, the evaporations *in situ* can provide moisture to fogs, leading to the maximum of the cloud water mixing ratio close to the sea surface; in deep fogs the mixing ratio peaks at the upper level due to cooling there. The SAT is 1-2℃ lower than the SST where fog is shallow (Guo 2009, Zhang 2010, Qi, 2010). The positive differences of the SAT-SST maintains in summer fogs according to the simulated results (Fu et al., 2010, Ren and Zhang, 2011) which is consistent with the observations.

Contradictory result was obtained by Huang et al. (2010). They found by observations that the longwave radiation at the fog top can warm and dry the SAT by entrainment leading to SAT>SST and the warm advection contribute to the warmer SAT too; Gao et al. (2007) obtained the positive difference of SAT-SST from modeling results. The former case is related to a fog at the coast of the South China Sea with intense lowe level warm/moist jet, and the latter one is associated with a Yellow Sea fog produced by a fast moving warm front. It seems that the SAT keeps warmer than the SST if warm advection is extremely strong, the situation that is common for fog formation at the coast of the South China Sea (He et al., 2008; Qu et al., 2008). These discrepancies indicate the complicated mechanisms involved in fogs.

The turbulence produced by wind shear is important at the beginning of fog formation, when the Richardson number (Ri) is less than 0.25 (Ri<0.25) below 20 m in height and the SAT is higher than the SST based on simulations (Guo, 2009; Qi, 2010; Zhang, 2010). The radiative cooling at fog top contribute more to the development of fog upward, when the Ri<0.25 exists at the mid-upper level of fogs. Similar results are obtained from observations (Huang et al., 2010). Two turbulent mixing tiers (Ri<0.25) are observed by soundings at Qingdao station in a summer fog (Ren and Zhang, 2010). One is at the upper level induced by the radiative cooling and the other at the lower level associated with wind shear. The radiative cooling effect seems hardly to influence the SAT much if the fog is deep enough, say more than 200 m in height. The contributions of the turbulence and radiation were discussed before using a theoretical model (Hu and Zhou, 1997; Hu et al., 2006). These latest achievements both support the previous results and provide details in real fogs quantitatively.

Ⅳ Fog forecast

Marked progresses have been made in the numerical fog forecast techniques in recent years though experiential and synoptic methods are still used operationally. The advanced weather forecast models, such as WRF (Weather research and forecasting model), RAMS (Regional Atmospheric Modeling System) and MM5 (The fifth-generation Pennsylvania State University/NCAR mesoscale model), are the foundation of the numerical fog forecast. Successful numerical simulations were operated by Fu et al. (2008, 2010), Gao et al. (2007, 2010a, 2010b), Guo (2009), Ren (2009), Qi (2010), Zhang (2010), Zhang and Ren (2010) and etc.. These simulations usually focus on typical sea fog cases.

In order to further improve modeling skills, 3DVAR and cycling 3DVAR schemes based on WRF's 3DVAR modules are used for data assimilation, which can obviously improve numerical modeling initial conditions. The modeling results show that the cycling 3DVAR scheme can figure out better

simulated sea fog coverage than the non-assimilated and 3DVAR ones when validated to satellite observations (Fig. 6). The improvements of initial conditions are mainly embodied in strengthening the stability of the marine atmospheric boundary layer (MABL) and in modifying winds of lower MABL. The assimilated initial conditions derived from WRF cycling 3DVAR scheme can provide better initial fields for RAMS than its built-in isentropic ones, because the former keeps the dynamic and physic balance and results in great improvement of modeling results (Gao et al., 2010a; Gao et al., 2010b). This experiment combines the two models together to make full use of their individual advantages.

A sea fog numerical forecast system has been put into experimental operation in the Ocean University of China. The system runs automatically and provides fog forecast in the coming 24 hours each day. Another fog forecast experiment was implemented from 30 June to 1 August, 2007 in National Meteorological Center. The results show that the numerical prediction system is able to predict sea fog with a satisfactory precision, especially heavy fog, which can provide helpful guidance for operational heavy fog prediction based on comparison with coastal observations. Yet the evaluations of the forecasting skill over seas remain a problem due to the lack of observations at seas and higher resolutions are required for the initial and boundary conditions (Huang et al., 2009b).

The simulated fog patches are identified as the cloud water mixing ratio is great than 0.1g/kg (Gao et al., 2007; Fu et al., 2010) and the horizontal visibility in fogs can be calculated from Stoelinga and Warner(1999) based on Koschmieder formulation （Koschmieder, 1924）:

$$X_{VIS} = -\ln \frac{0.02}{\beta},$$

in which, X_{VIS} is the visibility (m) and βis the extinction coefficient affected by cloud water (βcw), cloud ice (βci), snow (βsnow) and rain water (βrain).In spring and summer fogs, the algorithm only refers to cloud water:

$$X_{VIS} = -\ln \frac{0.02}{144.7(\rho \cdot q)^{0.88}},$$

where q is the liquid water content （kg/kg）, ρ the density of the air （g/m3 ）.

Ⅴ Microphysical characteristics of sea fog

The observations of the concentration and size of fog droplets and the liquid water contents (LWC) are implemented in the coastal area of the South China Sea (Wang et al., 2009; 2010). The liquid water contents have a wave-like variation during the sea fog developing phase. The increment of LWC is mainly contributed by the increase in the concentration of the larger droplets greater than 10μm. The droplet spectrum widens towards larger size as fog develops. The horizontal visibility is better related to LWC than to the droplet concentration. The average droplet spectrum is similar to Junge distribution, the average concentration is 57. 1 drops/cm^3, the average liquid water content is 0. 0183 g/m^3 and the average drop diameter is 4. 7μm. It is pity that there is no similar observations in the Yellow Sea in recent 20 years.

Ⅵ Summaries and discussions

Nowadays, sea fog climatology is far beyond the conventional statistics. The new results of the sea fog climatology provide explanations about the abrupt onset in April in the southern coast of Shandong Peninsula and an abrupt, basin-wide termination in August of fog season. The observations from the digital soundings demonstrate that spring fogs are shallow with strong temperature inversion

and dry layer while summer fogs are deep with weak stability and indistinct fog top. Instead of southerlies, northerlies can also produce fogs that are about 15% of the sea fogs in winter-spring in the Yellow and East China Sea, yet the mechanism in the process of moistening is unclear so far.

Cold phase (SAT<SST) often occurs in spring fogs due to intensified longwave radiation at fog tops, while warm phase (SAT>SST) is common in summer fogs because they are deep and the cooling at fog top is not as strong as in spring fogs due to plenty of moist air above, though all of these fogs are advection cooling ones. It is worth noting that the cold and warm phases may occur simultaneously but in different spots (often with different fog thickness), or appear at same spot but in different time in the duration of fog according to buoys and models. Therefore, cautions have to be paid to distinguish warm fog (SAT>SST) from cold fog (SAT<SST) just depending on one or two ship reports (e.g. the International Comprehensive Ocean-Atmosphere Data Set, or ICOADS) for any individual fog event.

Numerical fog forecast is still in the experiment stage at present, but it is the direction of fog forecast. Since fog is highly sensitive to the environmental conditions and is a "weak signal" compared with other weather phenomena, e.g. precipitation, great difficulties and huge challenges exist in this direction. The marine atmospheric boundary layer (MABL) in which sea fog occurs is hard to be simulated exactly by modeling, which influences the forecast heavily. Sparsely distributed observations over oceans are great obstacles for fog forecast. The sea fog research group in the Ocean University of China uses cycling 3DVAR and cycling Hybrid-ETKF-3DVAR to assimilate variety of data to improve the initial conditions, and the results are encouraging. Yet there is still a long way to go for the operational application. It is suggested that sea fog can hardly be forecasted successful with one single model and assemble forecast techniques will be a way out.

The microphysical characteristics and structures in the ABL are especially observed for sea fogs at the coast of the South China Sea, which help us understand the formation, development and decay of sea fogs. But such kind of observations is very rare in the Yellow and East China Sea in recent 20 years. A simple comparison shows that sea fogs are often connected with strong warm/moist advections in the South China Sea, whereas the warm/moist flows are not so robust in the Yellow Sea, which may lead to discrepancy in microphysical structures.

This review just focuses on aspects related to observations and mechanism. Other achievements, like fog detection by satellites, interannual variations of fog frequency and etc do not mentioned here.

Acknowledgement

This work is supported by 40975003 of NSFC, 20090132110008 of MOE, and GYHY200706031. Dr. Gang Fu and Dr. Shanhong Gao kindly provide with their latest papers.

Reference

Diao, X. X. (1992), Statistical analysis of sea fog near Qingdao adjacent sea. Marine Forecasts. 9 (3), 45– 55 (in Chinese).

Bai, H., and Zhang, S. P., Discuss about the characteristic area of the most direct water vapor source of the formation of sea fog over the adjacent marginal sea of Qingdao in Summer, 2010. Periodical of Ocean University of China. 40 (12) in print.

Fu G., Guo J. T., Angeline P., and Li P. Y., 2008. An Analysis and Modeling Study of a Sea Fog Event over the Yellow and Bohai Seas, J. Ocean Univ. Chin. 7(1), 27-34.

Fu, G., Li, P. Y., Crompton, J. G., Guo, J. T., Gao, S. H., and Zhang, S. P., 2010. An Observational and modeling study of a sea fog event over the Yellow Sea on 1 August 2003, Meteor. Atmos. Soc. 107, 149-159.

Gao, S. H., Lin, H., Shen, B., and Fu, G. (2007), A heavy sea fog event over the Yellow Sea in March 2005: analysis and

numerical modeling, Adv. Atmos. Sci. 24, 65-81.

Gao, S. H., Qi, Y. L., Zhang, S. B., and Fu, G., 2010a. Initial conditions improvement of seaf fog numerical modeling over the Yellow Sea by using cycling 3DVAR-Part 1: WRF numerical experiments. Periodical of Ocean University of China, 40(10),1-9.

Gao, S. H., Zhang, S. B., Qi, Y. L., and Fu, G., 2010b. Initial conditions improvement of seaf fog numerical modeling over the Yellow Sea by using cycling 3DVAR-Part 2: RAMS numerical experiments. Periodical of Ocean University of China, 40(11),1-10.

Guo, J. T. (2009), Study of formation and development mechanisms of sea fog: observational analysis and numerical modeling, Ph.d. Thesis, Ocean University of China.

He, Y. K., Huang, J., He, Z. G., and Wang, D. X., 2008, Interannual variability of spring sea fog over northern South China Sea, Journal of Tropical Oceanography, 27(5), 6-11

Hu, R. J., Dong, K. H., and Zhou, F. X., 2006. Numerical experiments with the advection，turbulence and radiation effects in the sea fog formation process, Advances in Marine Science, 24(2),156-165

Hu, R. J., and Zhou F. X., 1998, Effects of advection，turbulence and radiation on formation of sea fog Ⅰ·A theoretical analysis, Acta Oceanologica Sinica,12(1),25-32

Huang, B., Gao, S. H., Song, Y., Zhang, Z. H., and Zhao, W., 2009a, Analysis and observations for advective fog over the Yellow Sea, Advances in Marine Science, 27(1), 16-23

Huang, B., Chen, T., Chen, J., Deng L. T., 2009b, Simulation and test of sea fog numerical prediction system for Yellow Sea and Bohai Sea, Meteorological Science and Technology, 37(3), 271-275

Huang, H. J., Huang J., Mao, W. K., Liao, F., Li, X., Liu, W. H., and Yang, Y. Q., 2010, Characteristics of liquid water content of sea fog in Maoming area and its relationship with atmospheric horizontal visibility, Acta Oceanologica Sinica, 32(2),40-53

Huang, H. J., Huang, J., Liu, C. X., Yuan, J. N., Lü, W. H., Yang, Y. Q., Mao, W. K., and Liao, F., 2009, Microphysical characteristics of the sea fog in Maoming area, Acta Oceanologica Sinica, 31(2), 17-23

Huang, J., Wang, B., Zhou, F. X., Huang, F., Lü, W. H., Huang, M. G., Huang, H. J., Yang, Y. Q., and Mao, W. K., 2010. Turbulent Heat Exchange in a Warm Sea Fog Event on the Coast of South China, Chinese Journal of Atmospheric Sciences 134, 716-725.

Koschmieder, V. H., 1924. Theorie Der Horizontalen Sichtweite, Beitr. Phys. Atmos. 12, 33-53.

Ren Z. P., and Zhang, S. P., 2011, Structure characteristics of the Yellow Sea summer fog in the boundary layer and the comparison, Periodical of Ocean University of China, accepted.

Qi, Y. L., 2010. Study on the formation mechanism of typical advection fog occurred over the Yellow Sea, Master Thesis, Ocean University of China.

Qu, F. Q., Liu, S. D., Yi, Y. M., and Huang, J., 2008, The observation and analysis of a sea fog event in South China Sea, Journal of Tropical Meteorology, 24(5), 490-496

Stoelinga, M. T. and Warner, T. T., 1999. Nonhydrostatic, mesobeta-scale model simulations of cloud ceiling and visibility for an east coast winter precipitation event, J. Appl. Meteor. 38, 385-404.

Wang, B. H., Sea Fog, China Ocean Press, Beijing 1983. pp352.

Wang, H. G., and Qu, W. Z., 1997. Sea fog forecasts in Qingdao area. Mar. Forec., 14, 52-57 (in Chinese).

Wang, X., Huang, F., and Zou, F. X., 2006. Climatic characteristics of sea fog formation of the Huanghai Sea in summer Acta Oceanologica Sinica, 28(1), 26-34

Wang Ya-nan, Li Yongping, 2009, Climatological analysis of sea fog with cold air in the East China Sea and Yellow Sea, Journal of Tropical Meteorology, 25(2), 216-221

Zhang, H.Y., Zhou,F. X., and Zhang, X. H., 2005. Interannual change of sea fog over the Yellow Sea in spring. Oceanologia Limnologia Sinica，36，36-42 (in Chinese).

Zou, F. X., Wang, X., and Bao, X. W., 2004. Climatic characteristics of sea fog formation of the Huanghai Sea in spring, Acta Oceanologica Sinica, 26(3), 28-37

Zhang, S. B., 2010. Study on the Formulation of sea fog over the Yellow Sea related to high pressure, Master Thesis, Ocean University of China.

Zhang, S. P., Ren, Z. P., Liu, J. W., Yang, Y. Q., and Wang, X. G., 2008. Variations in the lower level of the PBL associated with the Yellow Sea Fog —new observations by L-Band Radar, J. Ocean Uni.China 7, 353-361.

Zhang, S. P., and Bao, X. W., 2008. The Main Advances in Sea Fog Research in China, Periodical of Ocean University of China. 38 (3), 359-366

Zhang, S. P., Yang, Y. Q., Wang, X. G., and Wei, J. S., 2008. Seasonal variations in the atmospheric stratification and relations with the Yellow Sea fog season, Periodical of Ocean University of China 38, 689-698.

Zhang, S. P., Xie, S. P., Liu, Q. Y., Yang, Y. Q., Wang, X. G., and Ren, Z. P., 2009. Seasonal variations of Yellow Sea Fog: observations and mechanisms, J. Climate 22, 6758-6772.

Zhang, S. P. and Ren, Z. P., 2010. The Influence of thermal effects of underlying surface on the spring sea fog over the Yellow Sea——observations and numerical simulation, Acta Meteorologica Sinica 68, 116-125.

Zhang, S. P., Liu, J. W., Xie, S. P., (2010), The Formation of a surface anticyclone in the spring Yellow and East China Seas, J. Meteo. Soc. Japan, revised has been submitted.

PROGRESS IN PHYSICAL OCEANOGRAPHY AND REGIONAL AIR-SEA INTERACTION IN THE SOUTH CHINA SEA IN 2006-2010

Dongxiao WANG ,Jian LI,Qiang WANG and Xuanru DING

(Key Laboratory of Tropical Marine Environment Dynamics, South China Sea Institute of Oceanology, Chinese Academy of Sciences, Guangzhou 510301, P.R. China)

Abstract: The progress made by Chinese researchers during 2006 to 2010 in physical oceanography of the South China Sea (SCS) and its regional ocean-atmosphere interaction was addressed here. It focuses on dynamic analyses of basic circulation types, meso-scale eddies, ocean waves, coastal upwelling, internal waves and tides, strait water-exchange, barrier layer, SCS Warm Current and regional air-sea interaction in the SCS. It also includes research progress in the Pearl River Estuary hydrology.

The South China Sea (SCS) is the largest marginal sea in the western Pacific Ocean, with numerous straits connecting to the ocean and water mass exchange with the Pacific and Indian Oceans. The temperature and salinity distribution, tidal mixing，meso-scale eddies, and basin-scale circulation are influenced by numerous straits, complex bottom topography and coastline, and enormous number of small islands, incurring the complicacy in circulation structure of the SCS. This has further resulted in the complicated spatial structure and distinct seasonal variation of the SCS circulation, including basin-scale, sub-basin-scale, and even meso-scale spatial structures, distinct seasonal and interannual variations as well as instantaneous variability.

The SCS circulation of multi-seasonal-and-spatial scales is formed upon a certain regional ocean-atmosphere interaction, whose formation is attributable to its own structural characteristics and closely related to external forces, such as monsoon and air-sea exchange. In recent years, many researchers believe in the existence of a tropical sub-system of East Asian monsoon in the SCS. Short-term abrupt weather phenomena such as typhoon may lead to strong meso-scale eddies in the surface layer of the ocean, causing distinct temperature drop in the upper ocean with the combined effect of direct cooling at the surface by wind. Large-scale monsoons and their wind-stress curls mainly impose a force on the basin-scale circulation to produce Ekman pumping, initiating variations at the depth of thermocline via divergence and convergence, while surface net heat flux and surface freshwater flux related to monsoon variations can influence the upper-layer ocean thermodynamics and dynamics of the SCS.

This report attempts to review the latest research progress on SCS oceanography contributed by Chinese researchers during 2006 and 2010 from the perspective of circulation dynamics and regional ocean-atmosphere interaction.

Ⅰ. Regional Oceanography of the SCS

The South China Sea (SCS) is a semi-enclosed marginal sea with deep a basin. The SCS is located at low latitudes, where the ocean circulations are driven principally by the Asia-Australia monsoon. Ocean circulation in the SCS is very complex and plays an important role in both the marine

environment and climate variability. Due to the monsoon-mountain interactions the seasonal spatial pattern of the sea surface wind stress curl is very specific. These distinct patterns induce different basin-scale circulation and gyre in summer and winter, respectively. The intensified western boundary currents associated with the cyclonic and anticyclonic gyres in the SCS play important roles in the sea surface temperature variability of the basin. The meso-scale eddies in the SCS are rather active and their formation mechanisms have been described in recent studies. The water exchange through the Luzon Strait and other straits could give rise to the relation between the Pacific and the SCS (Liu et al; 2008).

1 Dynamic Explanation of General Circulation Types in the SCS

Proceeding from the island rule theory and ocean data assimilation analysis, Wang *et al.* (2006) concluded that the wind stress variation in central-western equatorial Pacific region is a key factor in Luzon transport variation, while regional wind stress is only a secondary factor. An analysis of enormous SCS observation data leads to the conclusion that the main driving mechanism for the SCS circulation is JEBAR (joint effect of baroclinicity and relief), and secondarily IBWSR (Interaction Between the Wind Stress and Relief), with the terrain effect superior to the β effect, and data analysis of spring 1998 led to the discovery that Sverdrup relation is not valid in the SCS (Liao *et al.* 2007, 2008; Yuan *et al.* 2008).

Hong and Wang (2008) employed a high-resolution three-dimensional (3-D) ocean circulation model to study different effects of wind stress, Kuroshio invasion and bottom topography on the circulation in the northern SCS, concluding that Kuroshio invasion is the mechanism for high-pressure formation on the continental margin without distinct seasonal variations. Moreover, the SCS branch of the Kuroshio has a direct influence on the surface flow field, while wind stress is the main cause of seasonal variation of the SCS circulation. Without the barrier effect of Dongsha Island, the westward invasion of the Kuroshio would aggravate and the SCS branch of the Kuroshio would be strengthened.

Chern *et al.* (2010) observed, via annual-average wind-driven ideal model, that the three factors – wind-stress curl, inflow/outflow, and positive curl feedback from the left side of the Kuroshio—almost equally contribute to the consistent cyclonic circulation in the northern SCS. Besides, the northward movement of the Kuroshio is maintained by the north-south ridge in the Luzon Strait, hence an anticyclonic circulation is unlikely to be observed in the northern SCS.

Chao and Feng (2007) categorized the idealized SCS basin into Ekman layer, inertial layer, and friction layer. It is concluded through theoretical analysis that in wintertime a cyclonic circulation is dominant on all layers with negative correlation between flow speed and depth, while in summertime an anticyclonic circulation is dominant with negative correlation between flow speed and depth.

2 Strait Water-exchange and the SCS Circulation

Numerous straits around the SCS are connected with the open ocean, yet from the perspective of ocean circulation, the inflow and outflow of the Taiwan Strait, Bornean Strait, Palawan Strait, and the Luzon Strait are contained within the upper layer, with very limited influence on the mid-depth and deep circulations in the SCS. Located on the northern margin of the SCS and connected to the Northwest Pacific, the Luzon Strait is directly affected by the Kuroshio. The depth, geographical location, and existence of the western boundary current (WBC) and western boundary return flow determine the vertical structure of Luzon Strait transport.

Liu et al. (2010) discusses the intrusion of the Kuroshio into the SCS, and found the isopycnal surface tilted from the SCS to the North Pacific; and it was steeper in the lower layers than in the upper ones and strong vertical mixing taken place in the areas near 121 ℃E. The Kuroshio in high temperature and salinity intruded westward through Luzon Strait. The frequency of buoyancy was one order of magnitude greater than that of the common ones in the ocean, suggesting stronger stratification in the northeastern SCS. Yuan et al. (2006) used satellite ocean color, sea surface temperature, and altimeter data to study the surface Kuroshio path in the Luzon Strait area. The results suggest that the dominant path of surface Kuroshio intrusion in winter is a direct route from northeast of Luzon to southwest of Taiwan and then westward along the continental slope of northern South China Sea. Hysteresis of a western boundary current (WBC) flowing by a wide gap of a western boundary and the dynamics of the WBC variations associated with the impingement of meso-scale eddies from the eastern side of the gap are studies using a 1.5 layer reduced-gravity quasi-geostrophic ocean model. It is found that the hysteresis is controlled by the periodic penetrating and the leaping regimes of the vorticity balance, and meso-scale eddies approaching the gap from the eastern basin have significant impact on the WBC path inside the gap when the WBC is at a critical state along the hysteresis loop (Yuan and Wang, 2010). The WBC is prone to penetrating into the gap under northerly winds, and for southerly winds, the WBC is prone to leaping across the gap (Wang et al. 2010). When the Kuroshio is close to the critical states of hysteresis，both cyclonic and anti-cyclonic mesoscale eddies can induce transition of the Kuroshio path from an anti-cyclonic intrusion to a gap-leaping state in the Luzon Strait，whereas only cyclonic eddies can force the Kuroshio from the leaping path to an penetrating path (Yuan et al. 2008).

Wang et al. (2009) found TCs can induce a positive (negative) wind stress curl in the northwestern (southeastern) SCS in summer and a positive wind stress curl for the whole SCS in winter. TCs can affect both large-scale and mesoscale SCS ocean circulation, which suggests that studies including the effect of TCs are necessary to help improve the understanding of SCS ocean circulation dynamics. Wang et al. (2010) found the pattern and strength of the summer Asian monsoon wind stress curl over the SCS contribute to the interdecadal variability of the eastward current in the middle South China Sea (SCS) during summer.

Yuan *et al.* (2009) conducted research based on observation data and inverse method on the circulation of the Luzon Strait and the northern SCS circulation in March 1992, discovering that the Kuroshio mainly appears above 800 m and its invasion into the SCS takes place above 400 m, while the northern SCS circulation is dominated by a cyclonic circulation above 400 m to the east of 117.5 ℃E and an anticyclonic circulation below 400 m to the east of 119 ℃E. From August to September 1994, the Kuroshio above 400 m was close to the east coast of Taiwan while the distance increase on the 800-m layer; in the Luzon Strait, the Kuroshio invades into the SCS above 400 m, dominated by a cyclonic circulation with strong upwelling in the northern and central parts of the SCS (Yuan *et al.* 2007). An analysis of the observation data from April 22 to May 24, 1998 leads to the conclusion that the northern SCS is under cyclonic control while the central part is under anticyclonic control; the Kuroshio invasion is indistinct except for partial Kuroshio entry into the SCS above 300 m, while Vietnam costal jet appears above 300 m (Yuan *et al.* 2007). With buoy and observation data analysis, Yuan (2008) discovered that high oxygen water flows from the mid-layer in the SCS in the spring of 2002. Based on the analysis of observation data and satellite data of the Luzon Strait in 2002 (Yuan *et al.* 2009), the sandwich structure is distinctly demonstrated in Luzon Strait transport (LST).

Liu (2008) analyzed the seasonal variations of the subsurface layer and mid-depth water mass of the

SCS based on the same data, attempting at interpreting such seasonal variations by geostrophic flow and SCS meridional stream function. The numerical experiments conducted by Yu *et al.* (2008) show that major factors maintaining the subsurface salinity structure in the SCS include the Kuroshio, three secondary straits, freshwater flux, horizontal mixing by meso-scale eddies, and the driving force of regional monsoons. The research of Chen *et al.*（2007）demonstrates that the water of subsurface and mid depth is likely to leak into the east of the Taiwan Strait, before moving northwards to the west of the Okinawa Trough and then surging upwards to converge with waters of China East Sea. The northeastern continental shelf expansion features of the SCS based on the reflection seismograph survey conducted by Shao *et al.* (2007) show that the SCS bottom current from the Bashi Channel moves northwestwards along the continental slope in the northern SCS until entering the SCS. The above geological evidence demonstrates that the North Pacific flows into SCS through the Bashi Channel near the sill. Tian *et al.* (2006）discovered that sub-inertial current flows westwards above 100 m and eastwards below 100 m based on the hydrological data collected. This observation verifies the sandwich structure of the Luzon Strait flows, of which deep transport is 2 Sv.

Fang *et al.* (2006) discussed the low frequency variability of South China Sea (SCS) surface circulation through Empirical Orthogonal Function (EOF) analysis based on eleven years of sea surface height from satellite altimetry data are used to. The annual variability clearly agrees with previous studies, revealing the SCS response to seasonal fluctuations of the overlaying monsoon winds. The summer eastward jet off west coast of SCS is shown from the second seasonal EOF mode. Two new patterns of year-to-year and decadal variability are presented for the first time from measurements. Long term positive trend appears from 1993 to 2001 and reverses the sign of its trend again from 2001 to 2003. Abnormal events occur in 1994–1995, in 1997–1998 and in 2002 with different spatial scales regarding both basin-scale distribution and meso-scale variability located off the western SCS. Association of these events with the El Niño-Southern Oscillation is discussed. The transition period from cyclonic (anticyclonic) to anticyclonic (cyclonic) is January and February (August and September), expanding eastwards from the east coast of Vietnam. Except for the severe El Niño in 1997/1998, the sea level of the SCS has been rising between 1999 and 2001, yet the sea-level rise of the whole SCS in the summer of 2004 is lower than previous years and the anticyclonic circulation is weaker (Liu *et al.* 2008). In wintertime 1998, the north part of the SCS was controlled by a cold cyclone with an anticyclone close to Dongsha Island, while the central part was controlled by a strong cyclone and a weak anticyclone. The cyclonic control of the southern part was weak, yet with an anticyclonic circulation in the subsurface layer (Liao *et al.* 2008). In summer 2000, a distinct anticyclonic warm eddy of 300 km in scale and a cyclonic cold eddy existed to the most far western SCS. (Liao *et al.* 2007).

Based on hydrological data obtained in the Luzon Strait respectively in July 2007 and October 2005, Yang *et al.* (2010) discovered the structural difference between upper and mid layers; yet little variation is perceived in the bottom layer structure flowing westwards.

Proceeding from the survey in the Taltung Strait and Bashi Channel, Chang *et al.* (2010) concluded that the deep-sea flows are considerably influenced by tides, with varying structures perceived. Yet the geostrophic flow manifests intraseasonal variation rather than distinct seasonal variation. The research also shows that the Bashi Channel is a main passage for the deep overflow of the Luzon Strait. Zhang *et al.* (2010) conducted an analysis using altimeter data of 1997-2007 and annual output of global high-resolution HYCOM model of 2005-2006 to show the distinct intraseasonal variation of overall

flow volume in the Luzon Strait, which also varies with depth. The westward flow in the upper layer (0-300 m) manifests distinct seasonal and intraseasonal variations, while the eastward flow in the bottom layer (below 1200 m) has distinct seasonal variation yet the intraseasonal variation is also noticeable. Both eastward and westward flows in the mid-depth manifest distinct seasonal and intraseasonal variations, yet their net effect adds up to distinct intraseasonal variation as the two are equal in strength. The Rossby wave at a period of 90 to 150 days in the western Pacific is closely interrelated with the LST volume, which shows that the interaction between Rossby wave and Kuroshio may be the cause of intraseasonal variation in the LST.

3 SCS Warm Current

The SCS Warm Current (SCSWC) appears to the north of the southwestward current located in the northern part of the cyclonic circulation in the northern SCS. With the advancement in computing technology, an increasing number of high-definition models are employed in the research of the formation mechanism of the SCSWC. Hong and Wang (2006) discovered through dynamic diagnosis that the pressure gradient traversing the continental shelf and the geostrophic adaptation of cross-continental-shelf transport constitute the main reasons for the emergence of the northeastward current against the wind. With high-resolution 3-D ocean model, Chiang *et al.* (2008) attempted to show that the wind-stress relaxation is the main reason for the emergence of the SCSWC, while the invasion of the Kuroshio constitutes a strengthening factor and the high sea level in the Beibu Bay is the ultimate driving force of the SCSWC, hence the influence of Hainan Island is insignificant to the SCSWC. On the contrary, Yang *et al.* (2008) suggested that neither the invasion of the Kuroshio nor the relaxation of wind stress constitutes the main mechanism for the emergence of the SCSWC, and showed, through a simple model, that the chronic northward current of the Taiwan Strait is the main mechanism for the SCSWC. Wang *et al.* (2010) employed a high-resolution 3-D ocean model to discuss the mechanism for the emergence of the SCSWC from the perspective of vorticity. They discovered that the negative vorticity from JEBAR maintains the motion of the continental slope flow across the isobath, while deflected to the right, feeding into the SCSWC, thus becoming the source of the current. A momentum analysis led to the conclusion that the high-density belt on the continental slope as a result of the Kuroshio invasion causes the coastward pressure gradient on the continental slope, driving the SCSWC under geostrophic balance.

4 SCS Deep Circulation

The SCS circulation system is complicated, with the upper–ocean wind-driven circulation featuring seasonal variations. Due to the existence of deep water overflow in the Luzon Strait, a structure similar to thermohaline circulation exists in the SCS, which is in accordance with Stommel deep circulation theory. Li and Qu (2006) initiated a conceptual map of the SCS thermohaline circulation, which includes the three-layer water-exchange in the Luzon Strait, elevation structure of the upper and mid layers along the northern continental slope, deep-sea renewal component, and deep-sea internal cyclonic structure. As is shown by density structure and oxygen concentration distribution, the SCS deep circulation is basically a cyclonic structure, which corresponds with Stommel's deep-sea source and sink theory.

Wang (2010) recently proposed the first observation-based SCS deep geostrophic circulation map using thermal wind relation and the latest GDEM3.0 data. The northern part of the deep SCS has a cyclonic circulation with a strong deep WBC, while the southern part has a weak cyclonic circulation.

This result might be related to the sea-mountain distribution in the central SCS.

5 Ocean Data Analysis

He and Wang (2007) conducted an analysis of the wintertime characteristics of WBC in the SCS surface layer with drifting buoys from 2003 to 2006. Their findings showed that the source of the WBC in SCS surface layer is located in the northern SCS, with a velocity exceeding 0.8 m/s in the central part along the Vietnam coastline, and that the WBC in the SCS surface layer is maintained by the westward movement of the eastern boundary current and the Kuroshio invasion in December. Using the Argo data of October 2007, Zhou *et al.* (2010) found a southward flow existed along the coastline of Vietnam, starting at 15 °N, 111 °E and extending southward to 5 °N, reaching a depth of 1000 m. Water property analysis showed that no trace of the Kuroshio surface water or North Pacific Intermediate Water is perceived in the WBC during this period.

Li *et al.* (2006) conducted research on two cold surges with different intensities in the SCS in 2004 and their influences on sea-surface temperature (SST) on the basis of open-cruise data collected by automatic meteorological station mounted on the research vessel. Their findings showed that the slow southward movement and distinct on-land degeneration of the weak cold surge on September 22 did not cause any noticeable variation in SST in the SCS, while the fast southward movement and weaker on-land degeneration of the strong cold surge around October 2 caused a major drop in SST. Qiu *et al.* (2009) compared and rectified the AVHRR and TMI satellite data against the SST results obtained from the open cruises in an effort to assess the reliability of the two satellite SST products in the northern SCS.

6 Ocean Data Assimilation

With data assimilation, we can greatly improve the numerical simulations of the SCS. Ocean data assimilation provides high-quality reanalysis data for the regional oceanographic research of the SCS. As funded by the relevant national technology program, the SCS Institute of Oceanology under the Chinese Academy of Sciences has carried out a series of basic research in terms of ocean data assimilation of the SCS, through which the data assimilation systems based on the optimum interpolation, Ensemble Kalman Filter, Ensemble Kalman Smoother, among others, have been established.

An ocean data assimilation method is often used to obtain subsurface temperature from the SST. As the SCS lies in the monsoon system characterized by seasonally reversing wind, the depth of its mixed layer has relatively big seasonal change, though shallower than that of the open ocean. The relation between SST and subsurface temperature varies with depth in the SCS, different from that in the open ocean. Applied the ocean data assimilation to the SCS, and verified the difference in the performance of different SST scenarios in the SCS assimilation system to obtain the assimilation method best fit for the SCS, Shu *et al.* (2009) revealed that the method in which the main component of EOF is projected downward layer by layer on the basis of EOF decomposition, and the sea-surface information is projected downward layer by layer using the mutual relation between the two neighboring layers cannot destroy the temperature structure of subsurface layer, being a more effective method of optimum interpolation of SST.

Shu *et al.* (2010) built an Ensemble Kalman Filter assimilation model based on the Princeton Ocean Model (POM) in the northern SCS, adopted an RMS Ensemble Kalman Filter algorithm for the

assimilation to avoid the errors in observations, and introduced the local operator to eliminate the spurious correlation of samples in space and to increase the degree of freedom of samples simultaneously. Through this experiment, the Global High-Resolution Sea Surface Temperature (GHRSST) from June to July 2008 was assimilated, and the evaluation was performed for the assimilation result using the temperature/salinity data from the cruises during the Northern SCS Coastal Oceanographic Process Experiment (SCOPE) in summer 2008. Their results show that the temperature in the assimilated experiment improved the upwelling in the northern SCS, corrected the deviation of SST, and produced better vertical distribution of temperature.

Xiao *et al.* (2007) set up a POM-based SCS 3-D variational analysis assimilation model for the along-track assimilation of satellite altimeter data under the conditions that the error correlation of each track is taken into account and recursive filtering optimization algorithm is introduced. This system is evaluated using the temperature-salinity data during three cruise in spring 1998, summer 1998, and summer 2000, which shows that in contrast with the simulation result (without data assimilation), the temperature-salinity RMS error and deviation of the system are significantly reduced in both abnormal and normal years, and the error structure fit better with the normal distribution. Especially in the salinity field, this system can make freshwater lenses at the surface that results from precipitation and runoff, transmit the SSH information into the subsurface layer effectively, and reduce the error due to wind stress effectively (Xiao, 2006).

The National Marine Data and Information Service (NMDIS), SOA has established a China ocean reanalysis system (CORA) with multi-source observation data in offshore waters based on the multi-grid 3-D variational analysis. This system has been in the trial running for operation usage. In November 2009, the NMDIS completed the reanalysis product for over nearly 23 years from 1986 to 2008. This product has the horizontal resolution of 0.5 º, with 25 layers in the vertical direction, which has the widest area coverage, the longest time distribution, and the most assimilation data to date. After some preliminary evaluation, He *et al*. (2010) conclude that this product can better represent the large-scale circulation and thermal distribution, meso-scale physical processes, and multi-eddy structure in the SCS.

7 Hydrology of the Pearl River Estuary

The Pearl River Delta is formed by three river deltas in the west, north, and east, with river channels crisscrossed and water system closely packed (Ou, 2009). Under the joint influence of runoff, tidal flow, monsoon, continental shelf and terrain in the northern SCS, the dynamic processes in the PRE are relatively complicated. The Pearl River has the remarkable seasonal change in runoff, about 4,000 m^3/sec in winter and up to 20,100 m^3/sec in summer (Harrison *et al.,* 2008). In winter, the Pearl River suffers from very serious salt water intrusion as a result of low runoff, tidal stirring reinforcement; in summer, the strongly diluted water exists outside the estuary as a result of runoff increase and strengthened stratification. Therefore, the salt water intrusion in winter and diluted water in summer have been subjected to extensive research.

Salt water intrusion, also known as salt tide, is a unique phenomenon in estuary. The salt tide activity of the Pearl River Delta is mainly controlled by runoff and tide. As the saline water of the SCS continental shelf pushes upward along the main tidal outlets of the PRE with tidal currents, salt water spreading and brackish water mixing result in the more saline in the upper river, thus forming the salt tide (Bao *et al.* 2009). The difference in intensity of runoff and tide of eight major outlets in the PRE

leads to the difference in the movement of salt tide. According to years of monthly average chlorinity and simultaneous observation data of each outlet of the PRE, Ou (2009a) analyzed the spatial variability of salt tide activity using the clustering method. The result shows the salt tide activity of the PRE can spatially fall into two categories: one is the tide-dominated estuary, mainly referring to the Humen Outlet; the other is the runoff-dominated estuary including seven outlets such as the Yamen Outlet, Jiaomen Outlet, among others. The outlets of two different kinds are different in terms of brackish water mixing characteristics. The tide-dominated outlets are of vertically homogeneous mixing type and partially mixing type, while the runoff-dominated outlets are of layered type and partial mixing type in general (Ou *et al*., 2009b). Upon analysis of relationship between salt-water movement ascending distance and tidal elevation in three-month-long time series, Bao *et al*. (2009) revealed that salt-water ascending phenomenon of the Modaomen Outlet suddenly built up in just two days before and after the occurrence of the minimum tidal range of all the time, and swung on the achieved ascending high position for several days, and then gradually retreated from the Modaomen Outlet as the tidal force is reinforced, which made the intrusion of neap tide in the Modaomen Outlet stronger than that during the spring tide.

In summer, a great quantity of runoff flows into the PRE, which results in highly stratified water body. And the water body stratification is an important physical factor that contributes to the seasonal oxygen deficiency. After simulating and analyzing the formation of hypoxia in the bottom layer of the PRE using a 3-D ecological dynamic model, Luo *et al.* (2008) concluded that excessive nutrients and organic matters and freshwater runoff are the main factors that contribute to the hypoxia in the bottom layer, while the combination of tides and frontal mixing refrain the expansion of hypoxia. According to the research result of vertical transport of dissolved oxygen (DO) in the PRE by Zhang *et al*. (2010), tide, wind, and upwelling intermittently disrupted the stratification, which brought about the periodic change in DO vertical convection, direction and size of diffusion flux in the company of tide (Zhang et al. 2010). The mixture of runoff and each outlet of the Pearl River contribute to the formation of diluted water of the PRE. The plume front formed by the less dense diluted water on the shelf area outside the PRE is influenced by the complicated dynamic conditions in the northern SCS, and is the important integral part of the circulation in the northern SCS. Upon analysis of the month-by-month observation data for the northern SCS during 1978-1984, Ou *et al.* (2009b) revealed that the buoyant plume off the Pearl River Estuary (PRE), can be classified as four major horizontal buoyant plume types in summer: Offshore Bulge Spreading (Type I), West Alongshore Spreading (Type II), East Offshore Spreading (Type III), and Symmetrical Alongshore Spreading (Type IV). River-mouth conditions, winds and ambient coastal currents have inter-influences to the transport processes of the buoyant plume. It is found that all of the four types are surface-advected plumes by analyzing the vertical characteristic of the plumes, and the monthly variations of the river discharge affect the plume size dominantly. The correlation coefficient between the PRE plume size and the river discharge reaches 0.85 during the high river discharge season. A wind strength index has been introduced to examine the wind effect. It is confirmed that winds play a significant role in forming the plume morphology. The alongshore wind stress and the coastal currents determine the alongshore plume spreading. The impact of the ambient currents such as Dongsha Current and SCS Warm Current on the plume off the shelf has also assessed. The present study has demonstrated that both the river discharge and wind conditions affect the plume evolution. Based on analyses of observation data and model results, Gan *et al*. (2009a, 2010) revealed that diluted water in the PRE is mainly controlled by upwelling by summer monsoon after leaving the estuary and flowing into the northern SCS. The buoyancy flux of diluted water changed the upwelling

in the coastal and offshore areas.

Ⅱ. Meso-Scale Phenomena in the SCS

The SCS has a complicated coastline and many small islands; with the influence of monsoon and the Kuroshio intrusion, rich meso-scale features persist. As the observation shows the intensity of meso-scale signals is as large as that of currents in the SCS, its dynamics significance and influence on marine activities of mankind cannot be neglected. To strengthen the research on meso-scale phenomena in the SCS is therefore of great importance to the understanding and exploitation of the SCS natural resources.

1 Meso-Scale Eddies

Meso-scale eddies prevail in the ocean. These eddies, with high level of energy, horizontal scale of about 100-500 km and lifetime of about 20-200 days, are of rich structures.

Chen and Hou (2009) used fifteen years (1993–2007) of altimetric data, combined from different missions (ERS-1/2, TOPEX/Poseidon, Jason-1, and Envisat), to analyze the variability of the eddy kinetic energy (EKE) in the South China Sea (SCS). The highest EKE center was observed to the east of Vietnam (with a mean value of 509 cm^2/s^2) and the second highest EKE region was located to the southwest of Taiwan Island (with a mean value of 319 cm^2/s^2). They also found that the EKE structure is the consequence of the superposition of different variability components. Spectral analysis of the EKE interannual signal (IA-EKE) shows that the main periodicities of the IA-EKE to the east of Vietnam, to the southwest of Taiwan Island, and in the SCS are 3.75, 1.87, and 3.75 years, respectively. Correlation analysis shows that the IA-EKE has an obvious negative correlation with the SSTA in Niño3 (5°S–5°N, 90°W–150°W). El Niño–Southern Oscillation (ENSO) affects the IA-EKE variability in the SCS through an atmospheric bridge—wind stress curl over the SCS. The locations of the most remarkable EKE seasonal variabilities in the SCS are to the east of Vietnam, to the southwest of Taiwan, and to the west of Philippines in the seasonal cycle. The most obvious intra-annual and mesoscale variability, which may be the result of baroclinic instability of the background flow, are observed to the southwest of Taiwan Island. Wang *et al.* (2007) studied the generation of mesoscale eddies in the eastern South China Sea (SCS) in winters during August 1999 to July 2002 with a reduced-gravity model, and found that the orographic wind jets associated with the northeast winter monsoon and the gaps in the mountainous island chain along the eastern boundary of the SCS can spin up cyclonic and anticyclonic eddies over the SCS, suggesting that direct wind forcing could be an important generation mechanism for the rich eddy activity in the SCS, and that to simulate this mechanism the resolution of the wind forcing has to be high enough to resolve the local wind jets induced by orographic effects.

Li, Jin and Zhu (2007) suggested that the coupling and propagating features of mesoscale sea level variability between the western Pacific(WP)and the South China Sea(SCS)were studied based on time series analyses of satellite altimeter measured,along-track sea surface height anomalies(SSHA)along 21°N and the slope of the northern SCS. Significant propagation of mesoscale variability through the Luzon Strait was in the 45-day band which is very much likely a character of the Kuroshio originating from its low-latitude beginning. It is also suggested that the westward propagating Rossby waves will deform when they encounter the dynamical barrier of the Kuroshio.

Lin *et al*. (2007) identified the meso-scale eddies in the SCS during 1993-2002 using the TOPEX/Poseidon and ERS1/2 merged altimeter data, and conducted statistical analysis for their

temporal and spatial variations. According to their result, about 18 eddies occur averagely in the SCS per year. The inter-annual variation in the number of eddies is related to El Niño/La Niña to some certain extent. The areas where eddies occur mainly lie from the south of Vietnam to the southwest of Taiwan, characterized by northeast-southwest distribution, with the sea areas west of the Luzon Strait and southeast of Vitamin being the most likely, about 23% and 25%, respectively, in terms of occurrence probability. In terms of the occurrence place of eddy, spreading path and speed, occurrence probability and its contribution to the change in SSH, eddies can be roughly split into two relatively independent systems in the south and north along 17°N, and few eddies crosses over to the other system.

Liu and Hu (2009) studied the responses of the meso-scale eddies to the tropical cyclones Lingling 0123, Chanthu 0405, and Durian 0621 using TOPEX/Poseidon and Jason-1 altimeter, SeaWiFS, TMI, and other satellite remote sensing data to obtain the following results: (1) the cold eddies on the right hand side of 'Lingling' and 'Durian' strengthened after the tropical cyclones had passed, causing a drop in SSH and a sharp decline in SST as well as explosive rise in chlorophyll a; (2) the worm eddies on the left hand side of 'Lingling' and in the part of 'Chanthu' were weakened after the tropical cyclones had passed, causing a drop in SSH and a decline in SST but with minor change in chlorophyll a; and (3) when the tropical cyclones 'Lingling' and 'Chanthu' passed through the warm eddies, the intensity of tropical cyclones rapidly increased, which shows that warm eddies may help to strength tropical cyclones.

Yuan et al. (2007) studied the generation and propagation of the anti-cyclonic eddies northwest of Luzon of the Philippines in summer-fall, and found it is a seasonal phenomenon which is phase-locked to the onset of the southwesterly monsoon and the relaxation of the cyclonic wind curl in the northeastern South China Sea. The eddies originate from northwest of Luzon in summer, move across the northeastern South China Sea to reach the China continental slope in fall, and propagate southwestward along the continental slope in fall–winter, inducing shelfbreak current variations in the western South China Sea in fall–winter. Gengxin Chen et al. (2010a) analyzed the seasonal Luzon Warm Eddy (LWE) and found LWE extends vertically to more than 500 m water depth, with a higher temperature anomaly of 5℃ and lower salinity anomaly of 0.5 near the thermocline. The current speeds of the LWE are stronger in its uppermost 200 m, with a maximum speed of 0.6 m/s. And the LWE generally forms in July, intensifies in August and September, separates from the coast of Luzon in October and propagates westward, and weakens in December and disappears in February. The LWE's westward migration is approximately along 19°N latitude from northwest of Luzon to southeast of Hainan, with a mean speed of 6.6 cm/s.

Chen *et al.* (2010b) studied the eddy pair (an anti-cyclonic southern eddy and a cyclonic northern eddy) off eastern Vietnam and its impact on local thermohaline structure and found the eddy pair is a seasonal phenomenon usually found in the summer to fall and the eddy pair has an obvious impact on the thermohaline structure of the loacal upper ocean. The local wind stress curl plays an important role in the interannual variability of eddy pair.

2 Tides

Tides are the rise and fall of sea level due to the gravitational forces exerted by the Moon and the Sun. Customarily, the vertical fluctuation of sea water is known as the tide, while the horizontal motion is known as the tidal current.

Wang *et al*. (2009) conducted harmonic analysis and EOF using nearly 6-month temperature and meteorological data and flow velocity from three ATLAS buoys from October 1998 to April 1999, and studied the spatial structures of the tidal currents in the region. The harmonic analysis result showed that the diurnal tide prevailed in the area, the tidal ellipse rotated around depth, and the clockwise rotation of tide dominated. The tidal amplitude showed significant vertical change. Band-pass filtering on the current was performed for the actual measurement of 10-30 hours; the tidal current was been kept; EOF decomposition on the filtered current suggested the current in the deep basin of the SCS has relatively strong baroclinicity.

Si *et al.* (2010) computed fluctuating tidal and subtidal properties with the thermistor-chain and a ship-mounted Acoustic Doppler Current Profiler, and observed a large-amplitude nonlinear internal wave passing the site followed by a number of small ones. And they collected the tidal constituents from the TPXO7.1 dataset to evaluate these tidal characteristics.

Song *et al.* (2010) developed a new closure scheme in order to add the dissipation to the vertical movement (internal tide in particular). The basic assumption is that water parcel oscillates vertically and disturbs dynamic pressure, which can be affected by neighboring water body at the same time via viscosity. That is to say horizontal diffusion is reserved in the equation of vertical movement, thus the quasi-static pressure balance is introduced. In the z coordinate, the vertical velocity near sea ridges can be magnified. And such magnification can be attenuated by the new closure scheme as shown by the simulation results. When Cw=0.2, the vertical velocity of the simulation has been attenuated by 50% or so. Meanwhile, the simulated thermocline structure can be kept very well.

Tong *et al*. (2010) utilized the ECOM model to simulate the barotropic M2, S2, K1 and O1 tides in the SCS, and the SCS tidal energy flux and tidal energy dissipation. The results show that the barotropic M2, S2, K1 and O1 tides have energy fluxes of 38.93, 5.77, 29.73 and 28.97 GW, respectively, flowing into the SCS via the Luzon Strait. The energy fluxes of 2.42, 0.36, 8.67 and 7.86 GW flow into the Java Sea via the Karimata Strait from the SCS.

Xia *et al*. (2008) performed continuous observations for the bottom flow velocity in the outer continental shelf of the northern SCS over sand the wave areas. The results show that the strong flow at the bottom occasionally occurs at a velocity up to 30-77 cm/s in spite of relatively weak tidal and ocean currents. Upon the power spectral analysis of velocity time series, they found that numerous oscillating components are internal wave currents when the frequency is higher than the M2 tidal component, which demonstrates that the strong bottom current is caused by internal waves. The traveling speed of sand wave was calculated using the observed velocity. According to the calculation, the strong bottom flow can trigger the bottom sediment. Because the internal waves that spread in the northwest direction (up-slope direction) lead to the net flow in the southeast direction (down-slope direction), the sand waves move towards the southeast but at very low speed, and small-size sand waves move at the speed of less than 1.6 m a^{-1}. The bottom flow velocity driven by a strong typhoon was calculated using tide and storm surge coupled model. According to the calculation, the tide and storm surge coupling can move the bottom sand wave, while the moving direction of sand wave is related to the typhoon path, not always in the southeast direction, with the moving distance much smaller. The tide and storm surge coupling is not the main dynamic mechanism of sand wave movement.

Wu *et al.* (2007) provided the optimal assimilation evaluation for the parameters of the tide model in the northeastern SCS using the altimeter data. The model parameters include bottom-friction factors

and boundary conditions. The average value of derived optimal bottom-friction factor is 0.0085. The areas with relatively big value cover the northeast and southwest of Taiwan Island as well as the Luzon Strait, which are the areas with relatively strong internal tides.

3 Ocean Waves

We limit our discussion on the ocean waves in the SCS that are induced by wind. They are mainly wind waves and storm surges.

Chen et al. (2006) analyzed the seasonal character and time variation of offshore waves in China based on the TOPEX/Poseidon satellite altimeter data from December 1992 to March 2005. Analysis results show that the maximum average wave height is in winter, with the main wave areas in the Taiwan Strait, northern SCS, and southeastern sea area of Indochina Peninsula and east of the Luzon Strait, and the minimum is in summer; the transitional periods are spring and autumn. According to the study on wave time variation in rough sea areas during winter, annual variation is the main character of time variation, and seasonal variation is another important character of this sea area, which matches with the period of ENSO events perfectly.

Zhou et al. (2007) performed numerical calculations on the waves of the SCS during 1976–2005 using WAVEWATCH-III wave model with 30 years' reanalysis wind-field data as inputs. Based on their statistics and projection, the main character of waves in the SCS can be concluded as follows: 1) normal wave direction in the SCS is northeastward generally, accounting for 40% of the total occurrence frequency; strong wave direction in the northern SCS is eastward generally, while strong wave direction in the central and southern SCS is northeastward generally; 2) wave height is minimum in summer; while it is maximum in winter due to the impact of northeasterly monsoon; 3) wave height distribution of once-per-100-years under extreme conditions: significant wave height exceeds 18 m in the southeastern part of Hainan Island, and it is about 14 and 9 m averagely in the central and southern SCS.

Wang *et al.* (2008) found that continuous observation of sea water temperature and current during 18–30 September was examined to describe the upper ocean internal wave field response to Typhoon Damrey (0518). Power spectra of temperature and current time series indicate significant deviations from those obtained by using the deep ocean internal wave models characterized by a power law. They also found that the typhoon enhanced the kinetic energy in nearly all the frequency bands, especially in the surface water. The vertical energy density distribution, with its peak value at the surface, was an indication that the energy injected by the strong wind into the surface current could penetrate downward to the thermocline.

Integrating the current computation model and component geographic information system (GIS) effectively, Yin et al. (2008) established a visual wind-wave field model that takes tropical cyclone track and strength forecast as primary input parameters as well as a decision analysis system using GIS as the platform that has rapid diagnosis and analysis ability. They solved the key technology issues to integrate it into an operational system for the SCS waves.

4 Internal Waves

Internal solitary waves have significant impact on mixing and ecosystem on the edge of the continental shelf and have become hot research topic in physical oceanography in recent years in the

SCS.

Xu *et al.* (2010a) present that a sequence of internal solitary wave (ISW) packets propagating northwest was observed in September 2005, based on in-situ time series data from the acoustic Doppler current profiler (ADCP) and thermistor chain in Wenchang area. Both elevation and depression ISWs were observed at the same mooring location with amplitude of 35 m and 25 m respectively in different days. The main energy source of the waves is the diurnal tide and the wave packets were all riding on the troughs and shoulders of the internal tide, they were probably generated locally from the shelf break by the evolution of the internal tides due to nonlinear and dispersive effects. Xu *et al.* (2010b) summarized the characteristics of the ISWs and compared them with those of existing internal wave theories. Comparison between theoretical prediction and observation results shows that the high nonlinearity of these waves is better represented by the second-order extended Korteweg-de Vries (KdV) theory than the first-order KdV model.

Barotropic tides interacted with Double ridges in the Luzon Strait to form complicated baroclinic tide signals. Over the sea ridge, multiple baroclinic signals interacted and propagated to the west and then disintegrated into a series of internal solitary waves with large amplitude. The first solitary wave is closely followed by a second solitary wave and a series of internal coupled waves at small scale. Internal waves with small scale mainly concentrated in the upper 500 m and their energy would decay downwards. The internal waves with small scale are only generated from special horizontal velocity structure arisen out of the second internal solitary wave. By same wave velocity and propagation direction, this coupled system would propagate for a long distance and generate significant signals at the sea surface, which could appear in remote sensing images. By sensitivity tests, they found that the eastern sea ridge was the reason for the generation of the first internal tide, and strong high level internal tide signals would generate in the west. The waves generated between the two sea ridges would interfere with each other, and non-linear superposition would strengthen various signals in the whole area.

Ke *et al.* (2009) collected field data in the Wenchang waters, the northwestern SCS. They found that in late April strong internal solitary waves existed in the area, the amplitude of these waves was about 40 m, wave-generated baroclinic flows were almost 1 m/s, with propagation direction parallel to the tangential direction of the isobath and towards southwest. They identified these internal solitary waves as locally generated by tidal zonal and land interaction.

Shang *et al.* (2008) made frequency spectrum analysis on ocean current data of Acoustic Doppler Current Profiler (ADCP) obtained by fixed point observations in 1998. Their results indicated that the intensity of non-linear action between internal waves in the northern SCS would influence internal wave spectrum characteristics of the sea area. In the seasonal thermocline (at 22 and 58 m depth), due to the existence of strong non-linearity, spectral slope of internal waves tended to between σ^{-1} and σ^{-2}, the peak value of tidal-harmonic wave frequency with higher energy would present rare σ^{-3} progressively decrease with frequency. Below the seasonal thermocline (130m depth), non-linearity was relatively weak, observed spectrum characteristics of internal waves was similar to the standard Garrett-Munk internal wave spectrum, which all showed σ^{-2} spectral slope.

Yang *et al.* (2009) calculated critical periods of Rossby waves in the SCS using the World Ocean Atlas data and contrasted with those at the same latitude in the Pacific Ocean. The results indicated that critical periods of Rossby waves in the SCS would gradually increase with the increase of latitude. And

due to special terrain in the SCS, critical periods of Rossby waves in the SCS basin would distribute along northeast–southwest orientation, which was different from zonal distribution in the open ocean. By analyzing energy spectrum of the SSH anomaly in various grid points of the SCS, they found that the critical period in the mid basin was almost the same as the critical period of local Rossby waves; their values gradually increased with latitude, therefore, the model results were confirmed by observations.

Fan *et al.* (2008) analyzed the relationship between internal wave SAR images and radar band SIR-C/X-SAR multi-channel data in the SCS. For the ascending and descending internal wave SAR images, the characteristics of internal wave images was most obvious for the X wave, secondly by the C wave, and was the weakest in L wave. Li *et al.* (2009) simulated the internal waves excited by tide-terrain interaction and internal wave evolutions over the continental shelf break in the northeastern SCS using a 2-D non-hydrostatic ocean model. The research indicated that the interaction between tide and terrain could excite internal soliton wave train that propagated shoreward, which demonstrated the possibility of local generation of internal soliton waves in such sea area. But the amplitude of internal soliton waves locally generated was much smaller than those propagated from the Luzon Strait.

Shi *et al.* (2009) performed numerical simulations for large-amplitude internal soliton waves in the northeastern SCS (including deep basin and continental shelf break) under the circumstances of background flow field constituted by barotropic flood tide and baroclinic circulation, or barotropic ebb tide and baroclinic circulation. They found that barotropic tides had smaller influence on φ (z) and β but greater influence on α and c. The influence on α would gradually increase with the shoaling of water depth, but the influence on c was consistent; and α (absolute value) and c might be relatively larger when the direction of baroclinic circulation was the same as the one of barotropic tides. From diagnostic simulation of internal soliton waves, they found that barotropic tides had relatively small influence on main soliton wave shape and amplitude but had relatively large impact on non-linear evolution of the soliton waves.

Xie *et al.* (2010) used a continuously stratified nonlinear model to study the impact of topographical character on the generation of internal solitary waves over a sill by tidal flow. When the strength of imposed barotropic tides and the water stratification stay unchanged, the steepness of the sill slope can control both (a) whether or not the waves induced over a sill by tidal flow are linear internal waves or nonlinear internal solitary waves, and (b) the amplitude of the internal solitary waves generated. These conclusions are supported by a numerical experiment with a monthly-mean stratification and an actual seafloor topography from the Luzon Strait.

5 Barrier Layer

The analysis made by Pan *et al.* (2006) showed that barrier layers with distinct seasonal variation occur in the central SCS (10-19 °N, 108-122 °E). The largest probability for barrier layers to appear is in summer (52.8%), followed by autumn (41.0%), is the least (10.5%) in winter. In summer (August-September) of 2000, barrier layers were the most conspicuous, with an average thickness of about 14.2 m. Apart from the sea area (east of 114 °E, and west of Luzon Island) where barrier layers frequently occur, such layers are also noticeable in the southeastern sea area of Indochina Peninsula (12-14 °N, 110-114 °E). In spring (April-June) and autumn (December) of 1998, the average thickness of barrier layers reached 6.8 and 11.2 m, respectively. Barrier layers frequently appear in the sea area east of 114 °E and west of Luzon Island. Additionally, the possibility that barrier layers annually occur in the

west of Luzon Island (12-16 ℃N, 116-120 ℃E), the Zhongsha Islands and the Xisha Islands (16-18 ℃N, 110-116 ℃E) is over 20%. Relatively speaking, the probability of barrier layers occurring yearly in other sea areas is relatively small. Precipitation and southeastward Ekman drift act as the main causes why barrier layers occur in the central SCS in spring, summer, and autumn. Precipitation and southeastward Ekman drift clearly indicate the reasons why barrier layers frequently emerge in the western surrounding waters of Luzon Island in spring and summer; besides, heavy precipitation serves as the main cause for barrier layers to take place in summer in the southeastern sea area of Indochina Peninsula (12-14 ℃N, 110-114 ℃E), and anticyclonic eddy (warm eddy) may bring about stronger barrier layers.

6 Temperature Fronts

As an effective indicator for water masses of different properties, temperature front refers to region(s) where temperature varies the greatest. The northern continental shelf of the SCS, where water masses of various properties converge, acts as the sea area where temperature front frequently emerges. As usual, the temperature front stands for the region(s) where ocean variables vary drastically and is also the high productive area. The research on temperature front is conducive to acquire more details about the composition and variation of circulation system. With the help of 1989-2001 NOAA AVHRR data, Huang *et al.* (2006) studied temperature front emerging in the Taiwan Strait and its surrounding waters, indicating that the average strength, average maximal strength, and average width of temperature front are respectively 0.147, 0.281 /km, and 15.15 km. The characteristics of such front have conspicuous seasonal and interannual variation. Such front is so unstable that semi-circular frontal wave often emerges along the front. The time scale for emergence of front wave is about 1-7 d, the wavelength is around 35-133 km, the annual-average wavelength is 63 km, and the wave amplitude is 25-70 km. The fluctuation of frontal surface is extended to north-northeast, moving towards the north-northeast on the whole.

7 Coastal Upwelling

Cai *et al.* (2007) used a simple model to investigate the location, strength, and formation time of Vietnamese offshore current, and discovered that local wind-stress curl, non-linearity, topography, planetary vorticity advection, and water exchange between the SCS and the Sulu Sea have great impact on offshore location and strength of this current. When sea water flows in through the continental shelf of Sudan, the separation point will move further to the north; however, the stratification and Kuroshio intrusion have less influence on the separation point. In fact, the offshore location of the jet depends on the balance between Vietnamese offshore current and the southwestern branch (close to Vietnamese coast) of cyclonic circulation in the northern SCS, and its driving force is from the local positive local wind-stress curl.

Gan *et al.* (2009a) presented that observational and three-dimensional modeling studies reveal that the intensified upwelling in the northeastern South China Sea (NSCS) is formed as a result of intensified upslope advection of dense deep waters that cross the middle shelf toward the inner shelf over a distinctly eastward widened shelf. Induced by the respective widened shelf and the coastal promontory, the along-isobath variations of cross-isobath transport in the water column over the middle and inner shelves interactively characterize intensified upwelling in the NSCS.

Ⅲ. Air-Sea Interaction

The SCS and its surrounding waters have the highest SST and the strongest atmospheric convection on Earth. The onset of the SCS summer monsoon opens a moisture channel (Indian Ocean-SCS-Chinese Mainland), and water vapor transport during monsoon evolution plays a significant role in air-sea-land interaction in East Asia. Therefore, the air-sea interaction in the SCS is seen as the focus of research for many years. Numerous studies are published recently, providing more sound theoretical foundation and research methods to obtain further understanding of air-sea interaction in the SCS.

1 Fluxes at Air-Sea Interface

The influence of air-sea interaction on climate depends on the heat flux at the air-sea interface. Have summarized the previous research on air-sea transport exchange in the SCS, Yan *et al.* (2007) made comments on the 2008 "Asian Monsoon" Project, proposing an SCS transport project for long-term synchronous multi-point continuous observation to be urgently designed, in order to investigate the time evolution and interannual variation of air-sea interaction, to prepare parameterized schemes for boundary layers over the SCS and its surrounding waters, and to study the relationships between spatial and temporal distribution of the transport over the SCS and onset and evolution of summer monsoon over the SCS. From the analysis, it is elicited that the change of heat flux over the SCS has such conspicuous characteristics in intra-seasonal, annual, and interannual variations.

Having scrutinized the monthly data about latent heat detected by satellites in nine years from 1998 to 2006, Zeng et al. (2009a) discovered that the latent heat flux over the SCS has a conspicuous signal of intra-seasonal variation. The seasonal variation of latent heat flux in the SCS has two noticeable periods, 28-35 days and 49-56 days. The SCSM is closely correlated with the intra-seasonal variation of latent heat: the intra-seasonal change of latent heat in winter is stronger than that in summer. The amplitude of intra-seasonal variation of latent heat is 35 Wm^{-2} in winter and 80 Wm^{-2} in summer. In summer, the SCS latent heat flux has weak signals of east transport (1 °/day) and north transport (0.75 °/day), while in winter the flux is like standing waves. In summer, the intra-seasonal signals are mainly influenced by southwesterly monsoon, and in winter, however, they depend on wind speed and the specific humidity at the sea surface.

Based on the SSM/I satellite observation for 19 years, Zeng et al. (2009b) calculated the monthly evaporation rate of the SCS, elicited the net monthly freshwater flux with the help of rainfall monitored by SSM/I satellite, and analyzed their seasonal and interannual variations. The annual variation of SCS evaporation has two peaks, while rainfall and net freshwater flux each has one peak. From 1998 to 2001, evaporation in the SCS has an ascending trend, increasing by 1 mm/year; from 2001 to 2006, it falls by 1.9 mm/year. Rainfall and net freshwater flux in the SCS are in inverse proportion to Nino3 index.

The analysis made by Chen *et al.* (2007) for SCS heat flux based on multi-years' data indicated that the change of SCS heat flux has conspicuous characteristics in annual and interannual variations, and their periods are 0.5, 1, quasi-3 and 6-11 years respectively, of which the last two are consistent with the periods of drought and flood out-breakings in China. Consequently, it is suggested that the interannual variation of SCS heat flux plays an indispensable role in the distribution of droughts and floods in China.

The air-sea heat exchange in the SCS is large especially in tropical cyclones (Wu *et al.* 2009) and

Liang *et al.* (2009) used RegCM3 regional climate model to conduct numerical simulations for SCS heat flux before and after 2007 monsoon, aiming to understand the influence of air-sea heat flux on SCS monsoon onset and other fields. According to their results, RegCM3 is capable of simulating spatial distribution of each field, while it, by and large, has underestimated the magnitudes of SCS rainfall, SST, 500 hPa geopotential height, and 850 hPa wind. The variations in latent/sensible heat fluxes have large influence on the monsoon onset and other fields.

2 SCS Monsoon-related issues

The analysis of East Asian monsoon system reveals that SCS summer monsoon (SCSM) starts the earliest in Asian monsoons. The onset of SCSM heralds the conversion of air masses in Asian monsoon regions from winter situation to summer, the advent of summer monsoons in East Asia, and the inception of rainy season in eastern China. The onset time and strength of SCSM can influence the weather patters in eastern China.

The index of SCSM onset has many different definitions. In 2007, Ren *et al.* (2007) elicited vertically integrated moisture transport in the SCS from daily NCEP/NCAR reanalysis data of wind, specific humidity, and sea-level pressure during 1951-2000, defined the IVIMT as the index of SCSM onset, according to the analysis for moisture transport before and after the SCSM onset, to obtain the onset dates during the period. Further analysis revealed that this onset index could be used as reasonable onset dates of the SCSM.

With two sets of 42-year time series, ECMWF and NCEP, at hand, Zhou *et al.* (2010) tried to find out forecast factors closely related with early/late onsets of the SCSM. They also used the statistic analysis system (SAS) to design a formula to forecast onset date of SCSM.

Research has unveiled that the onset, maintenance, and variability of the SCSM is closely related to SST. Huang *et al.* (2008) used regional climate model (p-RCM 9) to simulate and investigate the influence of abnormal SCS SST on SCSM. The numerical simulations show that SCS SST in May is crucial to the onset date of SCSM: the continuously increasing/decreasing SCS SST in May drives the onset date earlier/later. The results of Zeng *et al.* (2008) showed that SST increases dramatically before the onset of the SCSM; after the monsoon is over, the SST spatial distribution changes: in the northern SCS, the SST continues to ascend, while it continuously decreases in the south. The fact that the sea surface absorbs heat before the onset of SCSM is the main reason why SST rises before the monsoon onset.

From satellite observations and the reanalysis data, Liu, Sun and Jiang (2009) investigates the late spring formation of warm water with temperature higher than 30 ℃ to the southwest of the Philippine Islands (8–18 ℃N, 115–120 ℃E). The results suggest that the blockage of the winter monsoon by the Philippine Islands results in this “Luzon warm water” (LWW) to the southwest of the Luzon Island and the “Vietnam cold tongue” (VCT) to the southeast of the Vietnam coast during winter and early spring in the South China Sea (SCS).

What is more, much attention should be paid to the relationships between atmospheric wind fields and SCSM. Lin *et al.* (2009) analyzed the relationship between SCS SST and local wind fields and characteristics of their seasonal variation, discussed the relationship between monsoon and the influence of local wind fields on SCS SST. Their conclusions signify that the relationship between abnormal SCS SST and unusual local wind fields have obvious seasonal variation: in summer,

abnormal SCS SST is evidently in inverse proportion to unusual zonal wind; while in winter, it is apparently in proportion to aberrant meridional wind. Such seasonal variations are closely related with features of East Asian monsoons (i.e., the prevailing wind has conspicuous seasonal variation). The study of Zhou *et al.* (2007) for the relationship between SCSM and meteorological fields reveals that the onset date of SCSM, at upper layers (200-100 hPa) is in proportion to zonal wind at the equator in the Indian Ocean in February of that year, and is in inverse proportion at lower layers (1000-700 hPa), similar to distribution features of dipoles; however, the situation is opposite at the central equatorial Pacific Ocean (160 °E-160 °W).

The research and analysis of the SCSM in recent years unveiled various features. Using wavelet analysis, Gu *et al.* (2007) analyzed the oscillation characteristics of strength index sequences of SCSM from 1948 to 2003, and conducted research on the relationship between the strength of SCSM at different time scales filtered with Lanczos filter and marine thermodynamic conditions provided by SODA product. They concluded that the strength change of SCSM has interannual variation for quasi four years, quasi nine years, and inter-decadal variation of around 38 years. Interannual variations are the strongest, while inter-decadal variation is the weakest. The strength of SCSM at different scales is considerably different spatially in terms of its relationship with ocean thermodynamic conditions.

Liu *et al.* (2009) introduced real-time multivariable MJO index (RMMs) proposed by Wheeler et al. to investigate the relationship between MJO index and activity index of SCS intra-seasonal oscillation (ISO). Their results show that MJO index has stable and high lag correlation with SCS ISO.

The analysis made by Fan *et al.* (2010) for circulation, distribution of precipitation, convection, temperature, and humidity before and after summer monsoons in 2004 and 2008 reveals that the monsoon in 2008 had an earlier onset (on May 4) than that in 2004 (on May 19). The Somali cross-equatorial flow before the onset in 2008 was weaker than that in 2004, and subtropical precipitation in 2008 never reached southern China like it did in 2004. In 2008, the strongest convection location was much closer to the south than that in 2004. During the period from the 5th week before the monsoon onset to the date of onset, the accumulated precipitation on Indochina Peninsula in 25 days in 2008 is about 61% of that in 2004, which makes large land-surface contrast, and thus results in different activities of SCSM. After the monsoon onsete, the warm and humid climate in the SCS in 2008 (2004) lasted to the end of October (the mid September), much longer in 2008 than in 2004.

The research conducted by Chen *et al.* (2009) on convection, circulation, and distribution of precipitation before and after the SCSM in 2007 shows that the convection in 2007 became stronger in the east cost of the Bay of Bengal, and then spread to the SCS; meanwhile, subtropical anticyclone withdrew eastward and moved to the north. The SCSM started in the middle/late May (29 weeks), after which the SCS was controlled by southwesterly wind, and the temperature difference between the south and the north in the low and middle latitudes in Asia (wind direction shear) shifted from positive/negative to negative/positive. During the period of the SCSM in 2007, the moisture transport and strengthened monsoon surge brought in more precipitation to eastern China.

Liu *et al.* (2009) found that the blockage of the winter monsoon by the Philippine Islands results in the “Luzon warm water” (LWW) to the southwest of the Luzon Island and the “Vietnamcold tongue” (VCT) to the southeast of the Vietnam coast during winter and early spring in the South China Sea (SCS), and it is a result of land–sea–winter monsoon interaction.

3 Tropical Cyclones

The SCS is one of three regions in the western Pacific Ocean where typhoon can form It is the where tropical cyclone frequently occurs, moving in from the western Pacific Ocean to forming over the SCS. In summer and autumn, a great deal of tropical cyclones form over the western Pacific Ocean that may evolve into typhoons or tropical storms. Further research on tropical cyclone to improve its forecast has a significant impact on guarding against disasters, mitigating their damages, and ensuring steady economic growth.

Using *Tropical Cyclone Year Boo*k compiled under the leadership of the China Meteorological Administration and global near-surface SODA data, Li *et al.* (2007) conducted research on the characteristics of temporal and spatial distribution of location frequency of tropical cyclone forming or passing through the SCS in the past 50 years, which indicates that the geographic distribution of location frequency for tropical cyclone from June to October mainly scatters around the SCS waters between 15 ºN and 22 ºN with obvious characteristics of inter-decadal variation. Before 1975, most of the ocean factors that influence the location frequency of tropical cyclone forming or passing through the SCS waters are La Niña events and the like, and after 1975, however, the are represented by El Niño events and the like.

Several researches have unveiled that the activity of tropical cyclone forming over the northwestern Pacific Ocean is evidently correlated with the SCSM (Mao *et al.* 2008). Based on the 1965 -2007 NCEP/ NCAR reanalysis data and tropical cyclone data by the Joint Typhoon Warning Center (JTWC), Huang *et al.* (2010) carried out preliminary research on the relationship between the onset of SCSM and the activity of tropical cyclone over the northwestern Pacific Ocean (including the SCS), which shows that with the number of tropical cyclone forming and its activity frequency over the northwestern Pacific Ocean (especially in the SCS), the onset of the SCSM increases obviously, comported with that before the onset. However, tropical cyclone emerges over the northwestern Pacific Ocean (west of 150 ºE) two pentads before the monsoon onset half of the time, which signifies tropical cyclone activity may act as one of the trigger mechanisms for the onset of SCSM. In most cases (77%), the SCSM onset is slightly earlier than usual, and tropical cyclone emerges frequently over the northwestern Pacific Ocean two pentads before the onset. In most cases (77%), SCSM starts slightly later than usual, and no tropical cyclone emerges in the two pentads before the onset and after the onset. The earlier onset of the monsoon is engendered by such complicated factors as ISO, emergence of tropical cyclone over the northwestern Pacific Ocean, and cold currents at low and middle latitudes, while the late onset is largely caused by ISO.

Shang *et al.* (2008) presents observations of ocean responses in the SCS subsequent to the passage of typhoon Lingling in November 2001, which show strong surface cooling and large scale Chla enhancement in winter. In particular, they applied the most recent satellite algorithms to differentiate Chla explicitly from CDOM, thus removing the ambigu-ity of whether the observed change was due to phyto-plankton or CDOM.

Typhoons can induce cooling wakes at the ocean surface, causing low sea surface temperature (SST) along their tracks. Yang and Tang (2010) used multi-satellite data to investigate the location of the cooling wake induced by 92 typhoons passing through the South China Sea (SCS) from 1998 to 2009. Analysis of the sequential merged microwave SST data revealed that Cooling wakes induced by typhoons mainly located within 100km along the side of typhoon tracks. It is showed that cold core

eddies, particularly strong cold eddies, existed in the pre-typhoon oceanic environment, may play a significant role in setting the strength and location of SST cooling induced by typhoons.

With the help of POM, an ocean circulation model, Zhang *et al.* (2007) obtained twin simulations for ocean circulation during the period that the SCS was affected by Typhoon "Faith" in 1998 with and without wave-induced stress taken into account. They analyzed the simulation results and compared them with the data collected from buoy observations. The preliminary results of analysis signified that if wave-induced stress is taken into account, simulation results are closer to the observation data, in terms of the maximal reduction in SST and near-inertial oscillation incurred by typhoon.

Through case study and historical statistics, Dai *et al.* (2010) illustrates the mechanism that tropical cyclone strengthens low-level jet stream over the SCS. They took tropical cyclone No. 0604, called 'Bilis', as an example, and used MM5, a meso-scale numerical model, for several numerical simulations. They results show that the powerful southwesterly monsoon prolonged the tropical cyclone life after its landfall, and increased precipitation from the tropical cyclone. Meantime, the influence of the tropical cyclone on southwesterly monsoon was noted. Finally, according to the statistics on 30 tropical cyclones from 1950 to 2009 with similar paths as Typhoon 'Bilis', they discovered that 80% of tropical cyclones are accompanied by positive anomaly of low-level wind speed in the SCS region.

Conclusion

From 2006 to 2010, Chinese scholars made unprecedented achievements on the SCS physical oceanography. The SCS observations, such as the SCS monsoon experiments, comprehensive scientific expedition in the Nansha Waters, and cruises to the northern SCS by the SCS Institute of Oceanology, Chinese Academy of Sciences, continuously unveil many interesting phenomena. The wide application of satellite remote sensing data with high accuracy and resolution has elevated the research on the SCS physical oceanography to a new high. Numerous numerical experiments provide mathematical approaches to reveal dynamic mechanisms for emergence and variation of the SCS circulation, and to forecast the SCS circulation. This paper does not cover all the results on the SCS physical oceanography in this period due to the limited space and deadline, but the research aforesaid brings in enough achievements to draw attention from colleagues from home and abroad on SCS issues. We are convinced that more research achievements in this field will be made to promote marine science in the SCS.

Acknowledgement:

This report is jointly sponsored by the Chinese Academy of Sciences (No. KZCX1-YW-12-01), the National Key Basic Research Program of China (2011CB403504), and the National Natural Science Funds (Nos. 40625017 and U0733002).

References:

1. Bao Yun, Liu Jiebin, Ren Jie, Xu Weiming, Qi Zhiming, (2009) :Research of Law and Dynamic Mechanism for Strong Saline Water Intrusion in Modaomen Waterway. Science in China Series G, 2009 39 (10): 1527-1534, (in Chinese with English abstract)

2. Cai Shuqun, Long Xiaomin, Wang Shengan.(2007): A model study of the summer Southeast Vietnam Offshore. Continental Shelf Research 27 (2007) 2357–2372

3. Chang, Y. T., W. L. Hsu, Tai J. H., Tang T. Y., Chang M. H. and Chao S.-Y. (2010): Cold deep water in the SCS.J. Oceanogr., 66, 183–190.

4. Chao Jiping and Feng Licheng, (2007): Formation of the f-plane quasi-geostrophic three-dimensional ocean circulation under wind-driven and the application of mass conservation. Chinese Journal of Geophysics Vo1.5O.No.5 Sep. (in Chinese with English abstract)

5. Chen Gengxin, Hou Yijun, Chu Xiaoqing, Qi Peng, Hu Po (2009); The variability of eddy kinetic energy in the South China Sea deduced from satellite altimeter data. Chinese Journal of Oceanology and Limnology Volume 27, Number 4, 943-954

6. Chen Gengxin, Hou Yijun，Zhang Qilong, Chu Xiaoqing. (2010a): The eddy pair off eastern Vietnam: Interannual variability and impact on thermohaline structure. Continental Shelf Research 30 (2010) 715–723

7. Chen Gengxin, Hou Yijun , Chu Xiaoqing and Qi Peng. (2010b): Vertical structure and evolution of the Luzon Warm Eddy. Chinese Journal of Oceanology and Limnology Volume 28, Number 5, 955-961

8. Chen Hongxia, Hua Feng, Yuan Yeli, (2006): Seasonal Characteristics and Temporal Variations of Ocean Wave in the Chinese Offshore Waters and Adjacent Sea Areas, Advances in Marine Science, (22): 436-445. (in Chinese with English abstract)

9. Chen Jinnian, Wang Hongna, Lv Xinyan, (2007): Variation feature of the sensible heat flux and latent heat flux in SCS, Advances in Water Science, 2007(18):390-397, (in Chinese with English abstract)

10. Chen Xiangya, Zhou Suoquan, Zhou Bing, (2009): Onset Process of SCS Summer Monsoon in 2007, Journal of Nanjing Institute of Meteorology, 2009(32):71-79. (in Chinese with English abstract)

11. Chern Chingsheng, Jan Sen, Wang Joe (2010): Numerical study of mean flow patterns in the SCS and the Luzon Strait. Ocean Dynamics 60:1047–1059

12. Chiang TzuLing, Wu ChauRon and Chao ShennYu, (2008): Physical and geographical origins of the SCS Warm Current. JOURNAL OF GEOPHYSICAL RESEARCH, VOL. 113, C08028

13. Dai Zhanpeng, Zhang Qinghong, (2010):The Interaction Between Tropical Cyclone and SCS Monsoon, Journal of Peking University, 2010:31-38, (in Chinese with English abstract)

14. Fan Kaiguo, Huang Weigen, He Mingxia, Fu Bin, (2008): Analysis of Internal Wave SAR Image with Multi-frequency, Marine Science Bulletin, 2008 (24): 110-114, (in Chinese with English abstract)

15. Fan Lingli, Guo Pinwen, (2010): Comparison of Characteristics Between SCS Summer Monsoon in 2004 and 2008, Journal of Tropical Meteorology, 2010(26):494-498, (in Chinese with English abstract)

16. Fang Wendong, Guo Junjian，Shi Ping and Mao Qingwen (2006): Low frequency variability of SCS surface circulation from 11 years of satellite altimeter data. GEOPHYSICAL RESEARCH LETTERS, VOL. 33, L22612,

17. Gan Janping, Cheung Y. Y., Guo X. and Li L. (2009a): Intensified upwelling over a widened shelf in the northeastern South China Sea，Journal of Geophysical Research，114

18. Gan, J., Li L., Wang D., Guo X., (2009b): Interaction of a river plume with coastal upwelling in the northeastern SCS. Continental Shelf Research, 29(4), 728-740.

19. Gan, J., Lu Z., Dai M., Cheung A. Y. Y., Liu H., Harrison, P. (2010): Biological response to intensified upwelling and to a river plume in the northeastern SCS: A modeling study. Journal of Geophysical Research, 115(C9), 1-19.

20. Gu Dejun, Ji Zhongping, Wang Dongxiao, (2007): The Relationship Between SCS Summer Monsoon Intensity and

Oceanic Thermodynamic Variables at Different Time Scale [J], Journal of Tropical Meteorology, 2007(23):14-20, (in Chinese with English abstract)

21. Harrison P., Yin K., Lee J., Gan J. (2008): Physical-biological coupling in the Pearl River Estuary. Continental Shelf Research.

22. He zhigang and Wang Dongxiao (2007): Surface pattern of the SCS western boundary current in winter。Advances in Geosciences Vol.12:ocean science

23. He Zhongjie, Han Guijun et al, (2010): Experiments on Assimilating of Satellite Data in the China Seas and Adjacent Seas, Periodical of Ocean University of China, 2010, 40-9, (in Chinese with English abstract)

24. Hong Bo and Wang Dongxiao, (2008): Sensitivity Study of the Seasonal Mean Circulation in the Northern SCS. ADVANCES IN ATMOSPHERIC SCIENCES，VOL 25 NO 5， 824—840

25. Hong Bo, Wang Dongxiao, (2006): Dynamic Diagnosis of Winter Windward Current in the North of SCS, Science Bulletin 9-14, Vol.51, Supplement II 2006.11, (in Chinese with English abstract)

26. Huang Anning, Zhang Yaocun, Huang Danqing, (2008): Numerical Study of the Impacts of SSTA in the SCS on the SCS Summer Monsoon, Chinese Journal of Atmospheric Sciences, 2008(32),640-652, (in Chinese with English abstract)

27. Huang Fei, Li Yuanni, Relationship Between the SCS Summer Monsoon Onset and the Tropical Cyclone Activity in the Western North Pacific, Periodical of Ocean University of China, 2010(40):1-10, (in Chinese with English abstract)

28. Huang Weigen, Lin Chuanlan, Lou Xiulin, Xiao Qingmei, Shi Aiqin, Jin Weimin, (2006):Satellite observations of the thermal front in the Taiwan Strait and its adjacent seas, Acta Oceanologica Sinica, 2006 (26): 49-55, (in Chinese with English abstract)

29. Ke Ziming, Yin Baoshu, Xu Zhenhua, Hou Yijun, (2009): The Characteristics of Internal Solitary Waves at Wenchang in the SCS, Oceanologia et Limnologia Sinica, 2009 (35): 269-274, (in Chinese with English abstract)

30. Li Chao, Zhang Yan, Wang Dongxiao, (2006): Impact of cold surges on sea surface temperature in SCS in autumn of 2004, Journal of Tropical Oceanography, 2006, 25 (2): 6-11, (in Chinese with English abstract)

31. Li Chunhui, Liu Chunxia, Cheng Zhengquan, (2007):The Characteristics of Temporal and Spatial Distribution of Tropical Cyclone Frequencies Over the SCS and Its Affecting Oceanic Factors in the Past 50yrs, Journal of Tropical Meteorology, 2007(23):341-347, (in Chinese with English abstract)

32. Li L. and Qu T. (2006): Thermohaline circulation in the deep SCS basin inferred from oxygen distributions, J. Geophys. Res.-Oceans, 111, C05017

33. Li Li, Jing C., Zhu D. (2007): Coupling and propagating of mesoscale sea level variability between the western Pacific and the South China Sea, Chinese Science Bulletin, 52(12), 1699-1707.

34. Li Qun, Chen Xu, Xu Zhaoting, Sunli, (2009): Numerical modeling on the nonlinear internal wave generation by the tide-shelf break interaction at the Northeastern SCS, Journal of Hydrodynamics, 2009 (24) Series A: 724-733, (in Chinese with English abstract)

35. Liang Wei, Li Xiuzhen, (2009):A Numerical Study on the Impact of Air-Sea Fluxes on the Onset of Summer Monsoon of SCS in 2007, Journal of the Graduates of Sun Yat-Sen University, 2009(30):82-89, (in Chinese with English abstract)

36. Liao Guanghong, Yuan Yaochu and Xu Xiaohua (2008): Three Dimensional Diagnostic Study of the Circulation in the South China Sea during Winter 1998. Journal of Oceanography, Vol. 64, pp. 803 to 814

37. Liao Guanghong, Yuan Yaochu and Xu Xiaohua (2007): Diagnostic Calculation of the Circulation in the South China Sea during Summer 1998. Journal of Oceanography, Vol. 63, pp. 161 to 178

38. Lin Ailan, Zhang Renhe, (2009): The impact of atmospheric wind at low level Oil sea surface temperature over the SCS and its relationship to monsoon, Marine Sciences, 2009(33). 95-100, (in Chinese with English abstract)

39. Lin Pengfei, Wang Fan, Chen Yongli, Tang Xiaohui, (2007): Temporal and spatial variation characteristics on eddies in the SCS, Acta Oceanologica Sinica, 2007(29):14-22, (in Chinese with English abstract)

40. Liu Changjian, Du Yan, (2008): Seasonal Variation of Subsurface and Intermediate Water Masses in the SCS, Oceanologia et Limnologia Sinica, 2008, 39 (1): 55-64, (in Chinese with English abstract)

41. Liu Guangping, Hu Jianyu, (2009): Response of the mesoscale eddies to tropical cyclones in the SCS: A Case Study, Journal of Oceanography in Taiwan Strait, 2009, (22) 3: 308-315, (in Chinese with English abstract)

42. Liu Qiang, Lu Bo, (2008): Seabed sediment acoustic attenuation in shallow seas of the SCS, Acta Oceanologica Sinica, 2008 (26): 48-55, (in Chinese with English abstract)

43. Liu Qinyu, Arata Kaneko and Su Jilan, (2008): Recent Progress in Studies of the South China Sea Circulation. Journal of Oceanography, Vol. 64, pp. 753 to 762, 2008

44. Liu Qinyu, Sun Chengxue, Jiang Xia,(2009): Formation of spring warm water southwest of the Philippine Islands: Winter monsoon wake effects. Dynamics of Atmospheres and Oceans 47 (2009) 154–164

45. Liu Yiling, Ju Jianhua, Lu Junmei, (2009): Relationship Between Tropical Low-frequency Oscillation and SCS Monsoon Intraseasonal Oscillation, Science and Technology Consulting Herald, 2009(14).1, (in Chinese with English abstract)

46. Liu Ze, Hou Yijun , Qi Peng and Hu Po. (2010): Observations of Kuroshio intrusion into the South China Sea. Chinese Journal of Oceanology and Limnology Volume 28, Number 5, 1012-1020

47. Luo Lin, Li Shiyu, Wang Dongxiao, (2008): Modelling of hypoxia in the Pearl River estuary in summer, Advances in Water Science, 2008, 19 (5), 729-735, (in Chinese with English abstract)

48. Mao J，Wu G，(2008): Influence of Typhoon Chanchu on the 2006 SCS summer monsoon onset[J]. Geophys Res Let t, 35, L12809

49. Ou S, Zhang H, Wang Dongxiao. (2009a): Dynamics of the buoyant plume off the Pearl River Estuary in summer [Internet]. Environmental Fluid Mechanics. 9(5):471-492.

50. Ou Suying, (2009b): Spatial Difference about Activity of Saline Water Intrusion in the Pearl (Zhujiang) River Delta, Scientia Geographica Sinica, 2009, 29(1), 89-92, (in Chinese with English abstract)

51. Pan Aijun, Wan Xiaofang, Xu Jindian, Guo Xiaogang, Wu Risheng, (2006): Barrier layer in the central SCS and its formation mechanism, Acta Oceanologica Sinica, 2006(26): 35-43, (in Chinese with English abstract)

52. Qiu Chunhua, Wang Dongxiao, Hiroshi Kawamura, Guan Lei, Qin Huiling, (2009): Validation of AVHRR and TMI-derived sea surface temperature in the northern SCS. Continental Shelf Research 29 2358-2366.

53. Ren Baohua, Zaheng Jianqiu, Du Jianwei, (2007): An Index of SCS Summer Monsoon Onset Based on Vertically Integrated Moisture Transport, Climatic and Environmental Research, 2007(12):503-514, (in Chinese with English abstract)

54. Shang Xiaodong, Lu Zhumin, Xie Xiaohui, Chen Guiying, (2009): Characteristics of internal-wave spectra on the continental slope of northern SCS, Journal of Tropical Oceanography, 2009 (22): 16-20, (in Chinese with English abstract)

55. Shang, S., L. Li,F. Sun, J. Wu, C. Hu, D. Chen, X. Ning,Y.Qiu, C.Zhang, and S.Shang (2008): Changes of temperature and bio-optical properties in the South China Sea in response to Typhoon Lingling, 2001, Geophys. Res. Lett., 35, L10602.

56. Shi Xingang, Fan Zhisong, Li Peiliang, (2009): Numerical Simulation for Influence of Barotropic Tidal Current on Large-amplitude Internal Solitary Waves in the Deep Sea in the Northeast SCS, Periodical of Ocean University of China, 2009 (34) s1: 297-302, (in Chinese with English abstract)

57. Shu Yeqiang, (2009b): Assimilation Study on Oceanographic Data of SCS for Sea Surface Temperature and Thermohaline Observation, SCS Institute of Oceanology Chinese Academy of Sciences, 2009.11, (in Chinese with English abstract)

58. Shu Yeqiang, Sui Dandan, Wang Weiwen, Xiao Xianjun, (2010): SST Assimilation Experiment in the Northern SCS Using Ensemble Kalman Filter, Journal of Tropical Oceanography, 2010, 29 (5): 10-16, (in Chinese with English abstract)

59. Shu Yeqiang, Wang Dongxiao, (2009a): Performance of Ocean data Reanalysis methods in the SCS,

APPLICATION, 2009.12, (in Chinese with English abstract)

60. Si Guangcheng, Hou Yijun, Qi Peng and Hu Po, (2010): Characteristics of nonlinear internal waves observed in the northern South China Sea. Chinese Journal of Oceanology and Limnology Volume 28, Number 5, 1068-1072

61. Song Dan, Thomas Pohlmann, Chen Xueen, Wu Dexing, (2010): The role of sea water viscidity in modeling the vertical movement of internal tides. Ocean Modelling 34 63–69

62. Tong Jingquan, Lei Fanghui, Mao Qingwen, Qi Yiquan, (2010): Tidal Energy Fluxes and Dissipation in the SCS Without Considering Tide-generated Potential Energy, Journal of Tropical Oceanography, 2010 (22): 1-7, (in Chinese with English abstract)

63. V. Vlasenko, N. Stashchuk, C. Guo, and X. Chen, Multimodal structure of baroclinic tides in the SCS. 2010 Nonlin. Processes Geophys., 17, 529–543

64. Wang Dongxiao, Liu Qinyan, Huang Ruixin, Du Yan,and Qu Tangdong，(2006): Interannual variability of the SCS throughflow inferred from wind data and an ocean data assimilation product. GEOPHYSICAL RESEARCH LETTERS, VOL. 33, L14605

65. Wang Dongxiao, Hong Bo, Gan Jianping and Xu Hongzhou, (2010): Numerical investigation on propulsion of the counter-wind current in the Northern SCS in winter. Deep Sea Research Part I: Oceanographic Research Papers Volume 57, Issue 10, October, Pages 1206-1221

66. Wang Gang , Qiao Fangli, Hou Yijun, Dai Dejun, Lin Min, Zhang Qilong and Yin Baoshu (2008): Response of internal waves to 2005 Typhoon Damrey over the northwestern shelf of the South China Sea Journal of Ocean University of China (English Edition) Volume 7, Number 3, 251-257

67. Wang Guihua，Chen Dake，Su Jilan, (2007): Winter Eddy Genesis in the Eastern South China Sea due to Orographic Wind Jets. JOURNAL OF PHYSICAL OCEANOGRAPHY VOLUME 38

68. Wang Guihua, Ling Zheng and Wang Chunzai, (2009): Influence of tropical cyclones on seasonal ocean circulation in the South China Sea. JOURNAL OF GEOPHYSICAL RESEARCH, VOL. 114, C10022

69. Wang G.-H，Xie S.-P，Huang R.-X, (2010): Deep SCS circulation. Geophys. Res. Lett., in press.

70. Wang Guihua, Wang Chunzai, Huang Ruixin, (2010): Interdecadal Variability of the Eastward Current in the South China Sea Associated with the Summer Asian Monsoon. Submitted to Journal of Climate (revised)

71. Wang Xuezhu, Li Peiliang, Zhang Tingting, (2009): Vertical structure of the tide current in the central deep basin of the SCS, Acta Oceanologica Sinica, 2009 (26): 20-27, (in Chinese with English abstract)

72. Wang Zheng, Yuan Dongliang, Hou Yijun. (2010): Effect of meridional wind on gap-leaping western boundary current. Chinese Journal of Oceanology and Limnology Vol. 28 No. 2, P. 354-358

73. Wu Disheng, Yang Hui, Wei Jiansu, Yu Shengbin, Chen Julong, Zhang Wenjing, Zhou Shuihua, Zhang Juan, Xia Huayong, (2009): Heat Exchange on Air-sea Interface of SCS and East China Sea in 1986, Journal of Tropical Meteorology, 2009(25):307-313, (in Chinese with English abstract)

74. Wu Ziku, Fan Haimei, (2007): Optimal Estimation of Parameters for a Tidal Model in the Northeast SCS, Journal of Hydrodynamics, Series. A, 2007 (24): 442-449, (in Chinese with English abstract)

75. Xia Huayong, Liu Yuqiang, Yang Yang, (2009): Internal-wave Characteristics of Strong Bottom Currents at the Sand-wave Zone of the Northern SCS and its Role in Sand-wave Motion, Journal of Tropical Oceanography, 2009 (22): 15-22, (in Chinese with English abstract)

76. Xiao Xianjun, Wang Dongxiao, Yan Changxiang, Zhu Jiang, (2007): Three-dimension Variational Oceanic Assimilation Model and its Verification in SCS, Progress in Natural Science, 2007, 17-3, (in Chinese with English abstract)

77. Xiao Xianjun, Wang Dongxiao，(2006):The assimilation experiment in the southwestern South China Sea in summer 2000

78. Xie Jieshuo, Cai Shuqun, He Yinghui (2010): A continuously stratified nonlinear model for internal solitary waves

in the northern South China Sea, Chinese Journal of Oceanology and Limnology Vol. 28 No. 5, P. 1040-1048

79. Xu Zhenhua, Yin Baoshu, Hou Yijun, (2010a): Highly nonlinear internal solitary waves over the continental shelf of the northwestern South China Sea. Chinese Journal of Oceanology and Limnology Volume 28, Number 5, 1049-1054

80. Xu Zhenhua, Yin Baoshu, Hou Yijun, Fan Zhisong and Antony K. Liu,(2010b): A study of internal solitary waves observed on the continental shelf in the northwestern South China Sea Acta Oceanologica Sinica Volume 29, Number 3, 18-25

81. Yan Junyue, Liu Jiumeng, Jiang Guorong, Wan Hui, Liu Yanju, Yao Huadong, (2007): Advances in the Study of Air-Sea Flux Exchange over the SCS, Advances in Earth Science, 2007(22):685-697, (in Chinese with English abstract)

82. Yang Jiayan, Wu Dexing, and Lin Xiaopei, (2008): On the dynamics of the SCS Warm Current. JOURNAL OF GEOPHYSICAL RESEARCH, VOL. 113, C08003, doi:10.1029/2007JC004427,

83. Yang Qi, Chen Guiying, Shang Xiaodong, (2010): Distribution characteristics of critical periods of Rossby waves and sea-surface height anomaly power spectra in the SCS, Journal of Tropical Oceanography, 2010 (22): 20-25, (in Chinese with English abstract)

84. Yang Qingxuan, Tian Jiwei, Zhao Wei. (2010): Observation of Luzon Strait transport in summer 2007. Deep-Sea Research,I57 670–676

85. Yang Xiaoxia, Tang Danling. (2010): Location of sea surface temperature cooling induced by typhoon in the South China Sea, JOURNAL OF TROPICAL OCEANOGRAPHY. 2010(29):26-31,(in Chinese with English abstract).

86. Yin Yi, Mao Qingwen, Wang Jing, Qi Yiquan, (2008a): A GIS-based component-oriented integrated system for analysis of tropical cyclone wind and wave fields in SCS, Journal of Tropical Oceanography, 2008 (22): 78-83, (in Chinese with English abstract)

87. Yin Yi, Wang Jing, Mao Qingwen, Qi Yiquan, (2008b):Prediction System of Typhoon Wind and Wave in the SCS Based on GIS, Marine Science Bulletin, 2008 (24): 76-81, (in Chinese with English abstract)

88. Yu Xiaoli, Xie Qiang, Wang Dongxiao, (2009):Diurnal cycle of marine atmospheric boundary layer during the 1998 summer monsoon onset over SCS, Journal of Tropical Oceanography, 2009(28): 31-35, (in Chinese with English abstract)

89. Yu Zuojun, Julian P. McCreary, Max Yaremchuk, Ryo Furue, (2008): Subsurface Salinity Balance in the SCS*. J. Phys. Oceanogr., 38, 527–539.

90. Yuan Dongliang and Wang Zheng (2011): Hysteresis and Dynamics of a Western Boundary Current Flowing by a Gap Forced by Impingement of Meso-scale Eddies. Accepted by JPO

91. Yuan Dongliang, Han Weiqing and Hu Dunxin (2006): Surface Kuroshio path in the Luzon Strait area derived from satellite remote sensing data. JOURNAL OF GEOPHYSICAL RESEARCH, VOL. 111, C11007,

92. Yuan Dongliang, Han Weiqing and Hu Dunxin. (2007): Anti-cyclonic eddies northwest of Luzon in summer–fall observed by satellite altimeters. GEOPHYSICAL RESEARCH LETTERS, VOL. 34, L13610, 6 PP., 2007

93. Yuan Dongliang, Li Ruixiang (2008): Dynamics of eddy—induced Kuroshio variability in Luzon Strait. JOURNAL OF TROPICAL OCEANOGRAPHY Vo1_27，NO．4 July

94. Yuan Yaochu, Liao Guanghong, Yang Chenghao. (2009): A diagnostic calculation of the circulation in the upper and middle layers of the Luzon Strait and the northern SCS during March 1992. Dynamics of Atmospheres and Oceans 47 86–113

95. Yuan, Y., G.-h. Liao, W. Guan, H. Wang, R. Lou, and H. Chen (2008): The circulation in the upper and middle layers of the Luzon Strait during spring 2002, J. Geophys. Res., 113, C06004, doi:10.1029/2007JC004546

96. Zeng L.L. and Wang D.X.., (2009a): Intraseasonal variability of latent-heat flux in the SCS, Theoretical and Applied Climatology,

97. Zeng Lili, Shi Ping, Wang Dongxiao, Chen Ju, (2009b): Seasonal and Interannual Variabilities of Evaporation and Net Freshwater Flux in the SCS, Chinese Journal of Geophysics, 2009(52):929-938, (in Chinese with English abstract)

98. Zeng Qiang, Zhang Yaocun, (2008): An Analysis of SST Variation During SCS Monsoon Onset Period in SCS,

Journal of Tropical Meteorology, 2008(24):44-50, (in Chinese with English abstract)

99. Zhang H, Li S. (2010): Effects of physical and biochemical processes on the dissolved oxygen budget for the Pearl River Estuary during summer. Journal of Marine Systems. 79(1-2):65-88.

100. Zhang Heng, Li Shiyu, (2010): Numerical Study on the Vertical Transport of Dissolved Oxygen in the Zhujiang (Pear1) River Estuary in Summer, Acta Oceanologica Sinica,, 32 (1), 34-46, 2010, (in Chinese with English abstract)

101. Zhang Zhengguang, Zhao Wei, Liu Qinyu. (2010): Sub-seasonal variability of Luzon Strait Transport in a high resolution global model. Acta Oceanol. Sin., Vol. 29, No. 3, P. 9-17

102. Zhang Zhixu , Qi Yiquan, Shi Ping, Wang Dongxiao.（2007）: Influence of wave induced stress on upper current in South China Sea during a typhoon process. JOURNAL OF TROPICAL OCEANO GRAPHY：Vol. 26 pp. 1 to 8

103. Zhou Hao, Lan Guangdong, Wen Zhiping, Cheng Bingyan, Li Yonghua, (2010): Forecast of the Onset Date of the SCS Summer Monsoon, ACTA Scientiarum Naturalium Universitatis Sunyatseni, 2010(49): 134-140, (in Chinese with English abstract)

104. Zhou Hao, Wen Zhiping, Lan Guangdong, (2007): Diagnosis of Relationships between the Onset of SCS Summer Monsoon and the Equatorial Zonal Wind, Chinese Journal of Atmospheric Sciences, 2007(31):950-962, (in Chinese with English abstract)

105. Zhou Hui, Yuan Dongliang , Li Ruixiang , He Lei , (2010): The Western SCS currents from measurements by Argo profiling floats during October to December 2007. Chinese Journal of Oceanology and Limnology Vol. 28 No. 2, P. 398-406

106. Zhou Liangming, Wu Lunyu, Guo Peifang, Wang Aifang, (2007): Simulation and study of wave in SCS using WAVEWATCH-Ⅲ, Journal of Tropical Oceanography, 2007 (22): 1-8, (in Chinese with English abstract)

ADVANCE IN BIOGEOCHEMICAL PROCESSES OF BIOGENIC ELEMENTS IN CHINA MARGINAL SEAS (2006-2010)

SONG Jinming

（Institute of Oceanology, Chinese Academy of Sciences, Qingdao 266071, P.R.China）

The main progress of chemical oceanography was focus on the marine biogeochemical processes of biogenic elements in China marginal seas from 2006 to 2010.The marginal seas form the linkage between the continent and the ocean. They mark the areas of interaction of rivers, lands, oceans, the atmosphere and sediments. Despite their relatively modest surface areas, yet they are important domains that influence global biogeochemical cycles. Marginal seas play a considerable role in the biogeochemical cycles of carbon, nitrogen and phosphorus because they receive massive inputs of these elements through upwelling and terrigenous inputs(Song, 2010). The marginal seas are also among the most biologically and geochemically active areas of the biosphere, and exchange large amounts of matter with the open oceans. The marginal seas have high sedimentation rates and act as filters and traps of both natural and anthropogenic materials transported from the continents to the open ocean. At least 80% of the terrigenous material delivered to the ocean today is trapped on the proximal shelves of the continents. On the other hand, the marginal seas are regions of higher net primary production relative to that of average global oceanic surface waters and play a significant role in the mitigation of effects of the anthropogenic perturbations through organic carbon storage and recycling within the global framework. The ocean margins can contribute an order of magnitude greater amount of dissolved and particulate organic matter to the interior of the Pacific than those derived from the surface open ocean. It was estimated that about half of the organic carbon input to the seabed of the North Pacific occurs within 500 km of the margin(Song et al., 2008)

The marginal seas are also especially susceptible to anthropogenic influence at a time when humans are strongly interfering in the global biogeochemical cycle of carbon, nitrogen and phosphorus. This interference has led to substantially increased loadings of the land and atmosphere with chemicals such as nutrients from these activities, especially in the marginal seas .

Ⅰ Marine Biogeochemical Processes of Biogenic Elements in China (2006-2010)

The China's marginal seas, including the Bohai Sea, the Yellow Sea, the East China Sea and the South China Sea, have a total area of 4.73×10^6 km^2. They form the linkage between the largest continent and the largest ocean in the world. Two of the largest rivers in the world, the Yangtze River and the Yellow River, together with the Pearl River whose flow is the second largest among rivers in China, empty into China marginal seas with large and ever increasing nutrient and carbon inputs.

Biogeochemical cycles can be dominated by different factors owing to the geomorphological and current systems in marginal seas. The amount of freshwater flow is an important factor due to its impact on buoyancy flux; upwelling is an important factor which is characteristically episodic in nature and which has been identified as having an important influence on the retention and exchange along those usually narrow shelves. The seasonal ice coverage also plays an important role in the air-sea exchange of gases and the land-to-sea flux of matter, especially in the polar margins. With respect to

the China marginal seas, the dominant factors are the fresh water input, the Kuroshio Intermediate Water which originates in the nutrient-rich South China Sea intermediate water and upwells onto the East China Sea continental shelf, the river input of nutrients and dissolved and particulate materials, the biological pump, and coastal anthropogenic activities such as mariculture and marine engineering, and the ecological disaster such as red tides and so on.

1 River Input

The continental fluxes of nutrients and organic matter have important impacts on marine ecosystems. In combination with freshwater discharge and the resulting stratification they can be crucial determinants of the productivity in coastal areas, especially in the estuaries of large rivers. Furthermore, continent-ocean fluxes are a principal source for nutrients to the world oceans, whose productivity is controlled by the availability of a few elements. A major fraction of terrigenous nutrients is bound in organic molecules and available to most primary producers only after bacterial mineralization.

Rivers serve as a major source of buoyancy and dissolved and particulate materials. They contribute significantly to the freshwater flow and terrestrial materials. The riverine fluxes of nutrients and organic matter have important impacts on marine ecosystems. The input of high concentrations of biologically important elements, along with the complex physical structure of buoyant freshwater plumes, lead to strong gradients in concentrations of and transformations among biogeochemical constituents in plume environments and can be crucial determinants of the productivity in marginal seas, especially in the estuaries of large rivers. The impacts of large rivers are important on a regional/continental scale and on a global scale but are especially significant to the continental shelf regions that receive the river input. It is primarily due to large rivers that approximately 40% of the global marine burial of organic matter occurs in deltaic environments (Song et al., 2008). The world's ten largest rivers transport approximately 40% of the fresh water and particulate materials entering the ocean.

In China, two of the largest rivers in the world, the Yangtze River and the Yellow River, together with the Pearl River whose flow is the second largest among rivers in China, empty into the China's marginal seas with large and ever increasing nutrient and carbon inputs. Annual discharge of rivers in China contributes 7% of the total global riverine discharge. They play a significant role in biogeochemical processes in China marginal seas(Song,2004).

Freshwater runoff from rivers into the seas is an important element of the dynamics over many continental shelves. Rivers serve as a major source of buoyancy which is a key mediating factor in transformation process in the coastal margins. On the one hand, buoyancy prevents the cold water from sinking there to large depths from the surface at high latitudes. On the other hand, buoyancy produces plumes and coastal currents locally. Since estuary outflows tend to be less saline and hence lighter than the ambient shelf water, a plume typically forms as the buoyant water spreads away from the mouth of the estuary and coastal currents develop downstream. Chemical and biological activities are greatly enhanced by the changed physical and optical environment within buoyant plumes.

With respect to the China marginal seas, freshwater input of the Yellow River, the Yangtze River, and the Pearl River has significant influence on the intensity of carbon source/sink in estuaries and the adjacent seas. With the development of the economy and the increasing demands for preventing floods and saving water resources in China, thousands of water conservancy projects have been constructed in the large river basins in recent decades, which reduced the freshwater flow to marginal seas. For instance, cutting back the Yangtze River outflow by a mere 10% will reduce the cross-shelf exchange by about 9% because of a reduced buoyancy effect, and at the same time, it will cut the onshore

nutrient supply by nearly the same amount (Song, 2010). It can therefore be expected that primary production and fish catch in the East China Sea will decrease proportionately. From the fresh water to the salty water, the Yangtze River mouth was gradually changed from strong carbon source to weak carbon sink.

Rivers contribute substantial amounts of dissolved and particulate materials to continental margins and subsequently to the ocean. These materials can largely influence the carbon source/sink in marginal seas. The riverine input of nutrients fuels a high biological production in coastal environments, making them an important layer in the global carbon cycle. The organic matter in suspended particulate material can be largely trapped in the estuary turbidity maxima, which intensifies microbial and micro-crustacean grazing activities. And thus the biological pump is strengthened. The riverine dissolved organic matter can be distributed throughout the ocean water column and its oceanic residence time is much shorter than that of marine dissolved organic matter. The regeneration of nutrients during rapid cycling of riverine dissolved organic matter could contribute to high rate of primary production in the coastal ocean.

Significant inputs of nutrients to the coastal zone arrive via rivers, which forms the foundation of high production in the continental margins. N, P, and Si are important limiting nutrients for production in marginal seas. Increasingly, these inputs are being greatly perturbed by anthropogenic activities. Rivers act as natural integrators of surficial processes, including human activities, within their drainage basins. With the development of economy and the increased demands for preventing floods and saving water resources in China, thousands of water conservancy projects have been constructed in the large river drainage basin during recent decades. Anthropogenic perturbations have caused considerable changes in riverine nutrient concentrations and fluxes to the sea. From the 1950s to 1970s, DIN and DIP concentration and flux have a slow increase, but a great increase after the 1980s due to the intensive application of chemical fertilizer and a large amount of chemical plants which came into operation after the 1980s. The chemical fertilizer applied to the Yangtze River drainage basin in 1991 was 48 times more than that in 1962. Annual dissolved silicon flux has decreased sharply since the 1950s, due to the decreased dissolved silicon concentration. Impoundment of reservoirs on rivers was responsible for the decreased dissolved silicon concentration. On the one hand, part of dissolved silicon is fixed by phytoplankton in the reservoirs. On the other hand, the reservoirs have reduced the sediment load to the sea, which has resulted in a decrease in dissolved silicon concentration.

In addition, the N:P:Si ratios of the inputs have been changed. It is well known that silicon plays an important role in the primary productivity of the aquatic ecosystem. Diatoms, accounting for 60% of all species of phytoplankton, take up silicon to form cell walls. Silicon is linked strongly to the carbon cycle through the activities of diatoms, the ‘workhorses of primary productivity. The sharply decreasing dissolved silicon flux and quickly increasing DIN and DIP fluxes into the sea have enhanced eutrophication and caused frequent harmful algal blooms in coastal waters. The highest record of red tides in the Yangtze River mouth is 19 times a year and the longest cumulative time is about 60 days, which caused great damage to mariculture and fishery production. The influence on biogeochemical processes by red tides will be discussed separately in the following part.

2 Coastal Anthropogenic Activities

Anthropogenic activities along the China marginal seas are mainly mariculture, sea reclamation and oil drilling projects. China is the developed country in mariculture, with the largest maricluture area and the largest yield in the world. The mariculture yield was 1.4×10^7 t in 2008, approximately two thirds of the total yield in the world. With respect to sea reclamation, there was three times of large sea

reclamation projects in the history of China, which were carried out for solar salt, enlarge agricultural land and maricluture, respectively. From 1949 to the end of the 20th century, the annual sea reclamation area was about 230~240km^2 per year. Now the fourth large sea reclamation projects are hot. It is planed that the sea reclamation projects will increase 700 km^2 lands annually, which are nearly equivalent to the area of Singapore.

Maricluture in China is primarily comprised of shellfish and seaweeds, which constitute about 90% of the total yield. Seaweeds and shellfish can greatly affect the biogeochemical processes. Algae affect the biogeochemical processes mainly through two ways: they transform the dissolved inorganic carbon to organic carbon via photosynthesis and the pCO_2 decreases; the absorption of nitrate and phosphate by phytoplankton will enlarge the alkalinity. Both of the ways will stimulate the diffusion of CO_2 into the seawater. In Sanggou Bay in the coastal of the Yellow Sea, the culture seaweeds can contribute to 37% of the total productivity in the bay, and it was estimated that about 3.3×10^5 t carbon is removed from the seawaters by mariculture of seaweeds in China coastal seas in 2002 (Song et al., 2008).

The shellfish can affect the biogeochemical processes through the following ways: they can use the HCO_3^- to form the shell; they can utilize organic material by filter feeding so that the quantity and composition of suspended particulate materials will be regulated; they can transport large amount of particulate materials by forming and deposition of fecal pellets, and thus the sedimentation rate will be enlarged; they excrete lots of nitrogen and phosphorus to the seawater. Part of the shell is transported into the deep sea, and most of the shell is harvested by human, both of which remove the carbon from the water. It was estimated that about 8.6×10^5 t carbon was removed from the seawater by mariculture of shellfish in China coastal seas in 2002 (Zhang et al., 2005). In addition, in the mariculture area, excretion of nitrogen and phosphorus by shellfish can satisfy 50% the nitrogen and phosphorus needed by phytoplankton, among which excretion of NH_4^+ and dissolved inorganic phosphorus can provide 40% and 39% of the nitrogen and phosphorus needed by phytoplankton, respectively(Song et al., 2008) . It was estimated that about 850t nitrogen and 78t phosphorus will diminish because of mariculture of shellfish and seaweeds (Song, 2010).

Furthermore, with respect to artificial bait which is primarily applied in shrimp mariculture and cage culture nowadays, baits feeding is an important factor affecting marine environment. Approximately 20% of the baits are not be utilized, which will be left into the water surroundings together with the excretions by shrimps and fish. In addition, instruments in mariculture area, such as cages and raft frames, can have effect on sea currents. The suspended mariculture of shellfish in Sanggou Bay reduced the tide speed by 35%~40% of the speed before mariculture, which would inevitably exert influence on carbon cycle processes.

Sea reclamation projects have reduced the capacity of the estuary to retain nutrients, as a result of the loss to reclamation of accommodation space for intertidal sedimentation. The huge loss of intertidal-wetland environment has had a severe impact on sediment and material fluxes. Reclamation and commercial/urban development in the estuary in the last 300 years has reduced the organic carbon storage capacity of the Humber estuary from about 3.2×10^5 t in the palaeo-estuary to no more than 2.5×10^3 t today, a more than 99% reduction in potential C_{org} storage capacity (Song, 2010). The total modern yearly sulphur deposition is approximately 2% of its value 2ka ago. The decreased organic carbon storage capacity and sulphur deposition rate in Humber estuary foreshow that the similar variations would possibly happen to China coastal area where sea reclamation projects are huge.

3 Biological Pump

A better understanding of the ability of the ocean to control atmospheric CO_2 levels will only be

gained from a quantitative investigation of the mechanism known as the biological pump(Song, 2008). The marine organisms act as a "biological pump", thus removing CO_2 and nutrients from the surface ocean and transferring these elements into the deeper ocean and ocean bottom(Song et al, 2008). The efficiency of biological pump can be affected by various factors. By altering the number, size, and density of particles in the ocean, the activities of different phytoplankton, zooplankton, and microbial species control the formation, degradation, fragmentation, and repackaging of rapidly sinking aggregates of particulate organic carbon (POC) and are responsible for much of the variation in the efficiency of the biological carbon pump.

Photosynthetic production by phytoplankton in the euphotic layer supplies organic material and energy to the aquatic food chain. Further, a possible decrease in pCO_2 in the surface sea water by phytoplankton photosynthesis can accelerate the transfer of CO_2 from the atmosphere to sea water. Thus, primary production in the euphoric zone is one of the most important processes, not only in material cycling in aquatic environments but also in carbon cycling in relation to global change. The carbon fixed by phytoplankton is about 2.22×10^8 t a^{-1} in the Bohai Sea, the Yellow Sea and the East China Sea, while that is 4.16×10^8 t a^{-1} in the South China Sea, about twice of that in the Bohai Sea, the Yellow Sea and the East China Sea(Song, 2010).

Inorganic carbon fixed by phytoplankton can be transformed into particulate materials after a series of biogeochemical processes(Song et al, 2008). Biological activities play an important role in the vertical transition of settling particulate matter (SPM). The Bohai Sea is a region of high productivity and turnover rate(Song et al, 2008). Zooplankton has high grazing pressure on phytoplankton. The growth rate of phytoplankton is about 0.43~0.73d^{-1}, and feeding rate of micro-zooplankton to phytoplankton is approximately 0.42~0.69 d^{-1}. In the bottom, grazing pressure of micro-zooplankton is 3 times of primary productivity (Song, 2010). According to Zhao et al.(2002), respiration can contribute 62% of the nutrients needed by photosynthesis, and excretion of zooplankton and regeneration in the water column can contribute 30% of the nutrients needed by photosynthesis. The high turnover rate of materials in the Bohai Sea makes little particulate organic carbon deposition onto the bottom, which can be confirmed by the low concentration of organic carbon in the sediments of the Bohai Sea. In the Yellow Sea, particulate organic matter in the Yellow Sea decreased from the surface to the bottom, and re-suspension of the sediment was the primary source of particulate matter in the bottom water. Particulate matter in the north South China Sea is mostly from organic materials of planktons. Vertical transportation of carbon in the East China Sea primarily relies on the particulate matters, and particulate organic carbon is mostly affected by biological activities in spring and by terrestrial input in autumn. Biogeochemical studies suggest very efficient recycling of organic carbon by bacterial and protozoan consumption in the shelf water of the East China Sea, but a finite amount of particulate organic carbon with a significant terrigenous fraction is exported from the shelf. The net fluxes of particulate organic carbon is larger in the East China Sea that in the Yellow Sea and south of Taiwan Strait.

4 Ecological Disasters

Marine ecological disasters, such as red tides, pathogenic microorganisms of marine fisheries, and invasion of alien species, can affect the environment of the seawater, the normal growth of marine organisms, and the marine ecological health conditions. Therefore, the transport of materials in marine environment and along the food chain will be changed, which can affect biogeochemistry in China marginal seas greatly. Red tides are the primary marine ecological disaster in China. Frequency of red tides in China marginal seas increased significantly in recent years. There were 698 red tides recorded

in the China's coastal area during 1960-2000, i.e. 4 times in the 1960s, 20 times in the 1970s, 75 times in the 1980s, 200 times in the 1990s, and 399 times in 2000. On average, red tide frequency changed from 3.3 during the 1960s-1980s to 54.5 during the 1990s-2000. The total area of red tides during 2001 to 2007 reached 124 850 km^2, which was significantly expanded while comparing with the historical records.

Red tide is a kind of phenomenon that some marine micro-algae, protozoa, or bacteria accumulate and reproduce rapidly in the water column. Algae bloom is a kind of phenomenon that algae reproduce rapidly in the water column. Commonly, algae blooms whose density of algae is up to a certain density are called red tides. Red tides assimilate lots of nutrients, increase dissolved oxygen at the beginning, and largely reduce the dissolved oxygen at the later period. During the red tides, dissolved oxygen, the transformation of nutrients, the primary productivity and sedimentation of chlorophyll a will be affected. There are often some species of phytoplankton which are poisonous and harmful to zooplankton or high levels. Through the food chain, the transformation of materials will be affected, such as reduce the biomass of organisms at the high levels. And thus, the carbon transformation will be disturbed.

In the regions where red tides often occurred, the primary productivity and transformation of nutrients are largely affected. Taking one such region in the East China Sea for example, the average primary productivity of the red tide tracking stations was 399.984 $mg \cdot m^{-3} \cdot h^{-1}$, while that of the surface water of the East China Sea was 10.091 $mg \cdot m^{-3} \cdot h^{-1}$(Song et al., 2008); the sediment in the region is the sink of dissolved inorganic nitrogen and phosphate, while in other area of the East China Sea dissolved inorganic nitrogen and phosphate mostly diffuse from the sediment; in addition, the sediment in the region is the source of silicon, while in other region of the East China Sea the sediment is mostly the sink of silicate; the sediment in the region can absorb 5.9% and 67% of the dissolved inorganic nitrogen and phosphate which are delivered by the Yangtze River; while silicate released from the sediment in the region can contribute to 7.8% of the total silicate in the water column(Song, 2010, Li et al,2004).

Red tides can also affect the feeding activities of the zooplankton. Some species of phytoplankton in the red tides are harmful. Through the selective predation, zooplankton can refuse eating harmful algae or reduce the feeding amount of such algae. With respect to the harmful algae that are in taken by zooplanktons, the assimilation efficiency, the feeding rate of the zooplankton to the nontoxic algae and the total productivity will also be reduced. And thus the material transportation efficiency along the food chain will also be reduced, which will decrease the carbon absorption.

2 Prospects for Biogeochemistry in the China's Marginal Seas

With the development of society and economy, anthropogenic activities (such as discharge of pollutants, mariculture, and coastal engineering, over fishing and so on) have greatly affected biogeochemical processes in the China's marginal seas in recent decades, which have influenced the social development in reverse(Song, 2010). In order to promote sustainable development of people and China seas, it is very important to understand the key marine biogeochemical cycles and related ecosystem processes that will be impacted by anthropogenic activities, the roles of ocean biogeochemistry and ecosystems in regulating anthropogenic activities, and the responses of key marine biogeochemical cycles, ecosystems and their interactions to anthropogenic activities(Song, 2010). In order to solve the problems, study on biogeochemistry of the China's marginal seas in the future should focus on the following issues: (1) understanding how biogeochemical cycles interact with

the food web dynamics, (2) effects of increasing anthropogenic CO_2 and acidification on marine biogeochemical cycles, ecosystems and their interactions, (3) the varying capacity of the ocean to store anthropogenic CO_2, (4) effects of changing supplies of macro- and micronutrients on biogeochemistry of marginal seas, (5) quantifying material transport within and across the continental shelf, transformation of materials within the water column and sediments, storage of materials in the coastal zone and air-sea exchange, (6) defining the terrestrial boundary condition for nutrient fluxes by better integration of river basin information, including sediment dynamics and organic inputs, (7) developing budgets and flux estimates for China marginal sea waters in order to understand and predict the impacts of anthropogenic activities and variation of biogeochemical cycles, and (8) biogeochemistry in aquaculture ecosystems.

In the Bohai Sea, biogeochemical processes are mainly affected by anthropogenic activities. In recent decades, freshwater discharge by the Yellow River into the Bohai Sea have decreased greatly, lots of materials have been transported into the Bohai Sea, nutrients regimes and structure of the ecosystem have changed a lot, and fishery resources have declined significantly. The Bohai Bay was the most affected part of the Bohai Sea in recent decades. It was the key region for biogeochemical study in the Bohai Sea. Study on biogeochemistry of the Bohai Sea in the future should focus on the following aspects: (1) defining the effect on material fluxes of the Yellow River by anthropogenic activities in the Yellow River drainage basin, (2) determination fluxes of terrestrial input of materials, (3) transfers of matter across the Bohai Sea interfaces (including air-sea interface, sediment-seawater interface and the interface between the Bohai Sea and Yellow Sea), (4) transformation of organic matter in marine food webs, (5) impacts of marine harvesting on end to end food webs and biogeochemical cycles, and (6) effects of changing supplies of macro- and micronutrients on biogeochemistry of the Bohai Sea.

In the Yellow Sea, biogeochemical processes are mainly affected by anthropogenic activities along the coastal zones in China and Korea. Mariculture is a kind of important anthropogenic activities in the Yellow Sea(Song et al, 2010). There are lots of mariculture zones along the coast of the Yellow Sea. These coastal areas were the key regions of study on biogeochemistry in the Yellow Sea. There are several key biogeochemical processes of the Yellow Sea that should be focused on in the future: (1) transformation mechanisms of nutrients in the water body of the aquaculture ecosystem, (2) budgets and controlling processes of primary biogenic elements in the aquaculture ecosystem, (3) the coupling mechanism of carbon-nitrogen-phosphorus in the aquaculture ecosystem, (4) the generating mechanism and eliminating ways of toxic substances in the aquaculture ecosystem, and (5) biogeochemistry of oxygen (mainly including fluxes and concentrations of oxygen), and (6) biogeochemistry of sulfur (mainly related to the sulfide in sediments) in the Yellow Sea.

With respect to the East China Sea, biogeochemical processes are greatly affected by the river input, sea currents, and the interactions with the open ocean. Because of the complicated environment in the Yangtze River estuary which is greatly affected by the riverine input, the upwelling and coastal currents, and anthropogenic activities(Li et al, 2004), it was the key region of study on estuarine biogeochemistry and biogeochemistry of the East China Sea. Study on biogeochemistry in the East China Sea in the future should focus on the following issues: (1) human influences on the river basin coastal zone interaction, (2) effects on nitrogen cycle (especially transformations involving N_2O) by changes in low-oxygen zones affect the nitrogen cycle, (3) impacts on biogeochemistry in the East China Sea by variation in physical forcing induced by climate change, (4) the varying capacity of the East China Sea to store anthropogenic CO_2, and (5) quantifying material transport within and across the

continental shelf.

As to the South China Sea, the Pearl River estuary and the Northern South China Sea can be greatly affected by anthropogenic activities; the coral ecosystem in the Nansha Islands is of high primary productivity and of distinct biogeochemical characteristics and can be affected greatly by variation in pH and anthropogenic activities(Song, 2004). These three regions are the important zones for study on biogeochemistry in the South China Sea. The following aspects are very important for biogeochemical researches in the South China Sea in the future: (1) effects of increasing anthropogenic CO_2 and acidification on the coral ecosystem in Nansha Islands and their interactions, (2) transformation of materials within the sediments, storage of materials in the coastal zone and air-sea exchange, (3) regeneration of nutrients in the water column, and (4) biogeochemistry of oxygen and sulfur.

Biogeochemical processes are very complicated and are affected by lots of factors (Song, 2010). It needs a good synthesis of marine chemistry, marine ecology, marine geology and physical oceanography. Therefore, scientists from a wide range of disciplines are needed to work together in order to solve the above problems and to get deeper insight into the biogeochemistry in China marginal seas in the future.

References

Chen CT (2008) Distributions of nutrients in the East China Sea and the South China Sea connection. Journal of Oceanography 64:737-751

Dai JC, Song JM, Li XG, Yuan HM, Li.N, Zheng GX (2007a) Environmental changes reflected by sedimentary geochemistry in recent hundred years of Jiaozhou Bay, North China. Environ Poll 145: 656 -667

Dai JC, Song JM, Li XG, Yuan HM, Zheng GX, Li N (2007b) Geochemical Records of Phosphorus in Jiaozhou Bay sediments -Implications for Environmental Changes in recent hundred years. Acta Oceanol Sin, 26(4): 132-147

Hu J, Peng P, Jia G, Mai B, Zhang G (2006) Distribution and sources of organic carbon, nitrogen and their isotopes in sediments of the subtropical Pearl River estuary and adjacent shelf, Southern China. Mar Chem 98:274-285

Hu J, Peng Pa, Jia G, Mai B, Zhang G (2006) Distribution and sources of organic carbon, nitrogen and their isotopes in sediments of the subtropical Pearl River estuary and adjacent shelf, Southern China. Marine Chemistry 98:274-285

Huang JJ, Wang SM, Chen YL (2007) Biogeochemical controls on distributions and flux of dissolved and particulate organic carbon in the Northern South China Sea. Deep-Sea Res Part II 54:1486-1503

Li M, Xu K, Watanabe M, Chen Z (2007) Long-term variations in dissolved silicate, nitrogen, and phosphorus flux from the Yangtze River into the East China Sea and impacts on estuarine ecosystem. Estuarine, Coastal and Shelf Science 71:3-12

Li XG, Song JM, Yuan HM (2004) Inorganic carbon of sediments in the Yangtze River Estuary and Jiaozhou Bay. Biogeochemistry. 77: 177-197

Liu KK, Kao SJ, Hu HC, Chou WC, Hung GW, Tseng CM (2007) Carbon isotopic composition of suspended and sinking particulate organic matter in the northern South China Sea: From production to deposition. Deep Sea Research Part II: Topical Studies in Oceanography 54:1504-1527

Ni HG, Lu FH, Luo XL, Tian HY, Zeng EY (2008) Riverine inputs of total organic carbon and suspended particulate matter from the Pearl River Delta to the coastal ocean off South China. Mar Pollut Bull 56(6):1150-1157

Qi X, Liu S, Zhang J (2006) Sediment-water fluxes of nutrients in the Yellow Sea and the East China Sea. Marine Sciences 30:9-15 (in Chinese with English abstract)

Song JM (2004) Biogeochemistry of China seas, Shandong Science and Technology Press, 1-591

Song JM(2010) Biogeochemical Processes of Biogenic Elements in China Marginal Seas[M]. Springer-Verlag GmbH & Zhejiang University Press, 1-662.

Song JM, Xu YF, Hu WP, Ni LY (2008) Biogeochemistry of Carbon in China Seas and Lakes, Science Press, 1-553

Wang CY, Wang XL, Sun BY, Su RG (2008) Ecotoxicological effect of Cu, Pb，Zn and Cd on *Prorocentrum donghaiense* Lu. China Environmental Science 28:264-268 (in Chinese with English abstract)

Wang PB, Song JM, Guo ZY, Li PC (2008) The release behavior of inorganic nitrogen and phosphorus in sediment during disturbance. Chin J Oceanol Limnol 26(2):197-202

Wang XL, Li KQ (2006) Marine environmental capacity of primary pollutants in the Bohai Sea, Beijing, Science Press (in Chinese with English abstract)

Wang XL, Xin Y, Shi F, Han XR, Zhu CJ, Shi XY (2007) The exchange rate and flux of macro-nutrients and the regulating factors at the seawater-sediment interface in the Bohai Sea. Periodical of Ocean University of China 37:795-800 (in Chinese with English abstract)

Xia J, Gao HW (2006) Simulation on seasonal cycle vertical structure of plankton ecosystem in eastern area of South Yellow Sea. Journal of Safety and Environment 6:59-65 (in Chinese with English abstract)

Yang GP, Jing WW, Li L, Kang ZQ, Song GS (2006) Distribution of dimethylsulfide and dimethylsulfoniopropionate in the surface microlayer and subsurface water of the Yellow Sea, China during spring. Journal of Marine Systems 62:22-34

Zhang LJ, Zhang Y (2008) The distribution of partial pressure of CO_2 in the Bohai Sea in summer. J Ocean Univ Chin 38: 635-639 (In Chinese with English abstract)

Zhang NX, Song JM, He ZP, Li XG, Yuan HM, Li N (2006) Influence of external source nitrate on dissolved inorganic carbon system in seawater simulation experiments. Marine Sciences 30:47-51 (in Chinese with English abstract)

Zhang P, Song, JM, Liu ZG (2007). PCBs and its coupling with eco-environments in the southern Yellow Sea surface sediments. Mar Poll Bull 54: 1105-1115

Zhang YS, Zhang FJ, Guo XW, Zhang MP (2006) Autumn flux of particulate settling observed at three representative stations in East China Sea. Oceanologia Et Limnologia Sinica 37:28-34 (in Chinese with English abstract)

Zheng GX, Song JM, Dai JC (2006) Effects of heavy metal (copper and cadmium) coupled with *Ulca pertusa* on marine inorganic carbon system in simulated experiments. Environmental Science 27:2445-2452 (in Chinese with English abstract)

Zheng GX, Song JM, Dai JC, Wang YM (2006). Distributions of chlorophyll a and carbon fixed strength of phytoplankton in autumn of the southern Huanghai Sea water. Acta Oceanol Sin, 25(3): 68-81

Zheng GX, Song JM, Sun YM, Dai JC, Zhang P (2008) Characteristics of nitrogen forms in the surface sediments of southwestern Nansha Trough, South China Sea. Chin J Oceanol limnol 26(3):280-288

ADVANCES IN SEA LEVEL RESEARCH IN CHINA FROM 2007-2011

ZUO Juncheng, LI Juan, LU Qing, CHEN Meixiang and XU Qing

（Institude of Physical Oceanography, HoHai University, Nanjing, 210098, P.R.C.）

Abstract

Global sea level change and regional ocean response obtain great attention from government and scientists, it is a key scientific problem in physical oceanography and atmospheric science, and one of the most important scientific problems in climate change. As an important exhibition of the response of ocean variation to climate change, the long term sea level trend has an extensive and far-reaching impact on offshore and coastal environment, ecosystem, and economical society. In this paper, recent progresses on sea level change and its impact on offshore and coastal environment in physical oceanography community in China since 2007 were reviewed systematically; The variation of global and regional sea level on different time scales were studied; mechanisms of sea level variation and change were discussed, such as dynamic effects on sea level change in different seas due to sea surface heat flux, freshwater flux, circulation, wind stress, and Rossby wave. The sea level change in 21st century is also predicted using statistical methods and numerical simulation methods, etc. Meanwhile, the short term ocean dynamical processes caused by sea level change such as tidal wave are discussed, the offshore and coastal environment like coastal erosion, seawater intrusion and soil salinization, estuarine saltwater intrusion, submerged coastal lowlands, and decline of mangroves is reviewed shortly, etc.

Key words: sea level change, mechanism, prediction, impact

Ⅰ Introduction

With the continuous increasing of CO2 emission due to human activities, global warming and sea level rise become one of the most important global environmental problems.

As sea level rise, most of the sedimentary coast is confronted with serious erosion, and coastal people have to deal with the ensuing coastal management. The most vulnerable regions are the low arenaceous or slimy coasts, where a little sea level rise can submerge large quantity of land and intensify seawater erosion, such as the Bohai Bay，the Yellow River Delta, the Yangtze River Delta and the Pearl River Delta in China.

Global, regional and local factors affect sea level variation together. Global mean sea level variation is mainly caused by the thermal expansion of the ocean, the melting and vanishing of the mountain icecap and glacier in Greenland and Antarctica. In some cases, regional and local factors like vertical movement of the earth crust and drainage of the surface water may induce a greater sea level change with a rate of 10 or 100 times larger than the absolute sea level rise caused by sea water mass variation and thermal expansion.

In the last 4 years from 2007 to 2010, a series of study have been developed on climate change,

sea level rise, impact and adaption, and a lot of creative achievements are obtained.

Ⅱ The of regulation of sea level change

Sea level varies in a lot of time period, like daily, seasonal, inter-annual, decadal and long-term trend etc. With the continuous abundance in ocean hydrologic observations and the increasing attention from scientist, great progress have been made on sea level variation regulation in recent years, and lot of new phenomena and regulation have been found.

1 Seasonal sea level variation

Global sea level has notable seasonal variation, the seasonal amplitude reaches up to 5～6cmin 15 ℃N～64 ℃N latitude band in the Northern Hemisphere during 1993-2003 , and about 2～3cm in the same latitude band in the Southern Hemisphere. In the Northern Hemisphere the maximum and minimum sea level height in a year occur in September and March, respectively, and it is in the opposite case in the Southern Hemisphere(Yan Mei, Zuo Juncheng et al.,2008).

Seasonal period of sea level variation is completely dominant in the north pacific during 1993-2006, with the remarkable period of 1a and 0.5a (Xu Shanshan,Zuo Juncheng et al.,2010), the highest sea level appears in September, and the lowest in March (Chen Meixiang,2009).

The sea level variation in the East China Seas is dominated by annual period. The amplitude of annual period is largest in the Bohai Sea, the second in the Yellow Sea, and the smallest in the East Sea, meanwhile it is smaller in the south of 30 ℃N in the East Sea than that in the Yangtze River estuary region (He Qianqian,2010). There is remarkable seasonal variation in the Topex/Poseidon sea level in the East China Sea, the lowest occurs in March and the highest in September, annual amplitude is up to 7.8cm (Yan Mei et.al., 2008). The sea level variation is also dominated by seasonal in the South China Sea, it is low from March to August and high from September to November (Tang Chaolian, et.al., 2009).

2 Interannual and decadal sea level variation, and long-term trend

The sea level in the north Pacific shows obvious inter-annual variation with the main quasi period of 28 months. The second and the forth EOF mode of monthly mean sea level show inter-annual variation, the second mode is ENSO mode, and the forth mode is both modulated by ENSO and PDO (Xu Shanshan, Zuo Juncheng, et.al., 2010). The sea level variation from 1955 to 2003 in the South China Sea shows 29 years period (Ding Rongrong et al., 2007).

From 1933 to 2003 the global mean sea level has a rising rate of 2.89mm/a, there into the mean sea level rising rates are 3.8, 2.2 and 2.1mm/a in the latitude band (15 ℃S~64 ℃S) of Southern hemisphere, in the latitude band (15 ℃N~64 ℃N) of Northern Hemisphere and low latitude band (15 ℃S~15 ℃N), respectively(Zuo et al.,2009).

The sea-level shows a rising trend in a large area of North Pacific during 1993-2006. Rising region is mainly located in low latitude of the west side of the ocean basin, while the decreasing region in in high latitude and low latitude of east side of the ocean basins (Chen Meixiang et al., 2009). The sea-level shows a rising trend with a rate of +4.5mm/a in Indo-Pacific warm pool area , while the rising rate of is 6.0 mm/a and 1.6 mm/a in the west Pacific warm pool and the Indian Ocean warm pool respectively (Cheng et al., 2008). The sea-level rising rate is 3.9mm/a during 1993-2006 in the South China Sea, and 3.6mm/a in the Pearl River Estuary (Shi Xiaojun et al.,2008). Since 1970, the Sea level along the east coast of Guangzhou shows a rsing trend with fluctuation and acceleration. Rising trend is

more obvious since 1987, and sea level variation is significantly affected by El Niño (Shen Dongfang et al., 2010).

Ⅲ The mechanism of Sea level variation

Sea level variation is significantly affected by the sea surface heat flux, freshwater flux, ocean circulation, wind stress and Rossby waves.

1The contribution of steric sea-level variation

Global mean steric sea level shows a clearly rising trend during 1955-2003 (Zhang Jianli et al., 2006). The liner rising rate of steric sea level in North Pacific is 1.4mm/a during 1993-2006, which takes about 47.5% of the total sea-level rise (Xu Shanshan, Zuo Juncheng et al., 2010).

Seasonal sea surface heat flux variation dominates the seasonal sea level variation, sea surface freshwater flux has a certain influence on the seasonal sea level variation. The annual amplitude of sea level variation in the Kuroshio and Gulf Stream area and in 20°S of the East Indian Ocean is mainly caused by steric effect. In tropical eastern Pacific Ocean, steric effect is only a part of the reason in the anuual sea level variation, and dynamic process has greater impact on the annual sea level variation (Yan Mei et al.，2008).

The steric sea level rise rate in the South China Sea is 4.2mm/a. The phase of the steric sea level variation leads Topex/Poseidon sea level by about 2 months (Ding Rongrong, Zuo Juncheng et al., 2007). In the South China Sea, the Topex/Poseidon sea level during 1993-2004, the steric sea level variation during 1945-2004 and inter-annual sea level variation analyzed from tide gauge data are all highly related to ENSO, The averaged mean sea level rising rate is about 4.8mm/a (Rong Zengrui et al., 2007). The specific heat capacity in the upper layer makes a great contribution to sea level change in the South China Sea. Heat budget changes sea level by affecting specific volume(Cheng et al.,2007).The specific heat capacity makes a great contribution to the sea level rise in the Western Pacific Warm Pool, but little in the Indian Ocean warm pool（Cheng et al, 2008).

In the East China Sea，the averaged sea level rise rate and the steric sea level rising rate during 1993-2003 is 4.9mm/a and 3.2mm/a respectively, so steric sea-level rise makes the major contribution to sea-level rise with about 64.5% (Yan Mei, Zuo Juncheng et al., 2008).

2 The influence of wind stress on sea-level variation

Wind stress mainly affects the long term sea level rising trend and inter-annual variation in the south of Kuroshio extension area, and it also contributes to the inter-annual sea-level variation in the north of Kuroshio extension area; wind stress can explain well the process of sea-level variation in equatorial region. Sverdrup transportation mainly affects the seasonal sea-level variation, especially in high latitude region; the long term trend and inter-annual variation of sea-level are mainly caused by the propagation of baroclinic Rossby wave (Chen Meixiang, 2009). ENSO influence the sea level variation of the East China Sea by local wind field (He Qianqian, Zuo Juncheng et al., 2010).

3 The influence of ocean circulation on sea level variation

Ocean circulation can influence significantly sea level variation in the East China Sea, the sea level on the left side of the Kuroshio principal axis will decrease when the Kuroshio flux increases, the sea level on the left side will rise when Kuroshio flux decreases, the Kuroshio flux and sea level vary in opposite phase on inter-annual scale, (He Qianqian, Zuo Juncheng et.al.,2010). During El Nino, the intensified Hadley circulation can enhance the cold and warm water exchange between the eastern

South China Sea and equatorial western Pacific, the decrease of water temperature and loss of sea water make the sea level fall in the South China Sea; at the same time, the construction and intensity of Walker circulation induce the sea level fall in the South China Sea (Shenchun, Zuo Juncheng et.al.,2010). ENSO influences wind field in the Bohai sea and the Yellow Sea through global atmospheric circulation, then the sea level in the Bohai sea and the Huanghai Sea is changed by local wind stress (Liu Xueyuang, Liu Yuguang et.al.,2009). In winter and summer, affected by the strong coastal current, dynamic height make a significant contribution to the coastal sea level variation in the South China Sea, especially in coastal area of Vietnam, Guangdong and Thailand gulf it is even over 90%. In spring and autumn, the dynamic height also contributes a lot, about 80%, to the coastal sea level variation. In the deep sea region, the contribution of dynamic height to the total sea level variation is about 50-60%, a little larger than that of steric height (Shen Chun et.al.,2010).

4 The influence of evaporation, precipitation and runoff on the sea level variation

The precipitation increased significantly in the western North Pacific, which contributes to the sea level rise; the precipitation decreased obviously in the central Mid-latitude ocean and eastern low-latitude ocean, and this caused the sea level dropped near the eastern boundary, during 1993 to 2006. The seasonal variation of precipitation mainly affected the seasonal sea level variation, and the variation of fresh water flux caused by evaporation and precipitation contributed 4.2% to sea level rise in the North Pacific during 1993 to 2006 (Chen Meixiang, 2009). Solar radiation, rainfall, runoff and wind stress has an impact on the seasonal variability of sea level in the Bohai Sea and the Yellow Sea (Liu Xueyuan, Liu Yuguang et al., 2009).

Ⅳ The prediction of long term sea level variation

Two methods are usually used to predict the long term sea level variation. One method is to analyze the major periods and rising rate of sea level variation through historical observations, and then extrapolate the future sea level change. The other method is to use a coupled climate model, which contains four separate models including atmosphere, ocean, land surface and sea-ice, to simulate the future sea level change under one assumption of scenario of global CO_2 emission.

The satellite altimeter data from 1993 to 2003 was analyzed with stochastic dynamic method, it shows that the mean rise rate of global sea level is 2.9mm/yr, twice of the rise rate of the whole 20^{th} century (Zuo et al., 2008). A method combining singular spectrum analysis and function of mean value generation was used to analyze monthly mean sea level data since 1950s at 6 tide gauge stations along the eastern China coast, it indicates that the maximum rising value in 2050 will not be no more than 16cm with the mean value of 9cm, while it is decreasing at Yantai station and Qinhuangdao station (Yuan linwang et al. 2008). Taking the global simulation results by CCSM3 (Community Climate System Model) under the IPCC SERE A2 scenario into account as the boundary forcing of the East China Sea to drive the regional ocean model of POP (Parallel Ocean Program), the sea level in the East China Sea at the end of 21st century will rise about 12-20cm. Sea-level rise in the Bohai Sea is relatively larger, up to 17cm; the rising value along the east coast (16cm) in the East China Sea is larger than that along the west coast (13cm). Sea level will rise by about 20cm near Ryukyu Islands (Chen Changlin et al., 2010).

Extrapolation of sea level rise in the future is easily influenced by the length and quality of data set, and the statistical method of data processing is also an uncertain factor. Furthermore, the sea level

variation are calculated on the assumption that the factors affecting the future result remain unchanged, so the changes of climate system can't be reflected well in the statistical method. On the other hand, climate changes can well simulated with numerical simulation, so numerical simulation are currently used to predictclimate change, and it is also a useful method to predict sea level change. However, poor knowledge of climate change, the uncertain of physical processes and chemical processed induced by clouds, sea, polar ice sheet and atmospheric concentrations of carbon dioxide, have prevent oceanographers from accurately predict the changes of climate. So the resolution improving may be a good means to study long time sea level variation. Besides, the variation of ocean circulation under the circumstances of climate change may also have a notable impact on the sea level variation (Yan Mei et al.,2008).

Ⅴ.The influence of sea-level variation on the offshore and coastal environment

1 The influence of sea level change on tidal wave

The increase of propagation speed of incident and reflected tidal waves, which caused by sea level rise will lead the changes of characteristics of amphidromic system (the position of amphidromic point, co-phase line and iso-amplitude line of tidal waves). It is found that, in the Bohai Sea, Yellow Sea and East China Sea, the co-phase lines of tidal waves will deflect anticlockwise after sea level rise relative to the current tidal system, the amphidromic point of tidal waves shift to some extent, and that there exist certain distribution pattern in the difference between the tidal amplitude after sea level rise and the current value. Also it can be seen from the numerical simulation that in the case of 1m rise of sea level, the highest increase of astronomical tidal level in Qingdao and Lian Yungang can reach 10~16cm, and the ocean chart datum can decrease by 10~12cm in some area (Yu Yifa et al., 2007).

The amphidromic point in this region will move to the southeast by about 14km and 25 km, respectively, when sea level rises by 3m and 5m in southern Yellow Sea. Along with that, co-phase lines and iso-amplitude lines will shift obviously, co-phase line will deflect counterclockwise. As the effect of this, tidal range will show different variation in different coastal region. Significant variation will occur in coast area near the non-tidal point (on the left and the top of Bay), while slight variation will occur in coast area far away from the non-tidal point (on the right and the top of Bay) (Wang Wei, Song Zhiyao et al., 2008).

2 The influence of sea level change on estuarine water level

The influence of sea-level rise on water level is very complicated in the pearl river delta estuary, the correlation coefficient of annual water level and sea-level at Deng Longshan station is 0.529 with the significant probability level of 0.01,which shows highly correlated. The sea-level rise contributes 20.1% to annual averagedwater level .(Kong Lan, Chen Xiaohong et al.,2010).

3 The effect of sea level rise upon saltwater intrusion in estuary

Sea level rise enhances the saltwater intrusion in estuary in dry season. In the developed Pearl River Delta region, the population affected by saltwater intrusion will increase by about 200,000 when salinity boundary goes upward 1km along river bank. With the fixed runoff, the intruded saline water line will move in upstream direction when sea level rises. In Hengmen waterway, the 250mg/L salinity isoline will upshift 1.1km, 2.0km, and 3.1km when sea level rises by 10cm, 30cm, and 60cm respectively, under the condition that the upstream runoff accounts for 97%, While the upshifting value will be 0.7km,0.8km, 1.7km when the upstream runoff accounts for 50% (Kong Lan, Chen Xiaohong et

al., 2010).

4 The influence of sea-level variation on coastal lowland

On one hand, sea-level rise causes shoreline to retreat by directly flooding the land, on the other hand, sea-level rise enhances ocean dynamical process and destroyes the steady balance of the coast, which finally leads to coastal erosion. The erosion rates in the Houjiang Bay and Shuidong Bay are 0.19-0.24m/a and 0.11~0.15m/a, respectively, when the sea-level rise rate is 2.0~2.5mm/a along Guangdong coast. The slight rise of sea level can inundate large area of low coastal plains, the coastline will be retreated by about 19~24m in the Houjiang Bay and about 12~15m in the Shuidong Bay after 100years (Li Zhilong et al., 2009).

On the basis of the SRTM altitude data in resolution of of 1/1200°×1/1200°, considering the estimated sea level rise in the 21st century simulated by CCSM (Climate System on that Model) and POP (Parallel Ocean Program) model in assumption of the IPCC SRES A2, the sea level variation caused by the crust subsidence, and the sea level variation caused by glacier melt, the coastal low land area submerged can be calculated when the extreme water level of 100-year return period occurs. Taking the 2000 year as the base year, the flooding area is calculated in the year of 2050 and 2080 in the whole China coastal zone, especially in the three major fragile regions, including Haihe river delta, Bohai bay and Laizhou bay delta, Yangtze river delta including Jiangsu coast and the northern coast of Zhejiang, and the Pearl river delta. The flooding area is 98.2988×10^3 km^2 by 2050 in the entire China coastal zone, and 5.0203×10^3 km^2, 64.141×10^3 km^2 and 15.337×10^3 km^2 in the three fragile delta regions. The flooding area in the entire China coastal zone is 104.9437×10^3 km^2, andare 5.1755×10^3 km^2, 67.802×10^3 km^2 and 17.209×10^3 km^2 in the three fragile delta regions by 2080 (Zuo Juncheng et al., 2010).

5 The influence of sea level change on mangroves coast

The response of mangrove ecosystem to sea level rise is far from simple landward migration. While the sediment rate of mangrove flat is equal to or greater than the rising rate of sea level, mangroves will grow stably or even toward the ocean; while the rising rate of sea level is greater than sediment rate of mangrove flat, mangrove may be damaged and migrate landward. If there exists a natural barrier (such as steep cliff) or an artificial barrier (such as seawall) in the rear, the transfer will be suffocated, resulting in the loss of the precious mangrove wetland resources (Zhang Qiaomin, 2007).

In general, deposition rate of most mangrove flat in China sea is close to or greater than the rising rate of sea level before 2030. Deposition of mangrove flat may "keep up" or even "surpass" sea level rise, the area of mangrove will basically remainstable. The rate of sea level rise will increase a lot after 2030, at that time a part of mangrove flat deposition will be less than sea level rise, especially in the coastal zone of less sediment and low deposition rate of mangrove flat (Zhang QiaoMin, 2007).

Ⅵ. Conclusion

As an important part of global change, sea level variation is a significant contributor in the global ocean circulation evolvement affected by climate change. In this paper, the latest development of the research in sea level variation in the last 2007-2010 in China is reviewed systematically. The variation of global and regional sea level on different time scales were studied; mechanisms of sea level variation and change were discussed, such as dynamic effects on sea level change in different seas due to sea surface heat flux, freshwater flux, circulation, wind stress, and Rossby wave. The sea level change in

21st century is also predicted using statistical methods and numerical simulation methods, etc. Meanwhile, the short term ocean dynamical processes caused by sea level change such as tidal wave are discussed, the offshore and coastal environment like coastal erosion, seawater intrusion and soil salinization, estuarine saltwater intrusion, submerged coastal lowlands, and decline of mangroves and coral reefs are all reviewed shortly, etc.

Reference:

Cao Yuenan, Zuo Juncheng, Du Ling, Li Lei, Li Peiliang. The Seasonal Variation of Sea Surface Height in the South China Sea: Characteristics and Mechanisms. Periodical of Ocean University of China. 2007, 37(Sup.Ⅱ): 031-038

Chen Changlin, Zuo Juncheng. Sea Level Changs of the China Sea in the 21st Century under SRES A2 Scenario. Acta Oceanologica Sinica. 2010 (accepted)

Chen Meixiang. Dynamics of Sea Level Variation in the North Pacific Ocean, Kuroshio Region of East Sea of China and Kuroshio Extension[D]. Qingdao: Ocean University of China, 2009

Cheng Xuhua, Qi Yiquan. Trends of Sea Level Variations in the South China Sea from Merged Altimetry Data [J]. Global and Planetary Change, 2007, 57(3/4): 371-382

Ding Rongrong. Sea Level Change in the South China Sea and Its Relations to the the Steric Height Variation and Wind [D]. Qingdao: Ocean University of China, 2007

Ding Rongrong, Zuo Juncheng, Du Ling, Li Lei, Li Peiliang. Sea Level Change in the South China Sea and Its Relations to the Steric Height Variation and Wind. Periodical of Ocean University of China. 2007, 37(Sup. Ⅱ): 023-030

Ding Rongrong, Zuo Juncheng, Du Lin, Li Lei, Li Peiling. Sea Level Change in the South China Sea and Its Relations to the Steric Height Variation and Wind. Periodical of Ocean University of China. 2007, 37 (sup. II): 023-030

He Qianqian, Zuo Juncheng, Chen Changlin, Chen Meixiang. Mechanism of Sea level variability in East China Sea and its response to ENSO. Journal of Hohai University(Natural Sciences), 2010(Accepted)

Kong Lan, Chen Xiaohong, Du Jian, Chen Dongwei. Impact of Sea-Level Rise on Salt Water Intrusion Based on Mathematical Model. Journal of Natural Resources. 2010, 25(7): 1097-1013

Kong Lan, Chen Xiaohong, Zhang Qiang, Peng Tao. Impacts of Rising Sea Level on Water Level Changes along the Pearl River Estuary, China. Ecology and Environmental Sciences. 2010, 19(2): 390-393

Li Jialin, Wang Lanhong, Zhang Renshun, Ge Yunjian, Qi Deli, Zhang Dianfa. Disaster Effects of Sea Level Rise——A Case of Jiangsu Coastal Lowland. Scientia Geographica Sinica. 2006, 26(1): 87-93

Li Zhilong, Li Zhiqiang, Chen Zishen. Sea Level Variation Analysis and Coastal Response in South China. Marine Science Bulletin. 2009, 28(6): 7-13

Lin Erda, Xu Yinlong, Jiang Jinhe et al.. National Assessment Report of Climate Change (Ⅱ): Climate change impacts and adaptation. Advances in Climate Change Research. 2006, 2(2): 51-56

Liu Xueyuan, Liu Yuguang, Guo Lin, Gu Yanzhen, Liu Yahao, Ma Yujuan. Mean Sea Level Change in East China Sea and its Response to ENSO. Marine Science Bulletin. 2009, 28(5): 35-48

Qiao Xin, Chen Ge. A Preliminary Analysis on the China Sea Level using 11 Years' TOPEX/Poseidon Altimeter Data. Marine Sciences. 2008, 32(1): 60-64

Rong Zengrui, Liu Yuguang, Zong Haibo et al. Interannual Sea Level Variability in the South China Sea and its Response to ENSO[J]. Global and Planetary Change, 2007, 55: 257-272

Rong Zengrui, Liu Yuguang, Chen Manchun, Zong Haibo, Xiu Peng, Wen Fan. Mean Sea Level Change in the Global Ocean and the South China Sea and Its Response to ENSO. Marine Science Bulletin. 2008, 27(1): 1-8

Shen Chun, Zuo Juncheng. Relationship between Sea-Surface Height Anomaly and ENSO and Atmospheric Circulation in the South China Sea. Journal of Hohai University(Natural Sciences), 2010(Accepted)

Shen Dongfang, Gong Zheng, Cheng Zemei, Yang Hui. Sea Level Change in Coastal Eastern Guangdong (Shanwei) in 1970-2009. Tropical Geography. 2010, 30(5): 461-465

Shen Qiang, E Dongchen, Qiao Xuejun. Decadal Variability and Regional Characteristics of Global Sea Level During the 20the Century. Geomatics and Information Science of Wuhan University. 2009, 34(4): 454-458

Shi Xiaojun, Chen Tegu, Yu Kefu. Sea-Level Changes in Zhujiang Estuary over Last 40 Years. Marine Geology & Quaternary Geology. 2008, 28(01): 127-134

Tang Chaolian, You Dawei, Chen Tegu, Chen Haiming, Yu Kefu. Sea-Level Changes along the Coast of Guangdong Province during 1986-2008. Tropical Geography. 2009, 29(5): 421-427

Wang Wei. Song Zhiyao, Lu Weiguo, Hu Ming. A Thoretical Analysis of the Responses of Coast Tidal Range to Sea Level Rise. The Ocean Engineering. 2008, 26(3): 94-97

Xu Shanshan, Zuo Juncheng, Chen Meixiang. North Pacific Sea Level Change and Its Impact Factors during 1993—2006. Periodical of Ocean University of China. 2010, 40(9): 024-032

Yan Mei. The Study of Thermodynamic Mechanism of Global Sea Level Variation[D]. Qingdao: Ocean University of China, 2008

Yan Mei, Zuo Juncheng, Du Ling et al.. Sea Level Variation/Chang and Steric Contribution in the East China Sea[A]. Proceeding of the Seventeenth (2007). International Offshore and Polar Engineering Conference[C], 2007

Yan Mei, Zuo Juncheng, Fu Shenbo, Chen Meixiang, Cao Yuenan. Advances on sea level variation research in global and China sea. Marine Environmental Science. 2008, 27(2): 197-200

Yan Yunfeng, Zuo Juncheng, Chen Meixiang. Influence of the Long-Term Sea Level Variation on Tidal Waves in the Eastern China Sea. Periodical of Ocean University of China. 2010, 40(11): 019-028

Yu Yifa, Liu Lan, Guo Mingke. Numerical Research on Tidal Waves Changes Due to Mean-Sea-Level Rise in the Bohai Sea, the Huanghai Sea and the East China Sea Ⅱ: Numerical Modeling of Tidal Waves after Mean-Sea-Level Rise in the Areas. Periodical of Ocean University of China. 2007, 37(1): 7-14

Yuan Linwang, Xie Zhiren, Yu Zhaoyuan. Long-term Prediction and Comparison of Sea-Level Change Based on the SSA and MGF Model. Geographical Research. 2008, 27(2): 305-313

Zhang Qiaoming. Responses of Tropical Biological Coasts to Global Change. Quaternary Sciences. 2007, 27(5): 834-844

Zuo Juncheng, Zhang Jianli, Du Ling et al.. Sea Level Variation/Change and Thermal Contribution in the Bering Sea[J]. Acta Oceanologica Sinica, 2005, 24(6): 36-45

Zuo Juncheng, Zhang Jianli, Du Li, Li Peiliang, Li Lei. Global Sea Level Change and Thermal Contribution. Journal of Ocean University of China, 2008, 8(1): 1-8

Zuo Juncheng, Yang Yiqiu, Chen Meixiang, Xu Qing, Zhang Jianli. Impacts of Sea-Level Rise on China's Coastal Zone under the Background of Climate Changes. Coastal Engineering. 2010(Accepted)

A REVIEW OF MARINE SEDIMENT DYNAMIC STUDIES IN CHINA: 2006-2010

Shu GAO[1] and Ai Jun WANG[2]

(1. Ministry of Education Key Laboratory for Coast and Island Development, Nanjing University, Nanjing 210093, P.R.China
2. Open Laboratory of Coast and Ocean Environmental Geology, Third Institute of Oceanography, State Oceanic Administration, Xiamen 361005, China)

Abstract: Research in marine sediment dynamics and related disciplines is carried out by the coastal engineers, physical oceanographers and marine geologists in mainland China. Progress in this research field has been made over the last four years (from July 2006 to June 2010), in terms of sediment transport and deposition processes, new methods and techniques, coastal morphodynamics, and marine sediment records for global change studies. Further development of marine sediment dynamic in the near future is anticipated in the basic research about the formation of sediment systems, such as the processes of benthic boundary layer, sediment resuspension and transport. It is also anticipated that the science of marine sediment dynamics will be involved more deeply in the earth system and global change sciences, especially in the study of the sediment sequence formation, continuity of sedimentary record, the requirement of information completeness for the past climate and environment changes, coastal morphodynamic simulation and marine ecosystem dynamics.

Keywords: Sediment dynamic processes; methods and techniques; coastal morphodynamics; sedimentary records and global change; China seas

YAPSO-China is submitting a national report on the recent research progress made by Chinese scientists, for the 25th IUGG (International Union of Geodesy and Geophysics) congress. As a part of the report, we intend to summarize in this contribution the research activities in marine sediment dynamics and related research fields, on the basis of a review of the papers published in refereed scientific journals between July 2006 and June 2010. These studies are concerned with the processes of sediment transport and accumulation, Methods and techniques for the research and their applications, coastal morphodynamics and marine sedimentary records associated with global change studies.

Ⅰ Process studies on sediment transport and accumulation

1 Shelf and deep water transport and accumulation processes

The continental shelf and deep sea environments have different transport and accumulation processes due to different hydrodynamic settings. On the continental shelf, tidal currents, waves and shelf circulations are the major factors and, therefore, sediment transport / accumulation patterns and related morphodynamics evolution are highly variable both in space and time. An end-member model reveals that, over the coastal waters of Lianyungang, from the shoreline towards the offshore areas

there are tidally-induced deposits, tide-wave mixed deposits and wave-dominated deposits, indicating the variations in hydrodynamics in the on-offshore direction (Zhang and Feng, 2009). In the shelf areas with strong tidal currents, the seabed sediment is highly mobile and large-scaled dunes are formed, as is observed in the Taiwan Strait (Du et al., 2008). Here, the bedform orientation is indicative of net sediment transport direction (Liu et al., 2007), and dune movement is further enhanced during storm events (Du et al., 2008). For the inner continental shelf, the sedimentary material and suspended solids are mainly derived from the rivers. Thus, the distribution of the seabed sediment is strongly influenced by the rivers, e.g., the sedimentary materials off the Yellow River and Mingjiang River mouths show clear source characteristics of the related catchments (Liu et al., 2009; Qiao et al., 2010). The sediment from the Changjiang River is sorted according to grain size after discharging into the shelf waters; the fine-grained material is subjected to long-distance transport towards the southeast, whilst the coarser material settles to the bed in a relatively short distance (Zhang et al., 2006). Further, on the shelf the movement of sediment is also influenced by shear fronts and plume fronts (Wang et al., 2007; Zheng et al., 2009), which generates significant spatial and temporal variations in suspended sediment concentration distributions. Further offshore, the transport of land-input materials are controlled by shelf circulation patterns such as the northern Yellow Sea, where sediment transport is related mainly to the Shandong Peninsula Longshore Current and the Yellow Sea Warm Current (Wang W et al., 2009; Bao et al., 2010). Off the Changjiang River mouth, the transport of suspended sediment is associated with the East China Sea shelf circulation patterns (Gao et al., 2007b). Similarly, outside the Hangzhou Bay, the suspended sediment concentration and transport rate are both reduced rapidly, with the shelf currents and gravity-induced currents being dominant over the tidal currents (Hu et al., 2009).

Seasonal upwelling and downwelling systems are formed on the shelf in response to monsoon climate, which influences the transport processes. To the east of the Pearl River mouth, downwelling patterns are generated by a combination of regional wind field, different Ekman effects in the surface and bottom waters, the cooling of surface water and the regional bathymetry, which modifies the dissolved oxygen distributions (Liu et al., 2010). In contrast, to the north and south of the Taiwan Strait upwelling is observed in summer (Hong et al., 2009). These varied patterns have an impact on the distribution and cycling of particulate organic carbon (Ye et al., 2008, 2009).

The transport from the shelf towards the deep sea is driven by turbidity currents (Wang et al., 2008) and extreme weather events and regional climate change, with different effects on different time scales (Meng et al., 2007; Li et al., 2009; Bian et al., 2010). On a short time scale, the East China Sea shelf water mass normally does not pass through the Kuroshio Current, but during extreme events (e.g., typhoons, winter cold outbreaks, intense internal waves, and turbidity currents) fine-grained materials may be transported to the Okinawa Trough (Bian et al., 2010). On hundred to thousand year time scales, regional rain fall patterns becomes an important factor for terrigenous sediment to be transported

towards the trough, in addition to extreme events such as earthquakes and storms (Li et al., 2009). On a thousand to ten thousand year scale (i.e., glacial-interglacial time scale), the shelf width change in response to sea level changes becomes the major factor for the material input, together with the changes in the intensity of the winter monsoon of the region (Meng et al., 2007).

2 Sediment transport and accumulation on tidal flats

Remarked spatial and temporal variations in current velocities, suspended sediment concentrations, bottom sediment distribution patterns and morphological features occur on tidal flats. The presence of salt marsh vegetation results in further complex patterns. Over the lower part of the intertidal zone, where waves are relatively large, significant resuspension occurs due to combined waves and tidal currents; towards the land, tidal currents is gradually reduced, generating different micro-scale bed morphological features (Liu et al., 2008). Resuspension and settling processes also result in a fining-upward trend in the water column; over the lower part of the intertidal zone the grain size of the bed materials are significantly different from the suspended sediment (Li et al., 2006，2008). Furthermore, the presence of the suspended sediment will reduce the near bed shear stress by 40-60% (Li et al., 2007).

The salt marsh vegetation reduces the wave energy rapidly; the rate of wave energy loss over a slat marsh may be 14 to 29 times as compared to that observed on a bare mudflat (Shi et al., 2010). In addition, tidal currents are also influenced by the salt marsh, which will affect the suspended sediment transport processes (Wang A J et al., 2010). Measurements indicate that net transport over salt marsh is directed towards the land, whilst net transport patterns on the bare mudflat in front of the salt marsh vary significantly, with complicated accretion and scour variations (Wang C et al., 2009). Salt marsh plants reduce the near bed flow, thus enhancing the settling flux and reducing resuspension flux; the trapping effect of the marsh produces cyclic sedimentation in response to seasonal and storms cycles (Yang et al., 2008) and influences the composition and geochemical properties of the bulk marsh sediment (Chen et al., 2007).

3 Transport and deposition processes in estuaries

Generally, the rivers in China are characterized by heavy sediment load. However, because of the large seasonal variations in river discharges and hydrodynamic conditions (Yang et al., 2006, 2008) the seabed sediment and suspended sediment distribution patterns can change significantly (Liu et al., 2007; Wang Y H et al., 2009; Pang et al., 2010). Thus, cyclic patterns in terms of grain size in sedimentary sequence are observed in cores (Zhang et al., 2008) It is found that the sedimentary materials in the middle part of the estuary are subjected to intense exchange between the bed and the water column (Liu et al., 2010) in response to active turbulence and energy dispersion in this section of the estuary (Liu et al., 2009). Intense resuspension occurs in many Chinese estuaries, resulting in high suspended sediment concentrations (Yang Y et al., 2006), and maximum turbidity values tend to lag behind maximum

vertical sediment fluxes (Yang Y et al., 2008). As a result, exchange of pollutant and nutrient materials between the water column and the bed is also intense (Gao et al., 2008; Ni et al., 2009). Estuarine mixing is enhanced by strong rectilinear tidal currents, although in some cases the net transport is not enhanced (Wu et al., 2006). In estuaries associated with high suspended sediment concentrations, hyperpycnal flow is generated (Huang et al., 2008).

Under natural conditions, fine-grained particles in the water column tend to exist in the form of flocs. In places where salinity and temperature are relatively stable, the current speed and the suspended sediment concentration represent the major factors for the formation of flocs, but these two factors affect different grain size fractions (Wang A J et al., 2009b). A critical current speed exists: when the current is weaker the critical value, the floc size increases with increasing current speed, but when the current exceeds the critical value the floc size will decrease (Cheng et al., 2007). If salinity fluctuations are large, then the formation of flocs becomes even more complicated, due to the combined effects of salinity and humus (Liu et al., 2008). In addition to current speed, the suspended sediment concentration itself also influences the floc size and, in turn, the settling flux (Wang A J et al., 2009b).

In China, human activities in the catchment tend to cause reduction in sediment discharges. This has led to decrease in deposition rate over the intertidal flat and subaqueous delta (Wei et al., 2007) and, in some places, seabed erosion (Yang S L et al., 2006). Further, the development of submarine dunes is also influenced (Li et al., 2008). It is anticipated that such influences will be associated with a larger spatial and temporal scale (Zhu et al., 2009).

4 Coastal zone processes in response to typhoon events

Whether or not extreme events will be intensified in response to global climate change is still a scientific problem (Liao and Fan, 2008). Nevertheless, the frequency of occurrence, the intensity and the ecological and environmental consequences of typhoons have been an important research topic in China. Typhoon events may enhance the chlorophyll-a concentration (Fu et al., 2009. Advective transport induced by strong winds and vertical mixing due large waves will affect the transport of suspended particles (Huang and Deng, 2007), which may enhance the sediment flux towards the deep sea (Bian et al., 2010). Further, in coastal waters typhoon-related waves enhance the near-bed shear stress and roughness length (Pan et al., 2009); as a result, the seabed material becomes more mobile, causing release of pollutants from the sedimentary layers and secondary water pollution (Li et al., 2010). Typhoon events are associated with rapid beach morphological changes (Qi et al., 2009a, 2009b) and extremely high suspended sediment concentrations on tidal flats (Wang A J et al., 2009a, 2009c). During a typhoon event, not only the bare flat but also the salt marsh tends to be eroding (Wang A J et al., 2009c). In sub-tidal areas, horizontal transport becomes intensified (Dai et al., 2009). Compared with the normal weather conditions, the sediment grain size of tidal deposits during storms become

coarse, more poorly sorted and more rounded (Wang J et al., 2006); it may be possible to determine the intensity and frequency of typhoons in history on the basis of tidal flat sedimentation features (Bai et al., 2006).

5 Sediment grain size trend analysis

The purpose of grain size trend analysis is to identify the direction of net sediment transport. For this type of analysis, there should be significant anisotropy of trend vectors, the relationship between the sampling depth and the time scale should established, the sampling interval should determined on the basis of geostatistical principle, the edge effect should be eliminated, the sampling sites should be within the same transport system, and the environment should be accretional (Gao, 2009). Some of these conditions have been also considered by the different authors (e.g., Wang G Q et al., 2007; Ma et al., 2008; Xu et al., 2010). Ma et al. (2008) applied the geostatistical method to analyse the grain size trend patterns in the Beibu (Tonkin) Gulf region and found that the net transport patterns identified are consistent with the other transport indications such as shelf circulation patterns.

Because the formation of grain size trends is associated with complicated sediment dynamic processes, it is important to consider the various factors that influence the spatial distributions of sedimentary materials (Gao, 2009). Yu and Gao (2008) used a one-dimensional model to simulate the formation of grain size trends due to bedload transport by rectilinear tidal currents. Such an approach may be further extended to include other modes of sediment transport (e.g., transport due to combined action of waves and currents, suspended sediment transport, and sediment materials being from different sources).

Ⅱ Development and application of new methods and techniques

1 Mathematical modelling

In China mathematical modeling has been applied widely to the analysis of coastal and shelf sediment dynamic processes. For example, Lu and Zhang (2006) calculated the seabed friction coefficient using a 2D model, Zhang et al. (2007) simulated the coupled processes of storms surges and astronomical tides on springs in the Taiwan Strait, Cai et al. (2007) modeled the western boundary effects of the South China Sea, and Han et al. (2008) studied the impact of typhoon on the suspended sediment concentration in the coastal waters of Rizhao, Shandong Peninsula.

Wang and Jiang (2007) established a 3D particle tracing model to simulate the seasonal changes in suspended sediment concentration over the Bohai, Yellow and East China Seas. Wang and Li (2009) used a sediment transport model for combined action of waves and currents to study the seasonal patterns of the movement of Yellow River derived sediment and the related processes. Qiao et al. (2008) used a 3D model to analyze the formation of the tidally-induced shear front off the Yellow River mouth and the suspended sediment transport patterns, and carried out a comparison with in situ measurements.

For estuarine and coastal process modeling, Xie et al. (2006, 2008) studied the formation of tidal channels floored with sandy materials and their morphological equilibrium conditions. Xie et al. (2009) also simulated the tidal channel morphology in Hangzhou Bay using the Delft3D model, taking cohesive fine-grained sediment transport into consideration. For the formation sedimentary records, Gao (2007a, 2009) modeled the preservation potential of tidal flat sequences. In the filed of mordynamic modeling, Ren et al. (2007) carried out long-term morphological evolution simulation for the Pear River delta, and Gao (2007b) studied the growth limit of the Changjiang River delta.

2 Remote sensing analysis

A number of researchers have attempted to obtain information on suspended sediment concentration in the water column using remote sensing techniques. Li et al. (2009) established the relationship between in situ suspended sediment concentration and a "suspension index" on the basis of TM reflectance for the Changjiang estuarine waters. Cui et al. (2009) used the suspended sediment and spectrum data to formulate an inverse model to determine the surface suspended sediment concentrations in the Bohai and Laizhou Bays. Fan and Huang (2010) also tried to establish a relationship between the remote sensing reflectance and the concentration. Similarly, Zhang et al (2008) proposed a quantitative model for the concentration on the basis of spectrum analysis and the determination of relevant parameters.

Time series of remote sensing images are useful in shoreline dynamics studies. Zhao et al. (2008) analyzed a series of satellite images to delineate the shoreline change patterns of the Changjiang River delta. In addition, satellite imagery has been also used to monitor vegetation changes in estuarine coastal environments (Shen et al., 2006), to measure the water content of tidal flat sediment (Zhang et al., 2008), and to detect water depth in shallow marine areas (Zhang et al., 2009).

3 In situ measurements of sediment dynamics

ADCP is generally a mature device to measure current velocities, but in certain types of environments the error is relatively large. To solve this problem, Xia and Liao (2010) proposed a procedure for data quality control and error reduction. Several authors continued to explore the method of obtaining suspended sediment concentration using the ADCP echo signal (Yang S L et al., 2006; Bai et al., 2009). Iy is found that when the grain size of the suspended material is stable the ADCP-based calculations may provide satisfactory data; however, if the grain size varies too much, then the correlation between the echo signal and the concentration becomes poor (Yuan et al., 2008).

Tripod systems are now widely used in seabed in situ observations. Yuan et al. (2008, 2009) analyzed the data sets obtained from tripod measurements, particularly those associated with sediment resuspension and settling processes, in an attempt to establish a relationship between the flow turbulence and the resuspension intensity. Further, the use of LISST-ST revealed that, under the condition of low current speeds, both current speed and suspended sediment concentration are

important factors for the development of flocs and floc settling velocity; when the concentration changes, the correlation between the floc size and settling velocity will be modified (Wang et al., 2009a).

4 Application of isotopic dating techniques

The ^{210}Pb and ^{137}Cs techniques are widely applied to estuaries and coastal embayments. In these coastal environments, intense human activities, complex hydrodynamic conditions and frequent accretion/erosion events generate a number of types of ^{210}Pb vertical distribution patterns and, therefore, the definition of deposition rate by ^{210}Pb measurements needs more detailed investigations (Long et al., 2007; Zhang et al., 2009; Liu Y L et al., 2010). Liu Z Y et al. (2010) proposed a depth-related deposition rate model, based upon Fourier series analysis; the deposition rate data obtained are highly correlated with the flooding, storm surges and human activity events of the region. Similarly, ^{137}Cs when applied to areas with unstable sedimentary environments has its limitations (Pan et al., 2008). ^{137}Cs dating requires that after accumulation dispersion of sediment will not occur; this is not the case when, for instance, the growth of salt marsh plants disturb the sedimentary layers (Wang et al., 2006).

5 Identifying sediment sources using tracers

Tracing methods may be quantitative or qualitative. Gao et al., (2009) used the heavy minerals as a tracer to establish sediment transport pathways qualitatively for the Yalu River estuarine areas; they found that a transport parting zone exists at the water depth of around 10 m. The use of rare earth elements as tracers is examined by Zhou et al. (2010); these authors pointed out that the relative content of rare earth elements may changed during transport and therefore caution should be taken in quantitative tracing analysis. Liu et al. used clay minerals as a tracer in sediment provenance analysis for the South China Sea region; further, they attempted to evaluate the contribution made by the Pearl River to the deposits in the various places of the region (Liu et al., 2008).

Ⅲ Coastal morphodynamics

1 Tidal inlet systems

Tidal currents are important in the formation and development of tidal inlets. Time-velocity asymmetry is not only controlled by regional tides, but it is also influenced by extremely events like storm surges (Gong et al., 2008). In addition, tidal inlet systems with different sizes may have different time-velocity asymmetric patterns (Gao, 2008). On tidal cycle time scales, the cross-sectional area may vary according spring-neap tidal cycles (Gong and Wang, 2006). Human activities also influence the stability of tidal inlets (Zhang et al., 2009). Because the entrance morphology of a tidal inlet is related to the entire system consisting of the tidal basin, the entrance channel and the flood and ebb deltas, quantitative simulation of the entrance evolution will require an understanding of the feedback processes between the hydrodynamic conditions, sediment transport and accumulation and entrance

morphology, together with an understanding the growth pattern of the tidal deltas in response to basin infilling processes (Gao, 2008).

2 Beach morphodynamics

Beach morphology is sensitive to the large scale offshore bathymetry (Zhao et al., 2006). In China, sand mining along the coastlines has a significant effect on the adjacent beach; for example, sanding near the Huiquan Bay, Qingdao, has caused the reduction of the height of the sand bars on the shore face (Zhuang et al.; 2009). In response to the human activities, the beaches are evolving towards a new equilibrium state (Li et al., 2007).

3 Morphodynamics of catchment-coast systems

Recent studies are concentrated upon the coastal morphological changes, suspended sediment composition changes and biogeochemical processes in response to catchment changes. Human activities in the catchment have caused changes in sediment sources, which in turn have caused coastal geomorphological adjustments (Zhu et al., 2009). Peng and Chen (2009) analyzed the hydrological data of the Yellow River for the last 60 years and identified the timing of the acrrection-erosion transfer on the adjacent coastlines. It is found that the coast near small mountainous rivers is more sensitive to catchment changes; Li et al. (2009) identified the accretion-erosion pattern changes at the Jiaojiang River mouth in association with the building of reservoirs in the catchment, and the engineering scheme for navigation channel improvements. The researchers also show continued concerns about the sedimentation and nutrient cycling patterns of the Changjiang estuary in response to the Three Gorges Dam construction (e.g., Li et al., 2007; Zhang et al., 2007; Gao and Wang, 2008).

Ⅳ Marine sedimentary records and global change studies

The study of "past global changes" to a large extent depends on the marine sedimentary records. In this research field, Sun et al. (2008) analyzed the mud deposit in the northern East China Sea in terms of "sensitive grain size constituents" and suggested that the transport of fine-grained sediment is influenced by climate change and can be reflected by the sedimentary characteristics. Xu et al. (2009) carried out a correlation analysis, to compare the eastern Asian monsoon climate changes as identified by the sensitive grain size parameters with those obtained from the Greenland ice-core analyses; such correlations are also supported by the clay mineral and abundant element analyses (Liu S F et al., 2010). However, Xu et al. (2010) pointed out that the information derived may vary if different methods for grain size parameter calculations were adopted.

Seismic stratigraphy has been used to study the record of environmental changes. Thus, Yang and Liu (2007) and Liu et al. (2007) analyzed high resolution shallow seismic records for the shallow marine areas near the Yellow River mouth; they identified the mechanisms for the formation of the various sedimentary structures and discussed about the resuspension processes and its influence on sediment transport in this region.

In terms of core analyses, Liu et al. (2008) studied the paleo-circulation patterns in the middle Holocene of the Bohai Bay area, on the basis of isotope, grain size, heavy minerals and geochemical compositions of core samples. Zhao et al. (2008) carried out major element analyses for the cores from the northern South China Sea and divided five sedimentary layers representing short-term climate change events. Based upon the analyses of sediment color, foramineferal abundance and ice-rafted detritus of the cores from the Chukchi Basin, northern Arctic Ocean, Wang et al. (2009) established the regional stratigraphic framework, identified seven ice-rafted transport events, and proposed a preliminary history of ice cap evolution of the region. Within a hundred year time scale, coastal sedimentary record may reflect the changing human activities. Yang and Zheng (2008) analyzed the sediment cores from the Yangpu Bay, Hainan Island; they stated that the sedimentary record revealed three stages of environmental pollution history of Yangpu Harbor i.e. period without pollution, before the 1970s; light pollution, the 1970s-1990s; and severe pollution, after the 1990s.

Ⅴ Future studies

Future progress in marine sediment dynamics will be dependent upon the studies on the basic scientific problems of the discipline and on the issues related to global change and earth system behavior. The basic scientific problems may include the contemporary processes for the formation of sedimentary systems, such as the processes of benthic boundary layer, resuspension, sediment transport and storm events. It is crucial to be able to quantify these processes. In terms of the global change and earth system studies, the scientists working in the field of sediment dynamics may contribute to an improved understanding of the formation of sedimentary systems, the stratigraphic continuity and resolution, the completeness of the sedimentary records for climate and environmental change research, coastal morphodynamic simulation and marine ecosystem dynamic processes.

References

Bai C G, Wang J, Xu Y H, 2006. Researches on coastal storm surge frequency during the warm period of Middle Holocene in central Jiangsu Province in China. Acta Oceanologica Sinica, 28(6), 78-85. (In Chinese, with English abstract)

Bai X F, Li S R, Gong D J, et al., 2009. Estimation of suspended sediment concentrations using Pulse-coherent Acoustic Doppler Profiler (PCADP). Chinese Journal of Oceanology and Limnology, 27, 260-265.

Bao X W, Li Z, Wang Y Z, et al., 2010. Sediment distribution features in the North Yellow Sea during summer and winter. Journal of Sediment Research, (2), 48-56. (In Chinese, with English abstract)

Bi C J, Chen Z L, Shen J, et al., 2009. Transfer and release of Hg from the Yangtze estuarine sediment during sediment resuspension event. Environmental Science, 30, 3256-3261. (In Chinese, with English abstract)

Bian C W, Jiang W S, Song D H, 2010. Terrigenous transportation to the Okinawa Trough and the influence of typhoons on suspended sediment concentration. Continental Shelf Research, 30, 1189-1199.

Chen Q Q, Meng Y, Zhou J Z, et al., 2007. Sedimentological and geochemical characteristics for evolution of salt marsh in the Changjiang River estuary in China. Acta Oceanologica Sinica, 29(6), 45-52. (In Chinese, with English abstract)

Cheng J, He Q, Xia X M, 2007. Characteristics of suspended fine sediment flocs in Changjiang (Yangtze) Estuary. Oceanologia et Limnologia Sinica, 38(4), 304-313. (In Chinese, with English abstract)

Cui T W, Zhang J, Ma Y, et al., 2009. The study on the distribution of suspended particulate matter in the Bohai Sea by remote sensing. Acta Oceanologica Sinica, 31(5), 10-18. (In Chinese, with English abstract)

Dai Z J, Zhang X L, Yan H, et al., 2009. Morphodynamic behavior of the mud coast in response to typhoon action. Ocean Engineering, 27(2), 63-69, 95. (In Chinese, with English abstract)

Du X Q, Li Y, Gao S, 2008. Characteristics of the large-scale sand waves, tidal flow structure and bedload transport over the Taiwan Bank in southern China. Acta Oceanologica Sinica, 30(5), 124-136. (In Chinese, with English abstract)

Fan H, Huang H J, 2010. Spectral signature of case II waters and its relationship with surface suspended solid concentration in the Yellow Sea and East China Sea. Oceanologia et Limnologia Sinica, 41(2), 161-166. (In Chinese, with English abstract)

Fu D Y. Pan D L, Ding Y Z, et al., 2009. Quantitative study of effects of the sea chlorophyll-a concentration by typhoon based on remote-sensing. Acta Oceanologica Sinica, 31(3), 46-56. (In Chinese, with English abstract)

Gao J H, Li J, Wang Y P, et al., 2009. Heavy mineral distributions and their implications for sediment dynamics in the Yalu Estuary and its adjacent sea area. Acta Oceanologica Sinica, 31(3), 84-94. (In Chinese, with English abstract)

Gao J H, Wang Y P, Pan S M, et al., 2007. Source and distribution of organic matter in seabed sediments of the Changjiang River estuary and its adjacent sea area. Acta Geographica Sinica, 62, 981-991. (In Chinese, with English abstract)

Gao L, Li D J, Ding P X, 2008. Variation of nutrients in response to the highly dynamic suspended particulate matter in the Changjiang (Yangtze River) plume. Continental Shelf Research, 28, 2393-2403.

Gao S, 2007a. Determination of preservation potential in tidal flat sedimentary records: a forward modeling approach. Quaternary Sciences, 27, 750-755. (In Chinese, with English abstract)

Gao S, 2007b. Modeling the growth limit of the Changjiang Delta. Geomorpholog, 85, 225-236.

Gao S, 2008. Morphodynamic processes of tidal inlets: a review. Advances in Earth Science, 23, 1237-1248. (In Chinese, with English abstract)

Gao S, 2009. Modeling the preservation potential of tidal flat sedimentary records，Jiangsu coast，eastern China. Continental Shelf Research, 29, 1927-1936.

Gao S, 2009. Grain size trend analysis: principle and applicability. Acta Sedimentologica Sinica, 27(5), 826-836. (In Chinese, with English abstract)

Gao S, Wang Y P, 2008. Changes in material fluxes from the Changjiang River and their implications on the adjoining continental shelf ecosystem. Continental Shelf Research, 28, 1490-1500.

Gong W P, Wang D R, 2006. Stability analysis and equilibrium area calculation of tidal inlet: a case study in Xincun inlet, Linshui, Hainan Island. Journal of Tropical Oceanography, 25(4), 31-41. (In Chinese, with English abstract)

Gong W P, Wang Y P, Wang D R, et al., 2008. Hydrodynamics under combined action of wave and tide and its implication for the sediment dynamics in Xincun Tidal Inlet, Hainan. Journal of Marine Science, 26(2), 1-12. (In Chinese, with English abstract)

Han S Z, Zheng Y X, Gao Z G, 2008. Numerical simulation of the suspended sediment under the effect of No.9711 tropic storm in the offshore zone of Rizhao. Periodical of Ocean University of China, 38, 868-874. (In Chinese, with English abstract)

Hong H S, Zhang C Y, Shang S L, et al. 2009. Inter-annual variability of summer coastal upwelling in the Taiwan Strait. Continental Shelf Research, 29, 479-484.

Hu R J, Wu J Z, Zhu L H, et al., 2009. Suspended sediment transport and deposition in the Zhoushan Archipelago sea area. Journal of Ocean University of China (Oceanic and Coastal Sea Research), 8, 343-351.

Huang H J, Liu Y X, Fan H, et al., 2008. Spatial-temporal change of density current at new outlet of the Huanghe (Yellow) River. Oceanologia et Limnologia Sinica, 39(1), 90-96. (In Chinese, with English abstract)

Huang L W, Deng J, 2007. Response of Yellow and East China Seas to a typhoon process. Oceanologia et Limnologia, 38, 246-252. (In Chinese, with English abstract)

Li B G, Wang C H, Zhou H Q, et al., 2009. Adjustment mechanism on the erosion and accretion of riverbved in the Jiaojiang Estuary in Zhejiang Province，China. Acta Oceanologica Sinica, 31(5), 89-100. (In Chinese, with English abstract)

Li B G, Zhang J, Zhou H Q, et al., 2007. Coastal evolution and erosional accretion dynamics on the subaqueous shore slope along the coast section at Ma'ao coast of Zhoushan Island in China. Acta Oceanologica Sinica, 29(6), 64-73. (In Chinese, with English abstract)

Li C S, Jiang B, Li A C, et al., 2009. Sedimentation rates and provenance analysis in the Southwestern Okinawa Trough since the mid-Holocene. Chinese Science Bulletin (Chinese version), 54, 1303-1310.

Li J, Gao S, Wang Y P, 2009. Studying the temporal and spatial changes of suspended sediment content in the Changjiang Estuary using a remote sensing quantitative method. Acta Oceanologica Sinica, 31(4), 167-175. (In Chinese, with English abstract)

Li P, Yang S L, Dai S B, et al., 2007. Accretion/erosion of the subaqueous delta at the Yangtze estuary in recent 10 years. Acta Geographica Sinica, 62(7), 707-716. (In Chinese, with English abstract)

Li W H, Cheng H Q, Li J F, et al., 2008. Temporal and spatial changes of dunes in the Changjiang (Yangtze) estuary, China. Estuarine, Coastal and Shelf Science, 77, 169-174.

Li Y H, Chen J, Chen J N, et al., 2010. Impact of typhoon "Fung-wong" on the distribution patterns of heavy metals in the Quanzhou Bay. Environmental Science, 31(6), 1450-1458. (In Chinese, with English abstract)

Li Z H, Gao S, Shen H T, et al., 2006. Characteristics of grain-size distributions of suspended sediment and its response to dynamics over the Dafeng tidalflat, Jiangsu coast in China. Acta Oceanologica Sinica, 28(4), 86-95. (In Chinese, with English abstract)

Li Z H, Gao S, Chen S L, 2007. Characteristics of tide-induced bottom boundary layers over the Dafeng intertidal flats，Jiangsu Province，China. The Ocean Engineering, 25(3), 53-60. (In Chinese, with English abstract)

Li Z H, Chen S L, Zhang G A, 2008. The study on grain-size distribution of suspended sediment and resuspension process on the Chongming east intertidal and subtidal zones in the Changjiang Estuary in China. Acta Oceanologica Sinica, 30(6), 154-163. (In Chinese, with English abstract)

Liao X B, Fan D D, 2008. Whether or not typhoons will be intensified by golobal warming: progress in paleo-storm research. Chinese Science Bulletin (Chinese version), 53, 1489-1502.

Liu C J, Xia H Y, Wang D X, 2010. The observation and analysis of eastern Guangdong coastal downwelling in the winter of 2006. Acta Oceanologica Sinica, 32(1), 1-9. (In Chinese, with English abstract)

Liu H, He Q, Ji X Q, et al., 2008. Sediment and geomorphology differentiation of tidal flat profiles combined wave and current actions：a case of the east Chongming tidal flat, Changjiang Estuary. Acta Sedimentologica Sinica, 26(5), 833-843. (In Chinese, with English abstract)

Liu H, He Q, Wang Y Y, et al., 2007. Temporal and spatial characteristics of surface sediment grain-size distribution in Changjiang Estuary. Acta Sedimentologica Sinica, 25(3), 445-455. (In Chinese, with English abstract)

Liu H, He Q, Wang Z B, et al., 2010. Dynamics and spatial variability of near-bottom sediment exchange in the Yangtze Estuary, China. Estuarine, Coastal and Shelf Science, 83, 322-330.

Liu H, Wu C Y, X W M, et al., 2009. Contrasts between estuarine and river systems in near-bed turbulent flows in the Zhujiang (Pearl River) Estuary, China. Estuarine, Coastal and Shelf Science, 83, 591-601.

Liu J, Saito Y, Wang H, et al., 2007. Sedimentary evolution of the Holocene subaqueous clinoform off the Shandong Peninsula in the Yellow Sea. Marine Geology, 236, 165-187.

Liu J G, Li A C, Chen M H, et al., 2008. Sedimentary changes during the Holocene in the Bohai Sea and its paleoenvironmental implication. Continental Shelf Research, 28, 1333-1339.

Liu Q Z, Li J F, Xu C H, et al., 2008. Flocculation process of fine-grained sediments by the combining effect of salinity and humus in the Changjiang Estuary in China. Acta Oceanologica Sinica, 30(3), 140-147. (In Chinese, with English abstract)

Liu S F, Liu Y G, Zhu A M, et al., 2009. Grain size trends and net transport patterns of surface sediments in the East China Sea inner continental shelf. Marine Geology & Quaternary Geology, 29(1), 1-6. (In Chinese, with English abstract)

Liu S F, Shi X F, Liu Y G, et al., 2010. Inner shelf muddy sedimentary record of the eastern Asian winter monsoon during middle

Holocene. Chinese Science Bulletin (Chinese version), 55, 1387-1396.

Liu Y L, Wang Y P, Gao J H, et al., 2010. Specific activity distribution patterns of lead-210 and sediment accumulation rates in the Jiaozhou Bay in Shandong Province, China. Acta Oceanologica Sinica, 32(1), 83-93. (In Chinese, with English abstract)

Liu Z F, Colin C, Huang W, et al., 2007. Clay minerals of the Pearl River catchment and their contribution to the South China Sea sediment. Chinese Science Bulletin (Chinese version), 52, 448-456.

Liu Z F, Tuo S T, Colin C, et al., 2008. Detrital fine-grain sediment contribution from Taiwan to the northern South China Sea and its relation to regional ocean circulation. Marine Geology, 255, 149-155.

Liu Z X, Berné S, Saito Y, et al., 2007. Internal architecture and mobility of tidal sand ridges in the East China Sea. Continental Shelf Research, 27, 1820-1834.

Liu Z Y, Pan S M, Cheng G B, et al., 2010. ^{210}Pb characteristic in the sediment cores from the Pearl River mouth and its environmental implication. Acta Sedimentologica Sinica, 28(1), 166-175. (In Chinese, with English abstract)

Long Z X, Yu X G, Wang J K, et al., 2007. Modern sedimentation rates and their influencing factors in the China's Xinglin Bay. Acta Oceanologica Sinica, 29(6), 155-160. (In Chinese, with English abstract)

Lu X Q, Zhang J C, 2006. Numerical study on spatially varying bottom friction coefficient of a 2D tidal model with adjoint method. Continental Shelf Research, 26, 1905-1923.

Ma F. Wang Y P, Li Y, et al., 2008. The application of geostatistics to analysis of grain size trend in the eastern Beibu Gulf. Acta Geographica Sinica, 63, 1207-1217. (In Chinese, with English abstract)

Meng X W, Du D W, Liu Y G, et al., 2007. Terrestrial flux in sediments from the Okinawa Trough and its response to climate changes over the past 35000a. Acta Oceanologica Sinica, 29(5), 74-80. (In Chinese, with English abstract)

Pan S M, Guo D Y, Liu Z Y, 2008. Sedimentation and erosion in Pui O salt marsh of Hong Kong from ^{137}Cs distribution in sediment. Acta Sedimentologica Sinica, 26, 655-660. (In Chinese, with English abstract)

Pan W R, Luo Z B, Zhang G R, et al., 2009. Characteristics of tide-induced bottom boundary layers in Xiamen Bay under the tropical cyclone conditions. Journal of Oceanography in Taiwan Strait, 28(4), 540-545. (In Chinese, with English abstract)

Pang C G, Yu W, Yang Y, 2010. Characteristics and its forming mechanism on grain size distribution of suspended matter at Changjiang Estuary. Environmental Science, 31(3), 618-625. (In Chinese, with English abstract)

Peng J, Chen S L, 2009. The variation process of water and sediment and its effect on the Yellow River delta over the six decades. Acta Geographica Sinica, 64, 1353-1362. (In Chinese, with English abstract)

Qi H S, Cai F, Lei G, et al., 2009a. Beach morphology in response to storm events, south China. Progress in Natural Sciences, 19(9), 975-985. (In Chinese, with English abstract)

Qi H S, Cai F, Su X Z, et al., 2009b. Study on geomorphologic process of beaches under tropical storm action. Acta Oceanologica Sinica, 31(1), 168-176. (In Chinese, with English abstract)

Qiao L L, Bao X W, Wu D X, et al., 2008. Numerical study of generation of the tidal shear front off the Yellow River mouth. Continental Shelf Research, 28, 1782-1790

Qiao S Q, Shi X F, Zhu A M, et al., 2010. Distribution and transport of suspended sediments off the Yellow River (Huanghe) mouth and the nearby Bohai Sea. Estuarine, Coastal and Shelf Science, 86, 337-344.

Ren J, Wu C Y, Bao Y, 2007. Approaches to morphological evolution in long-term morphodynamic model. Acta Oceanologica Sinica, 29(1), 76-80. (In Chinese, with English abstract)

Shen F, Zhou Y X, Zhang J, et al., 2006. Remote-sensing analysis on spatial-temporal variation in vegetation on Jiuduansha Wetland. Oceanologia et Limnologia Sinica, 37(6), 498-504. (In Chinese, with English abstract)

Shi B W, Yang S L, Luo X X, et al., 2010. A wave attenuation over the transitional zone of mudflat and salt marsh. Acta Oceanologica Sinica, 32(2), 174-178. (In Chinese, with English abstract)

Sun X Y, Li G X, Liu Y, et al., 2008. Response of environmental sensitive grain size group in core FJ04 from mud area in the north of East China Sea to East Asian Winter Monsoon evolvement. Marine Geology and Quaternary Geology, 28(4),

11-17. (In Chinese, with English abstract)

Wang A J, Gao S, Chen J, 2006. Application of ^{137}Cs chronology to coastal salt marshes. Marine Geology and Quaternary Geology, 26(5), 85-90. (In Chinese, with English abstract)

Wang A J, Gao S, Chen J, Li D Y, 2009a. Sediment dynamic responses of coastal salt marsh to typhoon "KAEMI" in Quanzhou Bay, Fujian Province, China. Chinese Science Bulletin, 54, 120-130.

Wang A J, Ye X, Chen J, 2009b. Observations and analysis of floc size and floc settling velocity of coastal salt marsh in Luoyuan Bay in Fujian Province, China. Acta Oceanologica Sinica, 31(2), 165-174. (In Chinese, with English abstract)

Wang A J, Ye X, Chen J, 2009c. Effects of typhoon on sedimentary processes of embayment tidal flat. Acta Oceanologica Sinica, 31(6), 77-86. (In Chinese, with English abstract)

Wang A J, Ye X, Huang C B, et al., 2010. Impacts of *Spartina alterniflora* on the transport of surface sediments in coastal saltmarshes of Quanzhou Bay. Journal of Oceanography in Taiwan Strait, 29(1), 66-72. (In Chinese, with English abstract)

Wang C, He B G, Zhou N C, et al., 2009. Cross-shore suspended sediment flux in the salt marsh pioneer zone of Chongming eastern beach in the Changjiang Estuary in China. Acta Oceanologica Sinica, 31(1), 143-151. (In Chinese, with English abstract)

Wang G Q, Shi X F, Liu Y G, et al., 2007. Grain-size trend analysis on the south branch of the Changjiang Estuary in China and its implication to sediment transportation. Acta Oceanologica Sinica, 29(6), 161-166. (In Chinese, with English abstract)

Wang H J, Yang Z S, Li Y H, et al., 2007. Dispersal pattern of suspended sediment in the shear frontal zone off the Huanghe (Yellow River) mouth. Continental Shelf Research, 27, 854-871.

Wang H L, Li G S, 2009. Numerical simulation on seasonal transportation of suspended sediment from Huanghe (Yellow) River to Bohai Sea. Oceanologia et Limnologia Sinica, 40(2), 129-137. (In Chinese, with English abstract)

Wang H R, Wang Y M, Qiu Y, et al., 2008. Development and its tectonic activity's origin of turbidity current sediment wave in Manila Trench，the South China Sea. Acta Sedimentologica Sinica, 26(1), 39-45. (In Chinese, with English abstract)

Wang J, Bai C G, Xu Y H, 2006. Mechanism of silt-mud couplet of mud tidal flat and discrimination criteria of storm surge sedimentation in the Middle Jiangsu Province. Acta Sedimentologica Sinica, 24(4), 562-569. (In Chinese, with English abstract)

Wang R J, Xiao W S, Li W B, et al., 2009. Late Quaternary ice-rafted sediment transport event: Chukchi Basin, Arctic Ocean. Chinese Science Bulletin (Chinese version), 54, 3761-3770.

Wang W, Li A C, Xu F J, et al., 2009. Distribution of surface sediments and sedimentary environment in the north Yellow Sea. Oceanologia et Limnologia Sinica, 40, 525-531. (In Chinese, with English abstract)

Wang Y H, Shen H T, Li J F, et al., 2009. Sedimentary features of sediment and their responses to dynamics in flood and ebb channel of the Changjiang Estuary. Acta Sedimentologica Sinica, 27(3), 511-517. (In Chinese, with English abstract)

Wang Y Z, Jiang W S, 2007. Numerical simulation of variations in winter and summer suspended material concentrations in the Bohai Sea，Yellow Sea and East China Sea. Advances in Marine Science, 25(1), 28-33. (In Chinese, with English abstract)

Wang Z H, Li L Q, Chen D C, et al., 2007b. Plume front and suspended sediment dispersal off the Yangtze (Changjiang) River mouth, China during non-flood season. Estuarine, Coastal and Shelf Science, 71, 60-67.

Wei T Y, Chen Z Y, Duan L Y, et al., 2007. Sedimentation rates in relation to sedimentary processes of the Yangtze Estuary, China. Estuarine, Coastal and Shelf Science, 71, 37-46.

Wu J X, Liu J T, Shen H T, et al., 2006. Dispersion of disposed dredged slurry in the meso-tidal Changjiang (Yangtze River) Estuary. Estuarine，Coastal and Shelf Science, 70, 663-672.

Xia H Y, Liao S Z, 2010. The quality control and the systematic error correction for the shipboard ADCP data off the Zhujiang River mouth. Acta Oceanologica Sinica, 32(3), 1-7. (In Chinese, with English abstract)

Xie D F, Gao S, Wang Y P, 2006. A preliminary modeling study on morphodynamic equilibrium of tidal channels floored with sandy sediments. Acta Oceanologica Sinica, 28(6), 86-93. (In Chinese, with English abstract)

Xie D F, Wang Z B, Gao S, et al., 2009. Modeling the tidal channel morphodynamics in a macro-tidal embayment，Hangzhou Bay，China. Continental Shelf Research, 29, 1757-1767.

Xu F J, Li A C, Wan S M, et al., 2009. The geological significance of environmental sensitive grain-size populations in the mud wedge of the East China Sea during the mid-Holocene. Acta Oceanologica Sinica, 31(3), 95-102. (In Chinese, with English abstract)

Xu X Y, Yi L, Yu H J, et al., 2010. The differences of grain-size parameters estimated with graphic and moment methods in coastal sediments. Acta Oceanologica Sinica, 32(2), 80-86. (In Chinese, with English abstract)

Xu Z W, Wang Y P, Li Y, et al., 2010. Sediment transport patterns in the eastern Beibu Gulf based on grain-size multivariate statistics and provenance analysis. Acta Oceanologica Sinica, 32(3), 67-78. (In Chinese, with English abstract)

Yang H L, Zheng Y L, 2008. The sediment records of environmental changes under interactions of nature with mankind during last hundred years in the Yangpu Bay of Hainan, China. Acta Oceanologica Sinica, 30(4), 95-103. (In Chinese, with English abstract)

Yang S L, Li H, Ysebaert T, et al., 2008. Spatial and temporal variations in sediment grain size in tidal wetlands，Yangtze Delta：on the role of physical and biotic controls. Estuarine, Coastal and Shelf Science, 77, 657-671.

Yang S L, Li M, Zhang W X, 2006a. Sensibility of delta forward coastal response to decrease in riverine sediment supply：a case study from the seaward coast of the Chongming Island in the Changjiang River delta. Geography and Geo-Information Science, 22(6), 62-65. (In Chinese, with English abstract)

Yang S L, Li P, Gao A, et al., 2006b. Observation of hydrographic and sedimentary processes over an intertidal flat based on ADP-XR and OBS-3A. Acta Oceanologica Sinica, 28(5), 56-63. (In Chinese, with English abstract)

Yang Y, Gao S, Wang Y P, 2008. Fine-grained sediment transport and resuspension process in tidal channel of the northern Hangzhou Bay in China. Acta Oceanologica Sinica, 30(2), 92-101. (In Chinese, with English abstract)

Yang Y, Wang Y P, Gao J H, et al., 2006. Hydrodynamics and fine-grained sediment resuspension in Changjiang Estuary during dry seasons. Journal of Nanjing University (Natural Sciences), 42, 643-655. (In Chinese, with English abstract)

Yang Z S, Liu J P, 2007. A unique Yellow-River-derived distal subaqueous delta in the Yellow Sea. Marine Geology, 240, 169-176.

Ye X, Li Y, Huang B Q, et al., 2008. Suspended particle size spectra of upwelling area in the Taiwan Strait during the summer of 2004. Acta Oceanologica Sinica, 30(2), 102-110. (In Chinese, with English abstract)

Ye X, Li Y, Huang B Q, 2009. Particle organic carbon in he southern Taiwan Strait during summer. Acta Oceanologica Sinica, 31(6), 87-99. (In Chinese, with English abstract)

Yu Q, Gao S, 2008. Simulation on sediment grain size trend with bedload transport under rectilinear tidal current. Oceanologia et Limnologia Sinica, 39(4), 297-304. (In Chinese, with English abstract)

Yuan Y, Wei H, Zhao L, et al., 2008. Observations of sediment resuspension and settling off the mouth of Jiaozhou Bay, Yellow Sea. Continental Shelf Research, 28, 2630-2643.

Yuan Y, Wei H, Zhao L, et al., 2009. Implications of intermittent turbulent bursts for sediment resuspension in a coastal bottom boundary layer: a field study in the western Yellow Sea, China. Marine Geology, 263, 87-96.

Yuan Y, Zhao L, Wei H, et al., 2008. Research on observing suspended sediment concentration using ADCP and LISST-100 instruments. Acta Oceanologica Sinica, 30(3), 48-55. (In Chinese, with English abstract)

Zhang C G, Zhang X, Chen M Y, et al., 2008. Study on remote sensing Quantitative model of suspended sediments in the coastal waters of Fujian. Journal of Natural Resources, 23(1), 150-160. (In Chinese, with English abstract)

Zhang C Y, Feng X L, 2009. The spatial distribution and analysis about the grain-size of sediments in the Lianyungang nearshore sea area. Acta Oceanologica Sinica, 31(4), 120-127. (In Chinese, with English abstract)

Zhang H J, Zhai S K, Fan D J, et al., 2007. Form characteristics and substance constituents of suspended sediment matters in the Yangtze River estuary area after the first-stage storage of the Three Gorges Project. Marine Geology & Quaternary Geology, 27(2), 1-10. (In Chinese, with English abstract)

Zhang N, Yin Y, Pan S M, et al., 2009. Modern sedimentation of tidal inlet-tidal basin system in Caofeidian coastal area，Bohai Bay，Northeastern China. Marine Geology & Quaternary Geology, 29(6), 25-34. (In Chinese, with English abstract)

Zhang R, Pan S M, Wang Y P, et al., 2009. Sedimentation rates and characteristics of radionuclide ^{210}Pb at the subaqueous delta in Changjiang Estuary. Acta Sedimentologica Sinica, 27(4), 704-713. (In Chinese, with English abstract)

Zhang R, Wang Y P, Gao J H, et al., 2008. The vertical sedimentary structure and its implications for environmental evolutions in the Changjiang Estuary in China. Acta Oceanologica Sinica, 30(2), 80-91. (In Chinese, with English abstract)

Zhang W Z, Hong H S, Shang S P, et al., 2007. A two-way nested coupled tide-surge model for the Taiwan Strait. Continental Shelf Research, 27, 1548-1576.

Zhang X D, Zhai S K, Xu S M, 2006. The application of grain-size end-member modeling to the shelf near the estuary of Changjiang River in China. Acta Oceanologica Sinica, 28(4), 159-166. (In Chinese, with English abstract)

Zhang Y, Zhang D, Hu P X, 2008. Water content of soil on outcrop beach measured by remote sensing. Acta Oceanologica Sinica, 30(5), 29-34. (In Chinese, with English abstract)

Zhang Y, Zhang Y, Zhang D, et al., 2009. An underwater bathymetry reversion in the radial sand ridge group region of the southern Huanghai Sea using the remote sensing technology. Acta Oceanologica Sinica, 31(3), 39-45. (In Chinese, with English abstract)

Zhao B, Guo H Q, Yan Y E, et al., 2008. A simple waterline approach for tidelands using multi-temporal satellite images: a case study in the Yangtze Delta. Estuarine, Coastal and Shelf Science, 77, 134-142.

Zhao H Q, Han X B, Chen R H, et al., 2008. Characteristics of main elements and their paleoenvironment significance of Core 191 in the northern South China Sea. Acta Oceanologica Sinica, 30(6), 85-93. (In Chinese, with English abstract)

Zhao Y X, Liu B H, Li X S, et al., 2006. Topography feature and migration of submarine sand waves in Jiaozhou Bay mouth. Oceanologia et Limnologia Sinica, 37(5), 464-471. (In Chinese, with English abstract)

Zheng Y M, Kang J C, Zhong W, et al., 2009. Salinity distribution of diluted water and plume front of early summer and late autumn in 2004 off Changjiang (Yangtze) Estuary. Oceanoligia et Limnologia Sinica, 40, 275-282. (In Chinese, with English abstract)

Zhou H, Ran W J, Jiang G J, et al., 2007. A flume experiment on flocculation settling of fine-grained sediment in moving water. Oceanologia et Limnologia Sinica, 38(2), 124-130. (In Chinese, with English abstract)

Zhou X J, Jiang F Q, Li A C, et al., 2010. A preliminary study on fingerprinting approach in marine sediment dynamics with the rare earth elements. Acta Oceanologica Sinica, 32, 67-82. (In Chinese, with English abstract)

Zhu L H, Wu J Z, Hu R J, et al., 2009. Geomorphological evolution of the Liaohe River delta in recent 20 years. Acta Geographica Sinica, 64, 357-367. (In Chinese, with English abstract)

Zhuang L H, Yan J, Chnag F M, et al., 2009. Short-term morphological changes after sand-digging during a sand sculpture activity. Chinese Journal of Oceanology and Limnology, 27, 966-974.